MECHANISTIC STUDIES OF GERMYLENE AND DIGERMENE REACTIONS

MECHANISTIC STUDIES OF THE REACTIONS OF TRANSIENT

DIARYLGERMYLENES AND TETRAARYLDIGERMENES IN SOLUTION

By

LAWRENCE ANDREW HUCK, B.Sc.(Honours)

A Thesis

Submitted to the School of Graduate Studies

in Partial Fulfillment of the Requirements

for the Degree

Doctor of Philosophy

McMaster University

DOCTOR OF PHILOSOPHY (2010)   McMaster University

(Chemistry)   Hamilton, Ontario

TITLE: Mechanistic Studies of the Reactions of Transient
                Diarylgermylenes and Tetraaryldigermenes in Solution

AUTHOR: Lawrence Andrew Huck
                B.Sc. (Honours, Co-op, University of Victoria)

SUPERVISOR: Professor William J. Leigh

NUMBER OF PAGES: xxv, 278

ABSTRACT

The reactivity of diarylgermylenes (GeAr$_2$, **Ga-g**) with tetrahydrofuran, diethylamine, acetic acid, carbon tetrachloride and isoprene has been studied in hexanes solution, while the reactivity of the germylene-Lewis bases complexes **37** and **44** with methanesulfonic acid and sodium hydroxide has been studied in methanol and THF solution. Dimerization of germylenes yields digermenes (Ar$_2$Ge=GeAr$_2$, **DGa-g**) and the reactivity of these species with diethylamine, acetic acid, and carbon tetrachloride has been examined. In addition to product studies, laser flash photolysis is used to generate and monitor these species over their lifetimes (< 20 μs) to determine absolute rate (k) and equilibrium (K) constants for the reactions. Aromatic substituent effects on k and K provide insight into the electronic demands of the transition state, while the effects of temperature on k and K leads to the activation and thermodynamic parameters, respectively.

Reaction of germylenes with acetic acid yields the corresponding O-H insertion product (**40**); a two-step mechanism is proposed, Lewis acid-base complexation followed by proton transfer. Generation of germylenes in THF and MeOH leads to the immediate formation of the corresponding Lewis acid-base complex (**37** and **44**). In both solvents, the decay of the complex is accelerated by methanesulfonic acid but in neither case could evidence for a germyl cation be found. The decay of the germylene-MeOH complex (**44**) is accelerated by NaOMe; in one case a germyl anion (**52**) was detected. Reaction of germylenes with CCl$_4$ gives products consistent with halogen atom abstraction by the germylene. The data suggest a mechanism involving fast reversible germylene-CCl$_4$

complexation followed by a rate-determining dissociative inner-sphere electron transfer to yield the Ph_2GeCl/CCl_3 radical pair (**60**), whose primary fate is cage escape. Data on the reactions of **37** with CCl_4 in hexanes containing THF and neat THF are most consistent with a mechanism that yields an ion pair. Germylenes are scavenged by isoprene to form the vinylgermirane **24** as the kinetic product, while the germacyclo-pentenes **23** are the thermodynamic products. A π-complex (**77**) prior to formation of **24** is proposed. It is believed that **23** forms from a (1+4) cycloaddition reaction of the germylene with isoprene rather than a [1,3]-sigmatropic rearrangement of **24**.

Digermenes react with acetic acid to yield products consistent with formal addition of acetic acid across the Ge=Ge bond; the kinetic data are consistent with nucleophilic attack by the carbonyl oxygen at germanium as the initial step in the reaction. Reaction of digermenes with CCl_4 gives the 1,2-dichlorodigermane. A double halogen atom abstraction mechanism, with the digermene behaving as an electron donor, is proposed.

ACKNOWLEDGEMENTS

TABLE OF CONTENTS

LIST OF FIGURES

LIST OF TABLES

Chapter 1 - Introduction

1.1. Thesis Overview

Germylenes are the germanium analogues of carbenes and have the general

formula GeR_2 (R = alkyl group, aryl group, hydrogen, halogen, etc.) while digermenes are

the germanium analogues of alkenes and have the general formula $R_2Ge=GeR_2$. The

reactivity of both species is highly dependent on substituent. For simple R groups (*e.g.*

CH_3, C_6H_5) germylenes undergo dimerization and subsequent oligomerization in the

absence of a scavenger at close to diffusion controlled rates; digermenes do so as well but

more slowly. Because the lifetimes of these transients are on the order of microseconds,

fast time-resolved spectroscopy is employed to detect these intermediates and study their

reactivity. This thesis presents the results of detailed mechanistic studies of a number of

germylene and digermene reactions. These results contribute to the knowledge of the

chemistry of the Group 14 reactive intermediates.

1.2. Nomenclature

The heavy Group 14 carbene analogues (MR_2, M = Si, Ge, Sn) are known as

metallylenes. Given that silicon and germanium are semi-metals, this term is a bit

misleading. Because the Group 14 elements are collectively known as the *tetrels*, the

more appropriate term is *tetrelylenes*,[1, 2] but such nomenclature is rarely used. The alkene

analogues, $R_2M=CR_2$ and $R_2M=MR_2$ (M = Si, Ge, Sn), are known as *metallenes* and

dimetallenes, respectively. It has been noted that since the structure and chemical

reactivity of these molecules are very different from those of alkenes, these terms are also

inappropriate.[3] The preferred though rarely used term for the latter is *dimetallylene* (or

ditetrelylene).[3] Table 1.1 lists a selection of Group 14 functionalities and the common

nomenclature.

Table 1.1. Nomenclature for some Group 14 functional groups.

M	Metallylene [a] MR_2	Metallene $R_2C=MR_2$	Dimetallene $R_2M=MR_2$	Metallane MR_4
Si	silylene	silene	disilene	silane
Ge	germylene	germene	digermene	germane
Sn	stannylene	stannene	distannene	stannane

a. In the older literature, these were often named using the tetravalent term with the suffix "diyl". (*e.g.* germylenes = germanediyls.)

1.3. Germylenes – Structure and Synthesis

1.3.1. Electronic Structure and Thermodynamics

Divalent Group 14 species have two non-bonding electrons on M. There are two

possible ground-state electronic configurations, the *singlet* and *triplet* (Figure 1.1). In

dialkyl- and diaryl carbenes, the energy difference between the singlet and triplet states

(ΔE_{ST}) is generally only a few kcal/mol and thus the multiplicity of the lower energy state

depends on the substituent[4-6] as well as the solvent[7]. For example, phenylchlorocarbene

is a ground state singlet while diphenylcarbene is a ground state triplet.[6] The situation

changes markedly in metallylenes. With only two reported exceptions,[8, 9] the lowest

energy electronic configuration for metallylenes is the singlet. Table 1.2 shows

calculated ΔE_{ST} values for the simplest Group 14 divalent species MH_2. Apeloig *et al.*

have suggested that the majority of the difference between the singlet energies of CH_2 and

SiH_2 is because of reduced electron-electron repulsion of the frontier electrons due to the

increasing size of the sp^2 orbital as Group 14 is descended.[10]
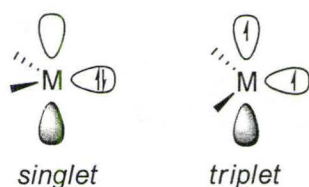
Figure 1.1. Singlet and triplet electronic configurations of divalent Group 14 species. In most cases, $E_{singlet} < E_{triplet}$ for M = Si, Ge, Sn.

singlet   triplet

A term used to describe divalent species in Group 14 is the *divalent state stabilization energy* (DSSE),[11, 12] which is the difference between the M-X bond dissociation enthalpies (D) of MX_4 and $\cdot MX_3$ (eqs 1.1-1.2). The more stable the divalent species, the lower the D value of the latter reaction leading to a greater DSSE. DSSE values for CH_2/MH_2 are listed in Table 1.2.

$$
\begin{array}{llll}
MX_4 \longrightarrow & \cdot MX_3 + & X\cdot & D(X\text{-}MX_3) \\
\cdot MX_3 \longrightarrow & :MX_2 + & X\cdot & D(X\text{-}MX_2)
\end{array}
\tag{1.1}
$$
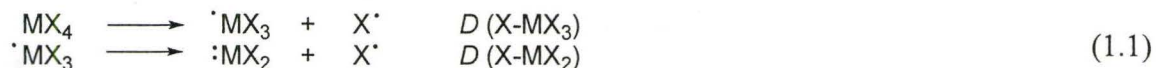
$$
DSSE = D(X\text{-}MX_3) - D(X\text{-}MX_2)
\tag{1.2}
$$

Table 1.2. Calculated singlet-triplet energy gap (ΔE_{ST}) and the divalent state stabilization energies (DSSE) for CH_2, SiH_2, GeH_2, and SnH_2. Units: kcal/mol.

	ΔE_{ST} [a]	DSSE
CH_2 ($^1A_1$)	-10.4	-12 [b]
($^3B_1$)		-6 [b]
SiH_2	+20.0	+19 [c]
GeH_2	+22.0	+26 [d]
SnH_2	+23.4	+26 [e]

a. CCSD(T)/EC; Reference 13. A positive value indicates a singlet ground state. *b*. MP4SDTQ(FC)/6-311G**//MP2(FU)/6-31G* ; see reference 14 for details. *c*. Experimental; reference 15. *d*. Experimental; Reference 16;. *e*. BAC-MP4(298K); Reference 17.

1.3.2. Synthesis of Germylenes

Carbenes are usually prepared from two common classes of compounds, namely diazo compounds (**1**) and diazirenes (**2**).[18, 19] No germanium analogues of these compounds are known. Germanimines ($R_2Ge=NR'$) readily dimerize and react with nucleophiles including THF, which undergoes ring opening.[20] Germadiazirenes can be viewed as the (1+2)-cycloaddition product of GeR_2 and N_2. Walsh *et al.* were unable to detect products from the reaction of SiH_2 and molecular nitrogen, although presumably the activation barrier for this reaction is very high.[21] An analogous reaction with germylenes would not be expected to occur because of the higher DSSE. If these species were to be prepared by any method they should immediately dissociate to the parent metallylene and N_2.

Germylenes can be prepared by reductive dehalogenation of R_2GeX_2 (*e.g.* eq 1.3)[22, 23] and by reaction of organolithium reagents with $GeCl_2$-dioxane (*e.g.* eq 1.4).[24] These reactions are often used in the synthesis of stable germylenes.

$$\text{(1.3)}$$

$$\text{(1.4)}$$

R = 2,4,6-trimethylphenyl
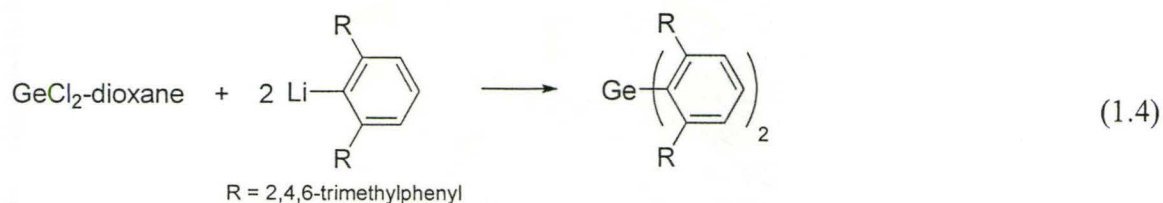
The most widely used class of compounds for the thermal generation of GeR_2 (R

= alkyl) is the germanorbornadiene (**3**), which produces GeR_2 and tetraphenylnaphthalene

(*e.g.* eq 1.5).[25, 26] Cyclotrigermanes (**4**) undergo thermolysis to yield germylenes,

although this is more frequently used when the product of interest is the concomitantly-

generated doubly-bonded species (*e.g.* eq 1.6). Both **3** and **4** give the same products upon

photolysis as they do upon thermolysis.[27-29] Thermal α-elimination (*e.g.* eq 1.7) will also

yield germylenes but the process is generally reversible.[30, 31]

$$R_2Ge \quad + \quad \text{(tetraphenylnaphthalene)} \tag{1.5}$$

$$R_2Ge \quad + \quad R_2Ge{=}GeR_2 \tag{1.6}$$

$$HGeCl_3 \; \rightleftarrows_{\Delta} \; GeCl_2 \; + \; HCl \tag{1.7}$$
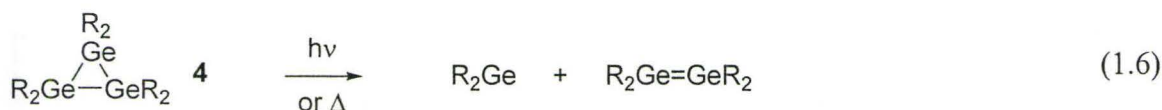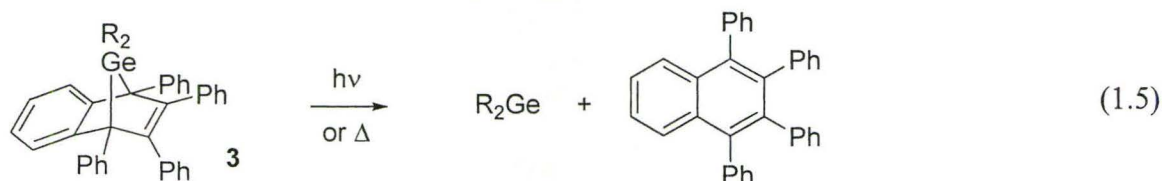
Commonly used photochemical germylene precursors include trimetallanes (*e.g.*

eq 1.8),[32] germadiazides (*e.g.* eq 1.9),[33] and germacyclopentenes (*e.g.* eq 1.10).[34] Both

trimetallanes and germadiazides undergo competing photochemical reactions which

reduces their suitability as germylene precursors in time-resolved spectroscopic studies.

Trimetallanes undergo competitive homolytic bond cleavage and rearrangement to a

germahexatriene derivative when R = Ph,[29, 35] while germadiazides produce a low

chemical yield of the germylene[33] and may also yield germanimines and other transient

products.[36, 37] Germacyclopentenes are ideally suited for mechanistic studies because

they yield germylenes in high chemical and quantum yield, and have no competing

reactions that interfere with the direct detection of the germylene.[34, 38]

$$\begin{array}{c} \text{R} \quad \text{R} \\ \text{Me}_3\text{Si} \overset{\text{Ge}}{\diagdown} \text{SiMe}_3 \end{array} \xrightarrow{\text{h}\nu} \begin{bmatrix} \text{GeR}_2 + \text{Si}_2\text{Me}_6 \end{bmatrix} + \qquad + \qquad \qquad \text{Ge(R)SiMe}_3 \qquad (1.8)$$

[Me₃SiGeR₂ + ˙SiMe₃]   SiMe₃
                                            when R = Ph

$$\text{Me}_2\text{Ge(N}_3)_2 \xrightarrow{\text{h}\nu} \text{GeMe}_2 + 3\,\text{N}_2 \qquad (1.9)$$
ca. 30%

$$\text{R}_2\text{Ge} \xrightarrow{\text{h}\nu} \text{R}_2\text{Ge} + \qquad \qquad (1.10)$$
> 90%
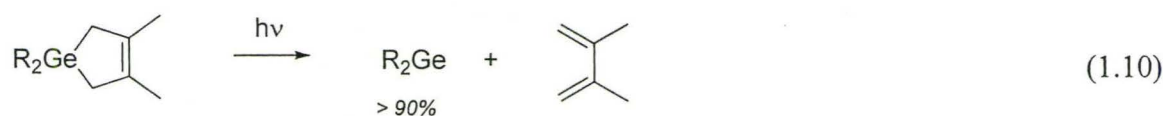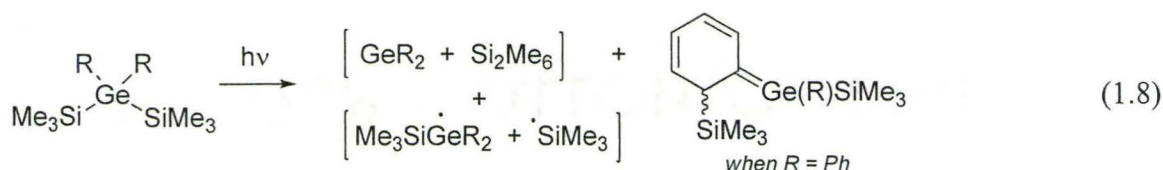
1.4. Germylenes - Reactivity

In the absence of a scavenger, sterically unencumbered germylenes (*e.g.* GeMe₂,

GePh₂) dimerize at close to diffusion controlled rates to yield the corresponding

digermenes. Dimerization can be slowed by

sterically bulky and/or thermodynamically

stablizing substituents on germanium as shown in

examples **5**[22] and **6**[39]. These are known as *stable*

germylenes and their x-ray crystal structures have

been determined.[22,39]
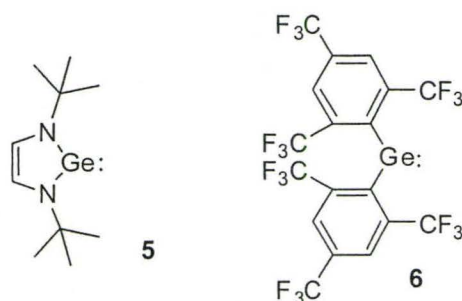
The chemical reactions of germylenes have been outlined in several reviews.[25, 40-

47] This thesis focuses on the reactivity of transient germylenes in four general classes of

reactions: (i) complexation with Lewis bases, (ii) insertion into σ bonds, (iii) addition to π-bonds, (iv) halogen atom abstraction. The following section summarizes the available data for the germylene reactions studied in this thesis, with a focus on $GePh_2$. Brief comparisons of germylene reactivity with the corresponding reactivity of silylenes and singlet carbenes are also given when appropriate. Comparisons are made with the ground state singlet silylene $SiPh_2$ and the ground state singlet phenylchlorocarbene (PhCCl, **7**) and dichlorocarbene (CCl_2).

1.4.1. Complexation with Lewis bases

Lewis acid-base complexation between germylenes and Lewis bases such as ethers, amines, and other heteroatom containing nucleophiles (Nu) is well known (*e.g.* eq 1.11).[25] Many complexes of this type have been detected by Ando *et al.* in rigid matrixes at low temperature.[48, 49] In these experiments, a photochemical GeR_2 precursor (R = alkyl or aryl) is frozen in a hydrocarbon matrix at 77 K in the presence of a Lewis base (amines, phosphines, ethers, sulphides, halocarbons, alcohols). Irradiation of the matrix yields the germylene, which is detected using UV spectroscopy. Annealing of the matrix leads to the appearance of a absorbance band which can be assigned to the corresponding germylene-nucleophile donor complex. In each case, the lowest energy absorbance maximum of the complex is blue shifted relative to that of the free germylene, as shown in Table 1.3.

GeMe$_2$ + [cyclic ether structure] $\longrightarrow$ [cyclic ether structure with Me$_2$Ge]   (1.11)

Me$_2$Ge
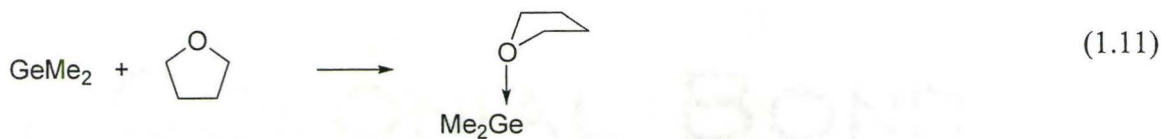
From fluid solution at ambient temperature, complexes of the type $X_2Ge \leftarrow Nu$ (X = halogen) are isolable as solids[50-53] because of the stability afforded by extensive intermolecular coordination.[54] Germylene complexes of the type $R_2Ge \leftarrow Nu$ (R = alkyl, aryl) are not isolable because while complexation slows oligomerization, is does not eliminate it – only germanium oligomers $(GeR_2)_n$ are isolated.[55, 56] Complexes of GeMe$_2$, GeMePh, GePh$_2$, and GeMes$_2$ (Mes = mesityl = 2,4,6-trimethylphenyl) can be detected at ambient temperature in hexanes solution by laser flash photolysis.[34, 57-59] As shown in Table 1.3, in both low temperatures matrixes and hexanes solution at ambient temperature, the absorbance maxima of the complexes in hexanes solution are blue shifted relative to the free germylene. Furthermore the absorbance maxima observed in the matrix is blue shifted relative to the absorbance maximum observed in fluid solution.

Table 1.3. Absorbance maxima (nm) of GePh$_2$ and GeMes$_2$ and the corresponding ether donor complexes in matrixes at 77 K and in hexanes solutions at ambient temperature.

	Matrix (77 K)^a	Hexanes (298 K)
GeMe$_2$	420	480 ^{c}
GePh$_2$	466	500 ^{c}
GeMes$_2$	550	560 ^{c}
Ph$_2$Ge← THF ^{b}	325	355 ^{d}
Mes$_2$Ge← THF ^{b}	360	360 ^{d}

a. Reference 49; 3:7 3-methylpentane:2-methylbutane. *b*. in the matrix 2-methyltetrahydrofuran was used. *c*. Reference 34. *d*. Reference 58.

Complexation is reversible (eqs 1.12-1.14) and the equilibrium constants are positively correlated with the basicity of the nucleophile (Table 1.4), as given by the gas phase proton affinity.[60] Forward rate constants for the approach to equilibrium between free $GePh_2$ and a number of $GePh_2$-nucleophile complexes have been measured and the values are all within a factor of 10 or less of the diffusional rate constant ($k_{diff} \approx 2.15 \times 10^{10}$ $M^{-1}s^{-1}$ in hexanes at 23 °C).[61] The relationship between the basicity of the nucleophile and the equilibrium constant suggests the germylene acts as the electrophile in these reactions.

Table 1.4. Kinetic and thermodynamic data of the formation of various $GePh_2$-Lewis base complexes in hexanes at 25 °C.

	k_Q / 10^9 $M^{-1}s^{-1}$	K_{eq} / 10^3 M^{-1}	λ_{max} / nm [c]
MeOH [a]	6.1 ± 1.1	3.3 ± 0.8	350
THF [a]	6.3 ± 0.6	23 ± 5	360
NEt_3 [b]	2.8 ± 0.9	> 20	330
$NHEt_2$ [b]	7.29 ± 0.09	> 20	320
$^nBuNH_2$ [b]	10.1 ± 0.6	> 20	310

a. Reference 58. *b.* Reference 57. *c.* λ_{max} $GePh_2$ = 500 nm.

$$GePh_2 \; + \; CH_3OH \; \rightleftharpoons \; Ph_2Ge \leftarrow O\overset{CH_3}{\underset{H}{\diagdown}} \qquad\qquad (1.12)$$

$$GePh_2 \; + \; \text{(tetrahydrofuran)} \; \rightleftharpoons \; Ph_2Ge \leftarrow O\text{(tetrahydrofuran)} \qquad\qquad (1.13)$$

$$GePh_2 \; + \; NR_3 \; \rightleftharpoons \; Ph_2Ge \leftarrow NR_3 \qquad\qquad (1.14)$$
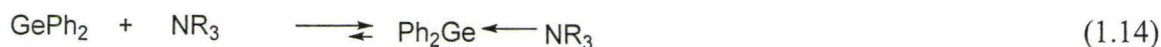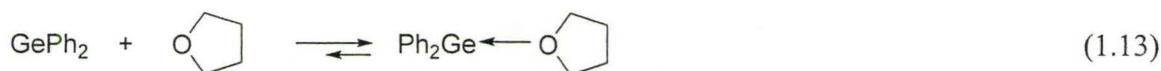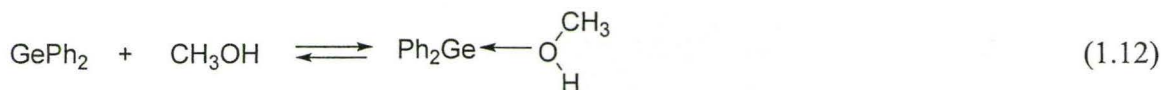
It should be noted that the discussion in this and subsequent sections of the thesis pertain to germylenes of the type GeR_2 (R = alkyl, aryl) and may not necessarily apply to

compounds of the type GeX_2 and GeRX, where X = halogen. W. P. Neumann observed

that "germylene dihalides sometimes behave as germylenes and sometimes they do

not"[25]. For example, $GeCl_2$ readily inserts into a variety of C-Cl bonds (*e.g. n*-BuCl),[30]

whereas $GeMe_2$ does not, instead favouring halogen abstraction to (ultimately) yield

Me_2GeCl_2.[62] This difference is likely a result of intermolecular coordination of GeRX in

solution (Figure 1.2).[31] The stabilization afforded by this coordination suppresses the

dimerization of GeRX and GeX_2 in solution and can be expected to affect other aspects of

germylene reactivity similarly.[31] Dihalogermylenes also exhibit extensive intermolecular

coordination in the solid state.[52, 53, 63, 64]
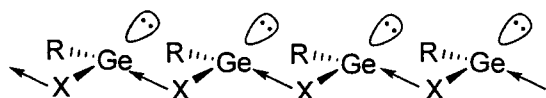
Figure 1.2. Intermolecular coordination of GeRX.

The complexation of silylenes with nucleophiles has also been thoroughly

studied.[65, 66] Complexation of THF with $SiPh_2$ occurs ca. five times faster than with

$GePh_2$ ($k_{THF} = 1.5 \times 10^{10}$ M^{-1}s^{-1}) and the equilibrium constant is at least one thousand

times greater ($K_{eq} > 10^5$ M^{-1}).[67] Both differences can be attributed to the greater bond

strength of Si-O compared to Ge-O (SiO $\approx$ 106 kcal/mol, GeO $\approx$ 85 kcal/mol).[68]

Halocarbenes have a lower electrophilicity because of donation of the halogen lone pairs

into the vacant *p*-orbital,[69] and complexation with singlet carbenes by aliphatic ethers is

not observed.[70, 71] Carbene complexation with *N*-donors is well known,[72] particularly the

complexation with pyridine.[73] The complexation of CCl_2 with pyridine in cyclohexane

solution at ambient temperature proceeds at the diffusion controlled rate.[74]

1.4.2. Insertion into the OH bonds of alcohols and carboxylic acids

The insertion of germylenes into the OH bond of alcohols (eq 1.15) is often employed to trap transient germylenes allowing their presence in the reaction to be inferred.[25, 40, 75] Ando *et al.* detected complexes between diarylgermylenes and aliphatic alcohols in low temperature matrixes by UV-vis spectroscopy (*vide supra*).[49] In one experiment examining the complexation of $GePh_2$ with ethanol, the corresponding ethoxygermane was isolated upon warming of the matrix, and the intermediacy of the complex in the mechanism was proposed. Kinetic studies for the reactions of transient germylenes ($GeMe_2$, $GePh_2$, and $GeMes_2$) with alcohols (MeOH, *t*-BuOH) were carried out in hexanes at ambient temperature.[58] In each case complexation between the germylene and the alcohol was found to be reversible (K_{eq} = 300-23,000 M^{-1}) and the corresponding complexes could be detected as distinct transients in equilibrium with the free germylene. The kinetic data are consistent with forward rate constants for the approach to equilibrium of $k_{1\,(MeOH)} > 4 \times 10^9\,M^{-1}s^{-1}$ in all cases, followed by a slow proton transfer (see eq 1.15). The rate constant for the unimolecular decay of the $GePh_2$-MeOH complex was estimated at $\leq 10^4\,s^{-1}$, suggesting the product forming step may be susceptible to catalysis by a second molecule of methanol.[58]

$$GeR_2 \ + \ MeOH \ \underset{k_{-1}}{\overset{k_1}{\rightleftharpoons}} \ R_2Ge \leftarrow O\overset{CH_3}{\underset{H}{\diagup}} \ \overset{k_2}{\longrightarrow} \ \overset{OMe}{\underset{R_2GeH}{|}} \qquad (1.15)$$
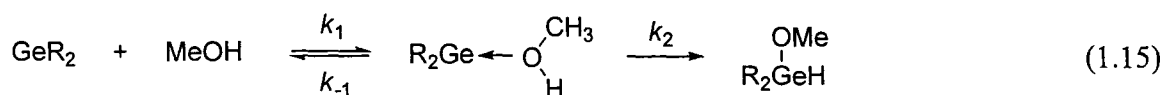
Insertion of germylenes into the OH bonds of carboxylic acids (eq 1.16) has also been studied, but less is known about the mechanism. Neumann and co-workers identified the products of the reactions of $GeMe_2$ with cyclohexanecarboxylic acid and benzoic acid and found that the more acidic substrate leads to a more stable product (*i.e.* the equilibrium constant is larger and the product is favoured).[76] Rate constants for the reactions of $GeMe_2$, GeMePh, $GePh_2$, and $GeMes_2$ with acetic acid have been measured in hexanes solution at 25 °C and are in the range of $k_{HOAc} \approx 1-8 \times 10^9 \ M^{-1}s^{-1}$ in the order $GeMes_2 < GePh_2 < GeMePh < GeMe_2$.[34, 57-59] Unlike with methanol, a complex between the germylene and the acid could not be detected and there was no indication of reversibility.

$$GeR_2 \quad + \quad MeCO_2H \quad \xrightarrow{k_{HOAc}} \quad R_2\overset{O-\overset{\displaystyle O}{\diagdown}}{\underset{H}{Ge}} \qquad\qquad (1.16)$$
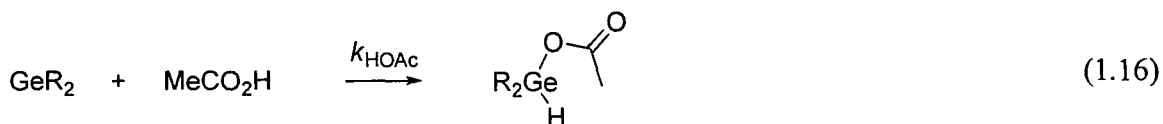
$SiPh_2$ reacts more rapidly than $GePh_2$ with both MeOH and HOAc ($k_Q = 1.3 \times 10^{10} \ M^{-1}s^{-1}$ and $1.0 \times 10^{10} \ M^{-1}s^{-1}$, respectively).[67, 77] The $SiPh_2$-MeOH complex is much shorter lived ($\tau = 0.04 \ \mu s$; recorded in the presence of 0.15 mM MeOH) than the $GePh_2$-MeOH complex ($\tau = 10 \ \mu s$; recorded in the presence of 5.0 mM MeOH), a difference that again can be rationalized by the stronger Si-O bond. No evidence could be obtained for the formation of an intermediate complex between $SiPh_2$ and HOAc.

Rate constants for the reactions of carbene 7 with MeOH and HOAc are both $k_Q \approx 3 \times 10^9 \ M^{-1}s^{-1}$ in isooctane at 20 °C ($k_{diff} = 1.3 \times 10^{10} \ M^{-1}s^{-1}$).[78, 79] No evidence for a transient intermediate that might be assigned to the corresponding carbene complex could

be obtained in either case.

1.4.3. Insertion into the NH bonds of amines and amides

Germylene insertion into the NH bond of amines and amides is known, although the products are not stable.[34, 76] Compounds containing the GeH moiety are more acidic than the corresponding CH compounds,[80] and this higher acidity likely contributes to the instability of the compounds. Decomposition would be especially problematic in the presence of any free amine and even the germylene/NH insertion product contains a basic site. The reactions of $GeMe_2$, $GeMePh$, and $GePh_2$ with n-butylamine (for example) have been studied in hexanes solution and the rate constants are all close to the diffusion limit in hexanes at 25 °C ($k_{BuNH2} = 1.0\text{-}1.3 \times 10^{10}$ $M^{-1}s^{-1}$).[38, 57, 59]

Gu and Weber have shown that $SiMe_2$ undergoes insertion into the NH bond of primary and secondary amines in solution.[81] There does not appear to be any kinetic data on the reaction of silylenes with amines in solution, although gas phase kinetic studies of the reactions of SiH_2 with NH_3 and $HNMe_2$ have been reported, but the authors were unable to reach a conclusion on the involvement of a Lewis acid-base complex between the silylenes and the amine.[82, 83] The reaction of CCl_2 with tertiary amines leads primarily to CH insertion, while NH insertion has been observed with other amines.[84] The rate constant for the reaction of (p-chlorophenyl)chlorocarbene with $HNEt_2$, which yields the corresponding NH insertion product, is $k = 2 \times 10^9$ $M^{-1}s^{-1}$ at 27 °C in isooctane.[85]

1.4.4. Halogen atom abstraction from CCl$_4$ and other halocarbons

The reaction of metallylenes with halocarbons, particularly carbon tetrachloride, has been extensively studied over the past few decades.[44, 62, 86-93] The mechanism has been shown to involve radical intermediates prior to the formation of the final product, which (formally) involves abstraction of two chlorine atoms from CCl$_4$ by the germylene (eq 1.17).

$$GeMe_2 \ + \ CCl_4 \longrightarrow Me_2Ge\begin{smallmatrix}Cl\\ \\Cl\end{smallmatrix} \qquad (1.17)$$

Two products are often observed in the reaction of metallylenes with halocarbons: those resulting from formal insertion of the metallylene (MR$_2$) into the R'-X bond (R$_2$R'MX, **8**) and/or those resulting from the formal abstraction of two halogen atoms from R'-X (R$_2$MX$_2$, **9**). *A priori*, these might be considered to be derived from a common radical pair intermediate (**10**), the primary product of reaction of the metallylene and halocarbon (eq 1.18), in which case the product yields should depend on the relative magnitudes of the rate constants for cage recombination (k_R) and cage escape (k_E). The ratio k_R/k_E should be proportional to solvent viscosity, while the ratio [**8**]/[**9**] should depend on k_R, k_E and k_{abs}[R'X].

$$
\begin{array}{l}
MR_2 + R'X \xrightarrow{k_1} \overline{R_2M\overset{\bullet}{X} \quad \overset{\bullet}{R'}} \xrightarrow{k_R} R_2R'MX \\
\phantom{MR_2 + R'X \xrightarrow{k_1}} \mathbf{10} \mathbf{8} \\
\phantom{MR_2 + R'X \xrightarrow{k_1}} \Big\downarrow k_E \\
\overset{\bullet}{R'} + R_2MX_2 \xleftarrow{k_{abs}[R'X]} R_2M\overset{\bullet}{X} + \overset{\bullet}{R'} \longrightarrow \textit{other radical products} \\
 \mathbf{9}
\end{array}
\qquad (1.18)
$$

The nature of the halocarbon affects the product ratio. For example, scavenging

of GeMe$_2$ with CCl$_4$ gives **9** (R = Me, X = Cl) as the only detectable product. When

benzyl bromide is employed as a GeMe$_2$ scavenger both **8** and **9** are isolated (R = Me, R'

= CH$_2$Ph, X = Br) but with allyl bromide only **8** is detected (R = Me, R' = CHCH$_2$, X =

Br).[62] Furthermore CIDNP* effects also vary; for example, CCl$_4$ shows evidence of

radical intermediates whereas allyl halides do not. It has been proposed that these

variations ultimately arise from differences in the reduction potentials of the halocarbons,

and that the halocarbons with the highest reduction potential undergo the most rapid

reaction, ultimately leading to the formation of the dichlorogermane.[94] Relative to other

halocarbons, CCl$_4$ represents an extreme in the reactivity (*i.e.* consecutive halogen atom

abstraction dominates while C-X insertion does not.) It has been noted that CCl$_4$ is one

of the most efficient electron transfer oxidants because of its high reduction potential.[95, 96]

Consider the reaction between GeMe$_2$ and CCl$_4$, which yields Me$_2$GeCl$_2$ and

C$_2$Cl$_6$ as the major products.[97] CIDNP effects led to a proposed mechanism involving the

intermediacy of a caged singlet radical pair (**11**),[62] the dominant fate of which is cage

escape. Alternative mechanisms have also been proposed. For example, Tomoda *et al.*

have suggested that the reaction of GeMe$_2$ with CCl$_4$ yields **12**, which

then thermally decomposes to give Me$_2$GeCl$_2$.[87] Analogous

suggestions have been made by Mochida *et al.* for the reaction of

GePh$_2$ with CCl$_4$.[89, 98] Egorov *et al.* isolated **12** and found it to be

$$\left[\overset{\textstyle\cdot}{Me_2GeCl} \quad \overset{\textstyle\cdot}{CCl_3} \right]^1$$

11

$$Me_2Ge\overset{\displaystyle CCl_3}{\underset{\displaystyle Cl}{\Big\langle}}$$

12

---
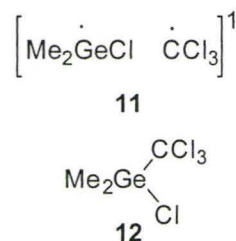
* Chemically Induced Dynamic Nuclear Polarization – changes in the intensity of the NMR signal(s) of a molecule
caused by the immediate precursor to that molecule possessing an unpaired electron. See Kaptein, R. *Adv. Free
Radical Chem.* **1975**, *5*, 319.

thermally and photochemically stable[99] so the intermediacy of **12** in the reaction of GeMe$_2$ with CCl$_4$ seems unlikely.

The reactions of GeMe$_2$, GeMePh, and GePh$_2$ with CCl$_4$ in hexanes solution occur relatively slowly compared to those with other scavengers ($k_{CCl4} \approx 10^7$ M^{-1}s^{-1}).[38, 57, 59] Rate constants for the reactions of GePh$_2$ with other halocarbons (CHCl$_3$, C$_2$Cl$_6$, C$_5$H$_{11}$Br) were all lower than that with CCl$_4$; the reasons for these differences are not yet clear as there does not appear to be a correlation of the rate constant with the reduction potential of the halocarbon.[57]

The rate constant for the reaction of SiPh$_2$ with CCl$_4$ is $k_{CCl4} = 10^9$ M^{-1}s^{-1}, approximately 100 times faster than the reaction of GePh$_2$ with CCl$_4$. Typical SiCl and GeCl bond strengths are *ca.* 97 and 81 kcal/mol, respectively, a difference of 16 kcal/mol.[68] However, typical SiO and GeO bond strengths are *ca.* 106 and 85 kcal/mol,[68] respectively (a difference of 21 kcal/mol) and the rate constants for the reaction of SiPh$_2$ and GePh$_2$ with methanol are both diffusion controlled. Thus clearly other factors besides bond strength play a role in the reaction of SiPh$_2$ and GePh$_2$ with CCl$_4$.

Platz and co-workers have examined the kinetics of the reaction of **7** with CCl$_4$ and other halocarbons in detail.[100] The ground state of **7** is the singlet and their proposed mechanism begins with halogen-bonding coordination[101] of the carbene lone pair and the chlorine (see eq 1.19). To reduce the subsequent electron-electron repulsion, the carbene crosses to the excited (open shell) singlet state surface from which chlorine atom abstraction completes the reaction.

$$\text{PhClC} \cdots \longrightarrow \text{Cl-CCl}_3 \longrightarrow \text{PhClC} \quad \text{Cl-CCl}_3 \longrightarrow \text{PhCCl}_2 + \overset{\cdot}{\text{C}}\text{Cl}_3 \qquad (1.19)$$

7
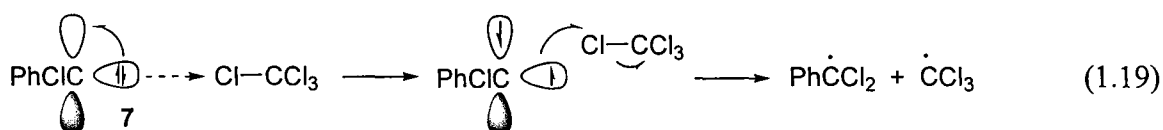
1.4.5. (1+2) Cycloadditions with alkenes

Considering the importance of the reaction of carbenes with alkenes to yield cyclopropanes,[6, 18, 69, 84, 102] it is not surprising that there is considerable interest in the corresponding reactions of silylenes and germylenes. Singlet carbenes add in a concerted, stereospecific manner to the alkene, whereas triplet carbenes add in a stepwise, non-stereospecific manner to the alkene. There have been a number of studies aimed at further understanding the mechanism of the reaction of singlet carbenes with alkenes.[103-110] The intermediacy of a π-complex (eq 1.20) has been proposed[105] and this has been supported by theoretical calculations for certain carbenes.[111, 112]

$$\overset{R}{\underset{R}{>}}: + \quad \rightleftharpoons \quad \overset{R}{\underset{R}{>}} \quad \longrightarrow \quad \overset{R}{\underset{R}{>}} \qquad (1.20)$$
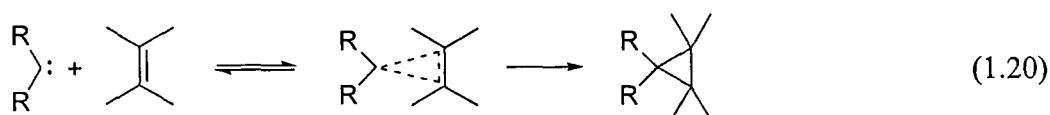
Like singlet carbenes, silylenes and germylenes undergo (1+2)-cycloadditions to yield the corresponding three-membered rings known as *metallianes* (**13**)(eq 1.21).[25, 65, 113] Metallianes are often thermally unstable[57, 114-117] because of the higher DSSE of the metallylene (relative to methylene), coupled with the higher ring strain of the metallirane (relative to cyclopropane).[116] While there are numerous examples of stable siliranes,[118-

17

[120] there are only three known examples of stable germiranes (**14-16**).[121, 122]

$$MR_2 + H_2C=CH_2 \longrightarrow \underset{\triangle}{\overset{R_2}{M}} \quad \mathbf{13} \tag{1.21}$$

14   **15**   **16**
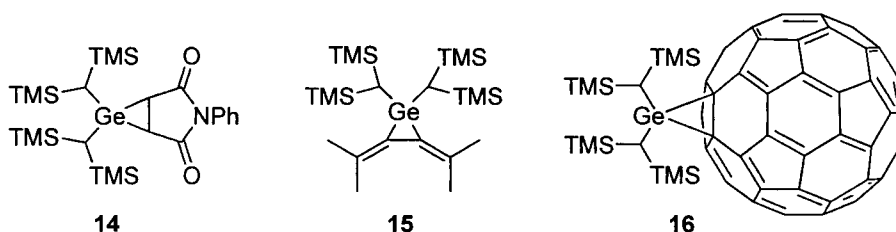
The reaction of SiPh$_2$ with 4,4-dimethylpent-1-ene

(DMP) proceeds with a rate constant of $k_{DMP} = 7.9 \times 10^9$ M^{-1}s^{-1}

17, M = Si
18, M = Ge
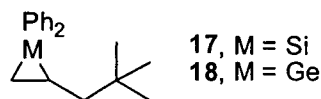
and leads to a species ($\lambda_{max} = 280$ nm) which does not decay over the maximum time

window of the experiment (ca. 1 s) and is therefore assigned to the corresponding silirane

17.[67] The reaction of DMP with GePh$_2$ proceeds with a similar rate constant ($k_{DMP} = (4.2$

$\pm 0.2) \times 10^9$ M^{-1}s^{-1}) yet the reaction is reversible on the microsecond timescale ($K_{eq} =$

2500 ± 600 M^{-1}), yielding a transient ($\lambda_{max} = 280$ nm) that decays with a lifetime of $\tau \approx$

1.5 ms.[57] Consistent with expectations based on the differences in DSSE, both the

reversibility and the shorter lifetime of the germylene-derived product compared to that

from the silylene support the assignment of the 280 nm species to the corresponding

germirane **18**.

1.4.6. (1+4) Cycloadditions with 1,3-dienes

Reactions of carbenes with 1,3-dienes has been examined and both (1+2) and

(1+4)-cycloadditions are possible.[123] The latter product has been detected only when the

diene is constrained in the *s*-cis conformation (eq 1.22) and the yields are low.[124-126] Both

pathways are symmetry allowed but the (1+2) addition is thought to be favoured because

there is less repulsion between the carbene lone pair and the diene π electrons (Figure

1.3).[127]

(2+1) product
89%

(4+1) product
11%

(1.22)
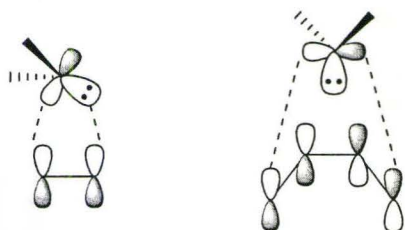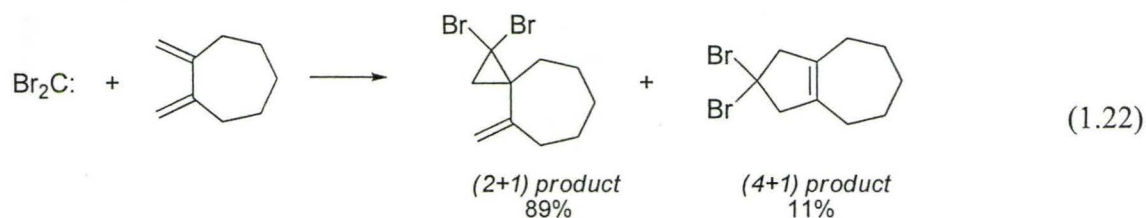
Figure 1.3. Symmetry allowed approach of the (1+2) [*left*] and (1+4) [*right*] addition of singlet methylene to 1,3-butadiene.[127]

Silylenes and germylenes react with 1,3-dienes to yields the formal (1+4)

cycloadduct (eq 1.23, **19**) as the major product, the former only when the silylenes are

generated via thermolysis.[25, 65] Unlike with carbenes, it is not necessary for the diene to

be constrained *s*-cis. The silacyclopentenes (**19**, M = Si) derived from silylenes and

dienes have random stereochemistry and it has been proposed that this randomization is

caused by a rearrangement of **20** to **19**, as shown in eq 1.24.[128-130] Direct (1+4) reactions

of silylenes with dienes[131] were generally thought to be a relatively minor pathway but

Tokitoh and co-workers have studied one system where the pathways are mutually

exclusive.[120] On the other hand, the reaction of germylenes with dienes yields **19**

stereospecifically which lends more support to the direct (1+4) mechanism.[132-134]

MR$_2$ + [allene structure] ⟶ R$_2$M[cyclopentene] **19**   (1.23)

MR$_2$ + [allene structure] ⟶ [R$_2$M bracketed structure] **20** $\xrightarrow{\Delta}$ R$_2$M[cyclopentene] **19**   (1.24)
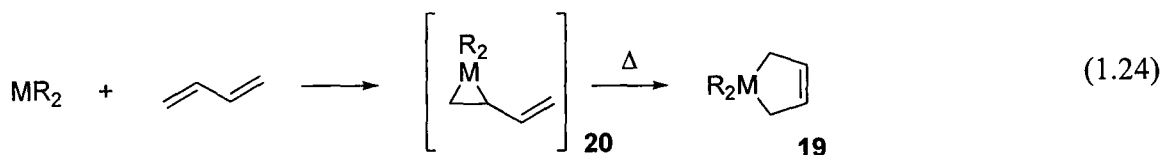
The rate constants for the reactions of SiMe$_2$ and SiPh$_2$ with isoprene and 2,3-dimethyl-1,3-butadiene (DMB) approach the diffusion limit in hexanes (k = 1.3-2.0 × 10^{10} M^{-1}s^{-1}).[67, 135] In each case a UV absorbing species assigned to the vinylsilirane was detected by flash photolysis (λ_{max} = 280 nm) and did not decay during the maximum time window of the experiment (~ 0.9 s).[67] In fact, the vinylsilirane derived from SiPh$_2$ and DMB (**21**) has been detected by ^{1}H NMR spectroscopy and was shown to isomerize to **22** in the dark over 48 hrs (eq 1.25).[67]

[structure] **21** $\xrightarrow{\tau < 48 \text{ hrs}}$ Ph$_2$Si[structure] **22**   (1.25)
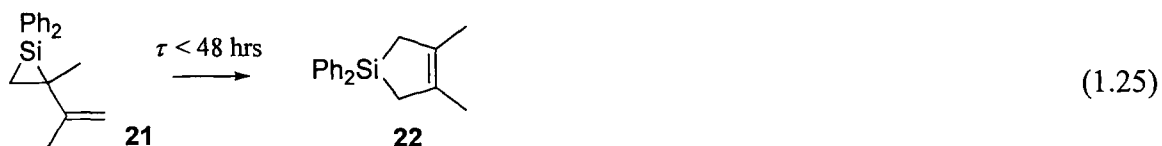
The reactions of GeMe$_2$,[38] GeMePh,[59] and GePh$_2$[57] with isoprene and DMB have been examined. With isoprene, the corresponding germacyclopentene is the major product observed in steady state photolysis experiments (eq 1.26, **23**). The absolute rate constants are about two times lower than the analogous reactions with silylenes (k_{diene} = 5-10 × 10^9 M^{-1} s^{-1}). The major difference in the case of germylenes compared to silylenes comes in the ability to detect an equilibrium between the free germylene and the vinylgermirane, particularly with GePh$_2$ (*e.g.* for GePh$_2$ + isoprene: K_{eq} ≈ 6000 M^{-1} in

hexanes at 25 °C).[57] The vinylgermirane (**24**, Ar = Ph) can be detected by flash

photolysis (λ_{max} = 290 nm) and decays over several hundred microseconds.[57] Again, the

ability to detect reversibility in the case of germanium and the fact that **24** has a shorter

lifetime than **21** is consistent with the greater DSSE of germylenes compared with

silylenes.

$$\text{GeAr}_2 \;+\; \underset{}{\text{}} \;\;\underset{k_{-1}}{\overset{k_1}{\rightleftharpoons}}\;\; \underset{\textbf{24}}{\overset{\text{Ar}_2\text{Ge}}{\triangle}} \;\longrightarrow\; \underset{\textbf{23}}{\text{Ar}_2\text{Ge}} \qquad (1.26)$$
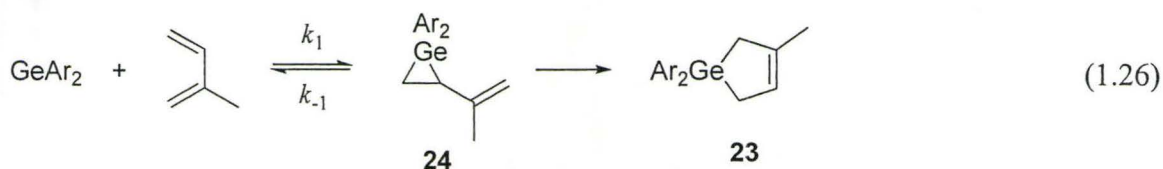
Only one study examining electronic factors on the reaction of germylenes and

dienes has been reported.[134] Dimethylgermylene was generated in the presence of a series

of 1,4-substituted-*E,E*-1,3-dienes and the composition of the resulting product mixtures

were determined (see eq 1.27 and Table 1.5). The products were formed

stereospecifically which led to the proposal of a concerted mechanism. Furthermore, a

positive correlation was noted between the yield of **25** and the resonance electron-

withdrawing ability of the diene substituents, leading to the conclusion that the germylene

plays the role of a nucleophile in the reaction with the diene (Figure 1.4).

$$\text{GeMe}_2 \;+\; R\text{—}\diagup\diagdown\text{—}R \;\;\xrightarrow{70\,°C}\;\; \underset{\textbf{25}}{\overset{R\diagup\underset{\text{Me}_2}{\text{Ge}}\diagdown R}{}} \;+\; \underset{\textbf{26}}{(\text{GeMe}_2)_n} \qquad (1.27)$$
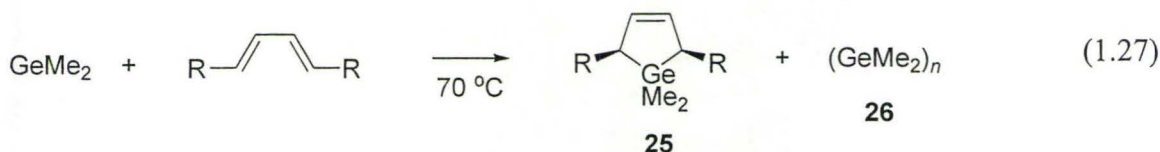
Table 1.5. Relative product yields from the reaction shown in eq 1.27.[134]

R	R [a]	% 25	% 26
NHCO$_2$Et	-0.38	0	100
OCOMe	-0.11	0	100
Ph	-0.13	10	90
CO$_2$Me	+0.11	70	30
CN	+0.15	90	10

a. R is the resonance substituent constant, which will be discussed below; however, a more positive value of *R* implies a stronger resonance acceptor. Values obtained from reference 136.
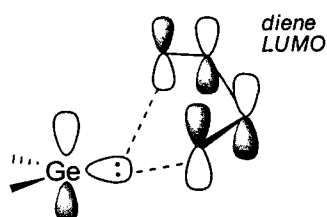
Figure 1.4. "Inverse" chelotropic transition state proposed by Köcher and Neumann for the reaction of germylenes with dienes.[134]

Several groups have investigated the reaction of silylenes and germylenes with alkenes and dienes via computational methods and it is suggested that a Lewis acid-base complex between the π-bond and the metallylene ("π-complex") is a minimum on the potential energy surface prior to the formation of **27**.[117, 131, 137-141] Nag & Gaspar reported a detailed computational study on the reactions of silylenes and germylenes with 1,3-dienes, which suggested that the direct (1+4) cycloaddition of metallylenes to dienes to give **20** is favoured over rearrangement of **27** (eq 1.28).[141]

(1.28)
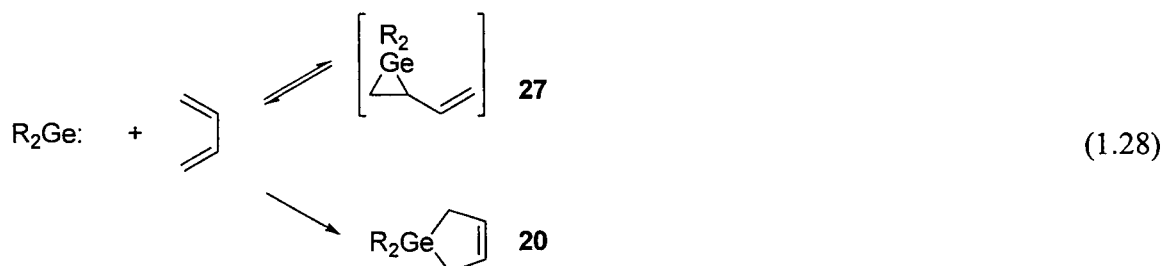
1.5. Digermenes – Structure and Synthesis

1.5.1. Geometry

Despite their formal analogy with alkenes, digermenes have little in common with the lightest doubly bonded species in Group 14. Consider first the geometry: the substituents of an alkene and the two carbons of the C=C bond lie in the same plane. Most higher dimetallenes, however, adopt what is known as a *trans bent* geometry.[3, 142-147] The distortion from planarity is most readily rationalized in terms of the donor-acceptor bonding model first proposed by Lappert,[148] where dimetallenes are viewed as metallylene dimers (see Figure 1.5). It has been suggested that a greater degree of *trans*-bending will be observed in dimetallenes derived from metallylenes with a more stable singlet ground state relative to the triplet (*i.e.* a larger ΔE_{ST}).[149]
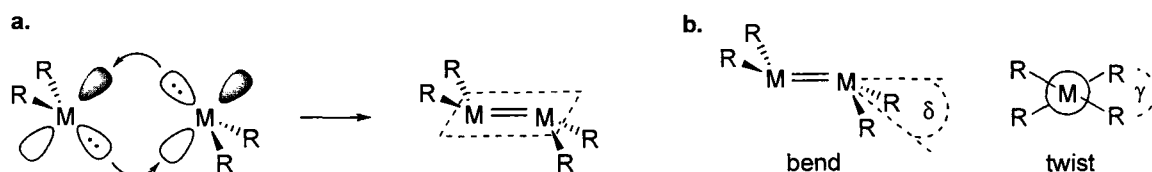
Figure 1.5. (a) The di-metallylene donor-acceptor model to explain the *trans bent* structure of dimetallenes. The dotted box outlines the plane of the M=M bond. (b) Bend and twist angles of dimetallenes, viewed down the M=M bond. The M=M plane bisects the R-M-R angle.

The molecular orbital view of dimetallenes considers π and σ^* orbitals (see Figure 1.6).[150] As the size of the metal increases down Group 14, the orbital size increases and the bonding orbitals become more diffuse. This reduces the electron density between the atoms, weakening the π bond and raising the energy of the π orbital. In addition the anti-

bonding character of the σ* orbital is decreased, thus lowering its energy. As $\Delta E_{\pi\text{-}\sigma^*}$

becomes smaller, a bending mode causes mixing of the π and σ* orbitals resulting in

pyramidalization at the metal center (a *pseudo*-Jahn-Teller distortion[151]). Consequently,

molecules displaying a high degree of trans-bending have electron density centered at the

metal atoms rather than between them.
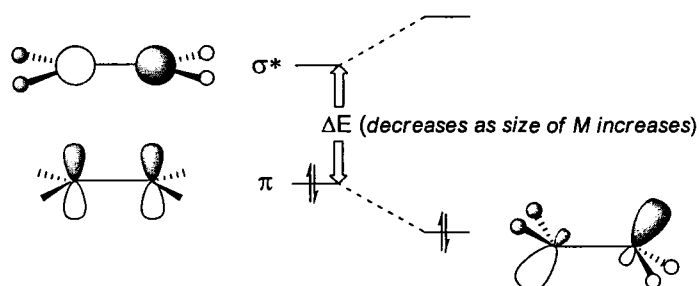
Figure 1.6. Pictorial representation of the *trans* bending of planar M_2H_4, caused by mixing of the π and σ* orbitals. Adapted from reference 150.

Substituents on the metal atoms also affect the amount of *trans* bending.[152] A

survey of the geometries of various digermenes shows that if the atom directly attached to

the germanium is silicon (Si is less electronegative than Ge)[153], a near-planar geometry

can result because more electron density remains between the M atoms and the π-bond is

stronger (*e.g.* R = SiMe^{i}Pr$_2$ δ = 0°, γ = 6°)[154]. On the other hand, those where the atom

directly bonded to the germanium is a carbon (C is more electronegative than Ge)[153],

display a greater degree of trans bending (*e.g.* R = CH(SiMe$_3$)$_2$ δ = 32°, γ = 0°).[155] Based

on a survey of the structural parameters of various tetra(alkyl substituted-aryl)digermenes,

there does not appear to be a correlation between the size of the substituent and the

degree of *trans*-bending.[156-159]

The calculated π-bond strengths of dimetallenes decrease down Group 14.[3, 12, 145]

The bond strength of a dimetallene is related to the DSSE of the metallylene in that the more stable the metallylene, the weaker the M=M bond. The weakest double bonds are the Sn=Sn double bonds – most known "stable" distannenes dissociate to stannylenes in solution.[3] The rotational barrier of the M=M bond is the simplest way of estimating the strength of the π-bond (D_π) while the M=M bond dissociation energy ($D_{M=M}$) is also an important parameter.[160] Calculated values of D_π and $D_{M=M}$ for the simplest dimetallenes $H_2M=MH_2$ are listed in Table 1.6.

Table 1.6. Calculated values of D_π and $D_{M=M}$ for $H_2M=MH_2$ (M = C, Si, Ge, Sn).[a]

	D_π	$D_{M=M}$
C	65[b]	173[c]
Si	25[d]	52.0[e]
Ge	25[d]	36.9[e]
Sn	20[f]	30.9[g]

a. Units: kcal/mol. b. MCSCF/6-31G(d); reference 161. c. experimental 298 K; reference 162. d. RHF-TCSCF DZP; reference 160. e. CCSD DZP//RHF-TCSCF DZP; reference 160. f. MCSCF/3-21(d); reference 163. g. PW91/TZDP; reference 164.

1.5.2. Synthesis

Digermenes may be formed indirectly through the dimerization of metallylenes[34, 165, 166] (eq 1.29) or directly by photolysis/thermolysis of cyclotrimetallanes (eq 1.30)[159, 167, 168] or digermanorbornadienes (eq 1.31).[169]

$$2\ R_2Ge \longrightarrow R_2Ge=GeR_2 \tag{1.29}$$

$$\begin{array}{c} R_2 \\ Ge \\ R_2Ge-GeR_2 \end{array} \xrightarrow[\text{or } \Delta]{h\nu} \quad R_2Ge \ + \ R_2Ge=GeR_2 \tag{1.30}$$

$$(1.31)$$
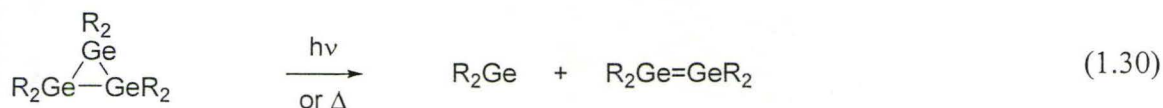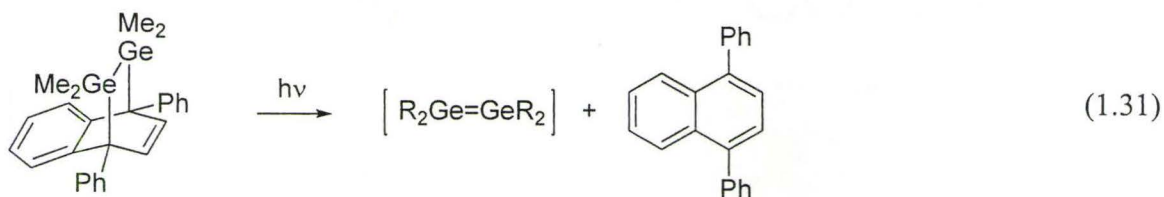
1.6. Digermenes – Reactivity

Digermenes and other dimetallenes are considerably more reactive than alkenes. Like germylenes, they are transient in nature, although there are many examples of stable digermenes resulting from the protection afforded by sterically bulky R groups.[165, 170] In the absence of a scavenger, sterically unencumbered digermenes undergo dimerization to a four membered ring (eq 1.32), and further oligomerization depending on the nature of the R group.[167]

$$(1.32)$$

The chemistry of digermenes has been outlined in several reviews.[20, 166, 170] The following section provides background information on some of the digermene reactions relevant to the work presented in this thesis.

1.6.1. Addition of the OH bond of alcohols, acetic acid and water.

Addition of the OH bonds of alcohols across the Ge=Ge bond of digermenes is well known (eq 1.33).[20, 170] The reactions of Ge_2R_4 (R = Me or Ph) with MeOH in hexanes proceed with rate constants $k = 1.9 \times 10^7$ $M^{-1}s^{-1}$ (R = Ph) and $k = 2.7 \times 10^6$ $M^{-1}s^{-1}$ (R = Me).[58] Rate determining nucleophilic attack by the oxygen at germanium is

proposed. Indeed, DFT calculations predict that the latter digermene has the higher energy LUMO, and should therefore be less reactive in a reaction where the initial step is nucleophilic attack at germanium.[38]

$$R_2Ge=GeR_2 \quad \xrightarrow{MeOH} \quad \overset{H}{\underset{|}{R_2Ge}}-\overset{OMe}{\underset{|}{GeR_2}} \qquad\qquad (1.33)$$

The OH addition of carboxylic acids are also known (*e.g.* see eq 1.34).[34, 159] Rate constants for the reactions of Ge_2Ph_4 and Ge_2Me_4 with acetic acid in hexanes are $k_{HOAc} <$ 4×10^7 $M^{-1}s^{-1}$ (R = Ph) and $k_{HOAc} = 2.8 \times 10^8$ $M^{-1}s^{-1}$ (R = Me). In this case, the methylated digermene reacts faster than the phenylated digermene, suggesting different mechanisms operate, possibly rate determining protonation by the acid.[58]

$$Mes_2Ge=GeMes_2 \quad \xrightarrow{HOAc} \quad \overset{H}{\underset{|}{Mes_2Ge}}-\overset{OAc}{\underset{|}{GeMes_2}} \qquad\qquad (1.34)$$
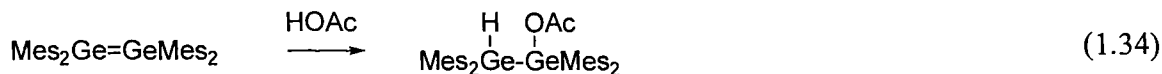
Baines and co-workers have reported the OH addition of water across the Ge=Ge bond of tetramesityldigermene, as shown in eq 1.35.[28] No kinetic information on this reaction has been reported.

$$Mes_2Ge=GeMes_2 \quad \xrightarrow{H_2O} \quad \overset{H}{\underset{|}{Mes_2Ge}}-\overset{OH}{\underset{|}{GeMes_2}} \qquad\qquad (1.35)$$
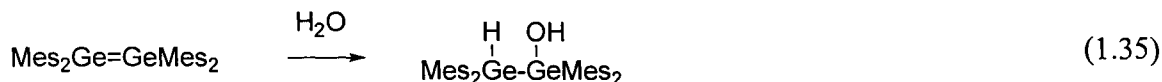
1.6.2. Addition of primary and secondary amines.

No conclusive evidence based on product studies that digermenes react with primary or secondary amines has yet been reported, [170] although laser flash photolysis experiments clearly show a reaction between Ge_2Ph_4 and Ge_2Me_4 with amines such as

H_2N^nBu (eq 1.36).[34, 58] The reactions of Ge_2R_4 with nBuNH$_2$ in hexanes proceeds with

$k_{R=Ph} = 4 \times 10^9$ M^{-1}s^{-1} and $k_{R=Me} = 5 \times 10^7$ M^{-1}s^{-1}.[34, 58] The difference in reactivity

parallels that described for alcohols (*i.e.* $k_{Ge2Ph4} > k_{Ge2Me4}$), suggesting that nucleophilic

attack by the amine at germanium is the initial step.

$$R_2Ge=GeR_2 \xrightarrow{H_2NR} \overset{\overset{H}{|}}{R_2Ge}-\overset{\overset{N(H)R}{|}}{GeR_2} \; ? \tag{1.36}$$
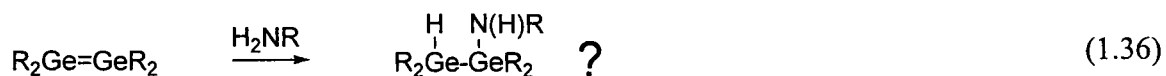
The NH addition of NH$_3$ to a conjugated disilene has been reported in one

instance.[171] No kinetic studies on the reactions of disilenes with amines have yet been

reported.

1.6.3. Reaction with halocarbons

Kira and co-workers carried out a detailed experimental and theoretical study of

the reaction of kinetically stable tetrasilyldisilenes (*e.g.* **28**) with CCl$_4$, CHCl$_3$, and

CH$_2$Cl$_2$ in hexane.[172] Two products were formed (**29** and **30**) in relative yields that varied

with the halocarbon. With CCl$_4$ as the disilene scavenger, only **29** was detected whereas

with CH$_2$Cl$_2$, only **30** (R' = CH$_2$Cl) was detected. With CHCl$_3$, both **29** and **30** (R' =

CHCl$_2$) were found. The yield of **29** relative to **30** increases with the rate constants for

chlorine atom abstraction from the halocarbons by silyl radicals.[172, 173] Mechanistic

details of these reactions were further probed by measuring activation parameters,

monitoring the reaction using electron paramagnetic resonance spectroscopy, and by

determining the reduction potential of the disilenes via cyclic voltammetry.

Computations were also used to examine the reaction. It was concluded that the

mechanism for disilene reaction first involves chlorine atom abstraction by the disilene to

generate the corresponding halodisilanyl and R′ radicals (eq 1.37).[172]

$$
R_2Si{=}SiR_2 \xrightarrow{R'Cl}
\left[
\begin{array}{c}
\underset{\overset{|}{\underset{\bullet}{}}}{R}\ \overset{R}{\underset{|}{\ }} \\
R{-}\underset{\overset{|}{\bullet}}{Si}{-}\underset{\overset{|}{Cl}}{Si}{-}R \ + \ {\cdot}R'
\end{array}
\right]
\begin{array}{c}
\xrightarrow{\text{escape}\ [R'Cl]} \\
\xrightarrow{\text{recombination}}
\end{array}
\begin{array}{c}
R{-}Si{-}Si{-}R \ \ \mathbf{29} \\
R{-}Si{-}Si{-}R \ \ \mathbf{30}
\end{array}
\qquad (1.37)
$$

28, R = t-BuMe₂Si
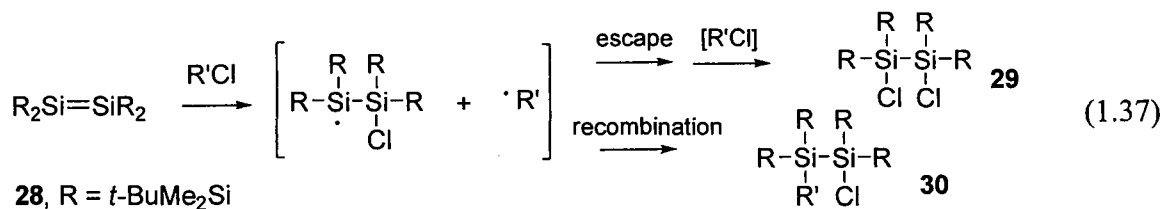
Mochida *et al.* have reported the major product of the reaction of $Me_2Ge{=}GeMe_2$

with CCl_4 to be the corresponding 1,2-dichlorodigermane (**31**, 71% yield by NMR),[169]

while Baines and co-workers found the major product of the reaction of the

$Mes_2Ge{=}GeMes_2$ with $CHCl_3$ to be **32** (25% isolated yield).[174] The reactions of

digermenes with halocarbons thus seems to parallel that of disilenes, which is reasonable

given that rate constants for chlorine atom abstraction by Group 14 radicals follow the

same trend with respect to the variation in the rate constant with R (in R-X).[175-177] As

noted in the case of the reaction of metallylenes with halocarbons, CCl_4 represents an

extreme in the reactivity, with double X abstraction favoured over X-C addition.

$$
\begin{array}{cc}
\underset{\overset{|}{Cl}}{Me}\ \ \underset{\overset{|}{Cl}}{Me} & \underset{\overset{|}{Cl}}{Mes}\ \ \underset{\overset{|}{CHCl_2}}{Mes} \\
Me{-}Ge{-}Ge{-}Me\ \ \mathbf{31} & Mes{-}Ge{-}Ge{-}Mes\ \ \mathbf{32}
\end{array}
$$

The reactions of Ge_2R_4 with CCl_4 in hexanes proceed with rate constants $k_{R=Ph} = 2$

$\times\ 10^6\ M^{-1}s^{-1}$ [57] and $k_{R=Me} = 2 \times 10^7\ M^{-1}s^{-1}$.[58] The reduced steric bulk at germanium in

Ge_2Me_4 relative to Ge_2Ph_4 likely enhances reactivity. Detailed product studies on these

reactions have not been carried out.

1.7. Applications of Germylene and Digermene Chemistry

Metallylenes, particularly SiH_2 and GeH_2, are important intermediates in the chemical vapour deposition process used in the manufacture of electronics.[178-181] Stable silylenes and germylene are involved in various organic reactions including C-H activation,[92] and Suzuki-type C-C bond forming reactions,[182] and have also been utilized to initiate the polymerization of a number of different organic compounds such as heterocycles,[183] alkenes,[184] alkynes and quinones.[185] Metallylenes are useful synthons in the preparation of stable organic and organo-Group 14 compounds,[186, 187] some of which show promising biological activity (e.g. anticancer).[188-191]

The starting point for the manufacture of most integrated circuits and memory chips involves the (001) crystal face of silicon and germanium.[192] Not surprisingly, there is interest in learning about the types of reactions these surfaces are expected to undergo. Si and Ge atoms pack in a tetrahedral arrangement and at the (001) surface, the exposed metal atoms have an unpaired electron.[193] These radicals are adjacent to an identical atom so it is often drawn as a double bond between the two atoms (see Figure 1.7).
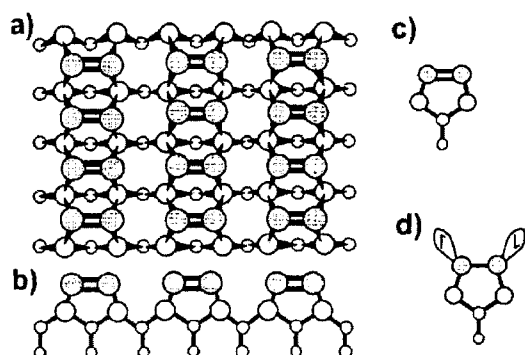
Figure 1.7. Schematic of the Si/Ge(001) surface. (a) Top view. Gray atoms represent M=M dimers in the surface layer. Deeper layers are depicted with smaller circles. (b) Side view. Surface dimers are depicted in gray. (c) Double bond and (d) diradical extremes of the surface M bonding. *(Reprinted from reference 192 with permission. © 2000 American Chemical Society.)*

Disilenes and digermenes have electronic structures loosely analogous to those of

the M=M dimers associated with these surfaces.[194-197] There is thus interest in using dimetallenes as small molecule mimics of the Si(001) and Ge(001) surfaces. While there are differences between the metal surface and a dimetallene in terms of the orientation and nature of the substitutents around the doubly bonded atoms, examination of molecular digermene reactivity nevertheless allows for the possibility to obtain information about surface chemistry.

1.8. Goals and outline of the thesis

For each of the reactions described in Sections 1.4 and 1.6, the major product has been identified and rate constants have been measured for germylenes such as $GeMe_2$, GeMePh, $GePh_2$, and/or $GeMes_2$ and the corresponding digermenes. Many important conclusions have been made from these data. With a more detailed study, the reaction mechanisms can be further addressed. As described by Bunnett:[198]

> "A reaction mechanism is a detailed description of a reacting system as it progresses from reactants to products. It includes identification of all intermediates that are involved, assessment of the characteristics of the transition state through which the reaction progresses, and recognition of the factors that affect reactivity."

The goal of this work is to answer various mechanistic questions pertaining to the reactions of germylenes and digermene discussed above. These questions include:

- Does the reaction of germylenes with acetic acid follow a similar path as that of germylenes and methanol (*i.e.* complexation followed by proton transfer) or does the acid protonate the germylene in the first step?

- Why is the reaction of germylenes with CCl_4, 100 times slower than the corresponding reaction with silylenes? Is an intermediate germylene-halocarbon complex involved in the reaction pathway? Does the digermene follow a similar reaction mechanism to that proposed for disilenes?

- What is the mechanism of the formal (1+2) and (1+4) cycloadditions reactions of germylene and alkenes and dienes? Is a π-complex similar to that proposed for the analogous carbene reactions involved as an intermediate? What is the mechanism for the isomerization of the initially formed (vinylgermirane) product to the thermodynamic (germacyclopentene) product?

Our attempts to answer these questions will rely primarily on detailed kinetic studies. Diarylgermylenes (**Ga-g**) and tetraaryldigermenes (**DGa-g**) will be utilized because substitution of the aromatic rings allows access to information about the electronic demands during the reaction (*vide infra*). Variation of both the rate (k) and equilibrium (K) constants with temperature provide further details, such as activation energies and thermodynamic parameters.

$GeAr_2$ **G**

$Ar_2Ge=GeAr_2$ **DG**

a. Ar = C_6H_5
b. Ar = $3,4\text{-}Me_2C_6H_3$
c. Ar = $4\text{-}MeC_6H_4$
d. Ar = $4\text{-}FC_6H_4$
e. Ar = $3\text{-}FC_6H_4$
f. Ar = $4\text{-}(CF_3)C_6H_4$
g. Ar = $3,3\text{-}(CF_3)_2C_6H_3$
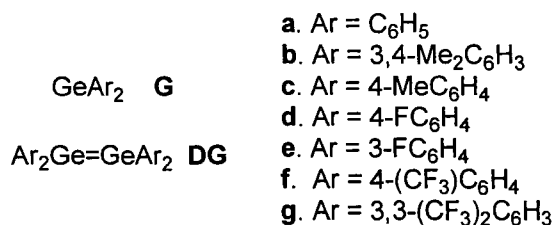
The remainder of Chapter 1 outlines the physical-organic "tools" used in our study of these reactions. Chapter 2 describes the synthesis of the diarylgermylene precursors,

and establishes the validity of using these substituted compounds to determine mechanistic information about germylene reactions. The technique of laser flash photolysis is described and explains how rate and equilibrium constants are obtained from these data.

The reactions of germylenes and digermenes are examined in the remaining chapters. Chapter 3 explores the complexation of $GeAr_2$ with various Lewis bases in hexanes solution such as diethylamine and acetic acid. The chemistry of $GeAr_2$ in coordinating solvents (THF and MeOH), where the reactive species is the corresponding Lewis acid-base complex, is also examined. Chapters 4 and 5 report the study of the reactions of $GeAr_2$ with CCl_4 and isoprene, respectively. These are important scavengers because they represent the two classes of molecules (halocarbons and unsaturated C-C bonds) that react with germylenes to form stable products containing (new) Ge-C bonds. Chapter 6 outlines a computational study of the (1+2) reaction of germylenes with alkenes and dienes. The objective was to determine what factors are likely to be important to the stability of the corresponding germirane. These results complement experimental data being obtained by others in our group. Finally, Chapter 7 describes all of the product and kinetic studies on the reactions of digermenes, with the scavengers acetic acid, diethylamine, and CCl_4.

1.9. Tools in the Analysis of Reaction Mechanisms

1.9.1. Substituent effects on equilibrium and rate constants - the Hammett equation

Knowledge of the changes in electron density distribution during a chemical reaction is important for elucidation of the mechanism. One method to probe this aspect of the reaction is to introduce a slight electronic perturbation into one of the reactants and note how this change affects the rate/equilibrium constants. Such perturbation can be achieved by replacement of a hydrogen atom on the aryl ring adjacent to a reactive site of a molecule with a substituent X such as CH_3, CF_3, or OCH_3. First defined by Louis Hammett in 1937,[199] it was noted that a number of these reactions (with equilibrium constants K_H and K_X) were related according to eq 1.38, where σ is a constant that depends on the ring substituent and its position, while ρ depends on the reaction, solvent and temperature. This structure-reactivity relationship is one of the most famous principles in physical-organic chemistry.

$$\log\left(\frac{K_X}{K_H}\right) = \sigma\rho \tag{1.38}$$

The dissociation of benzoic acid in water at 25°C (eq 1.39) is used to define the σ values (eq 1.38, where $\rho \equiv 1$). The acid dissociation constants of the substituted benzoic acids (K_X – eq 1.40) vary depending on the nature of X. For example, an electron withdrawing substituent such as p-CF_3 stabilizes the negative charge of the benzoate ion,

lowering its energy and thus increasing the acid dissociation constant relative to benzoic

acid. By definition, the σ value for hydrogen (H) substituent is $\sigma = 0$, so the σ value for

p-CF$_3$ is positive because $K_X > K_H$ ($\sigma_{p\text{-CF3}} = +0.54$). These σ values are defined only for

meta and *para* substituents to avoid the complication of steric interactions at the reactive

site from *ortho* substituents. The list of σ_{para} and σ_{meta} values for the substituents

employed in this thesis is given in Table 1.7.

$$K_H = \frac{k_{f\text{-H}}}{k_{r\text{-H}}} \qquad (1.39)$$

$$K_X = \frac{k_{f\text{-X}}}{k_{r\text{-X}}} \qquad (1.40)$$
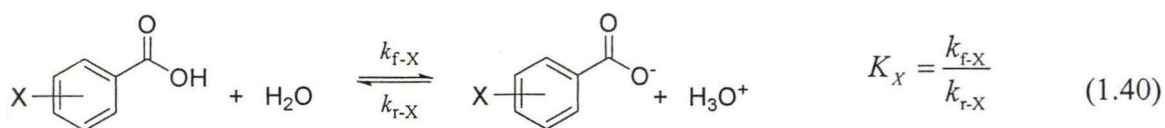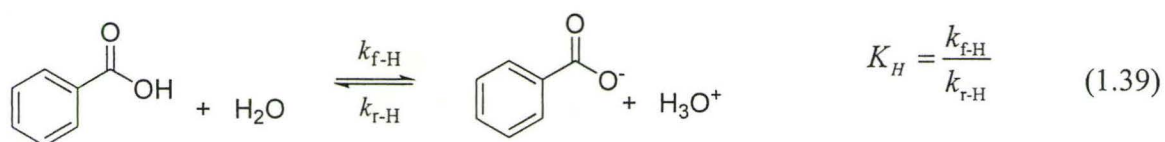
Electronic effects of the substituent can be transmitted through space (field

effects), through the σ-bonds (inductive effects) and via resonance. The separation of

these individual effects have been attempted and some of these values are listed in Table

1.7 where F is a measure of the *inductive* strength of a substituent and R is a measure of

the *resonance* strength of a substituent. The *para* substituent parameter σ_p is generally

considered to be the sum of the inductive and resonance components (eq 1.41)[136] There

is considerable discussion in the literature as to the validity of this simple treatment;[200-204]

however, the F and R values will be used in this thesis.

$$\sigma_p \approx F + R. \qquad (1.41)$$

Table 1.7. Hammett substituent constants used in this thesis.[136]

	σ_p	σ_m	F	R
CH_3	-0.17	-0.07	+0.01	-0.18
H	0	0	0	0
F	+0.06	+0.34	+0.45	-0.39
CF_3	+0.54	+0.43	+0.38	+0.16

Equilibrium constants are related to ΔG by eq 1.42, therefore any change in K_{eq} as a result of substitution is a manifestation of the changes to ΔG (eq 1.43). Recall from eq 1.38 that the logarithmic term in eq 1.43 is the definition of σ. The σ value is therefore a measure of $\Delta\Delta G$ caused by the aromatic substitution of benzoic acid.

$$\Delta G = -RT \ln K_{eq} \tag{1.42}$$

$$\Delta G_H - \Delta G_X = -RT \ln K_H + RT \ln K_X \tag{1.43}$$

$$\Delta\Delta G = -2.303 RT \log\left(\frac{K_X}{K_H}\right)$$

$$= -2.303 RT \sigma$$

Now consider a reaction unrelated to benzoic acid (denoted with $'$) in which we substitute the aromatic rings. A similar set of equations apply (eq 1.44).

$$\Delta G_{H'} - \Delta G_{X'} = -RT \ln K_{H'} + RT \ln K_{X'}$$

$$\Delta\Delta G' = -2.303 RT \log\left(\frac{K_{X'}}{K_{H'}}\right) \tag{1.44}$$

If a plot of log $(K_{X'}/K_{H'})$ *vs.* σ (eq 1.45) is linear this implies that the *nature* of the substituent effect on $\Delta\Delta G'$ is the same as on the pK_a of benzoic acid. Thus a *linear free*

energy relationship (LFER) exists between dissociated benzoic acid and the reaction of interest.[205] The slope of this line (ρ) indicates the magnitude of the substituent effect relative to the acidity of benzoic acid – if $|\rho| > 1$, the reaction is more sensitive to substituent and *vice versa*.

$$\log\left(\frac{K_{X}}{K_{H}}\right) = \sigma\rho \tag{1.45}$$

Substituents effect the values of ΔG (the free energy change between the reactant and product) and $\Delta G^{\ddagger}$ of a reaction (the free energy change between the reactant and transition state) (Figure 1.8). The former leads to changes in K_{eq} while the latter leads to changes in the rate constant k. LFERs exist between the rate constants of various reactions and the pK_as of substituted benzoic acids (σ). The Hammett equation for this relationship is essentially identical to that used with equilibrium constants (eq 1.46). The magnitude of the ρ value gives information regarding the charge distribution in the transition state of a reaction. For example if the slope (ρ) is positive, there is negative charge development in the transition state.

$$\log\left(\frac{k_{X}}{k_{H}}\right) = \sigma\rho \tag{1.46}$$

A final note is that often $\log K_x$ or $\log k_x$ is plotted against σ, rather than plotting $\log (K_x/K_H)$ or $\log (k_x/k_H)$ against σ. This change only affects the *y*-intercept and not the slope (ρ), which is the important parameter from these plots.
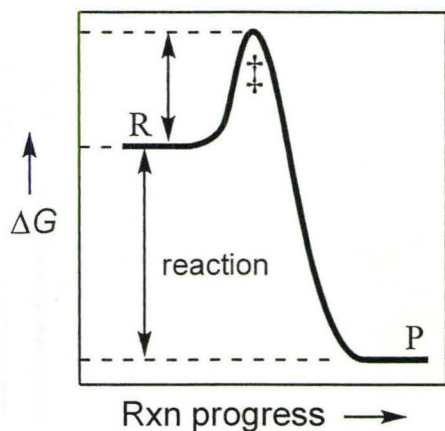
Figure 1.8. Typical reaction coordinate diagram for the exothermic conversion of reactants (R) to products (P) through the transition state, which is denoted with ‡.

1.9.2. Temperature Effects and the Determination of Enthalpies and Entropies

The relationship between the change in free energy (ΔG), enthalpy (ΔH) and entropy (ΔS) is given by eq 1.47, and applies regardless of whether the difference in question is between that of the reactants and products or the reactants and the transition state (Figure 1.8).[206] Note that the transition state refers to the point on the reaction coordinate diagram where the free energy (ΔG) is a maximum.[207]

$$\Delta G = \Delta H - T\Delta S \tag{1.47}$$

This relationship between the equilibrium constant and temperature can be obtained through substitution of ΔG in eq 1.47 with eq 1.42, and the result is the *van't Hoff equation* (eq 1.48), which gives the enthalpy (ΔH) and entropy (ΔS) of the reaction from a plot of log K vs. T^{-1}.[208] Inspection of this equation shows that when the temperature is increased, K_{eq} will decrease if the reaction is exothermic and the K_{eq} will

38

increase if the reaction is endothermic.[209]

$$\log K = \frac{1}{R \ln 10} \left(\Delta S - \frac{\Delta H}{T} \right) \tag{1.48}$$

For rate constants, k generally increases as the temperature is raised because more reactant molecules have sufficient energy to overcome the activation barrier and proceed to product. The relationship between the rate constant and temperature is given by the *Arrhenius equation* (eq 1.49), where A is the pre-exponential factor and E_a is the activation energy. The Arrhenius activation energy can be determined from a plot of $\ln k$ vs. T^{-1}. The larger the activation energy, the more sensitive the rate constant to changes in temperature. The *Eyring equation* (eq 1.50, where k is Boltzmann's constant and h is Planck's constant) provides the enthalpy of activation ($\Delta H^{\ddagger}$) and entropy of activation ($\Delta S^{\ddagger}$) from a plot of $\ln(k/T)$ vs. T^{-1}.

$$k = A \exp\left(\frac{-E_a}{RT} \right) \tag{1.49}$$

$$k = \frac{kT}{h} \exp\left(\frac{\Delta S^{\ddagger}}{R} \right) \exp\left(\frac{-\Delta H^{\ddagger}}{RT} \right) \tag{1.50}$$

For reactions in solution, E_a and $\Delta H^{\ddagger}$ differ only slightly (eq 1.51: $RT = +0.6$ kcal/mol at 25 °C).[210, 211] The entropy of activation ($\Delta S^{\ddagger}$) reflects the degree of organization in the transition state relative to that of the free reactants under the particular reaction conditions.[212] The activation entropy and the pre-exponential factor A

determined from the Arrhenius plot are related according to eq 1.52.

$$E_a = \Delta H^{\ddagger} + RT \tag{1.51}$$

$$\ln A = \frac{\Delta S^{\ddagger}}{R} + \ln \frac{kT}{h} + 1 \tag{1.52}$$

1.9.3. Kinetic Isotope Effect

A kinetic isotope effect (KIE) refers to a change in rate constant caused by the substitution of an isotopomer of a reactant in a given chemical reaction.[213] The KIE is normally expressed as the ratio of the rate constant observed with the "light" isomer divided by the rate constant observed with the "heavy" isomer (eq 1.53), and its magnitude provides mechanistic information. A KIE that results from isotopic substitution of an atom to which a bond is broken or formed is known as a primary KIE. Because deuterium substitution is the most common and is what is employed in this work, **H** will be used to refer to the light isomer and **D** the heavy isomer.

$$KIE = \frac{k_{light}}{k_{heavy}} = \frac{k_H}{k_D} \tag{1.53}$$

The origin of the KIE is in the difference between the zero point energies (ZPE) of the reactant and transition state of the reactions of **H** and **D**. The ZPE is the energy of a molecule in its lowest vibrational state at ambient temperature. Isotopic substitution does not significantly affect the C-L bond strength, and therefore the force constant for the bond vibration will be the same in both cases. The vibrational frequency will depend on the reduced mass of the C-L system and with **H** having the smaller reduced mass it has

the higher vibrational frequency and higher ZPE.[205] The observed rate constants will be

different if $E_a(\mathbf{H}) \neq E_a(\mathbf{D})$ (Figure 1.9).
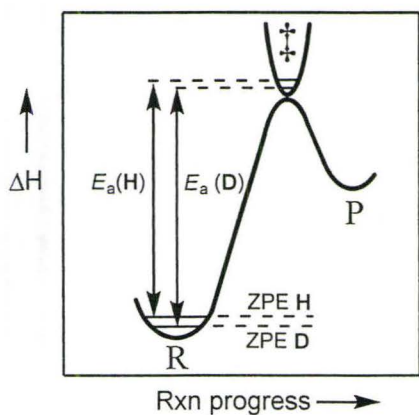
Figure 1.9. Reaction coordinate diagram illustrating the zero-point energies of H and D isotopomers.

A maximum KIE will be observed when the ΔZPE in the transition state is at a

minimum (*i.e.* $ZPE^{\ddagger}_{H} = ZPE^{\ddagger}_{D}$). This condition will be satisfied when the ZPE($\ddagger$) does

not depend on the mass of the isotope. There are three thermodynamic scenarios to

consider for a single-step H(D)-transfer reaction:

(1) a highly exothermic reaction will have a transition state that is early and "reactant

like" (Hammond-Leffler Postulate). There will be little cleavage of the bond C-L bond (L

= H or D) in the transition state and $\Delta ZPE_R \approx \Delta ZPE^{\ddagger}$ and KIE ≈ 1 (Figure 1.10).

(2) a highly endothermic reaction will have a transition state that is late and "product

like" and thus the transfer of L to the product is nearly complete in the transition state;

again the $\Delta ZPE_P \approx \Delta ZPE^{\ddagger}$ and KIE ≈ 1.

(3) a more thermoneutral reaction will have a transition state where the proton is partially

transferred and the C-L-C vibration will be symmetrical and will not depend on the

identity of L therefore $\Delta ZPE^{\ddagger} \approx 0$ and KIE > 1. The magnitude of the KIE will be largest

for reactions in which the transition state is linear and symmetric. Deviations of these

two properties will result in a reduction of the observed KIE. The theoretical maximum

KIE is 7.8 for the transfer of L between two carbon atoms.[206]
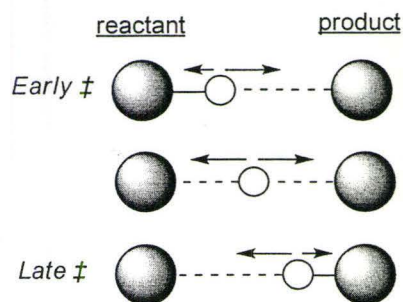
Figure 1.10. Diagram illustrating the relative degree of hydrogen transfer from reactant to product in reactions with an early, mid, and late transition state ($\ddagger$). The arrows show the relevant vibrations.

1.9.4. A note regarding data presented in this thesis.

A majority of the laser flash photolysis work presented in this thesis was carried

out in hexanes solution because this solvent should not (and indeed does not) complex

with the transient germylenes of interest. Great care was taken to ensure that the

glassware and solvent were anhydrous to minimize the complications due to formation of

germylene-water complexes. Chapter 3 and parts of Chapter 4 present studies carried out

in THF and although coordination with the germylene was the objective, the solvent was

dried. All solvents were deoxygenated via argon saturation prior to and during the

experiment. To increase readability, unless otherwise stated, descriptions of laser work

found in the text as well as within the figure and table captions which state that the data

were obtained in:

- <u>hexanes</u> should be interpreted as "anhydrous and deoxygenated hexanes at 25 °C"

- <u>THF</u> should be interpreted as "anhydrous and deoxygenated THF at 25 °C"

- <u>MeOH</u> should be interpreted as "deoxygenated MeOH at 25 °C".

Unless otherwise noted, all rate constants, Arrhenius parameters, and thermodynamic parameters presented in this thesis were obtained from linear least-squares fits of the data to the appropriate equations and errors are reported as twice the standard error ($\pm 2\sigma$).

1.10. References

1.   Wiberg, N. In *Silicon Chemistry. From the Atom to Extended Systems*, Jutzi, P.; Schubert, U., Eds. Wiley-VCH: Darmstadt, 2003; pp 85-99.
2.   Layfield, R. A. *Organomet. Chem.* **2005**, *32*, 171.
3.   Power, P. P. *J. Chem. Soc., Dalton Trans.* **1998**, 2939.
4.   Bauschlicher, C. W., Jr.; Schaefer, H. F.; Bagus, P. S. *J. Am. Chem. Soc.* **1977**, *99*, 7106.
5.   Tomioka, H. *Acc. Chem. Res.* **1997**, *30*, 315.
6.   Jones, M., Jr.; Moss, R. A. In *Reactive Intermediate Chemistry*, Moss, R. A.; Platz, M. S.; Jones, M., Jr., Eds. John Wiley & Sons: New York, 2004; pp 273-373.
7.   Wang, Y.; Hadad, C. M.; Toscano, J. P. *J. Am. Chem. Soc.* **2002**, *124*, 1761.
8.   Jiang, P.; Gaspar, P. P. *J. Am. Chem. Soc.* **2001**, *123*, 8622.
9.   Sekiguchi, A.; Tanaka, T.; Ichinohe, M.; Akiyama, K.; Tero-kubota, S. *J. Am. Chem. Soc.* **2003**, *125*, 4962.
10. Apeloig, Y.; Pauncz, R.; Karni, M.; West, R.; Steiner, W.; Chapman, D. *Organometallics* **2003**, *22*, 3250.
11. Walsh, R. *Acc. Chem. Res.* **1981**, *14*, 246.
12. Grev, R. S. *Adv. Organomet. Chem.* **1991**, *33*, 125.
13. Szabados, A.; Hargittai, M. *J. Phys. Chem. A* **2003**, *107*, 4314.
14. Pople, J. A.; Head-Gordon, M.; Fox, D. J.; Raghavachari, K.; Curtiss, L. A. *J. Chem. Phys.* **1989**, *90*, 5622.
15. Walsh, R.; Patai, S. In *The chemistry of organic silicon compounds*, Rappoport, Z., Ed. John Wiley & Sons Ltd.: 1989; pp 371-391.
16. Becerra, R.; Boganov, S. E.; Egorov, M. P.; Faustov, V. I.; Nefedov, O. M.; Walsh, R. *J. Am. Chem. Soc.* **1998**, *120*, 12657.

17. Allendorf, M. D.; Melius, C. F. *J. Phys. Chem. A* **2005**, *109*, 4939.
18. Moss, R. A.; Jones, M., Jr. In *Reactive Intermediates*, Jones, M., Jr.; Moss, R. A., Eds. John Wiley & Sons: New York, 1985; Vol. 3, pp 45-109.
19. Lowry, T. H.; Richardson, K. S., *Mechanism and Theory in Organic Chemistry*. 3rd ed.; Harper and Row: New York, 1987, p 546.
20. Barrau, J.; Escudié, J.; Satgé, J. *Chem. Rev.* **1990**, *90*, 283.
21. Becerra, R.; Cannady, P. J.; Walsh, R. *J. Phys. Chem. A* **2003**, *107*, 9588.
22. Herrmann, W. A.; Denk, M.; Behm, J.; Scherer, W.; Klingan, F. R.; Bock, H.; Solouki, B.; Wagner, M. *Angew. Chem. Int. Ed. Engl.* **1992**, *31*, 1485.
23. Takeda, N.; Tokitoh, N.; Okazaki, R. *Science of Synthesis* **2003**, *5*, 51.
24. Simons, R. S.; Pu, L.; Olmstead, M. M.; Power, P. P. *Organometallics* **1997**, *16*, 1920.
25. Neumann, W. P. *Chem. Rev.* **1991**, *91*, 311.
26. Harrington, C. R.; Leigh, W. J.; Chan, B. K.; Gaspar, P. P.; Zhou, D. *Can. J. Chem.* **2005**, *83*, 1324.
27. Tsumuraya, T.; Kabe, Y.; Ando, W. *J. Organomet. Chem.* **1994**, *482*, 131.
28. Baines, K. M.; Cooke, J. A.; Dixon, C. E.; Liu, H.; Netherton, M. R. *Organometallics* **1994**, *13*, 631.
29. Toltl, N. P.; Leigh, W. J.; Kollegger, G. M.; Stibbs, W. G.; Baines, K. M. *Organometallics* **1996**, *15*, 3732.
30. Satgé, J.; Massol, M.; Rivière, P. *J. Organomet. Chem.* **1973**, *56*, 1.
31. Massol, M.; Satgé, J.; Rivière, P.; Barrau, J. *J. Organomet. Chem.* **1970**, *22*, 599.
32. Bobbitt, K. L.; Maloney, V. M.; Gaspar, P. P. *Organometallics* **1991**, *10*, 2772.
33. Barrau, J.; Bean, D. L.; Welsh, K. M.; West, R.; Michl, J. *Organometallics* **1989**, *8*, 2606.
34. Leigh, W. J.; Harrington, C. R.; Vargas-Baca, I. *J. Am. Chem. Soc.* **2004**, *126*, 16105. (Errata: *J. Am. Chem. Soc.* **2006**, *128*, 1394.).
35. Lollmahomed, F.; Leigh, W. J. *Organometallics* **2009**, *28*, 3239.
36. Tsumuraya, T.; Ando, W. *Chem. Lett.* **1989**, 1043.
37. Baceiredo, A.; Bertrand, G.; Mazerolles, P. *Tetrahedron Lett.* **1981**, *22*, 2553.
38. Leigh, W. J.; Lollmahomed, F.; Harrington, C. R. *Organometallics* **2006**, *25*, 2055.
39. Bender, J. E. I.; Banaszak Holl, M. M.; Kampf, J. W. *Organometallics* **1997**, *16*, 2743.
40. Barrau, J.; Rima, G. *Coord. Chem. Rev.* **1998**, *178-180*, 593.
41. Weidenbruch, M. *Eur. J. Inorg. Chem.* **1999**, 373.
42. Tokitoh, N.; Okazaki, R. *Coord. Chem. Rev.* **2000**, *210*, 251.
43. Weidenbruch, M. *J. Organomet. Chem.* **2002**, *646*, 39.
44. Tokitoh, N.; Ando, W. In *Reactive Intermediate Chemistry*, Moss, R. A.; Platz, M. S.; Jones, M., Jr., Eds. John Wiley & Sons: New York, 2004; pp 651-715.
45. Becerra, R.; Walsh, R. *Phys. Chem. Chem. Phys.* **2007**, *9*, 2817.
46. Weinert, C. S. In *Comprehensive Organometallic Chemistry III*, Crabtree, R. H.; Mingos, D. M. P., Eds. Elsevier: Amsterdam, 2007; Vol. 3, pp 699-805.
47. Mizuhata, Y.; Sasamori, T.; Tokitoh, N. *Chem. Rev.* **2009**, *109*, 3479.

48. Ando, W.; Itoh, H.; Tsumuraya, T.; Yoshida, H. *Organometallics* **1988**, *7*, 1880.
49. Ando, W.; Itoh, H.; Tsumuraya, T. *Organometallics* **1989**, *8*, 2759.
50. Nefedov, O. M.; Kolesnikov, S. P.; Rogozhin, I. S. *Izv. Akad. Nauk SSSR, Ser. Khim. (Eng. trans.)* **1973**, 2824.
51. Bokii, N. G.; Struchkov, Y. T.; Kolesnikov, S. P.; Rogozhin, I. S.; Nefedov, O. M. *Izv. Akad. Nauk SSSR, Ser. Khim. (Eng. trans.)* **1975**, 812.
52. Denk, M. K.; Khan, M.; Lough, A. J.; Shuchi, K. *Acta Cryst.* **1998**, *C54*, 1830.
53. Tian, X.; Pape, T.; Mitzel, N. W. *Heteroat. Chem.* **2005**, *16*, 361.
54. Massol, M.; Rivière, P.; Barrau, J.; Satgé, J. *C. R. Acad. Sci., Ser. IIc* **1970**, *270*, 237.
55. Collins, S.; Murakami, S.; Snow, J. T.; Masamune, S. *Tetrahedron Lett.* **1985**, *26*, 1281.
56. Kolesnikov, S. P.; Egorov, M. P.; Dvornikov, A. S.; Kuz'min, V. A.; Nefedov, O. M. *Izv. Akad. Nauk SSSR, Ser. Khim. (Eng. trans.)* **1988**, 2654.
57. Leigh, W. J.; Harrington, C. R. *J. Am. Chem. Soc.* **2005**, *127*, 5084.
58. Leigh, W. J.; Lollmahomed, F.; Harrington, C. R.; McDonald, J. M. *Organometallics* **2006**, *25*, 5424.
59. Leigh, W. J.; Dumbrava, I.; Lollmahomed, F. *Can. J. Chem.* **2006**, *84*, 934.
60. Hunter, E. P. L.; Lias, S. G. *J. Phys. Chem. Ref. Data* **1998**, *27*, 413.
61. Murov, S. L.; Carmichael, I.; Hug, G. L., *Handbook of Photochemistry*. Dekker: New York, 1993.
62. Köcher, J.; Lehnig, M.; Neumann, W. P. *Organometallics* **1988**, *7*, 1201.
63. Trotter, J.; Akhtar, M.; Bartlett, N. *J. Chem. Soc. (A)* **1966**, 30.
64. Rouse, R. C.; Peacor, D. R.; Maxim, B. R. *Z. Kristallogr.* **1977**, *145*, 161.
65. Gaspar, P. P.; West, R. In *The chemistry of organic silicon compounds*, Rappoport, Z.; Apeloig, Y., Eds. John Wiley & Sons: New York, 1998; pp 2463-2568.
66. Belzner, J.; Ihmels, H. *Adv. Organomet. Chem.* **1999**, *43*, 1.
67. Moiseev, A. G.; Leigh, W. J. *Organometallics* **2007**, *26*, 6277.
68. Quane, D. *J. Inorg. Nucl. Chem.* **1971**, *33*, 2722.
69. Moss, R. A. *Acc. Chem. Res.* **1989**, *22*, 15.
70. Moss, R. A.; Wang, L.; Weintraub, E.; Krogh-Jespersen, K. *J. Phys. Chem. A* **2008**, *112*, 4651.
71. Moss, R. A.; Wang, L.; Odorisio, C. M.; Krogh-Jespersen, K. *J. Phys. Chem. A* **2010**, *114*, 209.
72. Padwa, A.; Hornbuckle, S. F. *Chem. Rev.* **1991**, *91*, 263.
73. Jackson, J. E.; Platz, M. S. In *Advances in Carbene Chemistry*, Brinker, U. H., Ed. Jai Press: Greenwich, Conn., 1994; Vol. 1, p 89.
74. Chateauneuf, J. E.; Johnson, R. P.; Kirchhoff, M. M. *J. Am. Chem. Soc.* **1990**, *12*, 3217.
75. Lappert, M. F.; Miles, S. J.; Atwood, J. L.; Zaworotko, M. J.; Carty, A. J. *J. Organomet. Chem.* **1981**, *212*, C4.
76. Klein, B.; Neumann, W. P.; Weisbeck, M. P.; Wienken, S. *J. Organomet. Chem.* **1993**, *446*, 149.

77.   Moiseev, A. G.; Leigh, W. J. *Organometallics* **2007**, *26*, 6268.

78.   Griller, D.; Liu, M. T. H.; Scaiano, J. C. *J. Am. Chem. Soc.* **1982**, *104*, 5549.

79.   Griller, D.; Liu, M. T. H.; Montgomery, C. R.; Scaiano, J. C.; Wong, P. C. *J. Org. Chem.* **1983**, *48*, 1359.

80.   Birchall, T.; Drummond, I. *Inorg. Chem.* **1972**, *11*, 250.

81.   Gu, T.-Y. Y.; Weber, W. P. *J. Organomet. Chem.* **1980**, *184*, 7.

82.   O'Neal, H. E.; Ring, M. A.; Martin, J. G.; Navio, M. T. *J. Phys. Chem. A* **1998**, *102*, 8493.

83.   Becerra, R.; Cannady, J. P.; Walsh, R. *Silicon Chem.* **2005**, *3*, 131.

84.   Kirmse, W., *Carbene Chemistry*. 2nd ed.; Academic Press: New York, 1971.

85.   Bonneau, R.; Liu, M. T. H. *J. Am. Chem. Soc.* **1991**, *113*, 9872.

86.   Ishikawa, M.; Nakagawa, K. I.; Katayama, S.; Kumada, M. *J. Organomet. Chem.* **1981**, *216*, C48.

87.   Tomoda, S.; Shimoda, M.; Takeuchi, Y.; Kajii, Y.; Obi, K.; Tanaka, I.; Honda, K. *J. Chem. Soc., Chem. Commun.* **1988**, 910.

88.   Oka, K.; Nakao, R. *J. Organomet. Chem.* **1990**, *390*, 7.

89.   Mochida, K.; Yoneda, I.; Wakasa, M. *J. Organomet. Chem.* **1990**, *399*, 53.

90.   Mochida, K.; Adachi, M.; Wakasa, M.; Hayashi, H. *Phosph. Sulf. Sil. Rel. Elem.* **1999**, *150-151*, 237.

91.   Adachi, M.; Mochida, K.; Wakasa, M.; Hayashi, H. *Main Group Met. Chem.* **1999**, *22*, 227.

92.   Miller, K. A.; Bartolin, J. M.; O'Neill, R. M.; Sweeder, R. D.; Owens, T. M.; Kampf, J. W.; Banaszak Holl, M. M.; Wells, N. J. *J. Am. Chem. Soc.* **2003**, *125*, 8986.

93.   Kavara, A.; Cousineau, K. D.; Rohr, A. D.; Kampf, J. W.; Banaszak Holl, M. M. *Organometallics* **2008**, *27*, 1041.

94.   Egorov, M. P.; Galminas, A. M.; Basova, A. A.; Nefedov, O. M. *Dokl. Akad. Nauk SSSR (Eng. trans.)* **1993**, *329*, 594.

95.   Eberson, L. *Acta Chem. Scand.* **1982**, *B36*, 533.

96.   von Stackelberg, M.; Stracke, W. *Z. Elektrochem.* **1948**, *53*, 118.

97.   Neumann, W. P.; Schriewer, M. *Tetrahedron Lett.* **1980**, *21*, 3273.

98.   Mochida, K.; Tokura, S. *Organometallics* **1992**, *11*, 2752.

99.   Egorov, M. P.; Dvornikov, A. S.; Ezhova, M. B.; Kuz'min, V. A.; Kolesnikov, S. P.; Nefedov, O. M. *Organomet. Chem. USSR* **1991**, *4*, 582.

100.   Jones, M. B.; Maloney, V. M.; Platz, M. S. *J. Am. Chem. Soc.* **1992**, *114*, 2163.

101.   Politzer, P.; Lane, P.; Concha, M. C.; Ma, Y.; Murray, J. S. *J. Mol. Model.* **2007**, *13*, 305.

102.   Moss, R. A. In *Carbenes*, Jones, M., Jr.; Moss, R. A., Eds. John Wiley & Sons: New York, 1973; Vol. 1, p 153.

103.   Brück, W.; Dürr, H. *Tetrahedron Lett.* **1982**, *23*, 2175.

104.   Moss, R. A.; Perez, L. A.; Turro, N. J.; Gould, I. R.; Hacker, N. P. *Tetrahedron Lett.* **1983**, *24*, 685.

105.   Platz, M. S. *Tetrahedron Lett.* **1983**, *24*, 4763.

106. Turro, N. J.; Cha, Y.; Gould, I. R. *Tetrahedron Lett.* **1985**, *26*, 5951.
107. Gould, I. R.; Turro, N. J.; Butcher, J., Jr.; Doubleday, C., Jr.; Hacker, N. P.; Lehr, G. F.; Moss, R. A.; Cox, D. P.; Guo, W.; Munjal, R. C.; Perez, L. A.; Fedorynski, M. *Tetrahedron* **1985**, *41*, 1587.
108. Moss, R. A.; Ławrynowicz, W.; Turro, N. J.; Gould, I. R.; Cha, Y. *J. Am. Chem. Soc.* **1986**, *108*, 7028.
109. Moss, R. A.; Turro, N. J. In *Kinetics and Spectroscopy of Carbenes and Biradicals*, Platz, M. S., Ed. Plenum Press: New York, 1990; pp 213-238.
110. Moss, R. A.; Wang, L.; Zhang, M.; Skalit, C.; Krogh-Jespersen, K. *J. Am. Chem. Soc.* **2008**, *130*, 5634.
111. Houk, K. N.; Rondon, N. G.; Mareda, J. *J. Am. Chem. Soc.* **1984**, *106*, 4291.
112. Houk, K. N.; Rondon, N. G.; Mareda, J. *Tetrahedron* **1985**, *41*, 1555.
113. Tortorelli, V. J.; Jones, M., Jr.; Wu, S.-h.; Li, Z.-h. *Organometallics* **1983**, *2*, 759.
114. Boatz, J. A.; Gordon, M. S. *J. Phys. Chem.* **1989**, *93*, 3025.
115. Nagase, S. *Polyhedron* **1991**, *10*, 1299.
116. Horner, D. A.; Grev, R. S.; Schaefer, H. F., III *J. Am. Chem. Soc.* **1992**, *114*, 2093.
117. Birukov, A. A.; Faustov, V. I.; Egorov, M. P.; Nefedov, O. M. *Russ. Chem. Bull., Int. Ed.* **2005**, *54*, 2003.
118. Zhang, S.; Conlin, R. T. *J. Am. Chem. Soc.* **1991**, *113*, 4272.
119. Kroke, E.; Willms, S.; Weidenbruch, M.; Saak, W.; Pohl, S.; Marsmann, H. *Tetrahedron Lett.* **1996**, *37*, 3675.
120. Takeda, N.; Tokitoh, N.; Okazaki, R. *Chem. Lett.* **2000**, 622.
121. Ando, W.; Ohgaki, H.; Kabe, Y. *Angew. Chem. Int. Ed. Eng.* **1994**, *33*, 659.
122. Kabe, Y.; Ohgaki, H.; Yamagaki, T.; Nakanishi, H.; Ando, W. *J. Organomet. Chem.* **2001**, *636*, 82.
123. Mayr, H.; Heigl, U. W. *Angew. Chem. Int. Ed. Engl.* **1985**, *24*, 579.
124. Jenneskens, L. W.; de Wolf, W. H.; Bickelhaupt, F. *Angew. Chem. Int. Ed. Engl.* **1985**, *24*, 585.
125. Le, N. A.; Jones, M., Jr.; Bickelhaupt, F.; de Wolf, W. H. *J. Am. Chem. Soc.* **1989**, *111*, 8491.
126. Lambert, J. B.; Ziemnicka-Merchant, B. T. *J. Org. Chem.* **1990**, *55*, 3460.
127. Fujimoto, H.; Hoffmann, R. *J. Phys. Chem.* **1974**, *78*, 1167.
128. Lei, D.; Hwang, R.-J.; Gaspar, P. P. *J. Organomet. Chem.* **1984**, *271*, 1.
129. Clarke, M. P.; Davidson, I. M. T. *J. Chem. Soc., Chem. Commun.* **1988**, 241.
130. Lei, D.; Gaspar, P. P. *Res. Chem. Intermed.* **1989**, *12*, 103.
131. Maier, E.; Olbrich, G. *Ber. Bunsen-Ges. Phys. Chem* **1986**, *90*, 86.
132. Schriewer, M.; Neumann, W. P. *Angew. Chem. Int. Ed. Engl.* **1981**, *20*, 1019.
133. Ma, E. C.-L.; Kobayashi, K.; Barzilai, M. W.; Gaspar, P. P. *J. Organomet. Chem.* **1982**, *224*, C13.
134. Köcher, J.; Neumann, W. P. *J. Am. Chem. Soc.* **1984**, *106*, 3861.
135. Moiseev, A. G.; Leigh, W. J. *J. Am. Chem. Soc.* **2006**, *128*, 14442.
136. Hansch, C.; Leo, A.; Taft, R. W. *Chem. Rev.* **1991**, *91*, 165.
137. Anwari, F.; Gordon, M. S. *Isr. J. Chem.* **1983**, *23*, 129.

138. Sakai, S. *Int. J. Quantum Chem.* **1998**, *70*, 291.
139. Su, M.-D.; Chu, S. Y. *J. Am. Chem. Soc.* **1999**, *121*, 11478.
140. Becerra, R.; Boganov, S. E.; Egorov, M. P.; Faustov, V. I.; Promyslov, V. M.; Nefedov, O. M.; Walsh, R. *Phys. Chem. Chem. Phys.* **2002**, *4*, 5079.
141. Nag, M.; Gaspar, P. P. *Organometallics* **2009**, *28*, 5612.
142. Trinquier, G.; Malrieu, J. P.; Rivière, P. *J. Am. Chem. Soc.* **1982**, *104*, 4529.
143. Trinquier, G.; Malrieu, J. P. *J. Am. Chem. Soc.* **1987**, *109*, 5303.
144. Malrieu, J. P.; Trinquier, G. *J. Am. Chem. Soc.* **1989**, *111*, 5916.
145. Driess, M.; Grützmacher, H. *Angew. Chem. Int. Ed. Engl.* **1996**, *35*, 828.
146. Power, P. P. *Chem. Rev.* **1999**, *99*, 3463.
147. Malcolm, N. O. J.; Gillespie, R. J.; Popelier, P. L. A. *J. Chem. Soc., Dalton Trans.* **2002**, 3333.
148. Davidson, P. J.; Harris, D. H.; Lappert, M. F. *J. Chem. Soc., Dalton Trans.* **1976**, 2268.
149. Chen, W. C.; Su, M.-D.; Chu, S. Y. *Organometallics* **2001**, *20*, 564.
150. Albright, T. A.; Burdett, J. K.; Whangbo, M. H., *Orbital Interactions in Chemistry*. John Wiley & Sons: New York, 1985; p 166.
151. Salem, L., *The Molecular Orbital Theory of Conjugated Systems*. W. A. Benjamin, Inc.: New York, 1966.
152. Liang, C.; Allen, L. C. *J. Am. Chem. Soc.* **1990**, *112*, 1039.
153. Allred, A. L.; Rochow, E. G. *J. Inorg. Nucl. Chem.* **1958**, *5*, 269.
154. Kira, M.; Iwamoto, T.; Maruyama, T.; Kabuto, C.; Sakurai, H. *Organometallics* **1996**, *15*, 3767.
155. Batcheller, S. A.; Tsumuraya, T.; Tempkin, O.; Davis, W. M.; Masamune, S. *J. Am. Chem. Soc.* **1990**, *112*, 9394.
156. Schäfer, H.; Saak, W.; Weidenbruch, M. *Organometallics* **1999**, *18*, 3159.
157. Stender, M.; Pu, L.; Power, P. P. *Organometallics* **2001**, *20*, 1820.
158. Pampuch, B.; Saak, W.; Weidenbruch, M. *J. Organomet. Chem.* **2006**, *691*, 3540.
159. Hurni, K. L.; Rupar, P. A.; Payne, N. C.; Baines, K. M. *Organometallics* **2007**, *26*, 5569.
160. Grev, R. S.; Schaefer, H. F., III; Baines, K. M. *J. Am. Chem. Soc.* **1990**, *112*, 9458.
161. Schmidt, M. W.; Truong, P. N.; Gordon, M. S. *J. Am. Chem. Soc.* **1987**, *109*, 5217.
162. Ervin, K. M.; Gronert, S.; Barlow, S. E.; Gilles, M. K.; Harrison, A. G.; Bierbaum, V. M.; DePuy, C. H.; Lineberger, W. C.; Ellison, G. B. *J. Am. Chem. Soc.* **1990**, *112*, 5750.
163. Windus, T. L.; Gordon, M. S. *J. Am. Chem. Soc.* **1992**, *114*, 9559.
164. Becerra, R.; Gaspar, P. P.; Harrington, C. R.; Leigh, W. J.; Vargas-Baca, I.; Walsh, R.; Zhou, D. *J. Am. Chem. Soc.* **2005**, *127*, 17469.
165. West, R.; Fink, M.; Michl, J. *Science* **1981**, *214*, 1343.
166. Tokitoh, N.; Okazaki, R. In *The chemistry of organic germanium, tin and lead compounds*, Rappoport, Z., Ed. John Wiley & Sons: New York, 2002; pp 843-901.
167. Ando, W.; Tsumuraya, T. *J. Chem. Soc., Chem. Commun.* **1989**, 770.

168. Tan, R. P.; Gillette, G. R.; Yokelson, H. B.; West, R.; Boudjouk, P. *Inorg. Synth.* **1992**, *29*, 19.

169. Mochida, K.; Kayamori, T.; Wakasa, M.; Hayashi, H.; Egorov, M. P. *Organometallics* **2000**, *19*, 3379.

170. Baines, K. M.; Stibbs, W. G. *Adv. Organomet. Chem.* **1996**, *39*, 275.

171. Boomgaarden, S.; Saak, W.; Weidenbruch, M.; Marsmann, H. *Z. Anorg. Allg. Chem.* **2001**, *627*, 349.

172. Kira, M.; Ishima, T.; Iwamoto, T.; Ichinohe, M. *J. Am. Chem. Soc.* **2001**, *123*, 1676.

173. Chatgilialoglu, C., *Organosilanes in Radical Chemistry*. John Wiley & Sons, Ltd.: Cornwall, 2004.

174. Samuel, M. S.; Jennings, M. C.; Baines, K. M. *Organometallics* **2001**, *20*, 590.

175. Hayashi, H.; Mochida, K. *Chem. Phys. Lett.* **1983**, *101*, 307.

176. Ito, O.; Hoteiya, K.; Watanabe, A.; Matsuda, M. *Bull. Chem. Soc. Jpn.* **1991**, *64*, 962.

177. Lalevée, J.; Blanchard, N.; Graff, B.; Allonas, X.; Fouassier, J. P. *J. Organomet. Chem.* **2008**, *693*, 3643.

178. Jang, S.-M.; Reif, R. *Appl. Phys. Lett.* **1992**, *60*, 707.

179. Isobe, C.; Cho, H. C.; Crowell, J. E. *Surf. Sci.* **1993**, *295*, 117.

180. Du, W.; Keeling, L. A.; Greenlief, C. M. *J. Vac. Sci. Technol., A* **1994**, *12*, 2281.

181. Veprek, S.; Prokop, J.; Glatz, F.; Merica, R.; Klingan, F. R.; Herrmann, W. A. *Chem. Mater.* **1996**, *8*, 825.

182. Fürstner, A.; Krause, H.; Lehmann, C. W. *Chem. Commun.* **2001**, 2372.

183. Dumitrescu, A.; Gornitzka, H.; Martin-Vaca, B.; Bourissou, D.; Bertrand, G.; Cazaux, J.-B. Use of stannylenes and germylenes as polymerization catalysts for heterocycles. US 0153717, 2003.

184. West, R.; Moser, D. F.; Haaf, M. Silylene catalysis of olefin polymerization. US 6,576,729, 2003.

185. Kobayashi, S.; Shoda, S.-I.; Cao, S.; Iwata, S.; Abe, M.; Yajima, K.; Yagi, K.; Hiraishi, M. *J. Macromol. Sci. - Pure Appl. Chem.* **1994**, *A31*, 1835.

186. Neumann, W. P.; Weisbeck, M. P.; Wienken, S. *Main Group Met. Chem.* **1994**, *17*, 151.

187. Ottosson, H.; Steel, P. G. *Chem. Eur. J.* **2006**, *12*, 1576.

188. Lukevics, E.; Ignatovich, L. In *The chemistry of organic germanium, tin and lead compounds*, Rappoport, Z., Ed. John Wiley & Sons: New York, 2002; pp 1653-1683.

189. Satgé, J. *Actual. Chim.* **2004**, 31.

190. Bains, W.; Tacke, R. *Curr. Opin. Drug Discovery Dev.* **2006**, *6*, 526.

191. Gately, S.; West, R. *Drug Dev. Res.* **2007**, *68*, 156.

192. Hamers, R. J.; Coulter, S. K.; Ellison, M. D.; Hovis, J. S.; Padowitz, D. F.; Schwartz, M. P.; Greenlief, C. M.; Russell, J. N. *Acc. Chem. Res.* **2000**, *33*, 617.

193. Loscutoff, P.; Bent, S. F. *Annu. Rev. Phys. Chem.* **2006**, *57*, 467.

194. Buriak, J. M. *Chem. Rev.* **2002**, *102*, 1271.

195. Wang, G. T.; Mui, C.; Musgrave, C. B.; Bent, S. F. *J. Am. Chem. Soc.* **2002**, *124*, 8990.

196. Bent, S. F. *J. Phys. Chem. B* **2002**, *106*, 2830.

197. Filler, M. A.; Van Deventer, J. A.; Keung, A. J.; Bent, S. F. *J. Am. Chem. Soc.* **2006**, *128*, 770.

198. Bunnett, J. F. In *Investigation of Rates and Mechanisms of Reactions. Part 1*, Bernasconi, C. F., Ed. John Wiley & Sons: New York, 1986; Vol. 6, p 253.

199. Hammett, L. P. *J. Am. Chem. Soc.* **1937**, *59*, 96.

200. Cherkasov, A. R.; Galkin, V. I.; Cherkasov, R. A. *Russ. Chem. Rev.* **1996**, *65*, 641.

201. Charton, M. *J. Phys. Org. Chem.* **1999**, *12*, 275.

202. Galkin, V. I. *J. Phys. Org. Chem.* **1999**, *12*, 283.

203. Wiberg, K. B. *J. Org. Chem.* **2002**, *67*, 1613.

204. Exner, O.; Böhm, S. *Curr. Org. Chem.* **2006**, *10*, 763.

205. Lowry, T. H.; Richardson, K. S., *Mechanism and Theory in Organic Chemistry*. 3rd ed.; Harper and Row: New York, 1987.

206. Espenson, J. H., *Chemical Kinetics and Reaction Mechanisms*. 2nd ed.; McGraw-Hill Book Co.: New York, 1995; p 155-180.

207. Muller, P. *Pure Appl. Chem.* **1994**, *66*, 1077.

208. MacQueen, J. T. *J. Chem. Ed.* **1967**, *44*, 755.

209. Atkins, P.; de Paula, J., *Physical Chemistry*. 7th ed.; W.H. Freeman & Co.: New York, 2002.

210. Pacey, P. D. *J. Chem. Ed.* **1981**, *58*, 612.

211. Laidler, K. J., *Chemical Kinetics*. 3rd ed.; HarperCollins: New York, 1987; p 112-115.

212. Carpenter, B. K., *Determination of Organic Reaction Mechanisms*. John Wiley & Sons: New York, 1984; p 123.

213. Anslyn, E. V.; Dougherty, D. A., *Modern Physical Organic Chemistry*. University Science Books: Sausalito, Calf., 2006; p 421-441.

Chapter 2 – Synthesis and Photochemistry of 1,1-Diarylgermacyclopentenes.

2.1. Overview

This chapter introduces the 1,1-diaryl-1-germacyclopent-3-enes (**33a-g**) which we employ as the precursors to the substituted diarylgermylenes **Ga-g**. The synthesis and initial photochemical and laser flash photolysis (LFP) experiments are described. An overview of the laser flash photolysis technique is given, along with a discussion of UV/visible spectroscopy. The methods used to determine rate and equilibrium constants from LFP data are also given. Dimerization rate constants for **Ga-f** to **DGa-f** are estimated.

2.2. The Choice of Aryl-Substituents.

The selection of the aromatic substituents in the germylene precursors was based on the following criteria: the substituents should (*i*) span a wide range of the Hammett σ scale from electron-donating to electron-withdrawing (*ii*) not alter the photochemistry of the precursor and (*iii*) not form a Lewis acid-base complex with the germylene. These restrictions, particularly *iii*, severely limit the possibilities because most of the strong electron-donating and electron-withdrawing substituents contain a heteroatom; heteroatoms (except fluorine because of its high electronegativity) are excluded because of the ability to form a Lewis acid-base complex with the germylene. The aromatic ring substituents are thus limited to alkyl substituents as electron donors (*e.g.* CH_3) and fluorine or fluorinated alkyl substituents as electron acceptors (*e.g.* CF_3).

51

2.3. Synthesis of 1,1-diarylgermacyclopentene (33a-g).

Compounds **33b-g** were prepared following a method similar to that reported for

the parent compound (**33a**).[1] The reaction sequence begins with the synthesis of $GeCl_2$-

dioxane (**34**, eq 2.1)[2] which is subsequently reacted with 2,3-dimethyl-1,3-butadiene

(DMB) to yield compound **35** (eq 2.2).[3] Reaction of **35** with two equivalents of the

appropriate aryl Grignard reagent yields **33a-g** in > 80% yield (eq 2.3).[1,4]

$$GeCl_4 + O(SiMe_2H)_2 + \quad \xrightarrow{\Delta} \quad \mathbf{34} \qquad (2.1)$$

$$\mathbf{34} + \underset{DMB}{} \quad \xrightarrow[THF]{\Delta} \quad Cl_2Ge \quad \mathbf{35} \qquad (2.2)$$

$$\mathbf{35} + ArMgBr \quad \xrightarrow[5°C]{THF} \quad Ar_2Ge \quad \mathbf{33a-g} \qquad (2.3)$$

a. Ar = C_6H_5
b. Ar = $3,4\text{-}Me_2C_6H_3$
c. Ar = $4\text{-}MeC_6H_4$
d. Ar = $4\text{-}FC_6H_4$
e. Ar = $3\text{-}FC_6H_4$
f. Ar = $4\text{-}(CF_3)C_6H_4$
g Ar = $3,5\text{-}(CF_3)_2C_6H_3$
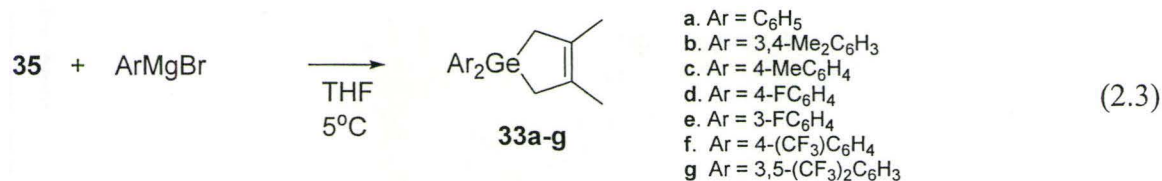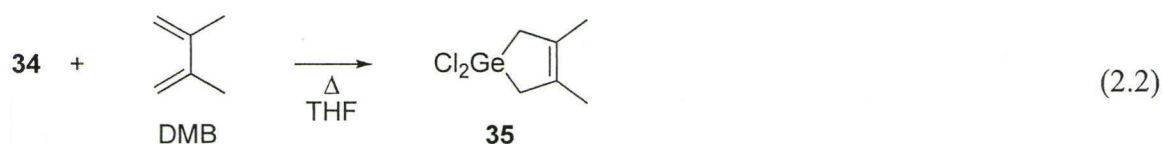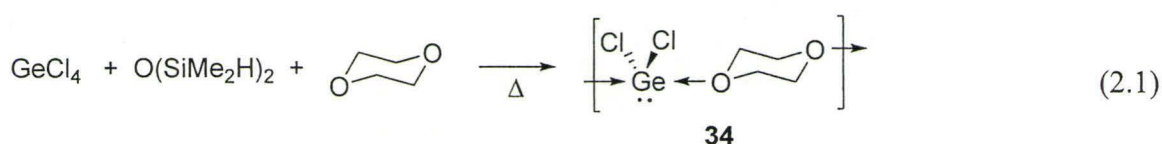
Purification of **33a-g** was achieved via silica gel column chromatography,

followed by multiple recrystallizations from hexanes. The purpose of the latter was to

remove any traces of biaryl that formed during the Grignard synthesis. Biaryl

complicates the laser flash photolysis experiments because the excited triplet state forms

with high efficiency ($\Phi_{ST} \sim 0.5$)[5] and the T^1-T^2 absorption has a very high extinction

coefficient ($\varepsilon_{360nm} = 38,500$ $M^{-1}cm^{-1}$ in hexanes).[5] Compounds **33a-g** are colourless

solids and were characterized by ^1H NMR, ^{13}C NMR, and IR spectroscopy, as well as

melting point, high-resolution mass spectrometry and combustion analysis. X-ray

crystallography was also utilized in one case (**33f**). These data are provided in Chapter 9. The UV spectra of **33a-g** were also recorded and are presented and discussed later in this chapter.

Certain spectral properties of **33a-g** can be correlated with Hammett sigma constants, although no strong correlations could be found. For example, the slope of the Hammett plot of the ^{13}C chemical shift of the aromatic carbon bonded to germanium is $\rho = +3 \pm 1$ ($r^2 = 0.70$). The melting ranges for these compounds spanned *ca.* 45-85 °C and it is noted that the compounds with exclusively *para* substituents generally have higher melting points, suggesting these are more tightly packed in the solid state.

The analogues **33a-g** were prepared at different times over the years in which the work described in this thesis was completed. The initial compounds were **33a,c,d,f** (H, p-Me, p-F, p-CF$_3$) and these were used in all experiments described in this thesis. In subsequent work it became clear that a greater coverage of the Hammett σ scale was necessary in order to make fully definitive mechanistic conclusions. To that end, compounds **33b** (mp-Me$_2$), **33e** (m-F) and **33g** (mm-(CF$_3$)$_2$) were prepared and used in some of the later studies that were undertaken.

2.4. Photochemistry of the germacyclopentenes

It was necessary to establish that the basic photochemistry of each of the germylene precursors **33b-g** is similar to that of **33a** (*i.e.* GeAr$_2$ is produced in high chemical and quantum yields). In a typical experiment, solutions of **33a** (the actinometer) and **33x** were prepared in C$_6$D$_{12}$ (*ca.* 0.02 M). Methanol (*ca.* 0.2 M) was

added to the solution to scavenge the germylene and Si_2Me_6 (ca. 2 mM) was added to the

solution as an integration standard. The solutions were placed in *quartz* NMR tubes,

purged with argon, sealed with a septum, and irradiated simultaneously with 254 nm light

in a merry-go-round apparatus. The progress of the reaction was monitored by ^1H NMR

spectroscopy (see Figure 2.1 for a representative example). As in the photolysis of **33a**,

the only products detectable upon photolysis of **33b-g** were the germylene-methanol

insertion products (**36**) and DMB (eq 2.4).

$$\textbf{33a-g} \xrightarrow[\substack{MeOH \\ C_6D_{12}}]{h\nu} \underset{\textbf{36}}{Ar_2Ge\overset{H}{\underset{OMe}{\diagup}}} + \ DMB \qquad (2.4)$$

Concentrations of the starting material and the products were determined by

integrating as many peaks as possible for each compound, using the Si_2Me_6 singlet as the

integration standard. In cases where a compound has more than one peak, each peak was

integrated, corrected for the number of protons responsible for the signal, and the values

were averaged. The concentrations of the starting material and products were then

plotted as a function of time (Figure 2.2) and the quantum yields for product formation

(Φ) were calculated from the relative slopes of the plots using eq 2.5. Chemical yields of

36 and DMB were calculated from the relative slopes of the plots using eq 2.6. The

results are listed in Table 2.1.
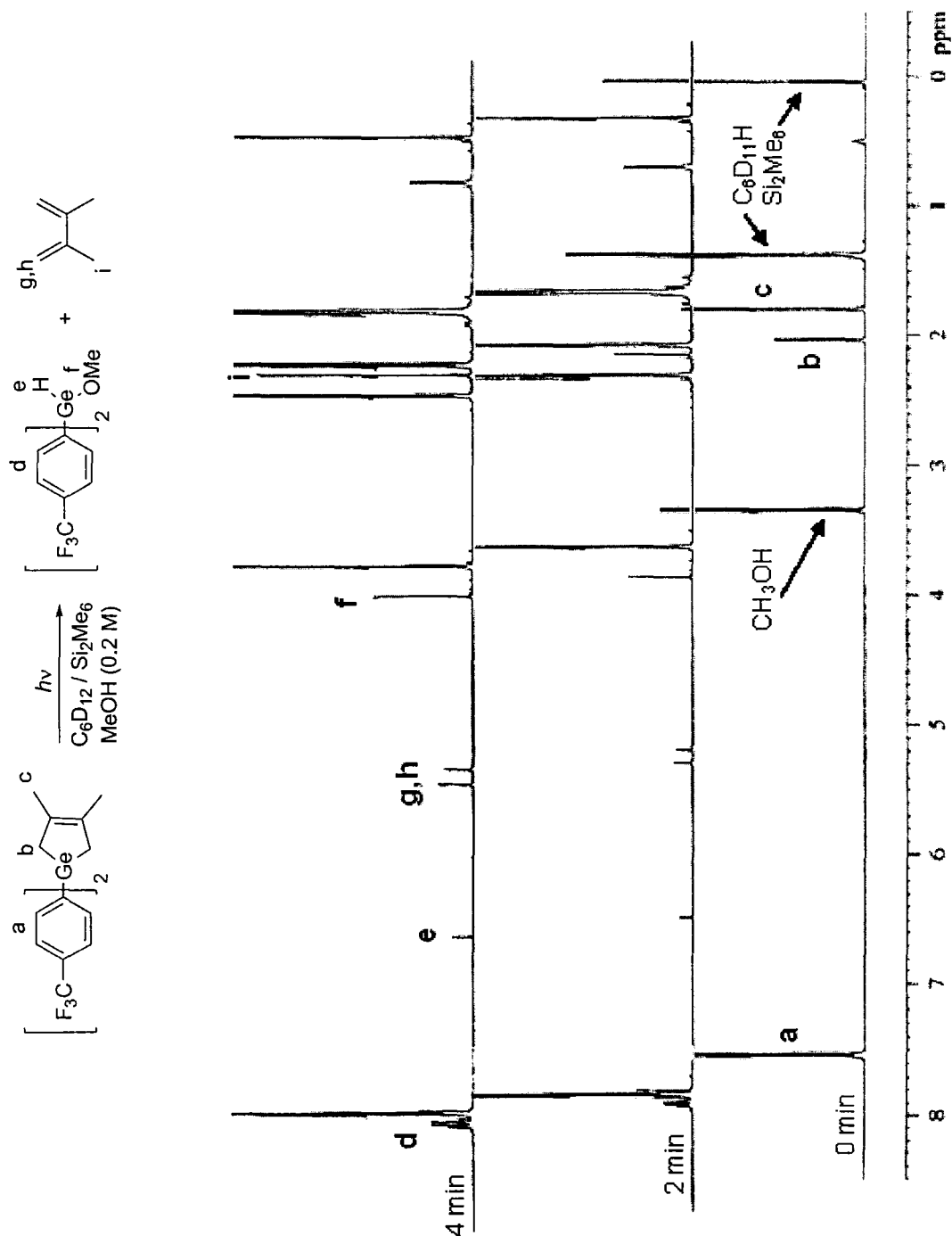
Figure 2.1. Representative ^{1}H NMR spectra from photolysis of **33f** in C_6D_{12} containing MeOH (0.2 M) and Si_2Me_6 (as internal integration standard). *(Reprinted from reference 4 with permission. © 2007 American Chemical Society.)*
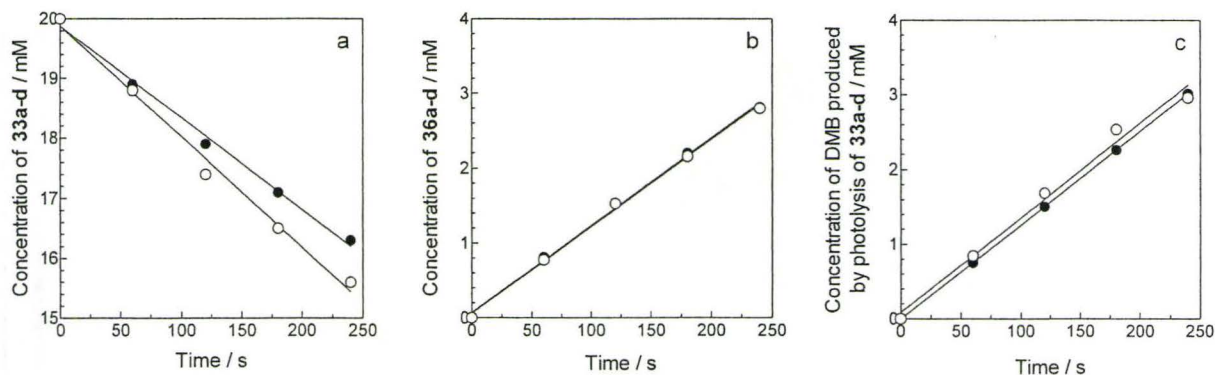
Figure 2.2. Concentration *vs.* time plots for (a) **33a,f**, (b) **36a,f**, and (c) DMB from photolysis of **33a,f** (0.02 M) in C_6D_{12} containing 0.2 M MeOH [(○ H)(● CF_3)].

$$\Phi_{36x} = \Phi_{33a}\left(\frac{d[36x]}{dt}\right)\left(\frac{d[36a]}{dt}\right)^{-1} \tag{2.5}$$

$$\% \, \text{yield}_{36x} = 100\left(\frac{d[36x]}{dt}\right)\left(\frac{-d[33a]}{dt}\right)^{-1}$$

$$\% \, \text{yield}_{DMB} = 100\left(\frac{d[DMB]}{dt}\right)\left(\frac{-d[33a]}{dt}\right)^{-1} \tag{2.6}$$

Table 2.1. Chemical and quantum yields for the formation of **36a-g** and DMB from the irradiation of **33a-g** (0.02 M) in C_6D_{12} containing MeOH (0.2 M).

33	Φ_{36}	Chemical yield / %	
		36a-g	DMB
a (H)	0.55 ± 0.07 [a]	86 ± 3	89 ± 3
b (m,p-Me_2)	0.35 ± 0.08	77 ± 3	82 ± 3
c (p-Me)	0.50 ± 0.09	82 ± 6	88 ± 9
d (p-F)	0.47 ± 0.10	81 ± 9	92 ± 11
e (m-F)	0.62 ± 0.09	88 ± 2	82 ± 2
f (p-CF_3)	0.55 ± 0.10	76 ± 6	88 ± 4
g (m,m-$CF_3)_2$	0.45 ± 0.09	83 ± 4	75 ± 4

a. reference 1.

The quantum yields of all the analogues are the same within the uncertainty limits. The chemical yields of germylene extrusion vary from 77-88%, but do not vary in a regular fashion with substituent. The reported chemical yield of **Ga** extrusion from **33a** is >95%.[1] The exact cause of this discrepancy is not known although it may be due to the use of a higher concentration of methanol (0.5 M) to scavenge the germylene.

2.5. UV-vis spectroscopy

2.5.1. Introduction

To determine absolute rate constants for the reactions of germylenes, digermenes and other transient species, direct detection is required and it must be possible to monitor the decay of the transient over a timescale of at least three times the lifetime of the transient (in the present case, $\tau < 1$ ms). The analyte must be generated immediately in high concentration and this can be achieved with a laser pulse. Furthermore, the chosen spectroscopic technique must have a rapid data acquisition time and be sensitive enough to detect transient species with concentrations in the range of 10^{-7}-10^{-5} M. There are a number of time-resolved spectroscopic techniques available for studying ground-state reactive intermediates including UV-visible, infrared, and Raman spectroscopies.[6-8] Whether a method is successful will depend on the analyte having the appropriate chromophore; for the detection of transient germylenes and digermenes, UV-vis spectroscopy is the most suitable method because of the (relatively) high values of the extinction coefficients in this region of the electromagnetic spectrum.

2.5.2. UV spectra of germylenes

Absorption of a photon of UV light results in an *n,p* electronic transition in the germylene from the ground state (S^0) to the first excited singlet state (S^1) (eq 2.7). Figure 2.3 shows the calculate HOMO and LUMO of $GeMe_2$. This transition occurs in the spectral range of 450-600 nm (λ_{max} $GeMe_2$ = 470 nm; $GePh_2$ = 500 nm; $GeMes_2$ = 560 nm in hexanes at 23°C.)[1] While these transitions are in a favourable location in the spectrum because they are well resolved from the absorbance spectrum of the precursor and solvent, their relatively small extinction coefficients make them challenging to detect (*e.g.* $\varepsilon_{GeMe2\,(470nm)}$ = 730 ± 300 $M^{-1}cm^{-1}$; $\varepsilon_{GePh2\,(500nm)}$ = 1850 ± 400 $M^{-1}cm^{-1}$).[1, 9]

(2.7)
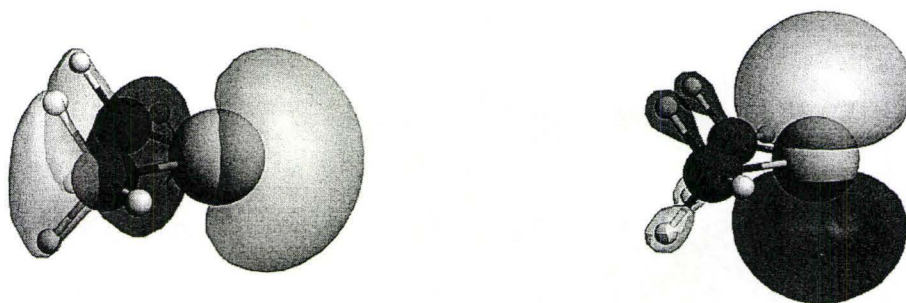
Figure 2.3. Dimethylgermylene ($GeMe_2$) HOMO (*left*) and LUMO (*right*). The figures were obtained by repeating the previously reported ADF calculation of $GeMe_2$ (PW91, TZDP, ZORA) in reference 1. Isosurface plotted at 0.044 a.u.

For germylenes (C_2 or C_{2v}) the *n,p* electronic transition is formally allowed;[10]

however, germylenes are hard to detect because the dipole-moment operator (μ), which is essentially a measure of the charge migration during the excitation, is small. The electron is being moved from one orbital to another on the same atom which does not result in a substantial migration of charge.

2.5.3. UV spectra of digermenes

For digermenes in the trans-bent geometry (C_{2h}), the π,π^* transition is also allowed. Relative to germylenes, there is a larger change in the transition moment μ resulting in a higher value of ε (e.g. Ge_2Ph_4 $\varepsilon_{440nm} > 6,000$ $M^{-1}cm^{-1}$ cf. $GePh_2 \approx 1850$ $M^{-1}cm^{-1}$)[1]. Digermenes can therefore be detected more easily at lower concentrations. Figure 2.4 shows the calculated HOMO and LUMO of $Me_2Ge=GeMe_2$ and also illustrates the trans-bent geometries common to disilenes, digermenes, and distannenes.
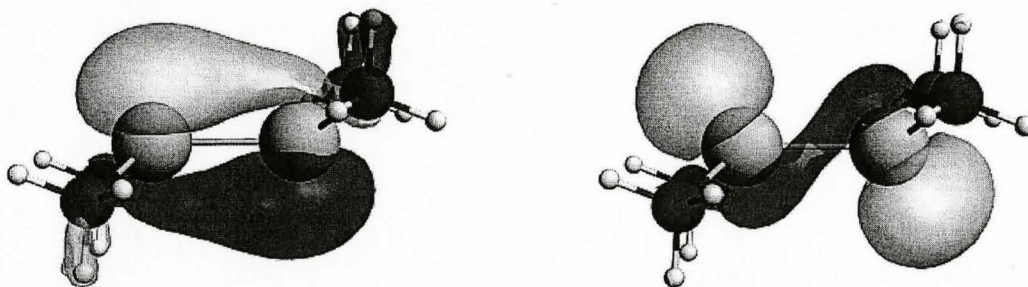
Figure 2.4. Tetramethyldigermene ($Me_2Ge=GeMe_2$) HOMO (*left*) and LUMO (*right*). The figures were obtained by repeating the previously reported ADF calculations of $Me_2Ge=GeMe_2$ (PW91, TZDP, ZORA) in reference 1. Isosurface plotted at 0.044 a.u.

2.5.4. UV spectra of germacyclopentenes

The UV spectra of **33a-g** are shown in Figure 2.5. Relative to the unsubstituted analogue **33a**, the benzenoid absorbance bands (the peaks *ca.* >245 nm) of **33b-g**: (1) are

more intense, (2) are red-shifted and (3) have less fine structure, as shown in Figure 2.5.
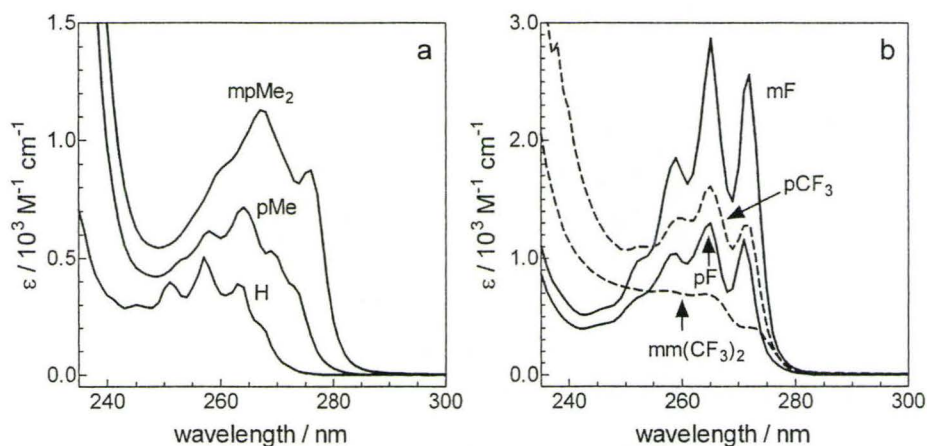
Figure 2.5. UV absorption spectra of (a) **33a,b,c** and (b) **33d,e,f,g** recorded in hexanes solution. Note the difference in the *y*-axis scales in the two graphs.

These changes are consistent with those observed in the UV spectrum of benzene upon substitution.[11] The lowest energy electronic transition of benzene ($^1B_{2u} \leftarrow \ ^1A_{1g}$) is symmetry forbidden but has a non-zero oscillator strength because of vibronic coupling. When the benzene ring is substituted, the symmetry of the molecule is lowered and the transition is no longer forbidden, yet the transition remains weak because of a small value of μ.[12] Benzene substitution leads to a red-shift regardless of the identity of the substituent;[13] upon substitution, the degeneracy of the HOMO and LUMO of benzene is lost and the gap HOMO-LUMO gap closes.[12, 14] Finally, the loss of fine structure implies a non-rigid excited state. It is believed that in the excited state, electronic energy is converted into vibrational energy of the substituents.[11] The loss of fine structure becomes greater as the ring becomes more highly substituted.

2.5.5. Laser flash photolysis

Laser flash photolysis (LFP) is a technique that employs a nanosecond-pulsed UV laser to generate a transient species, and fast time-resolved spectroscopy to detect it. In this work, UV-vis spectroscopy was the detection method employed. The UV absorbance at a given wavelength (corrected for the absorbance recorded prior to the laser pulse and therefore denoted ΔA) is monitored as a function of time. The absorbance (A) of the transient is related to its concentration (c) through the Beer-Lambert law (eq 2.8), where ε is the extinction coefficient and l is the distance the monitoring beam travels through the sample solution. The typical appearance of an absorbance-time profile recorded in a LFP experiment is shown in Figure 2.6. These data are used to determine absolute rate constants (k) for reactions of the transient species being monitored, a process that will be described in the next section.

$$A_\lambda = \varepsilon_\lambda cl \tag{2.8}$$
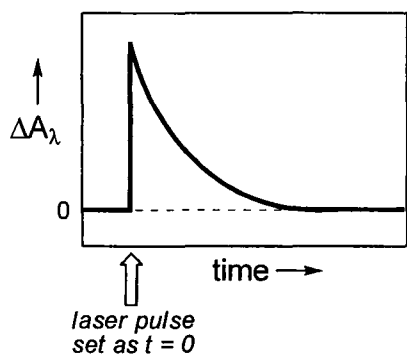
Figure 2.6. The general appearance of a transient decay profile recorded by LFP. A transient that is formed with the laser pulse manifests as a spike in the absorbance profile at $t = 0$.

2.6. Determination of rate and equilibrium constants by laser flash photolysis

This section addresses how data obtained from LFP experiments are analyzed in order to determine rate and equilibrium constants. Considered below are dimerization of the germylene and reaction of the germylene (or digermene) with a scavenger or quencher (Q). The latter has three commonly encountered scenarios:

(*i*) $K_{eq} > 25000$ M^{-1}, (*ii*) 1000 M$^{-1} < K_{eq} < 25000$ M^{-1} and (*iii*) $K_{eq} < 1000$ M^{-1}. Each of these will be discussed below.

Symbols used below:

[G] = germylene concentration at time t.   [G]$_0$ = initial germylene concentration
[G]$_e$ = germylene concentration at equilibrium [Q] = concentration of scavenger
[P] = product concentration at time t.   [P]$_e$ = product concentration at equilibrium
A = absorbance at time t.   A$_0$ = initial absorbance

2.6.1. Dimerization

In the absence of Q, the germylene dimerizes to the digermene. Dimerization is irreversible for the systems we study and can therefore be described by eq 2.9.[*] the integrated form of this equation is given in eq 2.10. Reorganization gives equation 2.11.

$$\frac{-d[G]}{dt} = 2k_{dim}[G]^2 \tag{2.9}$$

$$\frac{1}{[G]} = \frac{1}{[G]_0} + 2k_{dim}t \tag{2.10}$$

---

[*] The factor of 2 in this equation arises from the IUPAC convention of expressing an <u>elementary</u> reaction as: $aA + bB + \ldots \rightarrow pP + qQ + \ldots$, where $a,b,..,p,q$ are integers. The rate $\nu = (-1/a)\, d[A]/dt + \ldots = (1/p)d[P]/dt + \ldots$

$$[G] = \frac{[G]_0}{1 + 2k_{dim}[G]_0 t} \tag{2.11}$$

The experiment, however, measures absorbance and not concentration as is required by these equations. Substitution of concentration with absorbance (using eq 2.8) gives eq 2.12. The data are fit to this equation using a non-linear least-squares data fitting routine. Unless ε is known, we cannot determine k_{dim}. For $GePh_2$, ε_{500nm} has been measured and a value of the dimerization rate constant calculated ($k_{dim} = (1.2 \pm 0.2) \times 10^{10}$ M^{-1} s^{-1}).[1]

$$A = \frac{A_0}{1 + 2k_{dim}\left(\dfrac{A_0}{\varepsilon l}\right)t} \tag{2.12}$$

When a scavenger is added to the solution, a competition exists between dimerization and reaction with the scavenger. To address the kinetics of this scenario, consider the reversible reaction of G with Q to give a product (P) (eq 2.13a,b). The rate equation for the decay of the germylene is now described by eq 2.14. The concentration of Q in our experiments is always much higher than G so it may be regarded as constant and thus incorporated into k_Q (to give k_Q') (eq 2.15). Equation 2.15 can be further simplified by expressing the concentrations in terms of G only (eq 2.16).

$$G + G \xrightarrow{k_{dim}} G{=}G \tag{a}$$

$$G + Q \underset{k_{-Q}}{\overset{k_Q}{\rightleftharpoons}} P \tag{b}$$

(2.13)

$$\frac{-d[G]}{dt} = k_Q[G][Q] - k_{-Q}[P] + 2k_{dim}[G]^2 \tag{2.14}$$

$$\frac{-d[G]}{dt} = k'_Q[G] - k_{-Q}[P] + 2k_{dim}[G]^2 \tag{2.15}$$

$$\frac{-d[G]}{dt} = (k'_Q + k_{-Q})([G] - [G]_e) + 2k_{dim}[G]^2 \tag{2.16}$$

Kinetic simulations (KinTekSim 2.03)[15] were used to model the decay of the germylene at various values of k_Q and k_{-Q} from the scheme shown in eq 2.13. (These simulations are similar to ones previously reported by our group.[16]) In addition, the formation of the digermene was examined under these conditions with rate constants added to account for the reaction of the digermene with Q as well as digermene dimerization. The objective was to demonstrate how the relative values of the rate constants affect the appearance of the germylene decay trace. The appearance of the germylene decays will be discussed using three representative cases. The rate constants used in the simulations are listed in Table 2.2.

Table 2.2. Rate constants used in the kinetic simulations of the reaction of GeR_2 with Q.[a] Three representative cases have been chosen to represent the various types of germylene decays that are encountered in laser flash photolysis experiments.

	$k_Q / M^{-1} s^{-1}$	k_{-Q} / s^{-1}	K_{eq} / M^{-1} [b]
Irreversible (K_{eq} – large)	5×10^9	1×10^4	500,000
Reversible (K_{eq} – medium)	5×10^9	1×10^6	5,000
Reversible (K_{eq} – small)	5×10^9	1×10^8	50

a. dimerization rate constants for both the germylene and digermene were set at the diffusional rate constant in hexanes at 25 °C of 2.2×10^{10} $M^{-1}s^{-1}$, while reaction of the digermene with Q was set at 1×10^8 $M^{-1}s^{-1}$. b. $K_{eq} = k_Q/k_{-Q}$

2.6.2. "Irreversible" reactions: $K_{eq} > 25000$ M^{-1}.

In this situation, $k_Q \gg k_{-Q}$ and $[G]_e \sim 0$, so equation 2.16 simplifies to equation 2.17:

$$\frac{-d[G]}{dt} = k_Q'[G] + 2k_{dim}[G]^2 \tag{2.17}$$

At low [Q], a large portion of the decay of the germylene is a result of dimerization. At higher [Q], the decay is dominated by reaction with Q. At this point, the decay of the germylene fits well to the integrated rate equation for a pseudo-first-order reaction (eq 2.18), which yields the first-order decay coefficient (k_Q'). It is possible to directly substitute concentration with absorbance because the application of Beer's Law results in the cancellation of ε and l (eq 2.19).

$$[G] = [G]_0 e^{-k_Q' t} \tag{2.18}$$

$$A = A_0 e^{-k_Q' t} \tag{2.19}$$

The simulations for the irreversible reaction are shown in Figure 2.7. With the resolution of the instrument we are able to resolve the entire decay to "equilibrium" (which is essentially baseline when $K_{eq} > 25,000$ M^{-1}). A higher concentrations of Q, the germylene decays fit well to eq 2.18 because dimerization is suppressed – note how the digermene reaches its maximum yield more rapidly and that only sub-millimolar amounts of Q are required to produce a nearly static digermene concentration over the time window in which the germylene decay is recorded.
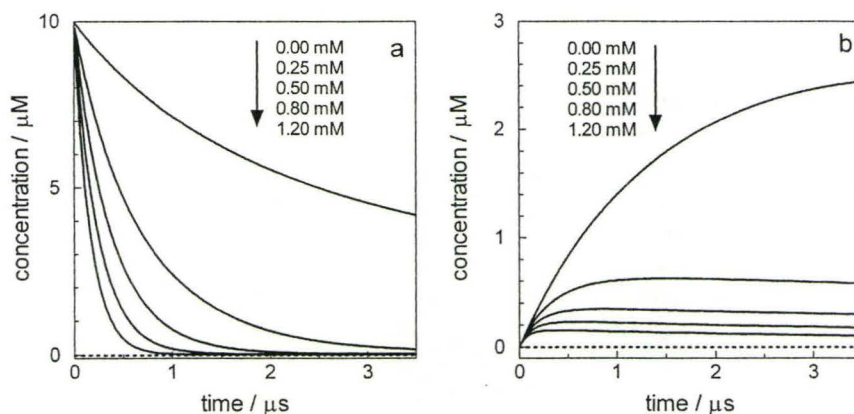
Figure 2.7. Simulated (a) germylene decay and (b) digermene growth profiles in the presence of various [Q] for a mechanism with a large K_{eq} (see text).

Because $k_Q' = k_Q[Q]$, a plot of k_Q' ($k_Q' \equiv k_{decay}$) vs. [Q] will yield a straight-line with slope k_Q provided the reaction is second-order overall, first-order in Q. In principle, the y-intercept should be zero; however, this would imply that in the absence of Q, the germylene does not decay. Decay in the absence of quencher occurs primarily because of dimerization but also because of reactions with trace impurities. The decay rate coefficient of the germylene at [Q] = 0 is labeled as k_0 and is the hypothetical pseudo-first-order rate constant for the decay of the germylene in the absence of scavenger. Thus the observed decay rate coefficient (k_{decay}) is described by eq 2.20.

$$k_{decay} \approx k_0 + k_Q[Q] \tag{2.20}$$

In cases where the reaction with Q is third-order overall, second order in Q, similar treatment of the data is valid because the concentration of Q is still constant over the duration of the transient decay. The difference is that now the plot of k_{decay} vs. [Q] will exhibit positive curvature (eq 2.21).

66

$$k_{\text{decay}} = k_0 + k_Q[Q]^2 \qquad\qquad (2.21)$$

2.6.3. Reversible reaction, intermediate K_{eq}: 1000 M^{-1} < K_{eq} < 25000 M^{-1}

When $K_{eq} < ca.$ 25000, neither k_{-Q} nor $[G]_e$ can be neglected, so equation 2.22 applies. Dimerization occurs during the time period in which the germylene decays are measured (see Figure 2.8); however, as [Q] increases, the contribution of dimerization to the germylene decay decreases, and the equation simplifies to that shown in eq 2.23, where k_{decay} is the rate coefficient for the approach to equilibrium.

$$\frac{-d[G]}{dt} = (k_Q' + k_{-Q})([G]-[G]_e) + 2k_{\text{dim}}[G]^2 \qquad\qquad (2.22)$$

$$\frac{-d[G]}{dt} = k_{\text{decay}}([G]-[G]_e) \qquad\qquad (2.23)$$

The observed decay is not to the baseline as it was in the previous case, but to a plateau the height of which is proportional to the concentration of germylene at equilibrium. A plot of k_{decay} vs. [Q] can therefore still be used to determine k_Q. (eq 2.24).

$$k_{\text{decay}} \approx k_0 + k_{-Q} + k_Q[Q] \qquad\qquad (2.24)$$
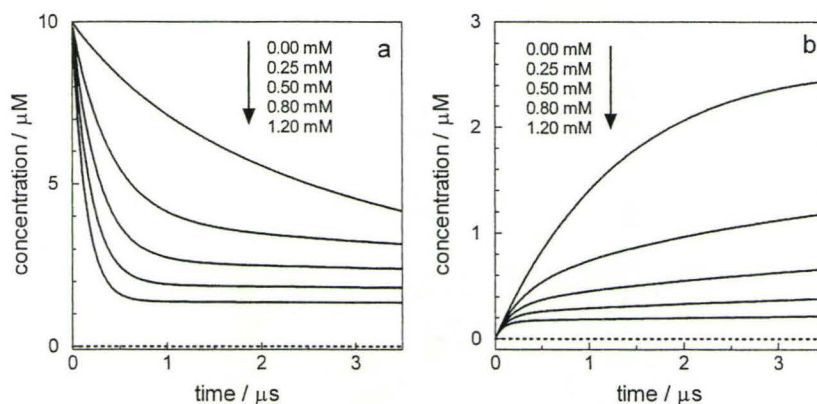
Figure 2.8. Simulated (a) germylene decay and (b) digermene growth profiles in the presence of various [Q] for a mechanism with intermediate values of K_{eq} (see text).

These data also allow the equilibrium constant to be determined. We know that the germylene concentration at equilibrium is proportional to the height of the plateau – a reasonable assumption given that the absorbance is roughly constant over the time scale monitored. The equilibrium concentration of the product is proportional to the difference between $A_0 - A_e$. The equation is set up as shown in eq 2.25 and rearrangement shows that a plot of A_0/A_e vs. [Q] should be linear with slope K_{eq} and y-intercept of 1 (eqs 2.26-2.27).

$$K_{eq} = \frac{(A_0 - A_e)}{A_e[Q]} \tag{2.25}$$

$$K_{eq}[Q] = \frac{A_0}{A_e} - \frac{A_e}{A_e} \tag{2.26}$$

$$\frac{A_0}{A_e} = K_{eq}[Q] + 1 \tag{2.27}$$

2.6.4. Reversible reaction, low K_{eq}: $K_{eq} < 1000$ M^{-1}.

As the reaction becomes more unfavourable, the behaviour of the germylene is much different than in the two scenarios described above. In this situation, addition of small concentrations of scavenger has almost no noticeable effect on the germylene decays when compared to the other scenarios at the same concentration of scavenger (Figure 2.9). This is largely a result of the fact that the difference between $[G]_0$ and $[G]_e$. is much smaller than it is in the other scenarios. Recall that the forward rate constant does not vary between these scenarios. Much larger concentrations are required before a noticeable change is observed and even in these cases it is difficult (usually impossible) to resolve the approach of the germylene to equilibrium and thus k_{decay} cannot be accurately measured. Instead what is observed is a decrease in the apparent initial maximum absorbance of the germylene. To calculate K_{eq}, the same equations used in the previous case are used (eq 2.25-2.27), except that the initial absorbance maximum in the absence of Q is taken to be the initial absorbance maximum at each concentration of Q.
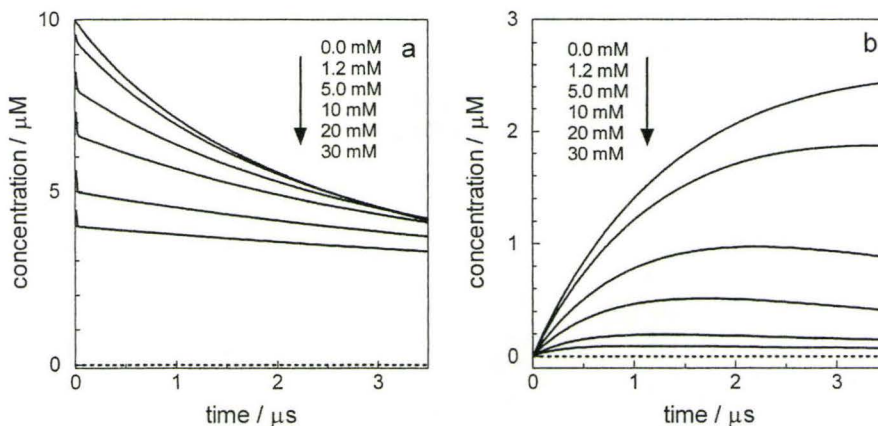
Figure 2.9. Simulated (a) germylene decay and (b) digermene growth profiles in the presence of various [Q] for a mechanism with low values of K_{eq} (see text).

2.7. Transient absorption spectra of 33a-f in hexanes. [†]

Comprehensive photochemical studies of **33a** were reported by Leigh,

Harrington, and Vargas-Baca in 2004.[1] Laser flash photolysis of **33a** (ca. 3 mM) in

hexanes leads to the immediate formation of diphenylgermylene (**Ga**; λ_{max} = 500, 300

nm) which then undergoes dimerization to tetraphenyldigermene (**DGa**; λ_{max} = 440, 290

nm) as shown in Figure 2.10. Assignment of the absorbance maxima of the germylene

and digermene was not straightforward – the photochemistry of the molecule was studied

in detail, as was the behaviour of these transients in the presence of various substrates.

Computational studies also support the identification. Several groups previously reported

transient UV-vis spectra assigned to $GePh_2$ in solution,[17-21] although there is a lack of

---

[†] The laser flash photolysis transient spectra of **33g** are different from the others and are instead discussed at the end of this chapter.

consistency in these data primarily because the precursors employed led to the formation

of additional transient products that complicated the interpretation of the UV spectra.
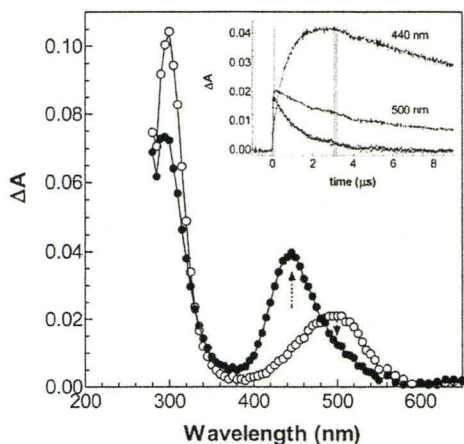
Figure 2.10. Transient absorption spectra from laser flash photolysis of a 3 mM solution of **33a** in dry, deoxygenated hexanes at 23°C recorded 55-170 ns (○) and 3.0-3.2 μs (●) after the 248 nm laser pulse. The inset shows the transient absorbance-time profiles recorded at 500nm and 440nm, while the unlabelled trace is $\Delta A_{500}-0.25\times\Delta A_{440}$. *(Reprinted from reference 1 with permission. © 2004 American Chemical Society.)*

Compounds **33a-f** have very similar transient UV-vis spectra (see Figure 2.11);

however, there is some variation between the substituted analogues in the long

wavelength absorbance bands, particularly with the germylenes (see Table 2.3). The

largest change was detected with the *para*-fluoro analogue. To determine whether this

shift was caused by complexation of the fluorine atoms of the precursor with the

germylene, the transient absorption spectrum of **33d** was recorded using 193 nm laser

excitation. Under these conditions, a much lower concentration of the

germacyclopentene is required (*ca.* 30 μM, ca. one thousand times lower than with 248

nm excitation). The spectra were similar to that recorded at higher precursor

concentrations, indicating that the spectral shift observed for this analogue cannot be

ascribed to complexation with the precursor. The magnitude of these spectral shifts

correlates weakly with the inductive electron-withdrawing ability (as characterized by the

F values)[22] although the slope of the Hammett plot is negligible ($\rho = +0.03 \pm 0.01$; $r^2 =$

0.855) from a plot of log (E_{max} / eV) vs. F, where $E_{max} = (1240$ eV / nm$)(\lambda$ /nm$)^{-1}$.

Table 2.3. Lowest energy UV-Vis transition (nm) of germylenes **Ga-f** and digermenes
DGa-f in hexanes.[a]

	$GeAr_2$	$Ar_2Ge=GeAr_2$
a (H)	500 ± 10	440 ± 5
b (m,p-Me$_2$)	500 ± 10	450 ± 5
c (p-Me)	495 ± 10	440 ± 5
d (p-F)	480 ± 10	440 ± 5
e (m-F)	485 ± 10	440 ± 5
f (p-CF$_3$)	490 ± 10	440 ± 5

a. Errors estimated based on how easily the wavelength of highest intensity for each transient can be
discerned. Spectra were recorded in 5 nm intervals.
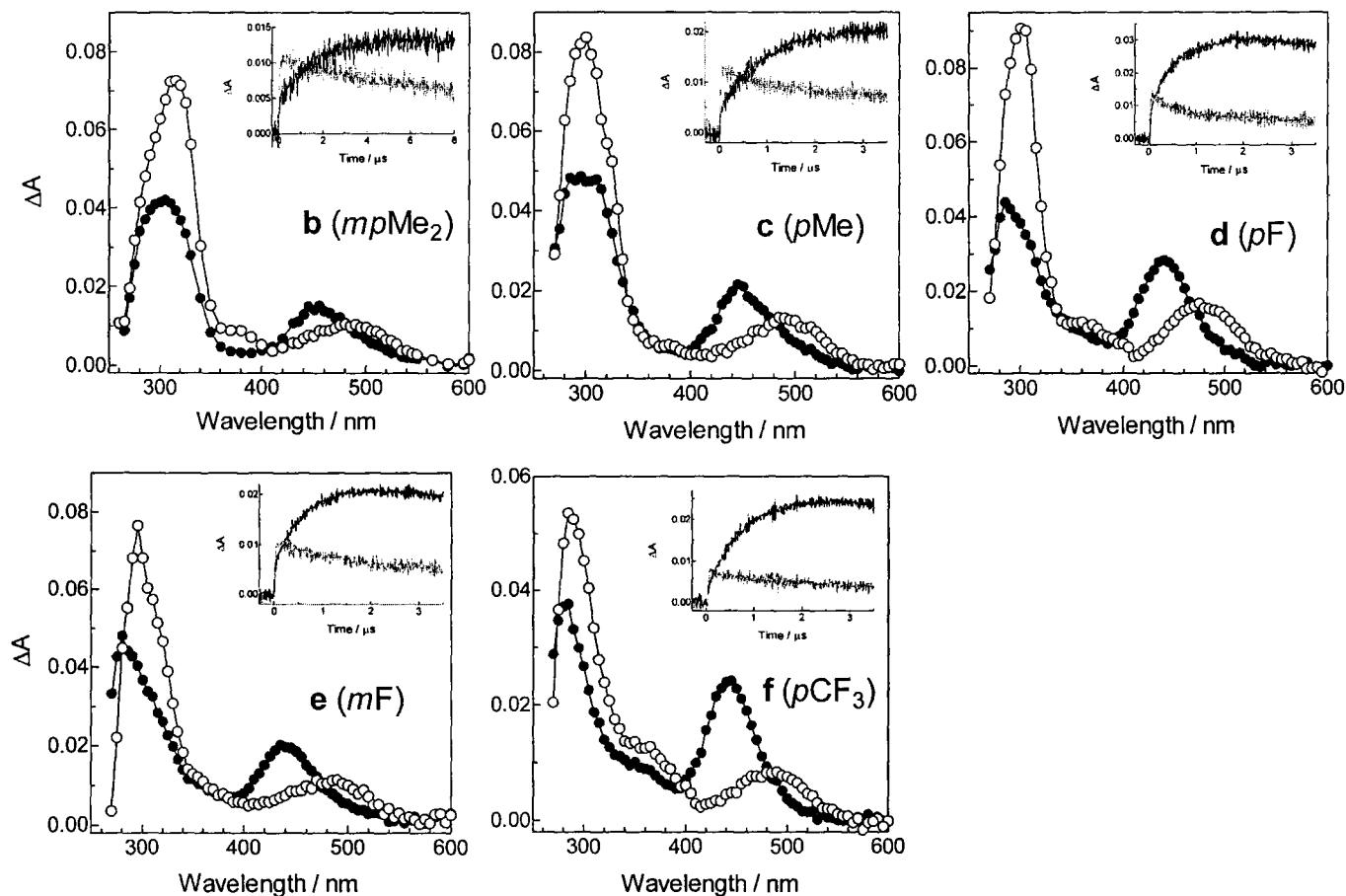
Figure 2.11. Transient absorption spectra from laser flash photolysis of **33b-f** (ca. 3 mM in hexanes) . The spectra labeled with ○ were recorded over the following time windows after the laser pulse: **b** 160-480 ns; **c** 77-96 ns; **d** 35-100 ns; **e** 58-90 ns; **f** 60-120 ns. The spectra labeled with ● were recorded over the following time windows after the laser pulse: **b** 7.20-7.70 μs; **c** 3.42-3.46 μs; **d** 3.56-3.58 μs; **e** 3.10-3.13 μs; **f** 3.46-3.48 μs. The insets show the absorbance-time profiles recorded at 500 nm (gray) and 440 nm (black). (*Spectra of **33b** recorded by S. Chitnis*)

2.8. Estimation of the dimerization rate constants (k_{dim}) of Ga-f in hexanes.

It is clear from Figure 2.11 that there is significant overlap of the germylene and digermene spectra; in fact the overlap is severe enough that it is impossible to isolate the transient decay profiles of the germylenes from those due to the digermene at any monitoring wavelength in the 300-530 nm range. To calculate the dimerization rate constants (k_{dim}) of the germylenes from the decay profiles (typically monitored at 500 nm), the contribution of the digermene to that signal must be subtracted so the 500 nm decay accurately represents the change in concentration of the germylene alone. To remove the underlying contribution of the growing absorbance of the digermene to the 500 nm decay, the relative extinction coefficients of the digermene at 440 nm (the wavelength at which the digermene is monitored) and 500 nm must be determined so that the correction shown in eq 2.28 can be applied.

$$\Delta A_{500\text{-corr}} = \Delta A_{500} - \Delta A_{440} \left(\frac{\varepsilon_{500-digermene}}{\varepsilon_{440-digermene}} \right) \tag{2.28}$$

The ratios $\varepsilon_{500}/\varepsilon_{440}$ for the digermenes **DGa-f** were determined by recording transient absorption spectra of solutions of **33a-f** (ca. 3 mM in hexane) containing 5-15 mM THF. In the presence of THF, the germylene forms a Lewis acid-base complex **37**, the absorbance maximum of which is *ca.* 360 nm (this will be discussed in more detail in Chapter 3). In the presence of these low concentrations of THF, the equilibrium shown in eq 2.29 is sufficiently shifted to the products that the free germylene is no longer

detectable, yet the digermene still forms.[23]

$$GeR_2 \ + \ O\hspace{-0.3em}\bigcirc \ \underset{k_{-1}}{\overset{k_1}{\rightleftharpoons}} \ R_2Ge \leftarrow O\hspace{-0.3em}\bigcirc \ \xrightarrow{\ \times 2\ } \ R_2Ge{=}GeR_2 \ + \ 2\,THF \hspace{3em} (2.29)$$

$$\mathbf{37}$$
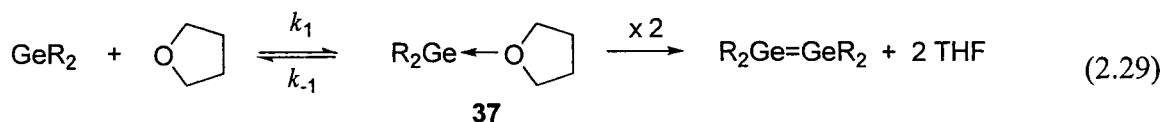
Figure 2.12 shows the spectrum of **33c** wherein the absorbance maximum of the corresponding complex **37c** is $\lambda_{max} = 360$ nm. Approximately 3.5 µs after the laser pulse, the digermene concentration reaches a maximum; therefore the spectrum recorded 3.55–3.57 µs after the laser pulse was used to calculate the relative digermene extinction coefficients by dividing the ΔA values at 440 and 500 nm. The resulting extinction coefficient ratios are listed in Table 2.4.
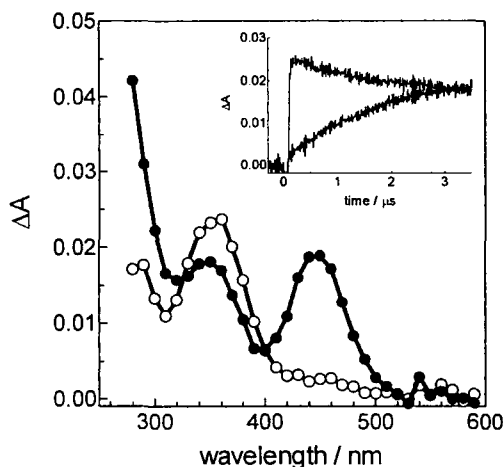
Figure 2.12. Transient absorption spectra from laser flash photolysis of a solution of **33c** (3 mM in hexanes) containing 13 mM THF (o) 122-147 ns and (●) 3.55-3.57 µs after the laser pulse. The inset shows absorbance-time profiles recorded at 360 nm (gray) and 440 nm (black).

Table 2.4. Ratio of the extinction coefficients (ε) of tetraaryldigermrenes **DGa-f** at 500 nm and 440 nm.

DG	$\varepsilon_{500nm}/\varepsilon_{440nm}$ [a]	**DG**	$\varepsilon_{500nm}/\varepsilon_{440nm}$ [a]
a (H)	0.15 [b]	**d** (p-F)	0.11
b (m,p-Me$_2$)	0.17	**e** (m-F)	0.12
c (p-Me)	0.15	**f** (p-CF$_3$)	0.14

a. Error estimated at ±0.02. *b*. Reference 1.

Using these extinction coefficient ratios and eq 2.28, the decays of **Ga-f** were corrected to remove the underlying digermene absorbance. The corrected decays are the unlabeled absorbance-time profiles shown in each of the graphs in Figure 2.13. These corrected decays were analyzed according to equation 2.12, yielding the solid (best-fit) lines in Figure 2.13. Equation 2.12 has two unknowns, ε and k_{dim}, so it is not possible to determine k_{dim} without knowing ε. Therefore only the ratio k_{dim}/ε can be calculated from analysis of the decay (Table 2.5).

Table 2.5. $k_{dim}/\varepsilon_{500nm}$ and k_{dim} for the dimerization of diarylgermylenes (**Ga-f**) to the corresponding tetraaryldigermenes (**DGa-f**) in hexanes. The latter was calculated assuming ε_{500nm} **Gb-f** = ε_{500nm} **Ga**.

DG	$k_{dim}/\varepsilon_{500nm}$ / 10^6 cm s^{-1}	k_{dim} / 10^{10} M^{-1}s^{-1}
a (H)	9 ± 2	1.7 ± 0.8
b (mp-Me$_2$)	4 ± 1	0.7 ± 0.2
c (p-Me)	8 ± 2	1.5 ± 0.8
d (p-F)	28 ± 8	5 ± 3 [a]
e (m-F)	21 ± 2	4 ± 1 [a]
f (p-CF$_3$)	28 ± 8	5 ± 3 [a]

a. Exceeds the diffusion limit: $k_{diff-hexanes}$ = 2.2 × 10^{10} M^{-1}s^{-1} at 25 °C.[24]

The extinction coefficient for GePh$_2$ at 500 nm is ε_{500nm} = 1850 ± 400 M^{-1}cm^{-1} [(1)] and the value of k_{dim} measured in this experiment is in agreement with the previously reported value.[1] The extinction coefficients for the germylenes **Gb-f** were not

determined. If we assume the extinction coefficients of **Gb-f** are similar to **Ga** (based on the similar Φ_{GeAr2} and $\Delta A_{500nm-max}$ values) the k_{dim} values for the more electron-poor germylenes can be seen to have somewhat faster dimerization rate constants, although clearly there are problems with this assumption because some of the k_{dim} values exceed the diffusion limit.
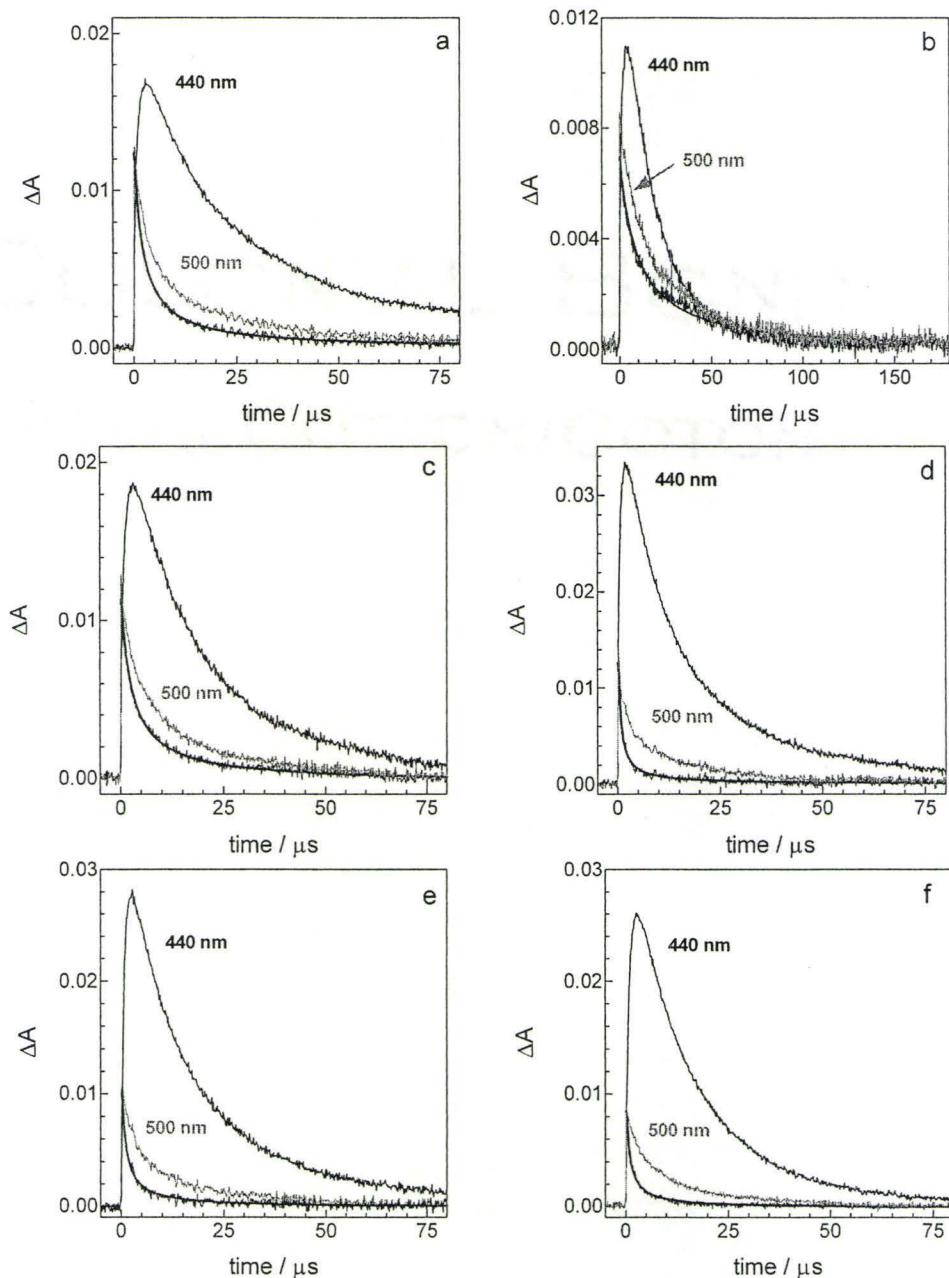
Figure 2.13. Absorbance-time profiles recorded at 440 nm and 500 nm by 248 nm laser flash photolysis of solutions of **33a-f** (ca. 3 mM) in hexanes. The lower, unlabelled traces are the corrected 500 nm decays, obtained by scaled subtraction of the 440 nm trace from the 500 nm one; the solid lines are the best fits of the data to eq 2.12.

2.9. Laser Flash Photolysis of 33g

The general appearance of a transient absorption spectra of a germacyclopentene recorded in the presence of a Lewis base was given in Figure 2.12. With this in mind, we can now discuss the transient absorption spectra of **33g** shown in Figure 2.14, which are different from those obtained with the other derivatives **33a-f**. Immediately after the laser pulse, one transient is formed (λ_{max} = 470 nm, $\tau \approx$ 200 ns) whose absorbance maximum is consistent with those observed with **Ga-f**; however, this germylene is much shorter lived than the other analogues and its decay gives rise to a second transient (λ_{max} = 350 nm, $\tau \approx$ 10 µs) whose absorbance maximum is similar to that observed with the other analogues in the presence of *O*-donors. The 350 nm transient decays over several microseconds, with the concomitant formation of a third transient (λ_{max} = 440 nm).
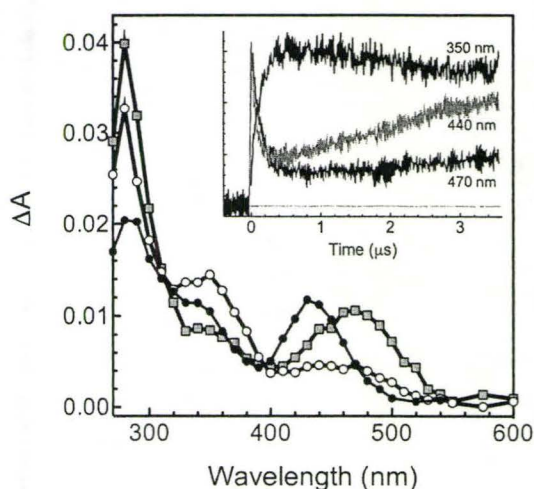
Figure 2.14. Transient absorption spectra of **33g** (3 mM) in hexanes recorded 58- 70 ns (■), 0.32-0.34 µs (○) and 9.6-9.9 µs (●) after the laser pulse. The inset shows the transient absorbance vs. time profiles recorded at 470 nm, 440 nm, and 350 nm. *(Reprinted from reference 25 with permission. © 2008 American Chemical Society.)*

The presence of four *m*-CF$_3$ groups in germylene **Gg** makes it the most electrophilic analogue in the series and thus potentially the most sensitive to traces of water or other Lewis base impurities. We initially suspected that the 350 nm transient

could be a complex between **Gg** and **33g** (either with the fluorine atoms or the C=C

bond), but experiments performed at lower concentrations of **33g** (0.5 mM; typical

concentration is 3 mM) resulted in weaker signals, as expected, but did not lead to

significant changes in the appearance or behaviour of the three transients. Despite

rigorous efforts to dry the solvent and remove other impurities, we were unable to

eliminate the formation of the 350 nm transient. Although we cannot conclusively

identify this transient, a reversibly formed complex between an impurity and **Gg** seems

most probable. The absorbance maximum and growth kinetics of the 440 nm transient

suggest the most reasonable assignment is the corresponding digermene **DGg** (eq 2.30).

$$\textbf{33g} \xrightarrow[\text{hexanes}]{h\nu} \underset{\text{(470 nm)}}{\text{GeAr}_2} \rightleftharpoons \underset{\text{(350 nm)}}{\text{complex ?}} \xrightarrow{\text{x 2}} \underset{\text{(440 nm)}}{\text{Ar}_2\text{Ge}=\text{GeAr}_2} \qquad (2.30)$$

$$\qquad\qquad\qquad \textbf{Gg} \qquad\qquad\qquad\qquad\qquad\qquad \textbf{DGg}$$
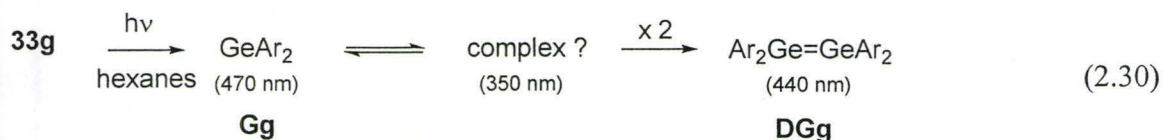
2.10. Summary

Compounds **33a-g** were synthesized from the reaction of two equivalents of an

aryl-Grignard reagent with **35**; variations in the UV spectra of **33a-g** were consistent with

those changes expected upon substitution of a benzene ring. Quantum and chemical

yields for the photochemical extrusion of the aryl substituted germylenes (**Ga-g**) and

DMB from the corresponding germacyclopentenes **33a-g** were measured in C_6D_{12}

solution by trapping the germylene with methanol (**36**). The quantum yields for the

extrusion of **Ga-g** are the same within experimental error ($\Phi \approx 0.5$), while the chemical

yields ranged from 77-88%. No other products could be detected in any case.

80

Laser flash photolysis of **33b-f** in hexanes leads to the prompt formation of the corresponding diarylgermylene (**Gb-f**; λ_{max} = 470-500 nm) which then undergoes dimerization to the corresponding tetraaryldigermene (**DGb-f**; λ_{max} ≈ 440 nm). These results are similar to those previously reported for **33a**.[25] There are only minor variations in the absorbance maxima of **Gb-f** and **DGb-f** with substituent. Although the dimerization rate constants were not explicitly determined, the k_{dim}/ε values suggest that the most electrophilic germylenes dimerize most rapidly. The laser flash photolysis behaviour of **33g** is somewhat different from the others in that the germylene has a much shorter lifetime and its decay leads to an intermediate transient product whose absorbance maximum (λ_{max} = 350 nm) is similar to those observed with the other germylenes in the presence of *O*-donors. This 350 nm transient is thus presently assigned to a Lewis acid-base complex between the germylene and an impurity and its decay gives rise to **DGg**.

2.11. References

1. Leigh, W. J.; Harrington, C. R.; Vargas-Baca, I. *J. Am. Chem. Soc.* **2004**, *126*, 16105. (Errata: *J. Am. Chem. Soc.* **2006**, *128*, 1394.).
2. Kolesnikov, S. P.; Rogozhin, I. S.; Nefedov, O. M. *Izv. Akad. Nauk SSSR, Ser. Khim. (Eng. trans.)* **1974**, 2379.
3. Massol, M.; Rivière, P.; Barrau, J.; Satgé, J. *C. R. Acad. Sci., Ser. IIc* **1970**, *270*, 237.
4. Huck, L. A.; Leigh, W. J. *Organometallics* **2007**, *26*, 1339.
5. Labhart, H.; Heinzelmann, W. *Chem. Phys. Lett.* **1969**, *4*, 20.
6. Bonneau, R.; Wirz, J.; Zuberbuhler, A. D. *Pure Appl. Chem.* **1997**, *69*, 979.
7. Toscano, J. P. *Adv. Photochem.* **2001**, *26*, 41.
8. Hamaguchi, H.; Gustafson, T. L. *Annu. Rev. Phys. Chem.* **1994**, *45*, 593.
9. Leigh, W. J.; Lollmahomed, F.; Harrington, C. R. *Organometallics* **2006**, *25*, 2055.
10. Orchin, M.; Jaffé, H. H., *Symmetry, Orbitals, and Spectra.* John Wiley & Sons: New York, 1971; p 204.

11.   Jaffé, H. H.; Orchin, M., *Theory and Applications of Ultraviolet Spectroscopy*. John Wiley and Sons: New York, 1962; p 242.

12.   Goodman, L.; Ross, I. G.; Shull, H. *J. Chem. Phys.* **1957**, *26*, 474.

13.   Doub, L.; Vandenbelt, J. M. *J. Am. Chem. Soc.* **1947**, *69*, 2714.

14.   Matsen, F. A. *J. Am. Chem. Soc.* **1950**, *72*, 5243.

15.   Barshop, B. A.; Wrenn, R. F.; Frieden, C. *Anal. Biochem.* **1983**, *130*, 134.

16.   Leigh, W. J.; Harrington, C. R. *J. Am. Chem. Soc.* **2005**, *127*, 5084.

17.   Mochida, K.; Wakasa, M.; Nakadaira, Y.; Sakaguchi, Y.; Hayashi, H. *Organometallics* **1988**, *7*, 1869.

18.   Konieczny, S.; Jacobs, S. J.; Braddock Wilking, J. K.; Gaspar, P. P. *J. Organomet. Chem.* **1988**, *341*, C17.

19.   Mochida, K.; Yoneda, I.; Wakasa, M. *J. Organomet. Chem.* **1990**, *399*, 53.

20.   Mochida, K.; Adachi, M.; Wakasa, M.; Hayashi, H. *Phosph. Sulf. Sil. Rel. Elem.* **1999**, *150-151*, 237.

21.   Leigh, W. J.; Toltl, N. P.; Apodeca, P.; Castruita, M.; Pannell, K. H. *Organometallics* **2000**, *19*, 3232.

22.   Hansch, C.; Leo, A.; Taft, R. W. *Chem. Rev.* **1991**, *91*, 165.

23.   Leigh, W. J.; Lollmahomed, F.; Harrington, C. R.; McDonald, J. M. *Organometallics* **2006**, *25*, 5424.

24.   Murov, S. L.; Carmichael, I.; Hug, G. L., *Handbook of Photochemistry*. Dekker: New York, 1993.

25.   Leigh, W. J.; Potter, G. D.; Huck, L. A.; Bhattacharya, A. *Organometallics* **2008**, *27*, 5948.

Chapter 3 – Reactions of Diarylgermylenes with Acetic Acid and Other Lewis Bases and the Effect of Lewis Acid-Base Complexation on Germylene Reactivity

3.1. Overview

This chapter presents the results from our initial mechanistic studies of germylene reactivity. At the time of the study only four analogues had been synthesized, the parent (H, **33a**) and the p-Me (**33c**), p-F (**33d**), and p-CF$_3$ (**33f**) analogues. We first looked at the Lewis acid-base complexation of germylenes **Ga,c,d,f** with tetrahydrofuran (THF) to form the corresponding complexes **37a,c,d,f** (eq 3.1). The rate constant for the reaction of GePh$_2$ with THF is $k_{THF} = (6.3 \pm 0.6) \times 10^9$ M^{-1}s^{-1}, while the equilibrium constant is $K_{eq} = (23 \pm 5) \times 10^3$ M^{-1},[1] so the results of this experiment would provide the first indication of whether our hypothesis that the rate and equilibrium constants should be sensitive to aromatic substitution is correct. Given that the reaction is a simple Lewis acid-base complexation, the prediction is that both k_Q and K_{eq} should increase with increasing electron withdrawing ability of the substituents. We would also learn through this study whether the spectra of the corresponding complexes are sensitive to polar-ring substituents.

$$\text{GeAr}_2 \;+\; \text{O}\langle\text{ring}\rangle \;\rightleftharpoons\; \text{Ar}_2\text{Ge} \leftarrow \text{O}\langle\text{ring}\rangle \qquad \textbf{37a,c,d,f} \qquad (3.1)$$
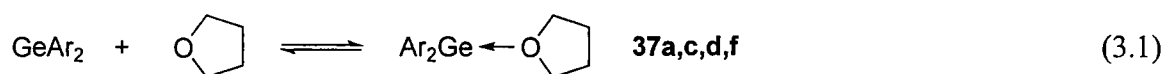
We then examined the reactions of **Ga,c,d,f** with diethylamine (HNEt$_2$). The rate constant for the reaction of GePh$_2$ with HNEt$_2$ is $k_{HNEt2} = 7.3 \times 10^9$ M^{-1}s^{-1}, while the equilibrium constant to form the germylene/amine complex (**38**) is too large to be accurately measured by LFP under the conditions of our experiments ($K_{eq} > 2.5 \times 10^4$ M$^-$

^{1}).^{2} It has been proposed that the NH insertion product (*e.g.* **39**) forms from the reaction of germylenes with amines and this study may be able to provide mechanistic details about the complexation and NH insertion steps (eq 3.2).

$$GeAr_2 \;+\; HNEt_2 \;\rightleftharpoons\; \underset{\textbf{38}}{Ar_2Ge \leftarrow N(H)Et_2} \;\overset{?}{\longrightarrow}\; \underset{\textbf{39}}{Ar_2\overset{H}{\underset{NEt_2}{Ge}}} \qquad (3.2)$$
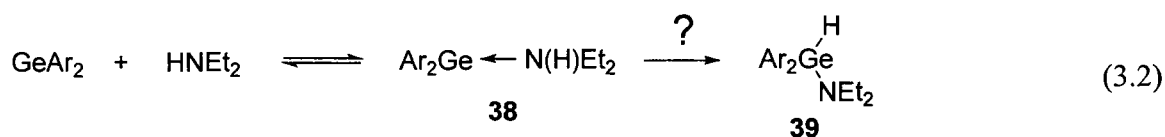
The reaction of diarylgermylenes with acetic acid yields the OH insertion product **40** (eq 3.3). The rate constant for the reaction of GePh$_2$ with HOAc is $k_{HOAc} = (3.9 \pm 0.7) \times 10^9 \, M^{-1}s^{-1}$.^{2} In principle, three mechanisms are possible for the reaction: (i) concerted OH insertion, (ii) complexation followed by proton transfer, and (iii) protonation followed by ion-pair combination. No evidence of a Lewis acid-base complex between the acid and germylene could be detected in the preliminary study.^{2}

$$GeAr_2 \;+\; MeCO_2H \;\longrightarrow\; \underset{H}{Ar_2Ge} \overset{O}{\underset{}{\diagdown}} \overset{O}{\diagup\!\diagdown} \quad \textbf{40} \qquad (3.3)$$
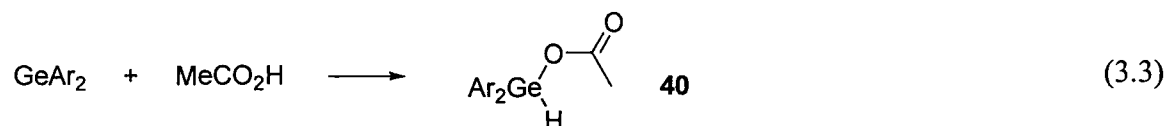
The final section of this chapter outlines my contribution to our group's initial studies of the reactivity of diarylgermylenes in the solvents THF and MeOH, where the reactive species is the corresponding Lewis acid-base complex **37** and **44**, respectively. These results build on the significant amount of data obtained by our group on the reaction of GeMe$_2$ and GePh$_2$ with THF and MeOH in hexane solution,^{1} and the results presented in the first part of this chapter on the reaction of **Ga,c,d,f** with THF in hexanes solution.

3.2. Complexation of Diarylgermylenes with THF in Hexanes.

In the presence of millimolar concentrations of THF, the decays of **Ga,c,d,f** are bimodal, exhibiting an initial rapid decay component and residual absorbance (*e.g.* Figure 3.1). At the same concentration of added THF, the intensity of the residual absorbance or plateau varied throughout the series with the most electron-rich germylenes exhibiting the highest plateau (Table 3.1). The bimodal form of the germylene decay in the presence of THF in which the plateau is non-zero is consistent with an equilibrium constant in the range of $1000 < K_{eq} < 25000 \text{ M}^{-1}$ (see Chapter 2). Equilibrium constants were estimated from the decays using eq 2.26, after correcting for the underlying contribution of the digermene to the germylene signal (Table 3.1). The (single) decay recorded for each of the substituted analogues was fit to first-order kinetics (eq 2.19), affording $k_{THF} \approx 1 \times 10^{10} \text{ M}^{-1}\text{s}^{-1}$ for each of the four germylenes. Based on these limited data we conclude that the forward rate constant is insensitive to aromatic substitution, as might be expected based on the magnitude of the rate constant. In each case, a new absorbance (λ_{max} ca. 360 nm) was observed to grow in on a similar time scale as the decay of the germylene absorbance. The absorbance maximum of the new transient did not vary significantly with substituent (Table 3.1).
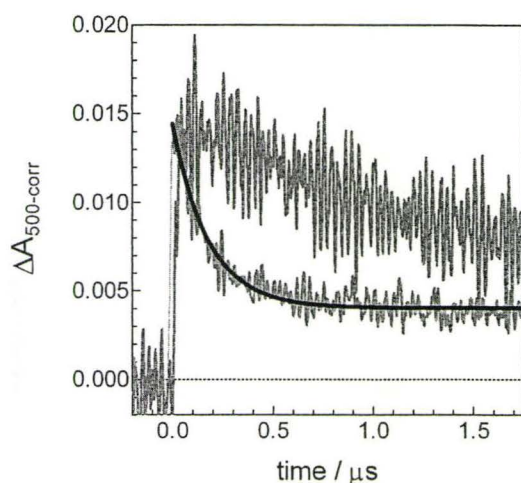
Figure 3.1. Corrected transient decay profiles of **Gc** (*p*-Me) in hexanes containing 0 mM (upper) and 0.50 mM (lower) THF. The solid line is the non-linear least squares fit of the data to first-order kinetics, according to eq 2.19.

Table 3.1. The concentration of THF, the resulting $\Delta A_0/\Delta A_{res}$ from the **Ga,c,d,f** transient decay profiles, and corresponding equilibrium constants for the complexation of **Ga,c,d,f** with THF. The absorbance maxima of **37a-f** in hexanes.

G	[THF] / mM	$\Delta A_0/\Delta A_{res}$	K_{eq} / 10^3 M^{-1}	37 λ_{max} / nm [a]
a (H)	0.40	7.5 ± 0.6	16 ± 3	355 ± 10 [b]
b (*mp*-Me$_2$)	-	-	-	370 [c]
c (*p*-Me)	0.50	3.6 ± 0.2	5 ± 1	355 ± 10
d (*p*-F)	0.35	8.4 ± 1.0	21 ± 4	345 ± 10
e (*m*-F)	-	-	-	345 ± 10
f (*p*-CF$_3$)	0.35	29 ± 12	> 25	350 ± 10

a. Obtained from spectra recorded in hexanes containing concentrations of THF (5-15 mM) at which the germylene could no longer be detected. *b*. Reference 1. *c*. shoulder.

The corrected absorbance-time profiles of the germylenes **Ga,c,d,f** in the presence of THF are consistent with reversible reaction of the germylenes with the ether to yield the corresponding GeAr$_2$-THF complex (**37**), as previously reported for the parent germylene GePh$_2$.[1] The forward rate constants were found to be insensitive to aromatic substituents, while the most electron-poor germylene exhibits the largest equilibrium constant. A linear Hammett correlation with K_{eq} was observed ($\rho_{Keq} = +1.3 \pm 0.2$; Figure

3.2) and these results confirm that the germylene does indeed play the role of the electrophile. Because the forward rate constant does not change with substituent ($\rho_{kf} \approx 0$), it is necessarily the reverse rate constant that is sensitive to substituent ($\rho_{kr} = -1.3 \pm 0.2$, as shown by eq 3.4. The dissociation of **37** occurs more rapidly with more electron-rich germylenes because the increased charge density at germanium destabilizes the complex (eq 3.5).

$$\log K_{eq} = \log\left(\frac{k_f}{k_r}\right) = \sigma\rho_{K_{eq}}$$
$$\log k_f - \log k_r = \sigma\rho_{K_{eq}} \tag{3.4}$$
$$\sigma\rho_{k_f} - \sigma\rho_{k_r} = \sigma\rho_{K_{eq}}$$
$$\rho_{k_f} - \rho_{k_r} = \rho_{K_{eq}}$$
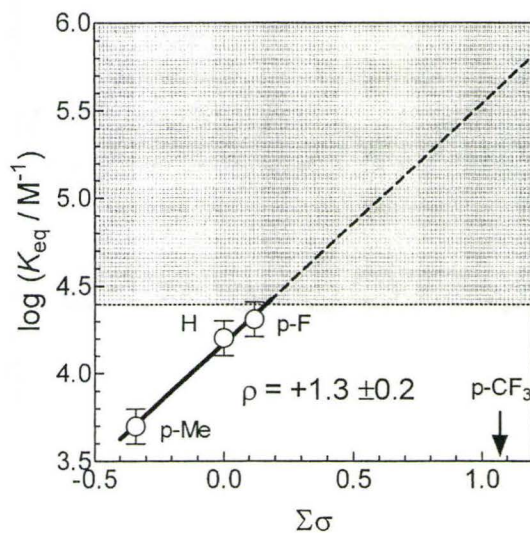
Figure 3.2. Hammett plot of the equilibrium constants for the Lewis-acid base complexation of $GeAr_2$ with THF in hexanes. The shaded area defines the range in which K_{eq} is too large to be measured with our system.

$$(3.5)$$
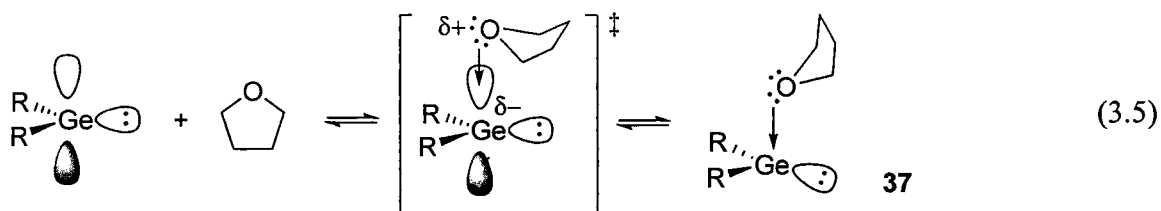
The effect of temperature on the equilibrium between GePh$_2$ and **37** was also investigated. Increasing the temperature did not have any detectable effect on the forward rate constant. At 60°C, the equilibrium constant was found to be $K_{eq} = (3,100 \pm 200)$ M^{-1}, as shown in Figure 3.3. This value is significantly smaller than the equilibrium constant measured at 25 °C ($K_{eq} = (16,000 \pm 3,000)$ M^{-1}). Using the equilibrium constants at these two temperatures, the van't Hoff equation (eq 1.48) was used to determine the thermodynamic parameters of the reaction. The enthalpy of complexation is $\Delta H = -11 \pm 2$ kcal/mol. The bond enthalpy for Ge-O covalent single bond is ca. -85 kcal/mol,[3] so clearly the interaction between the oxygen and germanium in **37** is quite weak, assuming the Ge-O interaction is the only change in bonding that takes place during the reaction. The entropy of complexation is $\Delta S = -24 \pm 5$ cal/K/mol. The negative value is reasonable because of the reduction in the degrees of freedom proceeding from reactants to product.
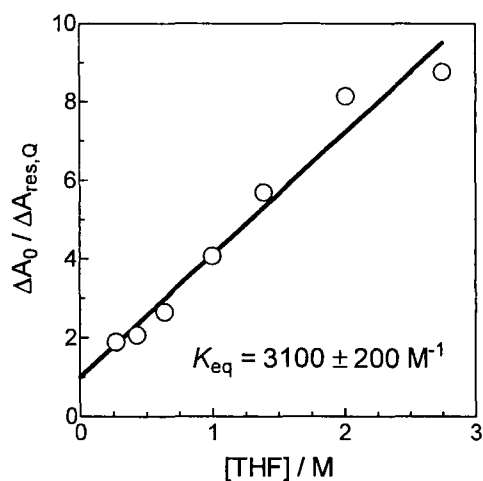
Figure 3.3. Plot of $(\Delta A_0/\Delta A_{res,Q})$ vs. [Q] for the reaction of $GePh_2$ with THF in hexanes at 60 °C. The data points were fit to eq 2.26, the slope of which yields K_{eq}.

The decay of **37** is accompanied by the formation of the digermene on a similar timescale (see Figure 2.12, p 75). The total yield of the digermene is minimally affected (in both total yield and growth time) by low concentrations of THF (<0.2 mM). In neat hexanes, the dimerization of the free germylene is diffusion controlled. In the presence of THF, the concentration of the free germylene is reduced; therefore, in order to maintain the same yield of the digermene there must be some contribution from reaction of the free germylene with **37** or between two molecules of **37** because the dimerization of the free germylene in hexanes already proceeds at the diffusion limit in hexanes. The growth time of the digermene absorbance increases with increasing concentrations of THF. Even at concentrations of THF where the germylene can no longer be detected (> 5 mM), the digermene still forms. It can thus be concluded that the digermene can form via any of the three pathways shown in eq 3.6.[1,4]

$$\text{GeR}_2 \;+\; \text{O} \underset{k_{-1}}{\overset{k_1}{\rightleftharpoons}} \text{R}_2\text{Ge} \leftarrow \text{O} \qquad \mathbf{37}$$

$$\boxed{k_{dim} > k_{dim}' > k_{dim}''}$$

(3.6)

$$\text{R}_2\text{Ge}{=}\text{GeR}_2$$

(arrows labelled $\times 2$, k_{dim}, k_{dim}', $\times 2$, k_{dim}'')
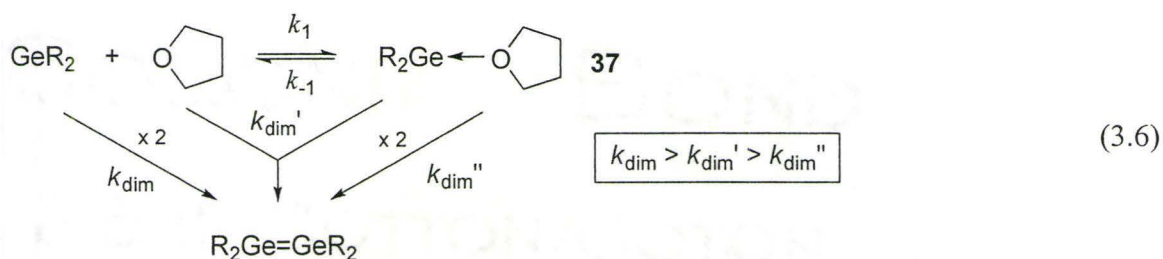
We turned to computational chemistry to provide additional insight into the nature

of the bonding in **37**, particularly whether there is any significant build-up of charge on

germanium due to complexation with the ether. Using $GeMe_2$ as the model germylene,

the geometry of $GeMe_2$-THF (**41**) was optimized in ADF using the same parameters that

have been previously employed by our group for germylene

calculations.[2] The calculated Hirshfeld charges[5, 6] for select atoms of

$$\text{Me}_2\text{Ge} \leftarrow \text{O} \qquad \mathbf{41}$$

the reactants and products are shown in Table 3.2.
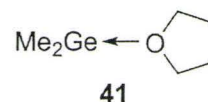
Table 3.2. Hirshfeld charges for select atoms (underlined) in $GeMe_2$, THF and $GeMe_2$-THF (**41**), calculated during the geometry optimization described in the text (PW91-TZ2P-ZORA). The $GeMe_2$ cation and anion are provided to put the charges into context.

Reactant	Charge	Product	Charge
<u>Ge</u>(CH₃)₂	+0.266	(H₃C)₂<u>Ge</u>--O(CH₂CH₂)₂	+0.144
Ge(<u>C</u>H₃)₂	-0.441 [a]	(H₃<u>C</u>)₂Ge--O(CH₂CH₂)₂	-0.455 [a]
<u>O</u>(CH₂CH₂)₂	-0.160	(H₃C)₂Ge--<u>O</u>(CH₂CH₂)₂	-0.065
<u>Ge</u>(CH₃)₂ [(+)]	+0.696	<u>Ge</u>(CH₃)₂ [(-)]	-0.349

a. sum of the charge on both carbon atoms.

In the free germylene, the germanium atom carries a partial positive charge,

which is reasonable because carbon is more electronegative than germanium.[7] Only a

minimal charge increase at germanium is predicted upon complexation with THF. Thus

the structures of these germylene-THF complexes are not drawn with partial/formal

charges. Instead, the complexation is represented with an arrow. The HOMO and

LUMO of **41** are shown in Figure 3.4, and the energies of these orbitals are listed in

Table 3.3 along with the energy of the corresponding orbitals of GeMe$_2$. Note that the

complexation by THF raises the energy of the both the HOMO and the LUMO of GeMe$_2$,

the latter more than the former thus increasing the energy gap between the two states

leading to the shorter wavelength (higher energy) transition observed in the transient

absorbance UV-vis spectra.
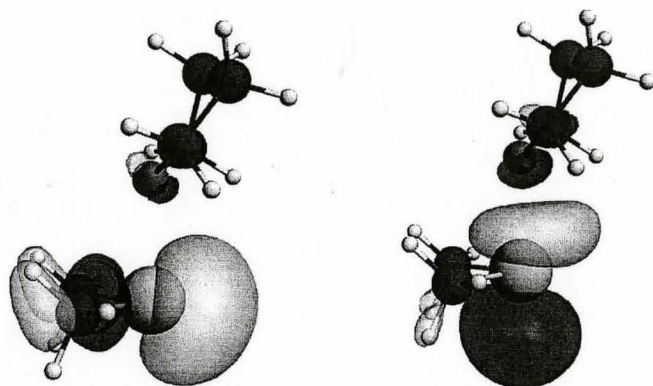
Figure 3.4. GeMe$_2$-THF (**41**) complex HOMO (*left*) and LUMO (*right*) as determined by DFT calculations (PW91,TZ2P,ZORA). Isosurface plotted at 0.044 a.u.

Table 3.3. Calculated energies (eV) of the HOMO and LUMO of GeMe$_2$ and **41** (ADF; PW91,TZ2P,ZORA).

	GeMe$_2$	**41**
HOMO	-5.112	-4.148
LUMO	-3.089	-1.012
$|\Delta|$	2.023	3.136

The enthalpy of complexation for the formation of **41** and the Ge-O distance

within **41** are similar to the Ge-O distance predicted in the GeH$_2$-water complex (**42**)

(Table 3.4).[8] To illustrate the difference between a Ge-O covalent bond and the Ge-O

interaction within the complex, the Ge-O bond distance in **43** (for which the x-ray crystal

structure has been determined) is also given.[9]

$$H_2Ge \leftarrow OH_2 \qquad \overset{\overset{H}{|}}{R-Ge} \atop R \diagdown OEt \quad \textbf{43}$$

42

R = CH(SiMe$_3$)$_2$
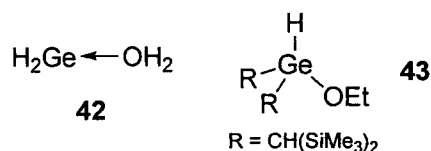
Table 3.4. Calculated enthalpy of complexation of the reactions of GeMe$_2$ with THF (to give **41**) and of GeH$_2$ and water (to give **42**). The experimental Ge-O bond length of **43** is given for comparison.

	ΔH_{298} / kcal mol^{-1}	Ge-O dist. / Å
41 [a]	-8.0	2.278
42 [b]	-11.6	2.258
43 [c]		1.797

a. PW91/TZ2P/ZORA. *b*. Reference 8; MP2/CEP-31g(2d,1p), ZPE corrected. *c*. Reference 9.

3.3. Complexation of Diarylgermylenes with HNEt$_2$ in Hexanes.

The decay rates of the germylenes **Ga,c,d,f** increase upon the addition of HNEt$_2$ as shown in Figure 3.5a. The decays plateau at the baseline for each [Q] and are thus representative of "irreversible" germylene scavenging (*i.e.* K_{eq} > 25,000 M^{-1}). The decay traces were fit to first-order kinetics and the resulting k_{decay} values increased in proportion to the concentration of added reagent (Figure 3.5b), leading to the k_{HNEt2} values listed in Table 3.5. A new transient formed (λ_{max} = 320 nm, $\tau \approx 200$ μs), which has been previously assigned to the germylene-amine complex **38**.[2]
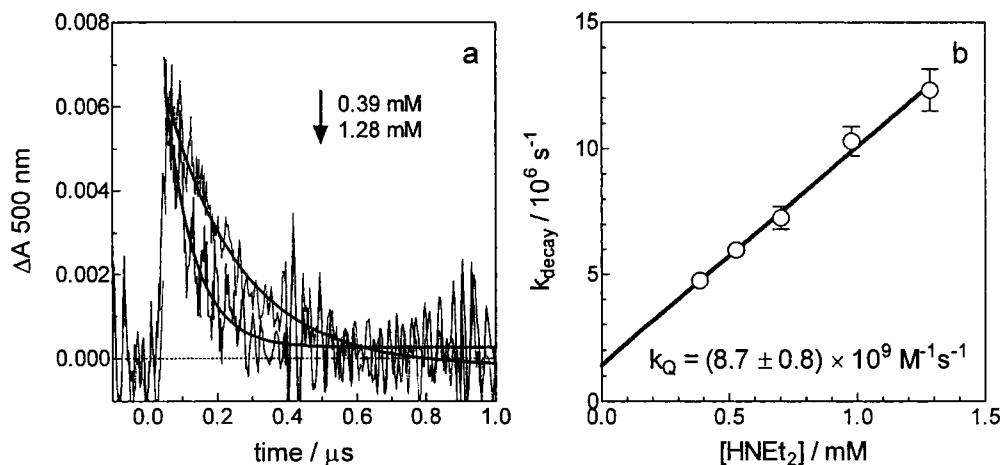
Figure 3.5. (a) Transient decay profiles recorded of **Gf** in hexanes in the presence of $HNEt_2$. The black lines are the non-linear least squares fit of the decays to eq 2.19. (b) Plot of k_{decay} vs. [Q] for the reaction of **Gc** with $HNEt_2$.

Table 3.5. Absolute rate constants for the reaction of **Ga,c,d,f** with $HNEt_2$ in hexanes.

G	k_{HNEt2} / 10^9 $M^{-1}s^{-1}$
a (H)	7.3 ± 0.9
c (p-Me)	6.9 ± 0.8
d (p-F)	7.3 ± 0.4
f (p-CF$_3$)	8.7 ± 0.8

A linear Hammett correlation of k_{HNEt2} with $\Sigma\sigma$ was observed the most electron deficient germylene reacting most rapidly with the amine ($\rho = +0.07 \pm 0.01$, see Figure 3.6). This positive Hammett ρ value is consistent with nucleophilic attack by the amine at germanium to yield **38**, as shown by eq 3.7. The larger equilibrium constants associated with formation of **38** relative to those measured for the formation of **37** (**G** + THF) are consistent with the higher basicity of the amine. We have been unable to identify any products (such as **39**) from the reaction of $GePh_2$ with diethylamine[2]

presumably because of the intrinsic instability of compounds of the type $R_2Ge(H)NR'_2$,[10] although slow proton transfer within **38** (relative to dissociation to the free germylene and amine) may also be a factor.

$$\tag{3.7}$$
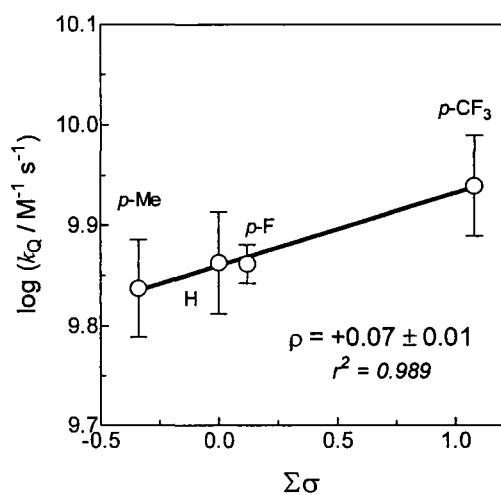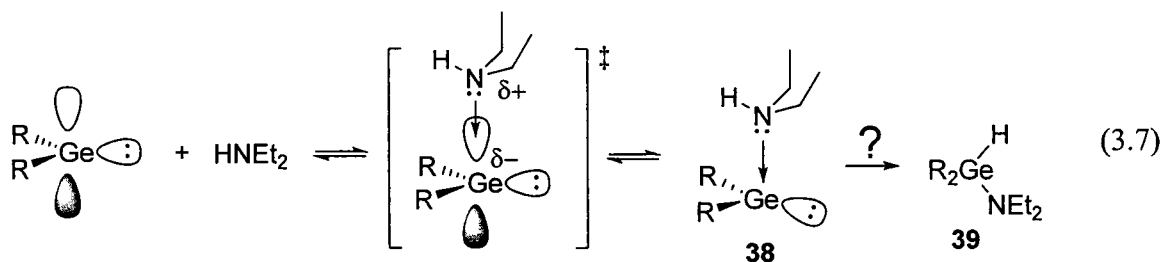
Figure 3.6. Hammett plot of the rate constants for the reactions of $GeAr_2$ with $HNEt_2$ in hexanes.

3.4. Reaction of Diarylgermylenes with Acetic Acid.

The reaction of acetic acid (HOAc) with germylenes is like that with alcohols in that the OH insertion product (**40**) is formed as the exclusive product.[2, 11] The reaction with $GePh_2$ with MeOH, which also yields the OH insertion product, begins with rapid complexation to give **44** ($k_{fast} \approx 6.1 \times 10^9$ $M^{-1}s^{-1}$)
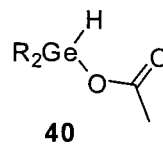
followed by a slow proton transfer to yield **36** ($k_{\text{slow}} \leq 10^4 \text{ s}^{-1}$), the latter step of which is likely catalyzed by a second molecule of methanol (eq 3.8).[1] Similar mechanistic details for the reaction of germylenes with acetic acid are not known. The reaction of GePh$_2$ with HOAc is irreversible and proceeds with a rate constant of $k_{\text{HOAc}} \approx 3.9 \times 10^9 \text{ M}^{-1}\text{s}^{-1}$; no intermediate was detected.[2]

$$\text{GeAr}_2 \quad + \quad \text{MeOH} \quad \underset{}{\overset{\text{fast}}{\rightleftharpoons}} \quad \underset{\textbf{44}}{\text{Ar}_2\text{Ge}\leftarrow \text{O}\overset{\text{CH}_3}{\underset{\text{H}}{}}} \quad \xrightarrow{\text{slow}} \quad \underset{\textbf{36}}{\text{Ar}_2\text{GeH}\overset{\text{OMe}}{}} \qquad (3.8)$$
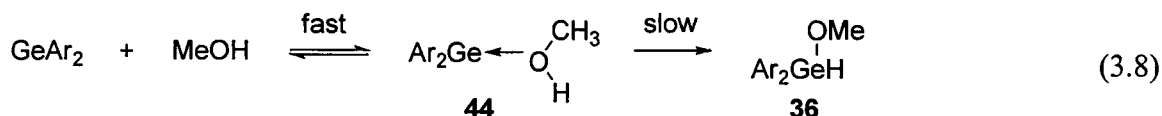
Given the difference in the pK_a's of methanol and acetic acid (Table 3.6), we were interested in whether the mechanism for the reaction of germylenes with acetic acid is similar to the mechanism for the reaction of germylenes with methanol (*i.e.* complexation followed by proton transfer) or whether protonation of the germanium lone pair occurs first because HOAc is a stronger acid than MeOH.

Table 3.6. Aqueous pK_a values and the gas phase proton affinities (PA) of acetic acid, ethyl acetate, methanol and THF.

	pK_a [a]	PA / kcal mol^{-1} [b]
Acetic acid	4.8	187
Ethyl acetate	-	200
THF	-	196
Methanol	32.0	180

a. Reference 12. *b.* Reference 13.

Solutions of **33a,c,d,f** (20 mM) in hexanes containing HOAc (0.4 M) were irradiated with 254 nm light for 2 hrs, the solvent was evaporated, the residue was dissolved in CDCl$_3$ and the ^{1}H NMR spectrum was obtained (See Figure 3.7). In each case, the corresponding acetoxygermane (**40a,c,d,f**) was identified as the major product,

showing that the aromatic substituents do not effect the course of the reaction. The

conversions in these experiments were quite high (> 90%), thus demonstrating the clean

photochemistry of the germacyclopentenes as well as the stability of the products

40a,c,d,f towards α-elimination or secondary photolysis. Similar experiments employing

methanol as the germylene scavenger show substantial decomposition of the product **36**

at similar conversions.
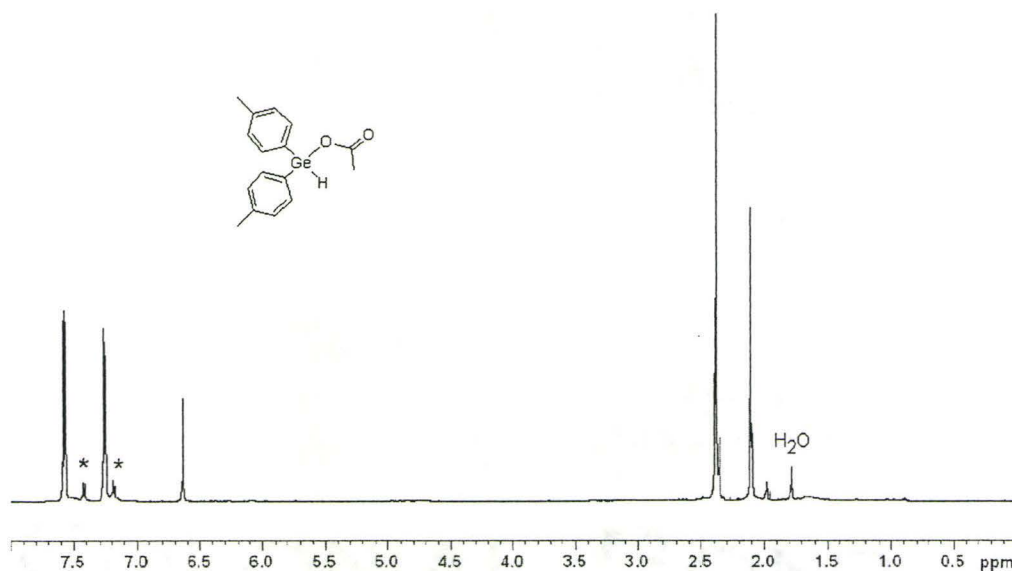
Figure 3.7. ^{1}H NMR spectrum of the crude reaction mixture from photolysis of **33c** in hexanes containing HOAc (0.4 M) after evaporation of the hexanes and re-dissolution in CDCl$_3$. The peaks marked with an asterisk are due to **33c**. *(Reprinted from reference 14 with permission. © 2007 American Chemical Society.)*

The decay rates of the germylenes **Ga,c,d,f** in hexanes increased in the presence

of HOAc (Figure 3.8a). The decay traces fit well to first-order kinetics and plots of k_{decay}

vs. [HOAc] were linear in each case (see Figure 3.8b which uses the experiment with **Gc**

as an example). The resulting rate constants are listed in Table 3.7. Rate constants for

the reaction of **Ga,c,f** with DOAc were measured under the same conditions and were

96

found to be the same within error as those measured with HOAc (Table 3.7). No new

transients could be detected in the transient absorption spectrum of **33a** recorded in

hexanes containing 0.5 mM HOAc (Figure 3.9).
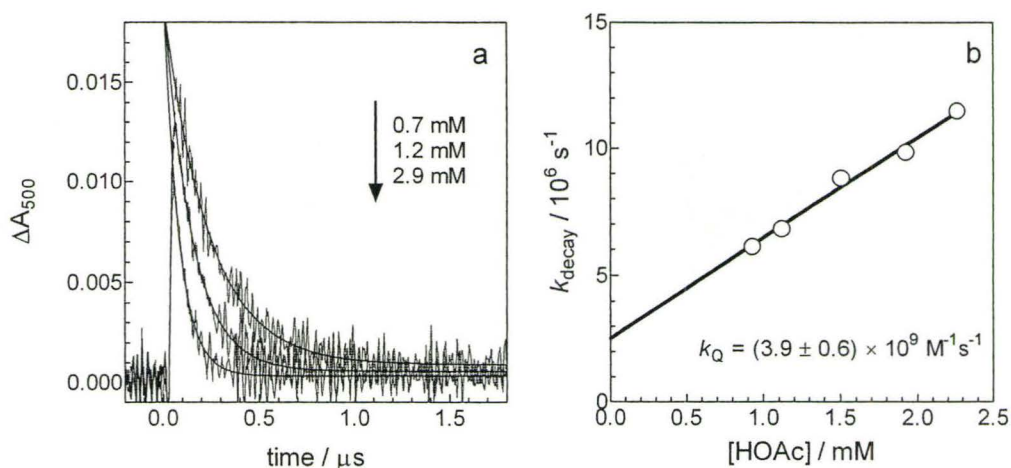
Figure 3.8. (a) Transient decay profiles of **Gc** in the presence of various concentrations of HOAc. The black lines are the non-linear least squares fit of to eq 2.19. (b) Plot of k_{decay} vs. [Q] for the reaction of **Gc** with HOAc in hexanes.

Table 3.7. Absolute rate constants for the reaction of **Ga,c,d,f** with acetic acid and acetic acid-*Od* in hexanes.

G	k_{HOAc} / 10^9 M^{-1}s^{-1}	k_{DOAc} / 10^9 M^{-1}s^{-1}
a (H)	3.9 ± 0.6	4.4 ± 0.6
c (*p*-Me)	3.4 ± 0.6	3.1 ± 0.8
d (*p*-F)	4.1 ± 0.8	-
f (*p*-CF$_3$)	6.2 ± 1.0	7.2 ± 0.9
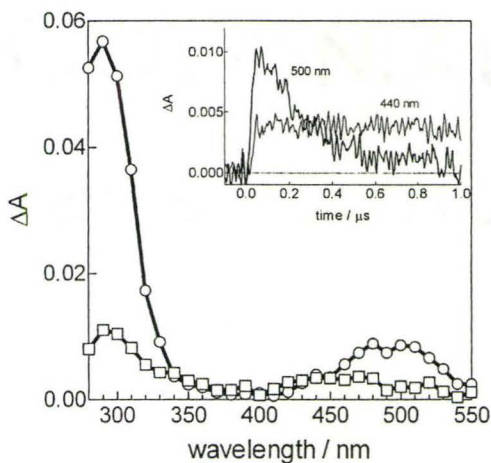
Figure 3.9. Transient absorption spectrum of **33a** in hexanes containing 0.5 mM HOAc recorded 99-106 ns (○) and 467-486 ns (□) after the laser pulse. The inset shows the absorbance-time profiles at 440 nm and 500 nm.

An excellent Hammett correlation with k_{HOAc} was observed ($\rho = +0.19 \pm 0.01$, see Figure 3.10) with the most electron deficient germylene (**Gf**) reacting most rapidly. The positive ρ value rules out protonation of the germylene by the acid occurring in the rate determining step of the reaction. Protonation is also mitigated by the lack of a kinetic isotope effect (KIE) with DOAc, although reactions with such large rate constants are generally not expected to display large KIEs. Most importantly, the positive ρ value indicates that the germylene plays the role of the electrophile in the reaction with the carboxylic acid. A mechanism beginning with complexation of the carbonyl oxygen of the acid with the germylene (**45**), followed by a rapid proton transfer to give **40** (eq 3.9) would be consistent with this result.
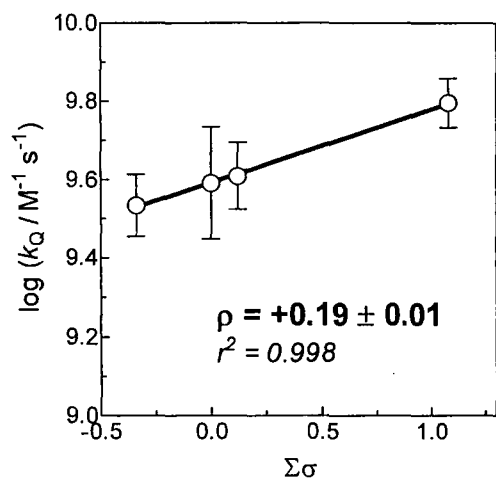
Figure 3.10. Hammett plot for the reaction of **Ga,c,d,f** with HOAc in hexanes.

$$\rho = +0.19 \pm 0.01$$
$$r^2 = 0.998$$

(3.9)
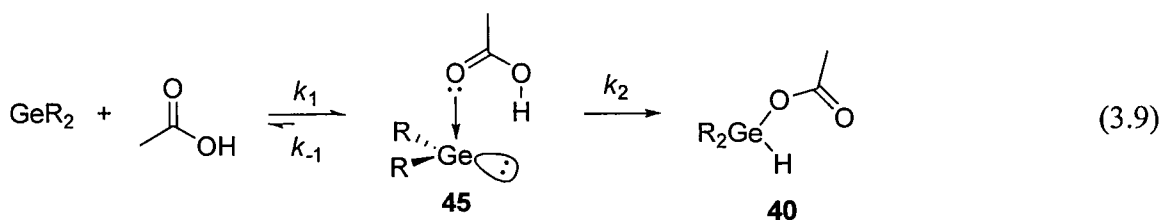
We were unable to detect the complex **45**, which suggests that if it is formed, it is a steady-state intermediate. The proton transfer step (k_2) must therefore occur more rapidly than **45** can dissociate to the free germylene and carboxylic acid (*i.e.* $k_2 \gg k_{-1}$). Because we cannot detect **45**, we hoped to obtain more information on this complexation step using a model compound. We reasoned that ethyl acetate (EtOAc) would be useful for this purpose (eq 3.10).

(3.10)
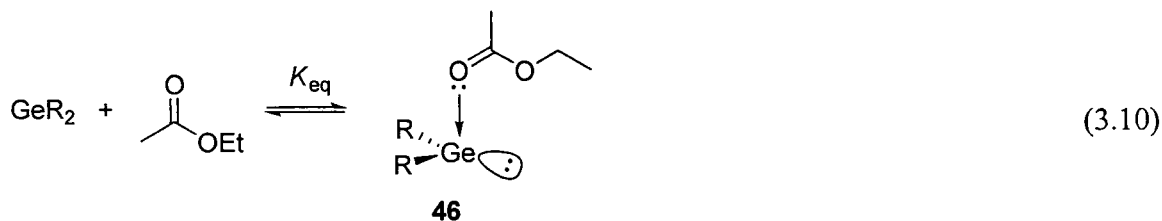
Photolysis of **33a** (30 mM) in C_6D_{12} in the presence of EtOAc (0.3 M) was monitored by ^1H NMR spectroscopy. DMB was the only product formed that could be identified. Substantial broadening of the aliphatic (δ 1.0-2.5) and aromatic (δ 6.9-7.7) resonances in the spectrum was observed, as were a number of minor peaks throughout the spectrum. These results are consistent with the primary reaction being oligo-merization of the germylene. Further identification of these products was not pursued.

Addition of millimolar concentrations of EtOAc to hexanes solutions of **33a,c,d,f** did not result in increases in the k_{decay} values of the corresponding germylenes. Instead, the apparent maximum yield of the germylene formed in the laser pulse decreased with increasing concentration of the ester (Figure 3.11a). Such effects are consistent with the *low K_{eq}* scenario described in Chapter 2 (*i.e.* $K_{eq} < 1000$ M^{-1}; $k_{forward} > 10^9$ $M^{-1}s^{-1}$). A transient absorption spectrum recorded in the presence of 30 mM EtOAc (Figure 3.11b) shows the formation of a new transient product exhibiting $\lambda_{max} = 360$ nm and $\tau = 10$-20 μs. Plots of $\Delta A_0/\Delta A_{0,EtOAc}$ vs. [EtOAc] were linear (Figure 3.11c) for each of **Ga,c,d,f**, allowing the determination of the equilibrium constant as described by eq 2.27. The largest equilibrium constant is found with the most electron deficient germylene (Table 3.8) and the Hammett plot has a positive slope of $\rho = +0.5 \pm 0.2$ as shown in Figure 3.11d. While the plot appears curved, these data are fit to a straight line due to the small number of points. The increase of K_{eq} with increasingly electron poor germylenes is consistent with the germylene behaving as an electrophile.
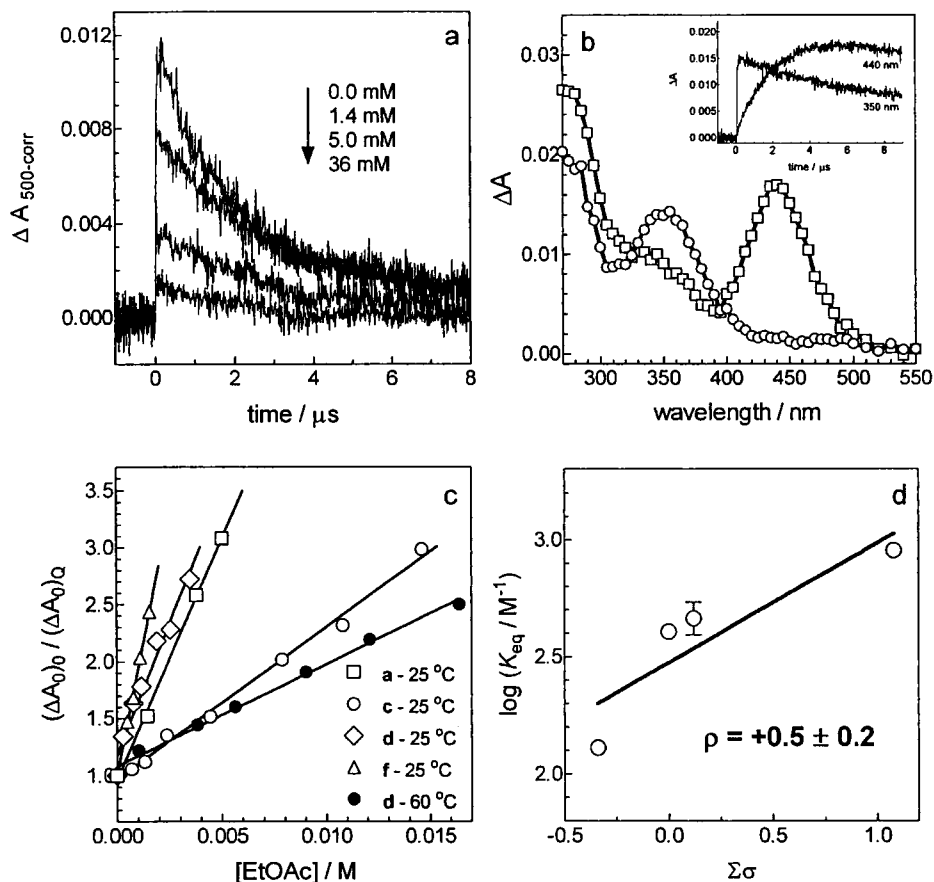
Figure 3.11. (a) Transient absorbance-time profiles of **Ga** recorded at 500 nm in the presence of EtOAc, corrected for the underlying absorbance due to **DGa**. (b) Transient UV/vis absorption spectra recorded by flash photolysis of a 3 mM solution of **33a** in hexane containing 30 mM EtOAc, 100 – 160 ns (○) and 6.6 – 6.7 μs (□) after the laser pulse; the inset shows transient absorption profiles recorded at 350 and 440 nm. (c) Plots of $(\Delta A_0)_0/(\Delta A_0)_Q$ for quenching of the peak signal intensities due to **Ga,c,d,f** by EtOAc in hexane at 25 °C and for **Ga** at 60 °C. (d) Hammett plot of K_{eq} for the reaction of diarylgermylenes with EtOAc in hexanes.

The new transient product that forms in the presence of EtOAc (λ_{max} = 350 nm, τ

= 10-20 μs) is thus assigned to the GePh$_2$-EtOAc complex **46** based on the similarities of

the absorbance maxima, transient lifetime, and Hammett ρ value to the germylene-THF

complex **37** (λ_{max} = 350 nm, τ = 10-20 μs).

Table 3.8. Equilibrium constants for the reaction of **Ga,c,d,f** with ethyl acetate in hexanes at 25°C unless otherwise noted.

G	K_{eq} / M^{-1}
a (H)	405 ± 7
a (H) – 60 °C	89 ± 7
c (*p*-Me)	29 ± 5
d (*p*-F)	460 ± 80
f (*p*-CF$_3$)	900 ± 25

As was observed with the GePh$_2$-THF reaction, the GePh$_2$-EtOAc equilibrium constant decreased when the temperature was increased from K_{eq} = (405 ± 7) M^{-1} at 25 °C to K_{eq} = (89 ± 7) M^{-1} at 60 °C. The thermodynamic parameters calculated from these two points are given in Table 3.9, along with those for the reaction with THF for comparison. The smaller ρ value exhibited by the reactions of the germylenes with EtOAc (assuming it is correct to treat the four points in Figure 3.11d as a straight line) indicates there is a smaller build up of positive charge at germanium; however, the thermodynamic data suggest the nature of the coordination is not significantly different.

Table 3.9. Hammett ρ values and thermodynamic parameters for the reactions of GePh$_2$ with THF and ethyl acetate in hexanes solution.

	ρ	ΔH / kcal/mol	ΔS / cal/K/mol
THF	+1.3 ± 0.2	-11 ± 2	-24 ± 5
EtOAc	+0.5 ± 0.2	-8.5 ± 0.6	-23 ± 2

The tetraaryldigermenes (**DG**, λ_{max} = 440 nm) can be detected at concentrations of EtOAc where the corresponding germylene can no longer be detected (for example, see Figure 3.11b). At low concentrations of EtOAc (< 5 mM), the maximum digermene

yield is higher than it is in the absence of the scavenger and the time required to reach the

maximum digermene yield increases (see Figure 3.12). Furthermore, the decay of the

digermene is insensitive to the presence of EtOAc.
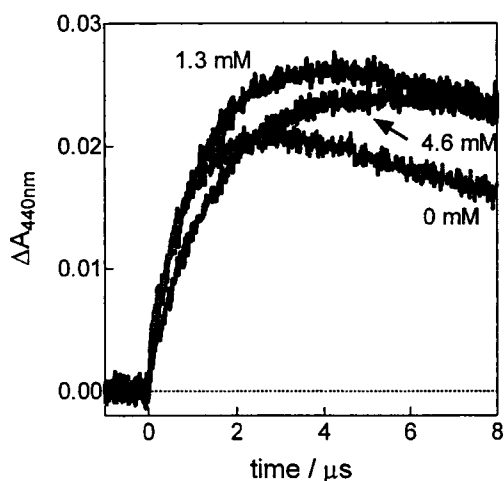
Figure 3.12. Transient absorbance vs. time profiles of **DGa** recorded in hexanes in the presence of various concentrations of ethyl acetate.

The increased yield of the digermene as the concentration of ethyl acetate is

increased is rationalized by the fact that reaction with the free germylene is a reaction that

contributes to the decay of the digermene; when the germylene is complexed this

contribution to the decay of the digermene is reduced. The increased growth time of the

digermene with increasing EtOAc concentration results from the fact that the rate

constant for dimerization of **46** is lower than that of the free germylene and/or because

the concentration of free germylene is reduced relative to its value in the absence of the

scavenger.[15]

The objective of studying ethyl acetate was to use it as a model for the proposed

first step in the reaction of the germylene with acetic acid. The reason we may not detect

a complex between the germylenes and acetic acid (**45**) is because it is a steady state

103

intermediate. In a two-step mechanism, the observed rate constant $k_{HOAc} = k_1 = 4 \times 10^9$

$M^{-1}s^{-1}$. If $K_{EtOAc} = K_{HOAc}$, then $k_{-1} \approx 10^7 \, s^{-1}$. The value of k_{-1} allows us to set a minimum

value for the rate constant of the proton transfer step at $k_2 \geq 10^8 \, s^{-1}$. If k_2 was lower than

this, we should be able to detect both the intermediate **45** as well as a KIE. But is the

value of k_2 reasonable? Recall that the H-migration within complex **44** in the reaction of

GePh$_2$ with MeOH occurs with an estimated rate constant of $k_2 \approx 10^4 \, s^{-1}$ (eq 3.11).[1] A

faster k_2 in the case of HOAc is reasonable because H-migration within **45** can proceed

via a cyclic five-membered transition state (eq 3.12) compared to a four-membered

transition state for the analogous process of **44**. Furthermore, the proton being

transferred within **45** is more acidic than the proton being transferred within **44**.

$$\text{GeR}_2 + \text{MeOH} \quad \underset{}{\overset{K_{eq} = 3300 \text{ M}^{-1}}{\rightleftharpoons}} \quad \underset{\textbf{44}}{\text{(intermediate)}} \quad \xrightarrow{k_2 \sim 10^4} \quad \underset{\textbf{36}}{R_2Ge\begin{smallmatrix} OMe \\ H \end{smallmatrix}} \qquad (3.11)$$

$$\text{GeR}_2 + \text{HOAc} \quad \underset{k_{-1} = 10^7 \text{ s}^{-1}}{\overset{k_1 = 10^9 \text{ M}^{-1}s^{-1}}{\rightleftharpoons}} \quad \underset{\textbf{45}}{\text{(intermediate)}} \quad \xrightarrow{k_2 > 10^8 \text{ s}^{-1}} \quad \underset{\textbf{40}}{R_2Ge\begin{smallmatrix} OAc \\ H \end{smallmatrix}} \qquad (3.12)$$
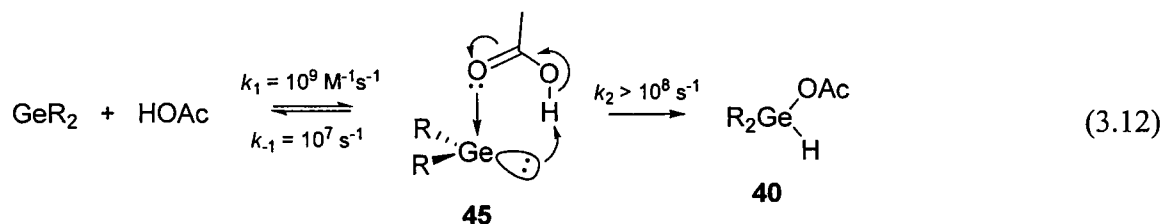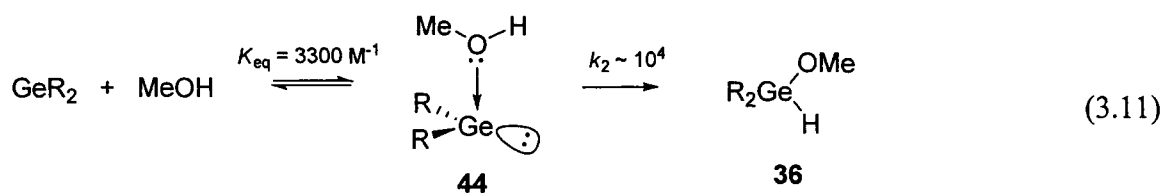
3.5. Some reactions of diarylgermylenes in tetrahydrofuran

3.5.1. Laser Photolysis of 33 in THF

Laser photolysis of **33a,c,d,e,f** in neat THF results in the prompt formation of a

transient absorbance centered at $\lambda_{max} \approx 340$ nm, which decays with mixed-order kinetics over several hundred microseconds (Figure 3.13a). Neither the absorbance maximum nor the lifetime are affected by aromatic substitution. The free germylene could not be detected under these conditions. Figure 3.13 shows the transient absorption spectra obtained by LFP of **33a** and **33e** in THF as examples of the typical appearance of the spectra of the substituted analogues. In neat THF, the digermene can be detected ($\lambda_{max} =$ 440 nm) provided, presumably, that the solvent is dry (Figure 3.13b – inset). Figure 3.14 shows the transient absorption spectra obtained by LFP of **33f** in THF which is atypical in that the lowest energy transition of the complex appears as a shoulder rather than a well-defined maximum.
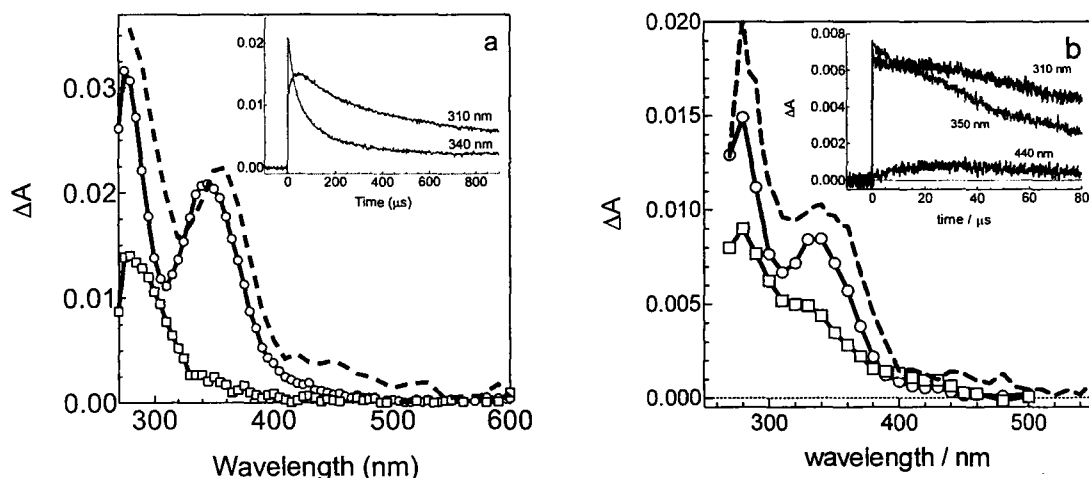
Figure 3.13. (a) Transient absorption spectra from laser flash photolysis of solution of **33a** in THF recorded 0 - 3.2 μs (○) and 500 - 506 μs (□) after the laser pulse (the insert shows transient decay traces recorded at 310 and 340 nm). The dashed line shows the spectrum obtained from the same compound in hexanes containing 2 mM THF, recorded 0.1-0.2 μs after the laser pulse. *(Spectrum recorded by C. Harrington. Reprinted from reference 4 with permission. © 2009 American Chemical Society.)* (b) Transient absorption spectra from laser flash photolysis of a solution of **33e** in THF, recorded 1.92-2.56 μs (○) and 53.6 – 54.7 μs (□) after the laser pulse. The inset shows the transient profiles recorded at 310, 350 and 440 nm. The dashed line shows the spectrum obtained from the same compound in hexanes containing 13 mM THF, recorded 83-96 ns after the laser pulse.
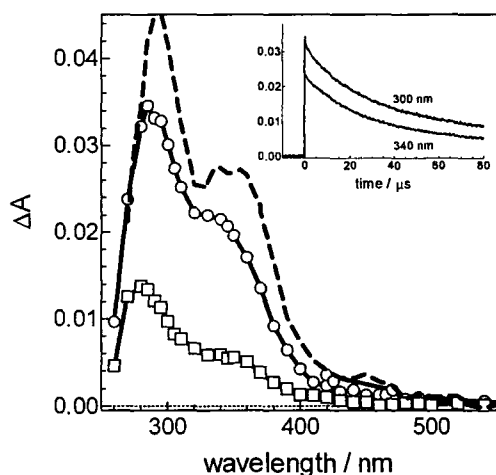
Figure 3.14. Transient absorption spectra from laser flash photolysis of a solution of **33f** in THF, recorded 1.92-2.24 μs (○) and 69.6 – 70.4 μs (□) after the laser pulse. The inset shows the transient profiles recorded at 300 and 340 nm. The dashed line shows the spectra obtained from the same compound in hexanes containing 4 mM THF, recorded 102-128 ns after the laser pulse.

The transient at 345 nm is assigned to **37**. The absorbance maximum of **37** in THF ($\lambda_{max} \approx 345$ nm) is similar to but somewhat blue shifted from that observed in hexane solution ($\lambda_{max} \approx 360$ nm). The germylene cannot be detected in any of these experiments, but this is expected because the free germylene cannot be detected in hexanes solution containing concentrations of THF greater than *ca.* 10 mM. The ability to detect the digermene is likely a result of how rigorously the solvent has been dried. When it is detected, the growth time is much longer than in hexanes, consistent with a smaller dimerization rate constant of **37** relative to that of the free germylenes.

3.5.2. Reaction of 37 **with methanesulfonic acid**

Product studies of the reactions of GeMe$_2$ with acetic and methanesulfonic acids in THF showed the formation of **47** in high yield and **48** in moderate yield, respectively (*F. Lollmahomed*).[4] The former is the same product that is formed from the reaction of GeMe$_2$ with HOAc in hexanes,[2] while the latter reaction was not explored in hexane solution. It was of interest to determine whether the germylene-THF complexes could be protonated, perhaps resulting in the formation of germyl cations. No new transients could be detected when the GeMe$_2$-THF complex was generated in the presence of MeSO$_3$H.[4]
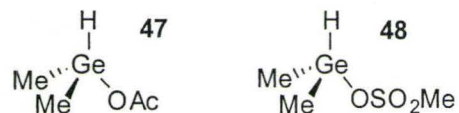
The decay rates of the complexes **37a,c,d,f** increased in the presence of methanesulfonic acid (MeSO$_3$H) (Figure 3.15a). The decays plateau at the baseline for each concentration of MeSO$_3$H indicating irreversible scavenging of the complex in each

case. The decay traces were fit to first-order kinetics and the resulting plots of k_{decay} vs.

[MeSO$_3$H] (Figure 3.15b) afforded the k_{MeSO3H} values listed in Table 3.10. The pK_a of

MeSO$_3$H in THF (p$K_{a\text{-}MeSO3H}$ $\approx$ 13-14)[16] dictates that the protonated form of the acid is

dominant – the percent dissociation under the conditions of our experiment is on the

order of 10^{-4} %. The transient absorption spectra of **33a** in THF recorded in the presence

of 62 mM MeSO$_3$H, shown in Figure 3.16, did not reveal the formation of any new

transients; similar results were obtained with **33c**.
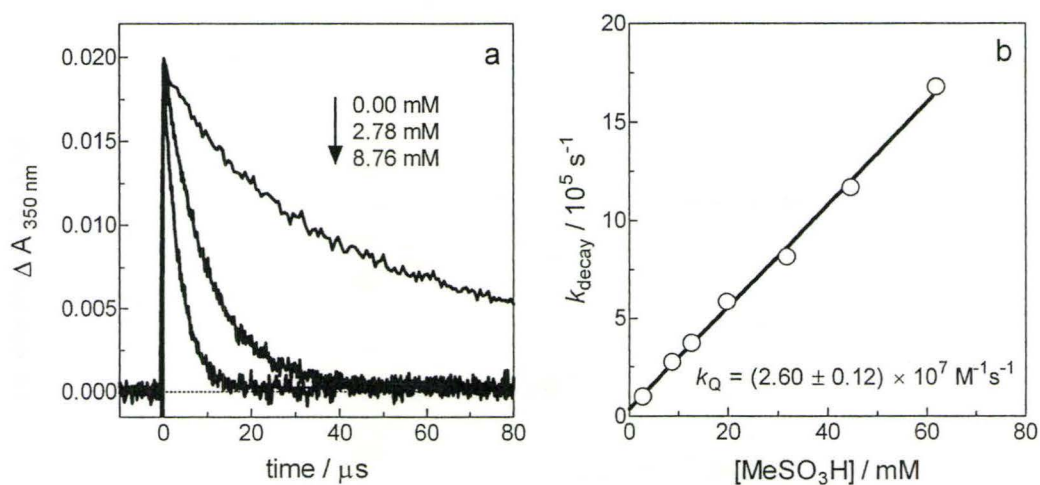
Figure 3.15. (a) Transient decay profiles of **37a** in the presence of MeSO$_3$H. The black lines are the non-linear least squares fit of the decays to first-order kinetics. (b) Plot of k_{decay} vs. [Q] for the reaction of **37a** with MeSO$_3$H.

Table 3.10. Rate constants for the reaction of **37a,c,d,f** with MeSO$_3$H in THF.

37	k_{MeSO3H} / 10^7 M^{-1}s^{-1}
a (H)	2.60 ± 0.12
c (*p*-Me)	2.79 ± 0.08
d (*p*-F)	2.32 ± 0.04
f (*p*-CF$_3$)	1.61 ± 0.03
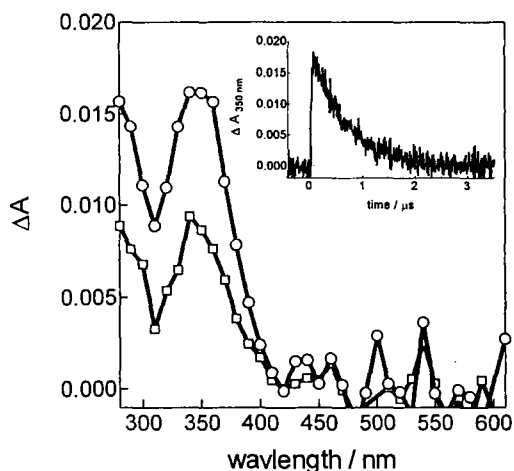
Figure 3.16. Transient absorbance spectra of **33a** in THF containing 62 mM $MeSO_3H$, recorded 109-134 ns (○) and 0.54-0.56 μs (□) after the laser pulse. The inset shows the absorbance-time profile measured at 350 nm.

A linear Hammett correlation with the rate constants was observed (ρ = -0.17 ± 0.01; see Figure 3.17). A negative slope is consistent with a build-up of positive charge in the transition state of the reaction, which is in turn consistent with the protonation of **37** (eq 3.13); however, the relatively small magnitude of the ρ value suggests that complete proton transfer to germanium at the transition state is unlikely. No new transients that might be assigned to the germyl cation **49** could be detected, even in the transient absorption spectra of one of the more electron-rich germylenes **Gc**.

(3.13)
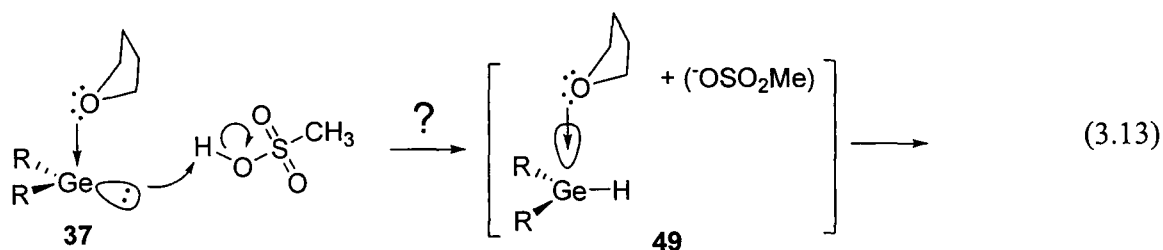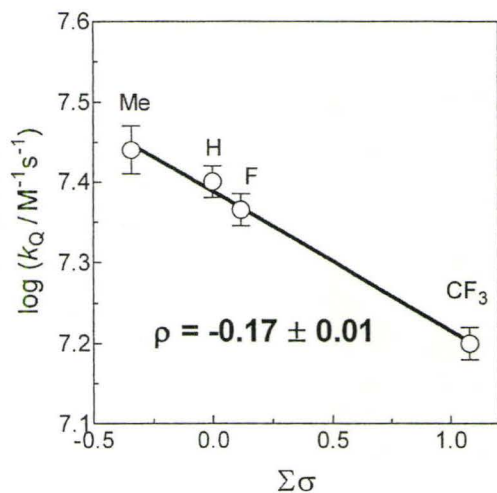
Figure 3.17. (a) Hammett plot for the reaction of **37a,c,d,f** with $MeSO_3H$ in THF.

3.6. Some reactions of diarylgermylenes in methanol

3.6.1. Photolysis of 33 in methanol

A product study was undertaken to ensure that **36** is produced in neat methanol as it is in hexanes containing methanol. Photolysis of **33a** in methanol, followed by evaporation of the solvent and ^1H NMR spectroscopic analysis confirmed that **36** is indeed produced; however, the digermoxane **50** was also detected (eq 3.14). The latter is consistent with reaction of **Ga** with water during the photolysis or with reaction of **36** with water during the work-up. The reaction of a germylene with water to yield a digermoxane has been reported.[17] Indeed, the yield of **50** was reduced when the experiment was repeated with sodium distilled methanol.

$$(3.14)$$

3.6.2. Laser flash photolysis of 33 in methanol

Laser flash photolysis of **33a,c,d,e,f** in methanol results in the prompt formation

of a transient absorbance centered at $\lambda_{max} \approx 325 \pm 5$ nm. Aromatic substitution does not

affect the absorbance maximum. The free germylene cannot be detected nor can the

growth of the 325 nm transient be resolved from the laser pulse. The digermene is not

expected to be detectable under these conditions (assuming it is formed at all) because it

reacts with methanol with a rate constant of $k = 1.9 \times 10^7$ M^{-1}s^{-1}.[1] Figure 3.18a shows the

transient absorption spectrum upon photolysis of **33a** and **33e** in MeOH, as examples of

the typical appearance of the spectra of the substituted analogues. Figure 3.19 shows the

transient absorption spectrum of **33f** in MeOH, which is atypical in that the lowest energy

transition of the complex appears as a shoulder rather than a well defined maximum.

Figure 3.18. (a) Transient absorption spectra from laser flash photolysis of **33a** in MeOH, recorded 0.19-0.83 μs (○) and 24.70-25.34 μs (□) after the laser pulse; the inset shows a transient decay trace recorded at 325 nm. The dotted line shows the spectrum obtained from the same compound in hexane containing 5 mM MeOH, recorded 90-116 ns after the pulse. *(Spectrum recorded by C. Harrington. Reprinted from reference 4 with permission. © 2009 American Chemical Society.)* (b) Transient absorption spectra from laser flash photolysis of a solution of **33e** (3 mM) in methanol, recorded 8.32-8.96 μs (○) and 19.5 – 20.5 μs (□) after the laser pulse. The inset shows the transient profile recorded at 320 nm.
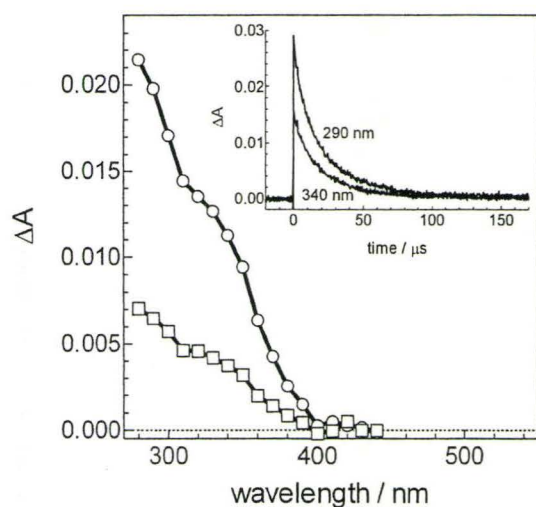
Figure 3.19. Transient absorption spectra from laser flash photolysis of **33f** in MeOH solution, recorded 4.16-5.12 μs (○) and 27.5-28.5 μs (□) after the laser pulse; the inset shows the transient decay traces recorded at 290 and 340 nm.

The 325 nm transients are assigned to the germylene-methanol complexes
44a,b,c,d,f. Under normal experimental conditions, such as those shown in Figure 3.18
and Figure 3.19, the complexes decay with mixed-order kinetics over several hundred
microseconds. At reduced laser intensities, however, the decays fit well to first-order
kinetics. (Reducing the laser intensity decreases the maximum yield of the complex, thus
reducing the probability of reaction between molecules of **44** therefore reducing any
second-order component of the decays.) The lifetimes did not vary significantly between
analogues ($\tau = 120 \pm 30$ µs; measured by S. Chitnis). The lifetimes of the complex **44f**
increased in methanol-O*d*, leading to a KIE of 2.5 ± 0.8 (measured by S. Chitnis).

The absorbance maximum of **44** in methanol is blue shifted relative to the
absorbance maximum of **44** in hexanes solution. It is possible that this shift is due to a
greater stabilization of the Ge-O interaction afforded by the more polar solvent or by the
coordination of a second molecule of methanol to the germylene.

The insensitivity of the decay rate coefficients of **44** to aromatic substitution
suggests that the transition state of the rate determining step for reaction of the complex
is only weakly polarized relative to that in the complex itself. The kinetic isotope effect
measured with MeOH/MeOD is consistent with solvent catalysed proton transfer within
44 to yield **36** with the proton transfer occurring in the rate determining step (eq 3.15).

(3.15)
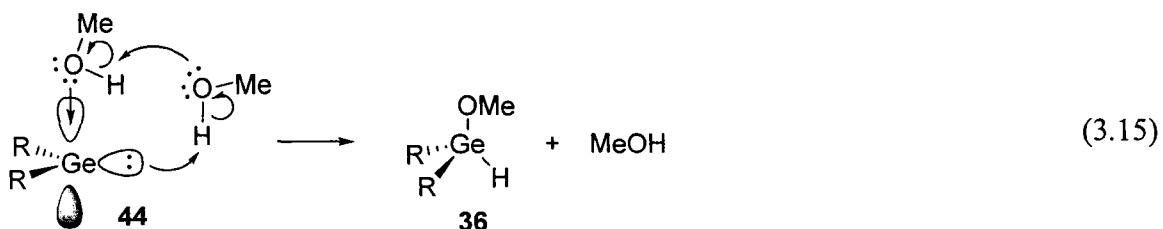
The next sections examine the reactivity of **44** in the presence of acid (MeSO$_3$H) and base (sodium methoxide). The objectives were to determine the nature of any catalysis that may be involved in the conversion of **44** to **36**, and to detect any cationic/anionic intermediates that might be involved.

3.6.3. Reaction of 44 with methanesulfonic acid

The decay rates of the complexes **44a,b,c,d,f** increased in the presence of methanesulfonic acid (MeSO$_3$H) (Figure 3.20a). The decay traces were fit to first-order kinetics and the resulting k_{decay} values increased in proportion to the concentration of added reagent (Figure 3.20b), leading to the k_{MeSO3H} values listed in Table 3.11. The rate constant for the reaction of **44-d-f** with MeSO$_3$D was 2.2 times slower than the reaction of **44f** with MeSO$_3$H in MeOH (Figure 3.21a). A transient absorption spectrum of **33a** recorded in MeOH in the presence of 0.9 mM MeSO$_3$H did not reveal the formation of any new transients.

44-d-f

R = (p-CF$_3$-C$_6$H$_4$)
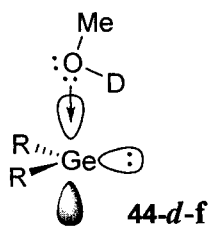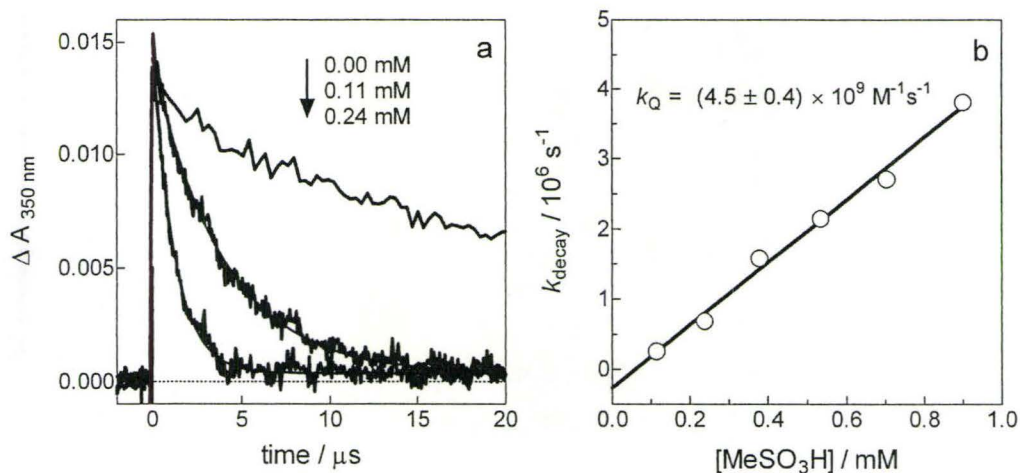
Figure 3.20. (a) Transient decay profiles of **44c** in methanol containing various concentrations of $MeSO_3H$. The black line is the non-linear least squares fit of the decay to first-order kinetics (eq 2.19). (b) Plot of k_{decay} vs. [Q] for the quenching of **44c** with $MeSO_3H$ in methanol.

Table 3.11. Absolute rate constants for the reaction of **44a,b,c,d,f** with methanesulfonic acid in methanol.

44	k_{MeSO3H} / 10^9 $M^{-1}s^{-1}$
a (H)	3.9 ± 0.2
b (mp-Me_2)	4.5 ± 0.5 [a]
c (p-Me)	4.5 ± 0.4
d (p-F)	2.04 ± 0.07
f (p-CF_3)	0.67 ± 0.03
f (p-CF_3) [b]	0.30 ± 0.02 [b]

a. Measured by S. Chitnis. b. for the reaction of the **44-d-f** with $MeSO_3D$ in MeOD.

A negative linear Hammett correlation of the rate constants was observed (ρ = -0.56 $\pm$ 0.08, Figure 3.21b), consistent with protonation in the transition state of the rate determining step for reaction of the complex. The results indicate a greater degree of polarization than is observed with the corresponding reaction in THF, which is

reasonable given the greater potential for transition state stabilization that is afforded by

the polar solvent. Further support for the proton transfer in the transition state came from

the observation of a KIE. Although these data are consistent with protonation of **44**, no

evidence for the formation of a cation could be found.
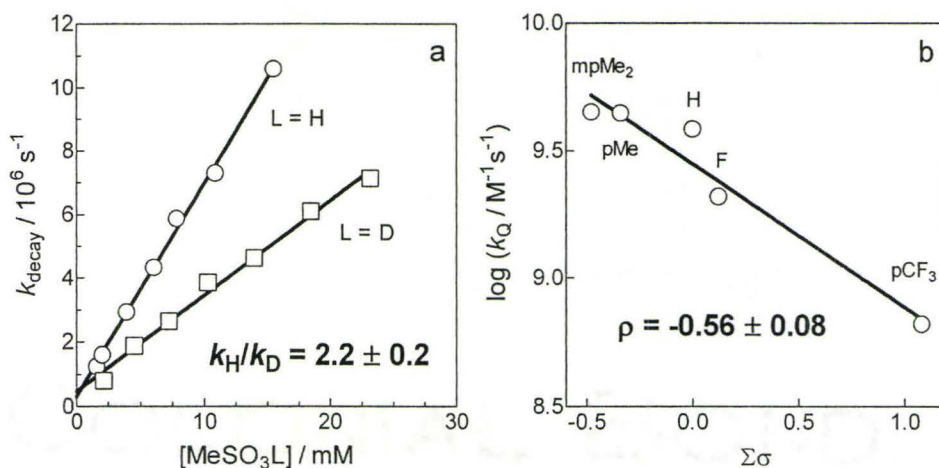
Figure 3.21. (a) Plot of k_{decay} vs. [MeSO$_3$L] for the reaction of **44f** and **44-*d*-f** with MeSO$_3$L in MeOL. (b) Hammett plot of the reaction of **44** with MeSO$_3$H in methanol.

Protonation of **44** in the transition state is supported by the Hammett and KIE

values. In methanol, MeSO$_3$H has a pK_a 2-3,[4] and over the concentration range studied in

a single experiment, the percent dissociation varies considerably. Figure 3.22 shows the

percent dissociation of MeSO$_3$H in methanol over the concentration range of MeSO$_3$H

employed in these experiments. The linear quenching plot of Figure 3.21b indicates that

the complex reacts with MeSO$_3$H and MeOH$_2^+$ with the same rate constant and is thus

consistent with general acid catalysis. A mechanism consistent with the available data is

shown in eq 3.16; the alternate H$^+$ source is MeSO$_3$H and this reaction is shown in eq

3.17.
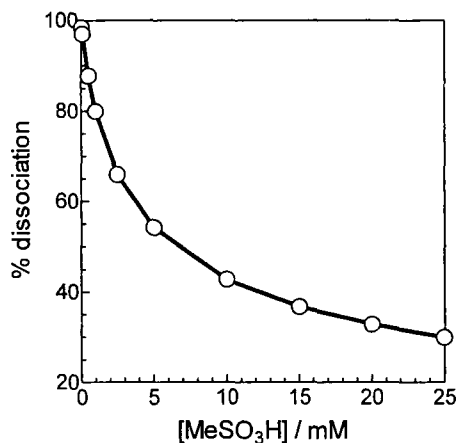
Figure 3.22. Percent dissociation of $MeSO_3H$ in methanol to $MeSO_3^-$ and $MeOH_2^+$, assuming $pK_a = 2.5$.

(3.16)

(3.17)
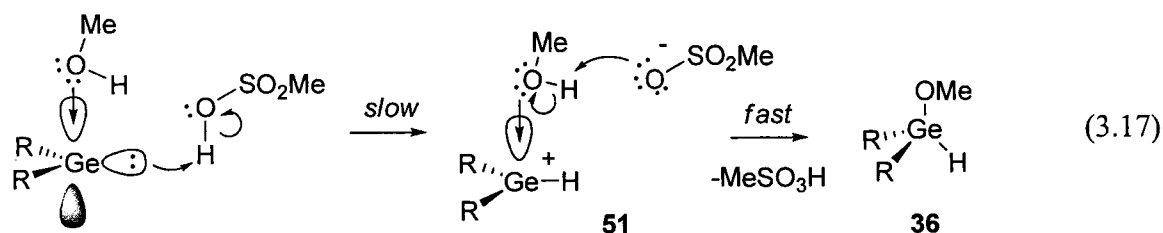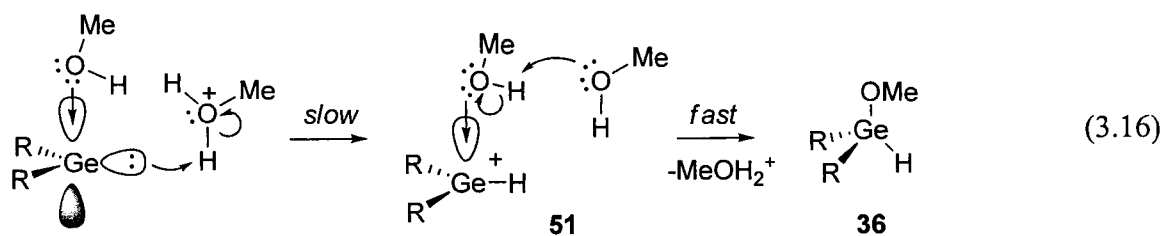
3.6.4. Reaction of 44 with sodium methoxide

The decay rates of the complexes **44a,b,c,d** (but not **44f**, *vide infra*) increased in the presence of sodium methoxide (NaOMe) as shown in Figure 3.23a. The decays plateau at the baseline for each concentration of the base, and each decay fit well to first-

order kinetics. The plot of k_{decay} vs. [NaOMe] (Figure 3.23b) afforded the k_{NaOMe} values

listed in Table 3.12. In contrast with the other analogues, the reaction of **44f** resulted in

the growth of a new transient ($\lambda_{max} \approx 310$-330 nm) the yield of which increased with

each successive addition of base (Figure 3.24). Because of the spectral overlap between

this new transient and **44f**, obtaining accurate decay kinetics for the reaction of **44f** with

NaOMe was not possible (*vide infra*). In order to estimate a rate constant, the decay

recorded at the lowest [NaOMe] studied was used to estimate k_{NaOMe} (Table 3.12).
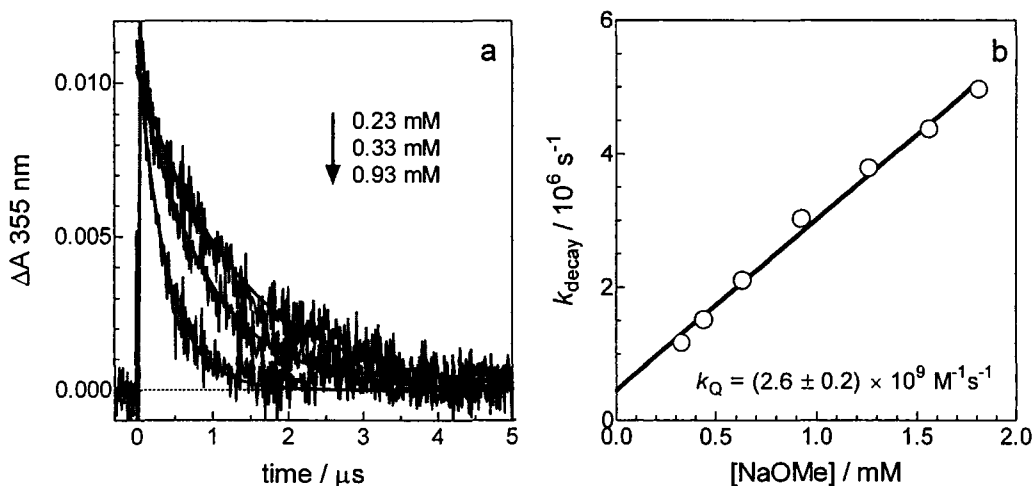
Figure 3.23. (a) Transient decay profiles of **44c** in methanol containing various concentrations of NaOMe. The black line is the non-linear least squares fit of the decay to first-order kinetics. (b) Plot of k_{decay} vs. [Q] for the quenching of **44c** with NaOMe in methanol.

Table 3.12. Rate constants for the reactions of **44a,b,c,d,f** with NaOMe in methanol.

44	k_{NaOMe} / 10^9 $M^{-1}s^{-1}$
a (H)	3.03 ± 0.06
b (mp-Me$_2$)	1.9 ± 0.4 [a]
c (p-Me)	2.6 ± 0.2
d (p-F)	4.0 ± 0.3
f (p-CF$_3$)	3.7 ± 0.5 [b]

a. measured by S. Chitnis. *b* based on a single data point recorded at the lowest [NaOMe] studied.
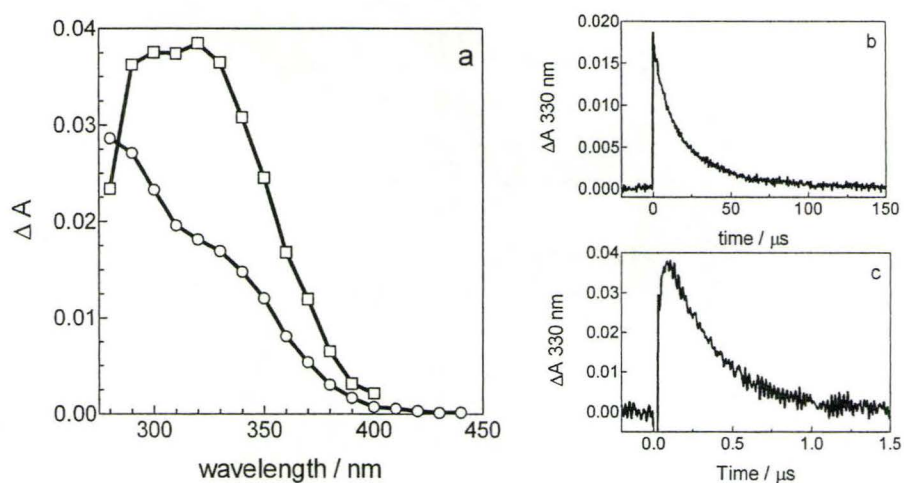
Figure 3.24. (a) Transient absorption spectra from laser flash photolysis of **33f** in methanol in the presence of 0 mM NaOMe (○) and 5.1 mM NaOMe (□) recorded 0.32-0.96 μs and 0.11-0.12 μs after the laser pulse, respectively. (b) Transient growth-decay profile recorded at 330 nm in the absence of NaOMe. (c) Transient growth-decay profile recorded at 330 nm in the presence of 5.1 mM NaOMe.

This transient is assigned to the germyl anion (**52**) based on the similarity of the spectrum to that previously assigned to Ph$_2$MeGe$^-$Li$^+$ (λ_{max} = 310 nm in THF)[18] and Me$_3$Ge$^-$[NBu$_4$]$^+$ (λ_{max} = 325 nm in HMPA)[19]. The fact this transient could only be detected with the trifluoromethyl analogue is reasonable because of the stabilization of the negative charge afforded by the substituent in this case (eq 3.18).

$$(3.18)$$
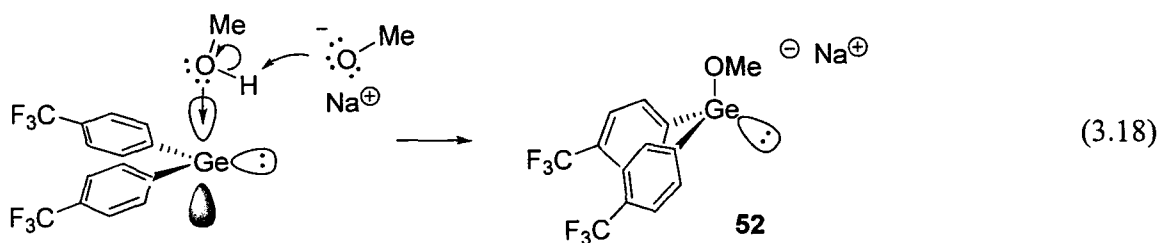
The Hammett plot of the rate constants for the reactions of **44a,b,c,d,f** with NaOMe in methanol is shown in Figure 3.25. Clearly the slope is positive over the substituents from mp-Me$_2$ to p-F, but how the p-CF$_3$ analogue fits on this plot is unclear. The formation of **52**, the spectrum of which overlaps that of **44f**, complicates the situation because it is not known how much uncertainty the presence of this additional transient will introduce into k_{decay}-**44f**. The positive ρ value over the range of mp-Me$_2$ to p-F is consistent with a build-up of negative charge at germanium in the transition state of rate-determining step of the mechanism (eq 3.19).
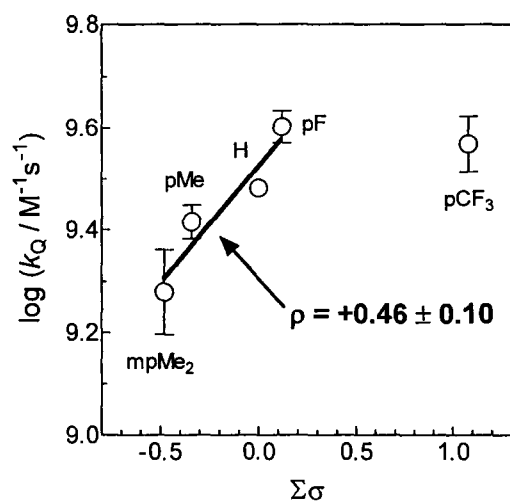
Figure 3.25. Hammett plot for the reaction of **44** with NaOMe in methanol.

(3.19)
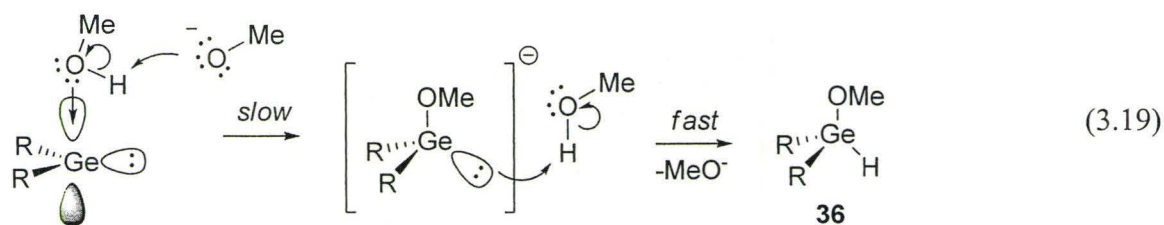
Data were later obtained (Ian Duffy - unpublished) for the reaction of the

germylene-MeOH complexes **44g** (*mm*-$(CF_3)_2$) and $(C_6F_5)_2$Ge-MeOH with NaOMe in

MeOH. The rate constants were found to be essentially the same as that measured with

44f. These data suggest that the value measured for the p-CF_3 analogue is likely real and

that the error introduced by the spectral overlap of the corresponding anion is minimal. A

probable reason for the plateau is that the diffusion limit for the reaction of sodium

methoxide in methanol has been reached. Although the generic diffusion rate constant in

methanol at 25 °C is $k_{diff} = 1.2 \times 10^{10}$ $M^{-1}s^{-1}$ and this value has not yet been reached,

sodium methoxide in methanol is highly solvated[20] and thus the diffusion rate constant

for the reaction of methoxide in methanol is likely smaller than in the absence of

solvation. The Hammett plot including these additional points is shown in Figure 3.26.
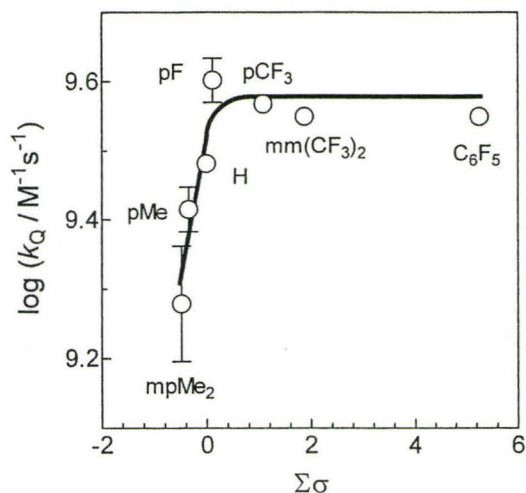
Figure 3.26. Hammett plot for the reaction of **44a-g** and $(C_6F_5)_2Ge\text{-MeOH}$ with NaOMe in methanol.

3.7. Summary

Aromatic substitution has little effect on the forward rate constant for the reversible reaction of germylenes with THF ($k \approx 10^{10}$ $M^{-1}s^{-1}$) but there is a large effect on the equilibrium constant ($K_{GePh2\text{-}THF} \approx 23,000$ M^{-1}; $\rho = +1.3$), consistent with the germylene playing the role of the electrophile in the Lewis acid-base complexation. The equilibrium constant for complexation of the germylene with $HNEt_2$ is sufficiently large that it cannot be measured by our LFP system ($K_{GePh2\text{-}HNEt2} > 25,000$ M^{-1}), while the forward rate constant for the approach to equilibrium is $k_{GePh2\text{-}HNEt2} = (7.3 \pm 0.9) \times 10^9$ $M^{-1}s^{-1}$. There is a small substituent effect on this rate constant ($\rho = +0.07 \pm 0.01$), suggestive of electrophilic behaviour by the germylene. No molecular products could be detected.

The reaction of diarylgermylenes with HOAc yields the corresponding

diarylacetoxygermane in high yield. Kinetic studies suggest the product is formed via a

two-step mechanism involving initial complexation followed by proton transfer. Ethyl

acetate was employed to model the proposed complexation step and to obtain

thermodynamic data on the Lewis acid-base equilibrium between the germylene and the

ester. From this we conclude that complexation is the rate-determining step with HOAc,

which occurs with a rate constant of $k_{\text{GePh2-HOAc}} = (3.9 \pm 0.6) \times 10^9 \, \text{M}^{-1}\text{s}^{-1}$. The

equilibrium constant for this complexation was estimated to be $K_1 \approx 400 \, \text{M}^{-1}$. The intra-

molecular proton transfer within the complex occurs with a rate constant of $k_2 > 10^8 \, \text{s}^{-1}$.

The behaviour of diarylgermylenes in the O-donor solvents MeOH and THF has

been examined. In both cases, generation of the germylene in these solvents leads to the

immediate formation of the corresponding Lewis acid-base complex, which decays over

tens of microseconds. In methanol, the OH insertion product is formed as expected based

on the known reactivity of germylenes with methanol in hexanes solution.

In tetrahydrofuran, the decay of the germylene-THF complex is accelerated by the

presence of acid. The rate constant ($k_{37\text{-MeSO3H}} = (2.6 \pm 0.1) \times 10^7 \, \text{M}^{-1}\text{s}^{-1}$) varies with

substituent in a manner consistent with a build-up of positive charge at germanium ($\rho = -$

0.17 ± 0.01). While it is reasonable to conclude this is due to protonation of the

germylene-THF complex by the acid, no spectroscopic evidence for a germyl cation

could be found.

In methanol, the decay of the germylene-MeOH complex is also accelerated by

the presence of acid leading to a rate constant of $k = (3.9 \pm 0.2) \times 10^9 \, \text{M}^{-1}\text{s}^{-1}$ for the

reaction of **44a** with MeSO$_3$H in methanol. Protonation of the complex in the rate

determining step is supported by the substituent effects (ρ = -0.56 ± 0.08) and a kinetic

isotope effect of KIE = 2.2 ± 0.2 was measured with **44f**. The results are consistent with

general acid catalysis in the formation of the OH insertion product. There was no

spectroscopic evidence for the formation of a germyl cation. The decay of the

germylene-MeOH complex is accelerated in the presence of NaOMe, leading to a rate

constant k = (3.0 ± 0.1) × 10^9 M^{-1}s^{-1} for the reaction of **44a** with NaOMe in methanol.

Deprotonation of the complex by methoxide is supported by the substituent effects (ρ =

+0.46 ± 0.10) and in one case (from LFP of **33f**), the growth of a new transient can be

detected in the presence of the base. The yield of this transient, which we have assigned

to the germyl anion **52**, increases with increasing methoxide concentration and can only

be detected with the most electron poor germylene (p-CF$_3$). The absorbance maximum of

this transient is in good agreement with the spectroscopic data of other germyl anions

reported in the literature.

3.8. References

1.   Leigh, W. J.; Lollmahomed, F.; Harrington, C. R.; McDonald, J. M. *Organometallics* **2006**, *25*, 5424.
2.   Leigh, W. J.; Harrington, C. R.; Vargas-Baca, I. *J. Am. Chem. Soc.* **2004**, *126*, 16105. (Errata: *J. Am. Chem. Soc.* **2006**, *128*, 1394.).
3.   Smith, D. W., *Inorganic Substances*. Cambridge University Press: Cambridge, UK, 1990.
4.   Lollmahomed, F.; Huck, L. A.; Chitnis, S. S.; Harrington, C. R.; Leigh, W. J. *Organometallics* **2009**, *28*, 1484.
5.   Hirshfeld, F. L. *Theor. Chim. Acta.* **1977**, *44*, 129.
6.   te Velde, G.; Bickelhaupt, F. M.; van Gisbergen, S. J. A.; Fonseca Guerra, C.; Baerends, E. J.; Snijders, J. G.; Ziegler, T. *J. Comput. Chem.* **2001**, *22*, 931.
7.   Allred, A. L.; Rochow, E. G. *J. Inorg. Nucl. Chem.* **1958**, *5*, 269.

8.   Schoeller, W. W.; Schneider, R. *Chem. Ber. Recl.* **1997**, *130*, 1013.

9.   Lappert, M. F.; Miles, S. J.; Atwood, J. L.; Zaworotko, M. J.; Carty, A. J. *J. Organomet. Chem.* **1981**, *212*, C4.

10. Rivière, P.; Rivière-Baudet, M.; Couret, C.; Satgé, J. *Synth. React. Inorg. Met. - Org. Chem.* **1974**, *4*, 295.

11. Klein, B.; Neumann, W. P.; Weisbeck, M. P.; Wienken, S. *J. Organomet. Chem.* **1993**, *446*, 149.

12. *CRC Handbook of Chemistry and Physics, Internet Version.* 90 ed.; CRC Press/Taylor and Francis: Boca Raton, FL, 2010.

13. Hunter, E. P. L.; Lias, S. G. *J. Phys. Chem. Ref. Data* **1998**, *27*, 413.

14. Huck, L. A.; Leigh, W. J. *Organometallics* **2007**, *26*, 1339.

15. Leigh, W. J.; Harrington, C. R. *J. Am. Chem. Soc.* **2005**, *127*, 5084.

16. Ding, F.; Smith, J. M.; Wang, H. *J. Org. Chem.* **2009**, *74*, 2679.

17. Neumann, W. P. *Chem. Rev.* **1991**, *91*, 311.

18. Mochida, K.; Wakasa, M.; Sakaguchi, Y.; Hayashi, H. *J. Am. Chem. Soc.* **1987**, *109*, 7942.

19. Mochida, K.; Suzuki, H.; Nanba, M.; Kugita, T.; Yokoyama, Y. *J. Organomet. Chem.* **1995**, *499*, 83.

20. Gold, V.; Grist, S. *J. Chem. Soc. B* **1971**, 1665.

Chapter 4 – Reactions of Diarylgermylenes with Carbon Tetrachloride

4.1. Overview

The reaction of germylenes with halocarbons has been extensively studied over the past few decades (see Chapter 1), with most of the work focused on the reactions with carbon tetrachloride (CCl_4).[1-10] The major germylene-derived product isolated after thermolysis of **53** in carbon tetrachloride is Me_2GeCl_2 (**54**)(eq 4.1).[11] When the reaction was performed within an NMR spectrometer, the CIDNP effects observed in the ^{1}H NMR spectrum led to a proposed mechanism involving the intermediacy of a caged singlet radical pair (**55**), the predominant fate of which is cage escape (eq 4.2).[2]

$$ (4.1) $$

$$ (4.2) $$

We undertook kinetic studies on the reaction of CCl_4 with **Ga-f** in both hexanes and THF solution. Product studies of the reaction of **Ga** and **37a** with CCl_4 in hexanes and THF, respectively, were also carried out. The results of these experiments are presented, followed by a discussion of the mechanistic implications.

4.2. Reaction of diarylgermylenes with CCl$_4$ in hexanes - Results

4.2.1. Product studies

The steady-state photolysis of **33a** (0.02 M) in C$_6$D$_{12}$ containing CCl$_4$ (0.05 M) was monitored by ^{1}H NMR spectroscopy; Figure 4.1 shows some representative spectra. The identifiable molecular products were **56-58** and DMB (eq 4.3). Product yields were determined from the (initial) slopes of the concentration vs. time plots (shown in Figure 4.2), relative to that for disappearance of the starting material. Based on the intensity of the aromatic and germyl hydride ^{1}H NMR resonances of **57**, it was estimated that approximately 50% of the material is deuterated (*i.e.* Ph$_2$GeDCl, **57-d**). A reaction in C$_6$H$_{12}$ performed under similar conditions was monitored by GC/MS, which allowed the detection of hexachloroethane (C$_2$Cl$_6$) and **59** in addition to **56-58** (eq 4.3). In addition to these major products, broadening of the baseline in the aromatic region was observed and became more pronounced with increased photolysis times. Significant amounts of unidentified material giving rise to resonances in the allylic (δ 3.5 ppm) and aliphatic (δ 1.5-2.2 ppm) regions of the NMR spectrum were also detected.

$$\text{Ph}_2\text{GeCl}_2 \; + \; \text{Ph}_2\text{GeHCl} \; + \; \text{Ph}_2\text{Ge(Cl)(CCl}_3) \; + \; \text{DMB}$$

| | **56** (30%) | **57** (18%) | **58** (4%) | DMB (76%) |

33a $\xrightarrow[\text{0.05 M CCl}_4]{h\nu}$

59 (19%)   (0.5%)

(4.3)
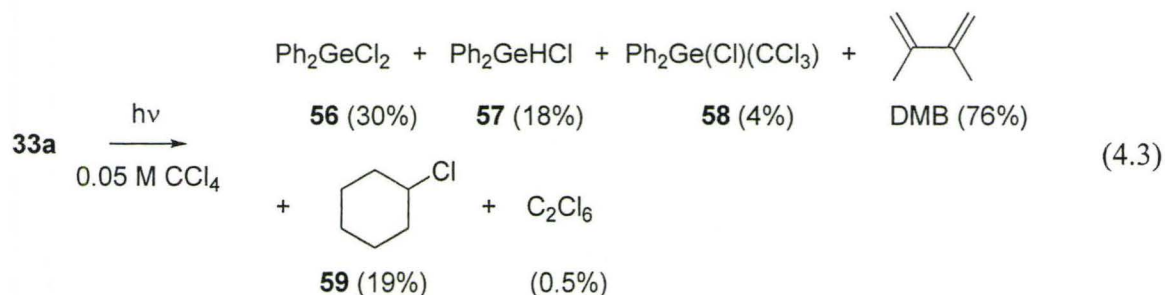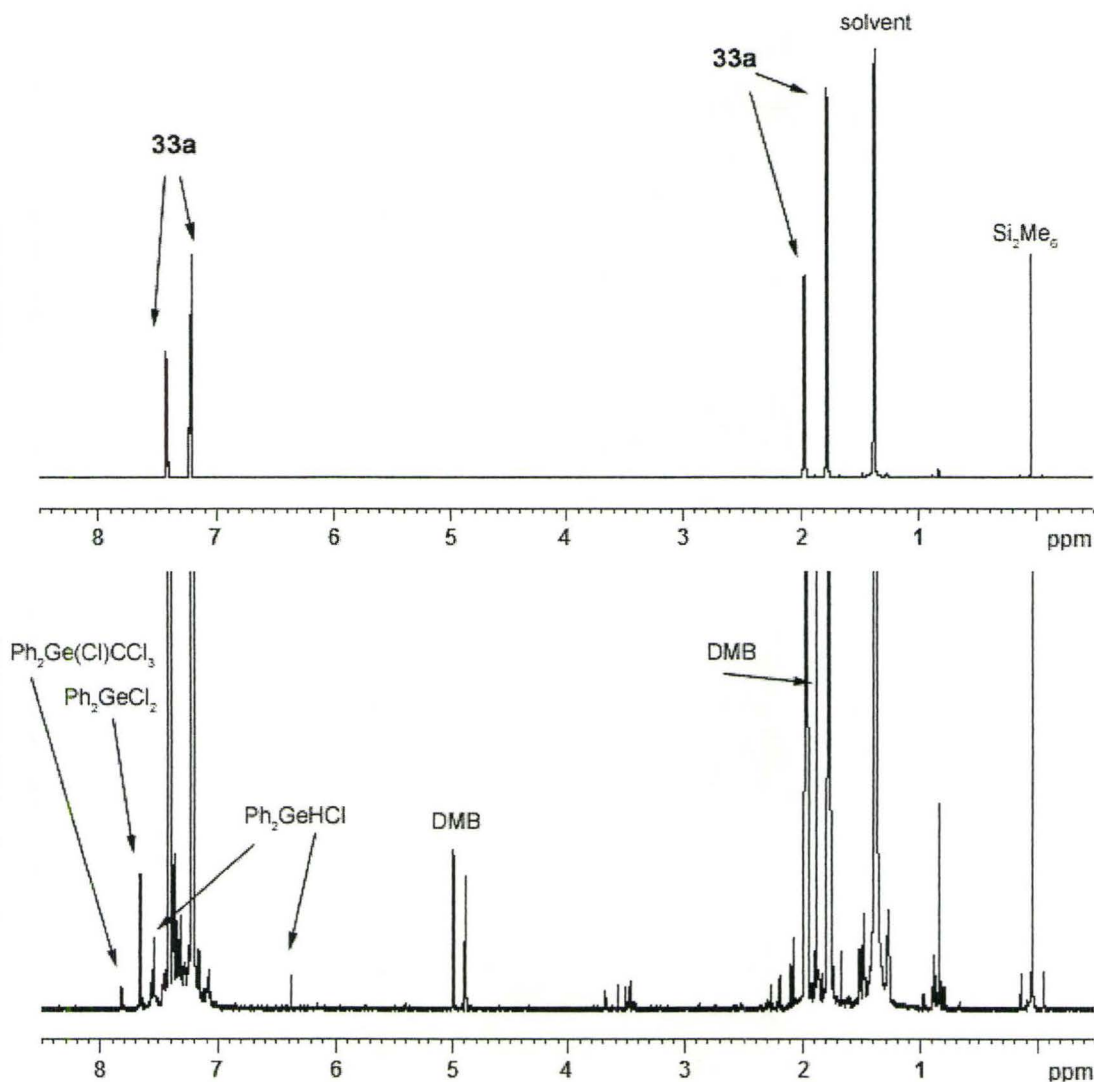
Figure 4.1. 600 MHz ^{1}H NMR spectrum of a 0.02 M solution of **33a** in C_6D_{12} containing CCl_4 (0.05 M) and Si_2Me_6 (3 mM) before (top) and after 254 nm photolysis for 200 s (bottom).

The presence of the hydrochlorogermane **57** was puzzling. In the earlier studies

by Neumann on the reaction of $GeMe_2$ with CCl_4, the corresponding product

(Me_2GeHCl) was not reported. The presence of **56, 59**, and C_2Cl_6 provide support for a

128

mechanism involving initial halogen atom abstraction from CCl_4, suggesting that the singlet radical-pair **60** is the primary product. The low yield of the radical-pair recombination reaction product (**58**) thus indicates that the

$$\left[Ph_2\overset{\bullet}{Ge}Cl \quad \overset{\bullet}{C}Cl_3 \right]$$
$$\mathbf{60}$$

dominant fate of **60** is cage-escape. If **57** is derived from the Ph_2GeCl radical, the H atom must come from the allylic positions of **33a** as these C-H bonds are predicted to have bond dissociation energies of roughly the same magnitude[12] as the resulting Ge-H bond,[13] making the reaction thermodynamically plausible. The formation of the deuterochloride **57-*d*** is rationalized as resulting from insertion of $GePh_2$ into DCl.[14] Indeed, acid was detected when moist litmus paper was exposed to the head space vapours above the steady-state photolysis solution after the experiment. To determine whether the reaction of $GePh_2$ with HCl was plausible under our reaction conditions, a solution of **33a** (0.04 M) in C_6D_{12} saturated with $HCl_{(g)}$ was irradiated, resulting in the formation of **57** in high yield (eq 4.4).

$$\mathbf{33a} \quad \xrightarrow[\substack{HCl_{(g)} \\ C_6D_{12}}]{h\nu} \quad Ph_2GeHCl \quad + \quad DMB \qquad\qquad (4.4)$$
$$\mathbf{57}\,(83 \pm 3\%) \quad (80 \pm 2\%)$$
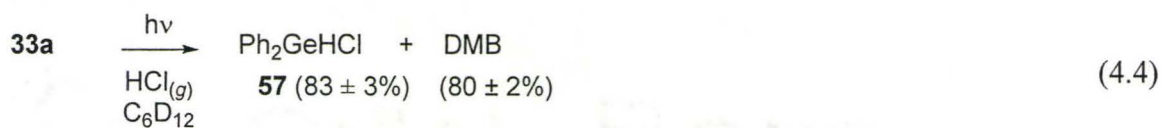
In the event that **57** is derived from the reaction of $GePh_2$ with H(D)Cl, what is the source? The concentrations of **33a** (0.02 M) and of CCl_4 (0.05 M) were such that 99.7% of the incident light is absorbed by **33a** ($\varepsilon_{254\,nm\,\mathbf{33a}} = 340$ M^{-1} cm^{-1} and $\varepsilon_{254\,nm\,CCl4} = 0.44$ M^{-1} cm^{-1}) thus chlorine atom generation from photolysis of CCl_4 (followed by H /D atom abstraction from the solvent) is the most likely source – chlorine atoms will abstract hydrogen atoms from hydrocarbon solvents at diffusion controlled rates.[15] (Another

possible source of HCl is hydrolysis of any of the chlorogermanes produced in the

reaction (56-58) by adventitious water.) If the primary source of H(D)Cl results from

photolysis of CCl_4, the concentration of H(D)Cl will be dependent on the concentration

of CCl_4. A number of experiments were performed at different concentrations of CCl_4

and the results are summarized in Table 4.1. Concentration vs. time plots are given in

Figure 4.2.

Table 4.1. Product yields (%) from photolysis of **33a** (0.02 M) with C_6D_{12} containing
various concentrations of CCl_4.

$[CCl_4]$ / M	Ph_2GeCl_2 (56)	$Ph_2GeH(D)Cl$ (57)	$Ph_2Ge(Cl)CCl_3$ (58)	DMB	%D (57-**d**)
0.006	9 ± 5	3 ± 1	*a*	82 ± 10	*a*
0.02	20 ± 4	22 ± 3	3.3 ± 0.7	96 ± 6	67
0.05	30 ± 5	18 ± 3	4.1 ± 0.7	76 ± 6	56
0.10	33 ± 4	27 ± 4	3.9 ± 0.5	78 ± 8	44

a. could not be measured.
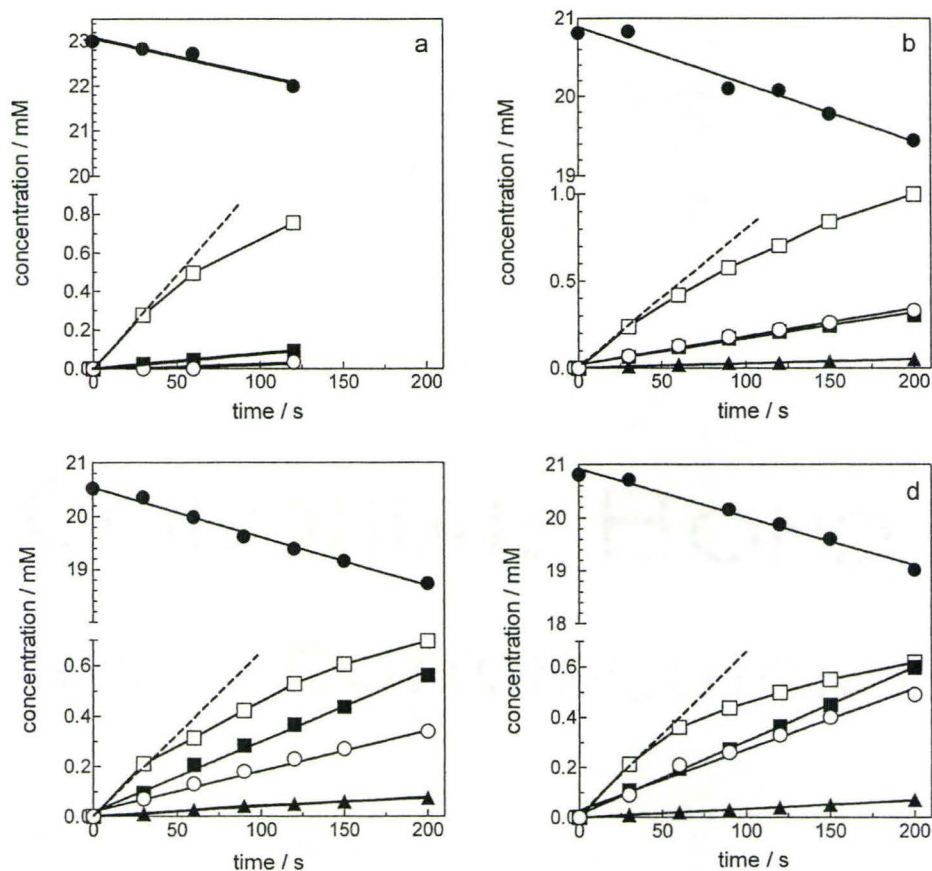
Figure 4.2. Concentration vs. time plots from steady state photolysis of **33a** (0.02 M, ●) in C_6D_{12} containing various concentrations of CCl_4 ((a) 0.006 M; (b) 0.02 M; (c) 0.05 M; (d) 0.10 M) as determined by ^1H NMR spectroscopy; **56** (■), **57** (O), **58** (▲), and DMB (□).

What is clear from these figures is that the consumption of DMB is more rapid at

higher concentrations of CCl_4 and the yield of **57** is highest with the highest

concentration of the halocarbon, which is consistent with the proposal that **57** is derived

from the initial photolysis of CCl_4. We suspected that radicals produced in the

$GePh_2/CCl_4$ reaction could add to DMB and lead to some of the unidentified aliphatic

products that were detected in the ^{1}H NMR spectrum. A solution of CCl_4 (0.25 M) and

DMB (15 mM) in C_6D_{12} solution was irradiated and the progress monitored by ^{1}H NMR

spectroscopy. As shown in Figure 4.3, some of the products observed in spectrum of the

GePh$_2$/CCl$_4$ reaction indeed correspond to radical addition to the diene. The

concentration vs. time plots of these unknown products formed in the steady-state

photolysis experiments of **33a** with CCl$_4$ *always* exhibited upward curvature. We also

ran a GC/MS of this photolysis mixture and compared it to that of the GePh$_2$/CCl$_4$

reaction; nearly all of the products that could be detected by GC/MS with a lower

retention time than **56-58** were present in the chromatogram of the diene/CCl$_4$ photolysis

mixture.
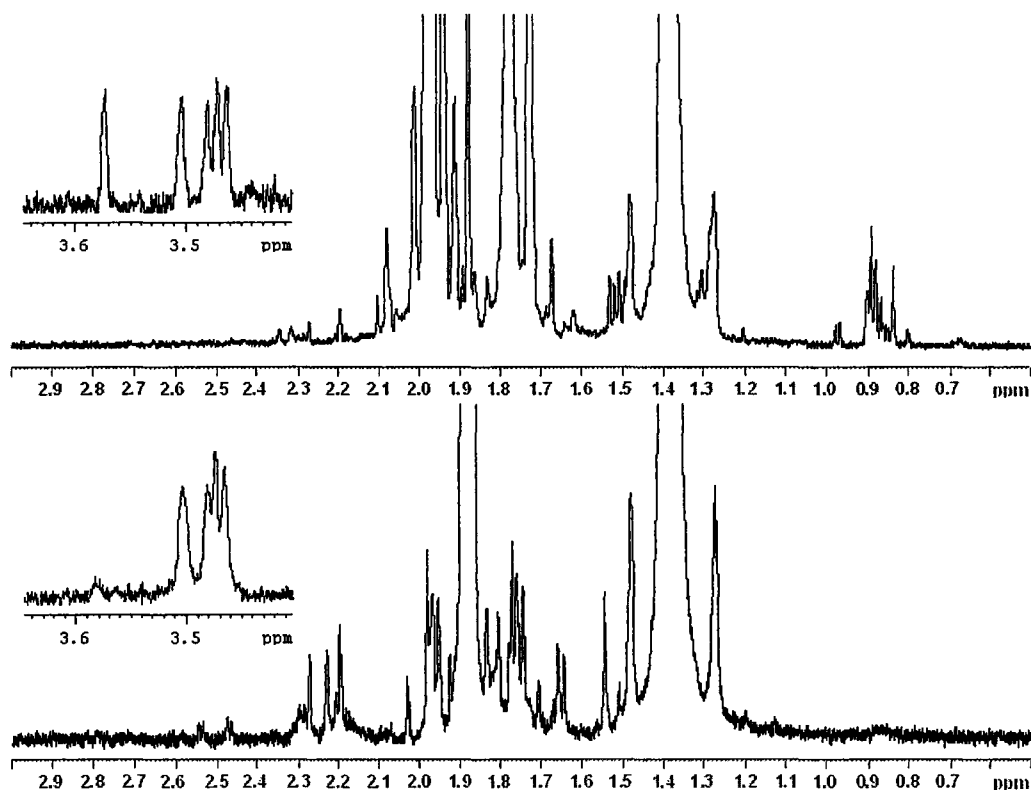
Figure 4.3. Selected regions of the ^{1}H NMR spectrum after photolysis of solutions of (*top*) **33a** (0.02 M) + CCl$_4$ (0.10 M) in C$_6$D$_{12}$ and (*bottom*) CCl$_4$ (0.25 M) + DMB (15 mM) in C$_6$D$_{12}$.

Each of the products shown in eq 4.3 was identified by NMR or GC/MS by spiking the mixture with an independently prepared sample. Compounds **56** and **57** were prepared following literature procedures.[16, 17] Compound **58** was prepared via reaction of PhMgBr with **61**, as described by eq 4.5. Compound **58** is a viscous liquid that underwent hydrolysis over several days to yield **62** (eq 4.6). The single crystal x-ray structure of **62** is shown in Figure 4.4.

$$\text{GeCl}_2\text{-dioxane} + \text{CCl}_4 \xrightarrow{\Delta} \text{Cl}_3\text{GeCCl}_3 \xrightarrow{2\text{ PhMgBr}} \text{Ph}_2\text{Ge(Cl)CCl}_3 \qquad (4.5)$$

$$\mathbf{34} \qquad\qquad\qquad \mathbf{61}\ (66\%) \qquad\qquad \mathbf{58}\ (11\%)$$

58 $\xrightarrow[\text{-HCl}]{\text{H}_2\text{O}}$

$$\text{Ph}^{\text{''}}\overset{\overset{\displaystyle \text{OH}}{|}}{\underset{\underset{\displaystyle \text{Ph}}{\diagup}}{\text{Ge}}}{}_{\diagdown}\text{CCl}_3$$

62

(4.6)
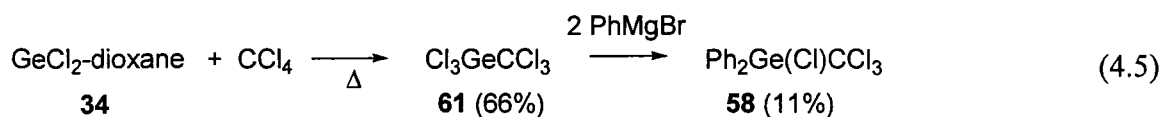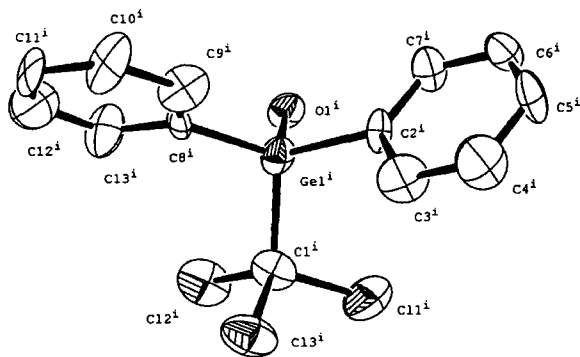
Figure 4.4. ORTEP diagram of **62** (50% probability ellipsoids). H atoms omitted for clarity. Select bond distances (Å): GeC^1 1.992(15); GeC^2 1.953(15); GeC^8 1.950(15); GeO 1.775(9). Additional details provided in Chapter 9.

The overall mass balance of germanium in the reaction of GePh$_2$ and CCl$_4$ is poor (ca. 40%; see eq 4.3). A MALDI mass spectrum of the reaction mixture shows the presence of several high molecular weight compounds (500 < M.W. < 1000 Da) containing two or three germanium atoms (Figure 4.5). The presence of these high molecular weight oligogermanes is consistent with the broadening of the aromatic region of the ^{1}H NMR spectrum that was observed over the course of the photolysis.[18, 19] The formation of oligogermanes will also lead to longer wavelength absorption in the UV-vis spectrum, an effect that depends on the molecular weight as well as chemical composition of the oligomers.[18] Although we were unable to identify any of these products by GC/MS, analysis showed that the six most intense peaks that elute with retention times longer than **58** (excluding residual **33a**) all undergo fragmentation to yield the PhGeCl ion.
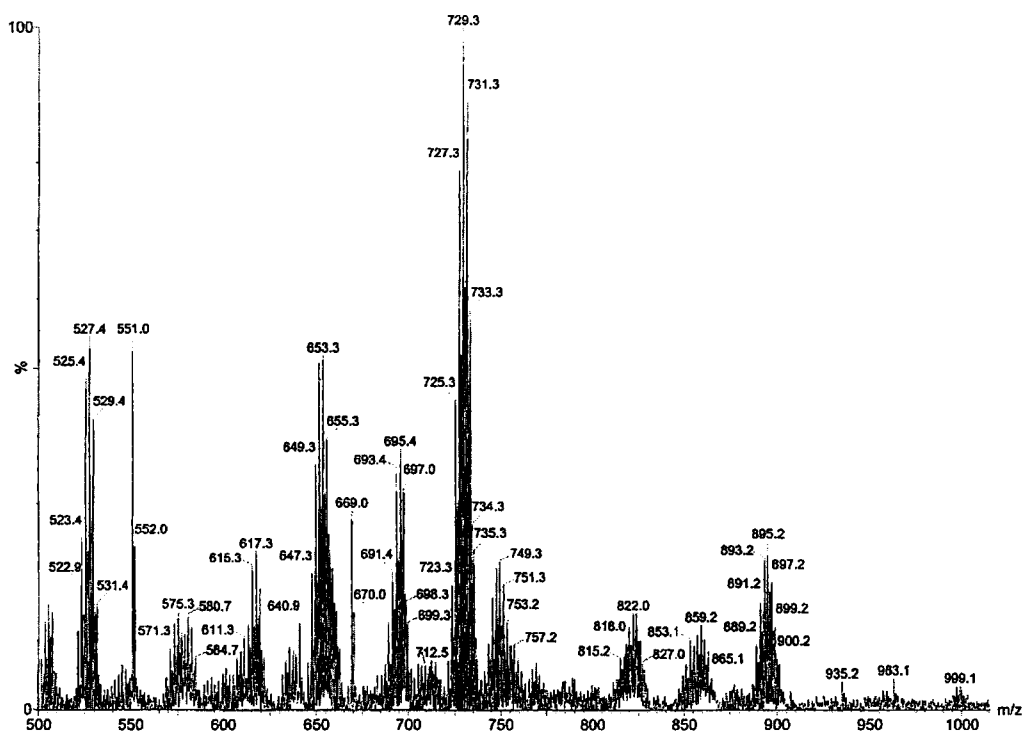
Figure 4.5. A MALDI mass spectrum of the mixture resulting from photolysis of a 0.02 M solution of **33a** in hexanes containing 0.05 M CCl₄.

4.2.2. Kinetics measurements by laser flash photolysis.

The decay rates of **Ga-f** in hexanes increased in the presence of CCl₄ as shown in Figure 4.6a. The decay traces fit to first-order kinetics in the presence of CCl₄ and the plots of k_{decay} vs. [CCl₄] were linear in each case (see Figure 4.6b) and afforded the rate constants listed in Table 4.2. The rate constant measured for the reaction of **Ga** with CCl₄ in hexanes is in agreement with the previously reported value.[20] A transient absorption spectrum of **33a** recorded in hexanes containing 0.5 M CCl₄ showed no changes in the relative intensities of the germylene absorbance maxima (500 nm and ca. 300 nm) and no new transients that could be ascribed to the formation of a Lewis acid-

135

base complex between the germylene and halocarbon could be detected.

Table 4.2. Absolute rate constants for the reactions of germylenes **Ga-f** with CCl_4 in hexanes.

G	k_{CCl4} / 10^6 $M^{-1}s^{-1}$
a (H)	11.6 ± 1.0
b (mp-Me_2)	12.3 ± 2.0
c (p-Me)	12.6 ± 4.0
d (p-F)	6.9 ± 1.6
e (m-F)	8.0 ± 0.8
f (p-CF_3)	2.6 ± 1.2
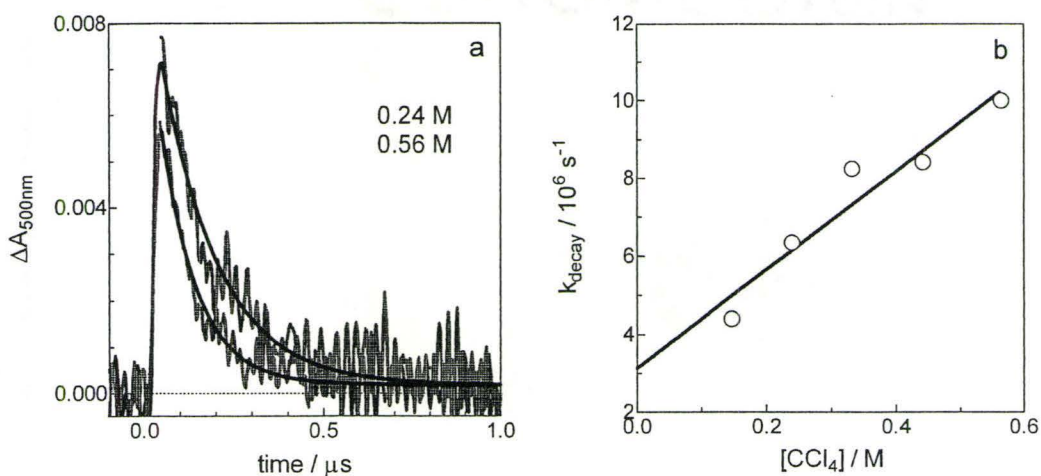
Figure 4.6. (a) Transient decay profiles of **Gc** (CH_3) in hexanes at containing of CCl_4. The black lines are the fit of the decays to first-order decay kinetics (eq 2.19). (b) Plot of k_{decay} vs. $[CCl_4]$ for the reaction of **Gc** with CCl_4 in hexanes.

LFP experiments require much lower concentration ratios of **33a** to CCl_4 than are employed in the steady-state photolysis experiments, so competing photolysis of CCl_4 in the laser experiments is of greater concern ($\varepsilon_{248\,nm\,33a} = 290$ M^{-1} cm^{-1} and $\varepsilon_{248\,nm\,CCl4} =$

1.23 M^{-1} cm^{-1}). Within the concentration range of CCl_4 required to produce detectable changes in the germylene decay rates, CCl_4 absorbs up to 40% of the laser light. The quantum yield for Cl-CCl_3 bond homolysis in the gas phase ($\Phi_{Cl} \approx 0.2$).[21] As described above, chlorine atoms will abstract hydrogen atoms to yield HCl and new carbon centered radicals, as well as add to DMB. To test whether the formation of such species will affect our kinetic experiments, a control experiment using **33d** (p-F) was performed. This analogue was chosen as it represents the mid-point on the Hammett σ scale. The decays of **Gd** and **DGd** in the presence of 0.03-0.5 M CCl_4 was monitored as a function of laser intensity, which was attenuated with neutral density filters. With both transients, the observed rate coefficients were approximately constant over the range of intensities studied (*ca.* 20-100% of the full laser power of *ca.* 100 mJ/pulse) thus indicating that co-absorption of the excitation pulse by CCl_4 has a negligible effect on our kinetic experiments. The yield of the germylene decreases slightly with each addition of CCl_4 (this can be seen in Figure 4.6a), but by no more than what would be expected due to screening of the excitation light by the halocarbon. This allows the additional conclusion that CCl_4 does not quench the excited state of **33** at the concentrations employed in these experiments.

A plot of the rate constants for the reactions of **Ga-f** with CCl_4 in hexane solution versus Hammett σ constant afforded a reaction constant of $\rho = -0.38 \pm 0.10$, as shown in Figure 4.7a. Rate constants for the reaction of **Ga** with CCl_4 in hexane were measured at several temperatures over the range of 10-60 °C. The Arrhenius plot, shown in Figure 4.7b, led to the values of $E_a = -0.7 \pm 0.7$ kcal/mol and log A = 7.0 ± 0.5 for the reaction of

the parent germylene **Ga** with CCl_4.
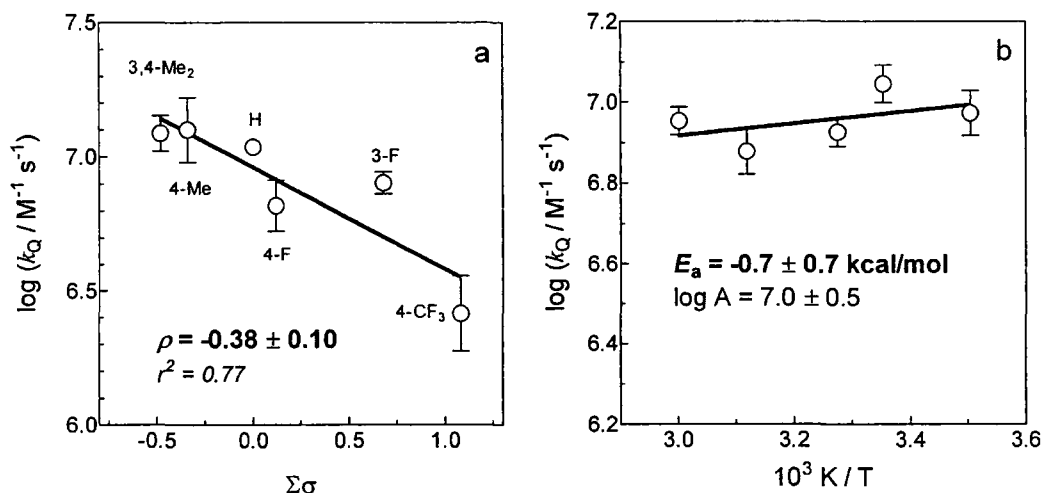
Figure 4.7. (a) Hammett plot of the rate constants for the reaction of **Ga-f** in hexanes. (b) Arrhenius plot of the reaction of $GePh_2$ with CCl_4 in hexanes determined over the range of 10-60 °C.

4.2.3. Low temperature matrix photolysis

It has been proposed that the reaction of germylenes with halocarbons begins with the formation of a Lewis acid-base complex with the halogen acting as the nucleophile[22] and this suggestion has received support from theoretical calculations.[23-25] Ando and co-workers detected the formation of a variety of germylenes-heteroatom complexes by UV-vis spectroscopy in hydrocarbon matrixes at 77 K.[26] Complexes of $GePh_2$ with chlorocyclohexane (**63a**, λ_{max} = 374 nm) and chlorobenzene (**63b**, λ_{max} = 403 nm) were reported.[26] Because no evidence for the formation of a complex between $GePh_2$ and CCl_4 (**63c**) could be found in the LFP experiments of **33a** in the presence of CCl_4, we turned to

138
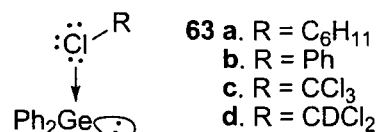
low temperature matrix photolysis to see if **63c** could be detected under these conditions.

The experiments involve cooling to 78 K a solution of a germylene precursor and the halocarbon in 3-methylpentane (3-MP). The freezing point of 3-MP is 110 K,[27] and by cooling the solution rapidly past this point, crystallization is bypassed leading to the formation of super-cooled liquid or glass.[28-30] The glass transition temperature (T_g) is defined as the temperature at which the viscosity is $\eta = 1 \times 10^{13}$ P and for 3-MP, $T_g \approx 77$ K.[28] The super-cooled liquid is disordered and can transmit radiation provided it does not contain a solute that absorbs that particular wavelength. Upon photolysis at 78 K, the germylene can be detected by UV-vis spectroscopy. As the matrix is warmed, the formation of a complex can be detected because the viscosity of 3-MP changes by several orders of magnitude over a few Kelvin (*e.g.* at 82 K $\eta_{3\text{-MP}} = 2.1 \times 10^{10}$ P).[31]

The absorbance maximum of GePh$_2$, produced from photolysis of **65** in 3-MP matrix, is 466 nm.[26, 32] Irradiation **33a** in a 3-MP at 78 K produces **64** (λ_{max} = 285 nm; Figure 4.8) either from direct photochemical rearrangement of

33a or from reaction of GePh$_2$ and DMB within the solvent cage.[33] We found instead that 1,1-diphenylgermacyclobutane (**66**) could be used as an efficient GePh$_2$ precursor in matrix experiments because the photolysis co-product (cyclopropane; eq 4.7) is unreactive.[34, 35]
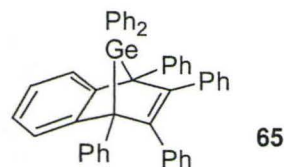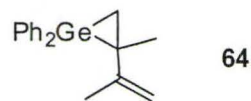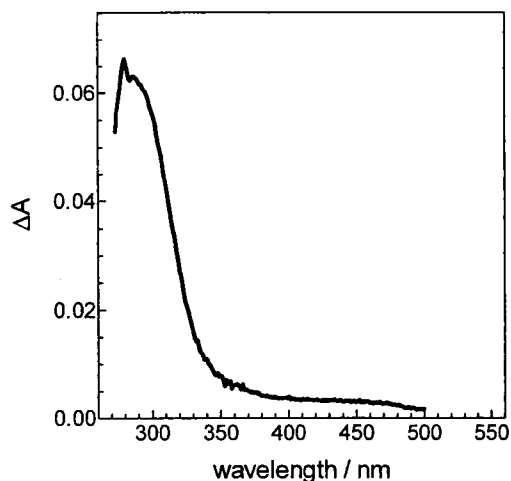
Figure 4.8. The difference between the UV-vis spectra recorded before and after 254 nm irradiation of a solution of **33a** in 3-MP at 78 K. *(Reprinted from reference 33 with permission. © 2007 Springer.)*

$$Ph_2Ge=CH_2 \quad + \quad H_2C=CH_2 \qquad \sim 60\%$$
$$67$$

$$Ph_2Ge \quad \quad h\nu \quad \Phi_{-GeCB} = 0.26 \pm 0.03 \qquad\qquad (4.7)$$
$$66$$

$$GePh_2 \quad + \quad \triangle \qquad \sim 20\%$$
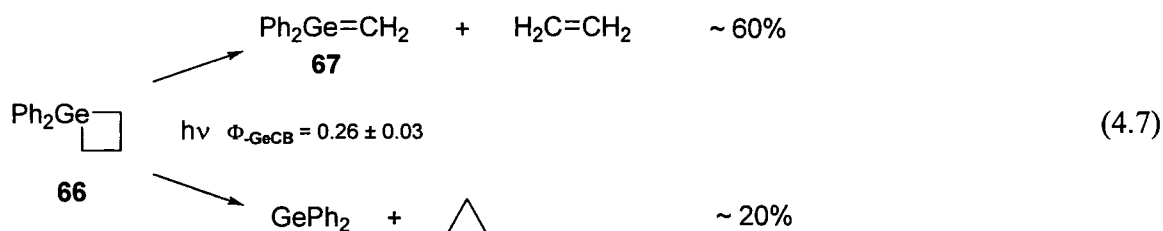
A solution of **66** in 3-MP was cooled to 78 K in a cryostat, which was then placed in a photochemical reactor equipped with 254 nm lamps. Photolysis results in the formation of three distinct absorbance bands, one centered at $\lambda_{max} = 460$ nm, a shoulder absorbance at $\lambda_{max} \approx 330$ nm, and an intense band centered below 300 nm; see Figure 4.9a. The absorbance at 330 nm is assigned to **67**,[34, 35] while the 460 nm absorbance band is assigned to $GePh_2$.[26, 32] The absorbance band at < 330 nm presumably has contributions from both species.

The matrix was irradiated until the new bands stabilized in intensity, and then left in the dark for 30 minutes at 78 K. No change was observed when the UV-vis spectrum

was re-recorded. The matrix was then warmed in 1 K increments and a UV spectrum

recorded at each temperature. At *ca*. 82 K, the intensity of the 460 nm absorbance began

to decrease and undergo a concomitant red-shift as shown in Figure 4.9a. The cause of

this shift of the absorbance maxima towards that of $GePh_2$ in hexanes at ambient

temperature (λ_{max} = 500 nm) is not clear; however, it may be due to the fact the

germylene is not formed in its minimum energy geometry. As the temperature is raised,

the decreasing viscosity allows the germylene to tend towards the minimum energy

geometry (*i.e.* the geometry in fluid solution at ambient temperature). Indeed, EPR

studies have demonstrated that the geometry of diarylcarbenes generated in a matrix

changes upon warming.[36, 37] The spectral shift may also be caused by differences in the

ground- and excited-state energy surfaces at these two temperatures.[38]

The procedure was repeated with a solution of **66** in 3-MP containing 0.15 M

CCl_4. The rates of growth of the absorbance bands were unaffected by the presence of

the halocarbon, as shown in Figure 4.9b. Upon warming, the red-shift of the 460 nm

signal was again observed but was accompanied by a more rapid decrease in intensity

(Figure 4.9b). This is consistent with a more rapid disappearance of $GePh_2$ in the

presence of CCl_4 but without formation of a detectable intermediate. Finally, the

procedure was repeated with a new solution of **66** in 3-MP containing 0.15 M $CDCl_3$.

The rates of growth of the three absorbance bands at 78 K were again unaffected by the

presence of the halocarbon, although the intensity of the **67** was larger in this experiment.

Upon warming of the matrix, there was a blue shift of the 460 nm band to 405 nm, as

shown in Figure 4.9c. Warming past approximately 88 K led to a gradual decrease in

intensity of the signal. This is again consistent with a halocarbon-induced reaction of

$GePh_2$, but via a detectable intermediate with its own discrete absorption spectrum.

Similar results with $CDCl_3$ were obtained using $(Ph_2Ge(SiMe_3))_2$ as the $GePh_2$ precursor.
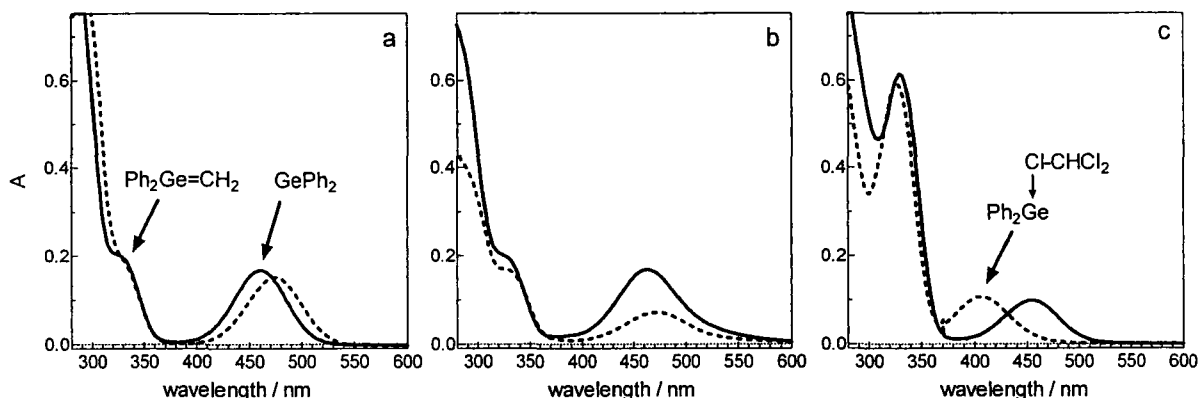
Figure 4.9. (a) UV/vis spectra (solid line) upon photolysis of a dry, deoxygenated 3-methylpentane matrix at 78 K containing **66**. The same matrix, warmed to roughly 87 K (dashed line). (b) As in (a) except the solution contained 0.15 M CCl_4. (c) As in (a) except the solution contained 0.15 M $CDCl_3$.

Interestingly, the results indicate that $GePh_2$ reacts with both CCl_4 and $CDCl_3$ at

82 K, but only with the latter does an intermediate build up in high enough concentrations

to be detected. Thus, the main difference in the two reaction pathways appears to be that

the barrier for further reaction of the intermediate is higher in the case of $CDCl_3$; with

CCl_4 it is too low for the intermediate to be detected.

We hypothesized that we may be able to detect a complex of $GePh_2$ and $CDCl_3$

(**63d**) because $CHCl_3$ reacts with $GePh_2$ at least 50× more slowly than CCl_4.[20] The new

absorbance detected at 405 nm is assigned to **63d**. This absorbance is in the spectral

range of the absorbance maxima of the germylene-chlorocarbon complexes reported by

Ando *et al.*[26] The possibility that the 405 nm absorbance is due to a complex between the germylene and adventitious water seems unlikely because all the experiments were performed under similar conditions and although the UV absorbance maximum of a germylene water complex has not been reported, the absorbance maxima of such species should be further to the blue based on the spectra reported for other germylene/*O*-donor complexes in 3-MP at 77 K (*e.g.* λ_{max} GePh$_2$-2-MeTHF: 325 nm and λ_{max} GePh$_2$-EtOH: 333 nm).[26]

4.3. Reaction of the diarylgermylene-THF complex with CCl$_4$ in THF - Results

4.3.1. Product studies

Photolysis of **33a** (0.02 M) in THF-d_8 containing CCl$_4$ (0.05 M) afforded the same products as were obtain in cyclohexane but in markedly different yields (eq 4.8). The formal C-Cl insertion product (**58**) is the major product under these conditions, the broadening of the baseline in the aromatic region is less severe, and the unidentified resonances in the δ 1.5-2.2 and δ 3.5 regions of the NMR spectrum are absent. Figure 4.10 shows the ^{1}H NMR spectrum before and after photolysis of a solution of **33a** in THF containing 0.05 M CCl$_4$; the total conversion is approximately 10%. The growth of the products follows the same pattern as in cyclohexane, except that the curvature in the concentration vs. time plot of DMB is much less pronounced than it is in C$_6$D$_{12}$ photolyses (see Figure 4.11). The amount of **57** present as **57-*d*** was approximately 20%. Note also that the concentration vs. time plot of **57** exhibits slight curvature at low photolysis times, consistent with its formation being due to the reaction of GePh$_2$ with

HCl. As we observed in C_6D_{12}, the yield of **57** varied somewhat from experiment to experiment, and the resonance in the ^{1}H NMR spectra due to trace amounts of water broadened upon irradiation, an effect consistent with the presence of HCl in the product mixture.[39] We noted that the area of this peak increased by *ca.* 15% over the course of the experiment. When a reaction under identical conditions (except using non-deuterated THF) was monitored by GC/MS, C_2Cl_6 was detected in trace amounts.

$$\textbf{33a} \xrightarrow[\substack{\text{THF-}d8 \\ 0.05\ \text{M CCl}_4}]{hv} \text{Ph}_2\text{GeCl}_2 \ + \ \text{Ph}_2\text{GeHCl} \ + \ \text{Ph}_2\text{Ge(Cl)(CCl}_3) \ + \ \text{DMB} \tag{4.8}$$

$$\textbf{56}\ (33\%) \qquad \textbf{57}\ (20\%) \qquad \textbf{58}\ (49\%) \qquad \text{DMB}\ (87\%)$$
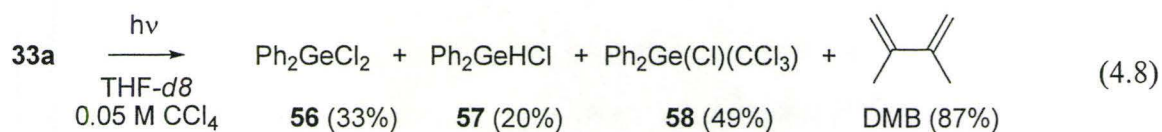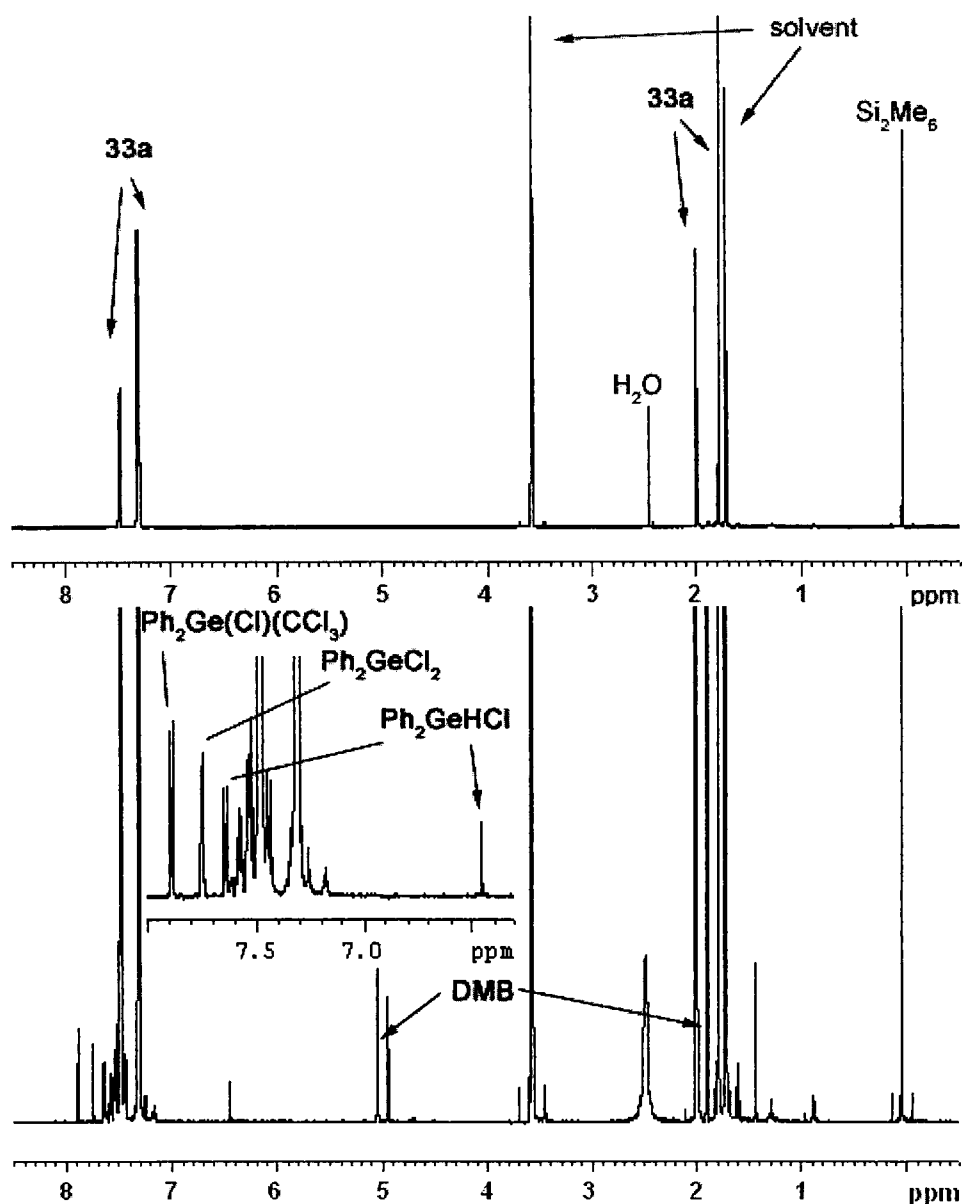
Figure 4.10. 600 MHz ^{1}H NMR spectrum of a 0.02 M solution of **33a** in THF-d_8 containing CCl_4 (0.05 M) and Si_2Me_6 (3 mM) before (*top*) and after photolysis for 200 s with 254 nm light (*bottom*). Note the broadening of the water peak, which is consistent with the presence of HCl.
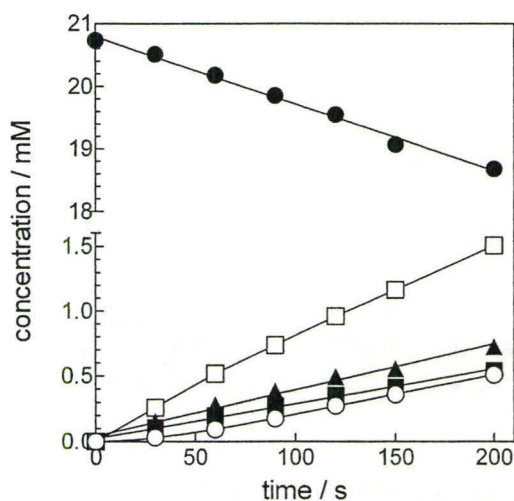
Figure 4.11. Product distribution upon 254 nm photolysis of **33a** (●) (0.02 M in THF-d_8) and in the presence of CCl_4 (0.05 M) as determined by ^{1}H NMR. **56** (■), **57** (○), **58** (▲), and DMB (□).

4.3.2. Kinetics measurements by laser flash photolysis

The decay rates of the germylenes **37a-f** in THF increased in the presence of

CCl_4, as shown in Figure 4.12a. The decays fit acceptably to first-order kinetics in the

presence of CCl_4 and k_{decay} increased in proportion to the concentration of added reagent

(see Figure 4.12b). The absolute rate constants obtained from the plots of k_{decay} vs.

[CCl_4] are listed in Table 4.3.

Table 4.3. Absolute rate constants for the reactions of the germylene-THF complexes (**37a-f**) with CCl_4 in THF.

37	k_{CCl4} / 10^6 $M^{-1}s^{-1}$
a (H)	4.3 ± 0.3
b (mp-Me$_2$)	6.4 ± 0.6
c (p-Me)	2.3 ± 0.2
d (p-F)	0.86 ± 0.07
e (m-F)	0.56 ± 0.08
f (p-CF$_3$)	1.3 ± 0.2
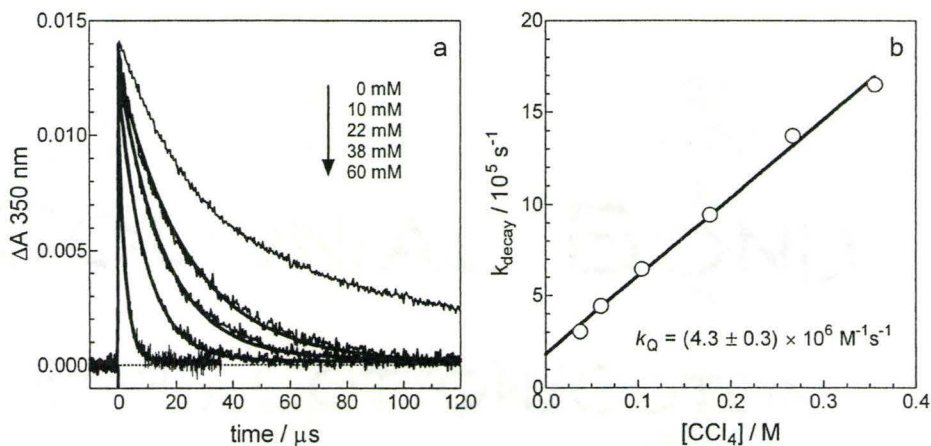
Figure 4.12. (a) Transient decay profiles of germylene-THF complex **37a** in THF containing various concentrations of CCl_4. The black lines are the fit of the decays to first-order kinetics. (b) Plot of k_{decay} vs. $[CCl_4]$.

The Hammett plot of the rate constants of the reaction of **37a-f** with CCl_4 in THF solution revealed a very poor correlation ($\rho = -0.5 \pm 0.3$) when the normal σ parameters (σ_m and σ_p) were used. A better correlation was found between $\log k$ and the inductive parameters (F) ($\rho = -0.84 \pm 0.16$). Figure 4.13 shows both of these Hammett plots.
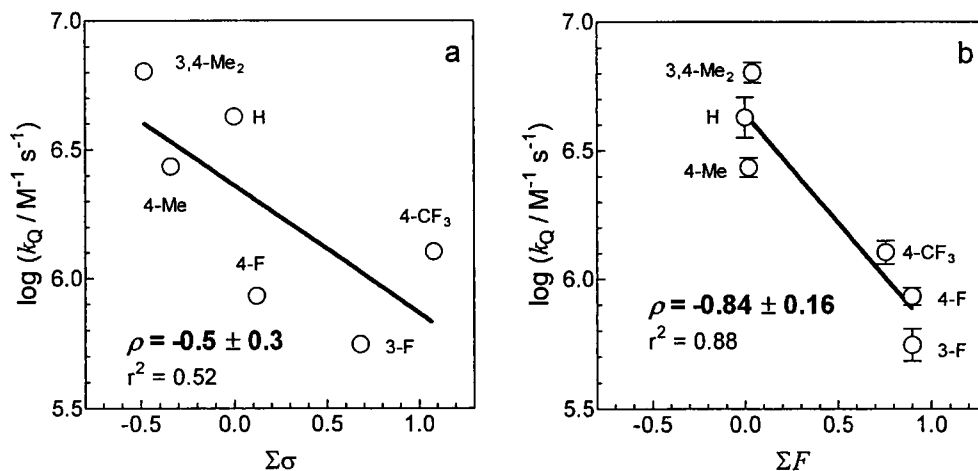
Figure 4.13. Hammett plot of the reaction of **37** with CCl_4 in THF (a) using the normal σ parameters and (b) using the inductive parameters F.

Rate constants for the reaction of **37a** with CCl_4 in THF were measured at several temperatures over the range of 10-60 °C. The Arrhenius plot is shown in Figure 4.14, which provided the Arrhenius parameters E_a = +5.9 ± 0.4 kcal/mol and log A = 10.9 ± 0.3. The latter term corresponds to an entropy of activation of $\Delta S^{\ddagger}$ = -11.6 ± 1.3 cal K^{-1} mol^{-1} at 25 °C.
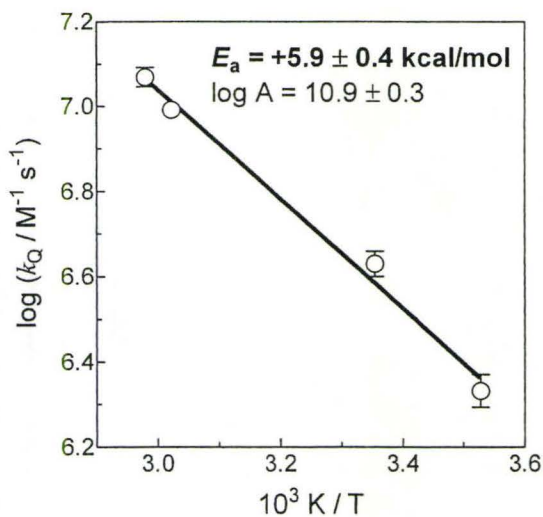
Figure 4.14. Arrhenius plot for the reaction of $GePh_2$-THF with CCl_4 in THF.

4.4. Discussion of the Mechanism of $GePh_2$ and $GePh_2$-THF with CCl_4

Consider first the results in hexanes solution. The products, especially **56** (Ph_2GeCl_2) and C_2Cl_6, are consistent with a mechanism that involves initial chlorine atom abstraction from CCl_4. Based on analogy with the reaction of $GeMe_2$ with CCl_4, it seems likely that the primary product should be the radical pair **60**. The low yield of **58** indicates that cage escape is the dominant fate of **60**. The Ph_2GeCl and CCl_3 free radicals can undergo a variety of further of reactions, such as abstraction or alkene additions, some of which are shown in Figure 4.15. In earlier experiments with $GeMe_2$ the yield of the dichlorogermane Me_2GeCl_2 was much higher (65-80%) because CCl_4 was the solvent.[11]
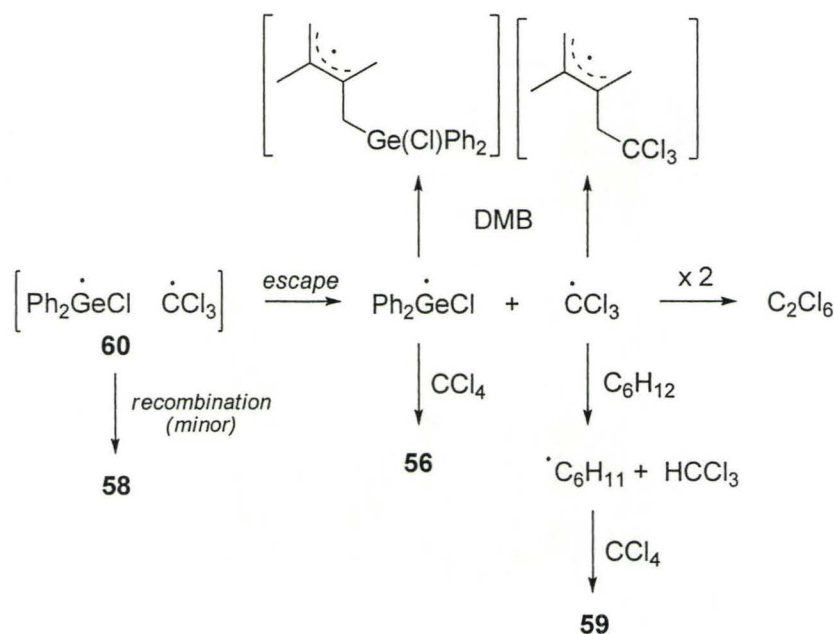
Figure 4.15. Reaction scheme outlining the probable fate of the singlet radical-pair **60**.

The negative ρ value suggests that positive charge accumulates at germanium in the transition state of the rate determining step (*i.e.* the germylene behaves as the electron *donor* in the reaction). Negative activation energies can result when the rate determining step is preceded by a fast, reversible step[40] or when a single step reaction has no enthalpic barrier.[41] A single step reaction in which the germylene acts as an electron donor is unlikely given the electrophilic nature of germylenes. A mechanism that could lead to both a negative ρ value and a negative activation energy is shown in eq 4.9. The first step is fast, reversible Lewis acid-base complexation to yield **63c**, which undergoes dissociative electron transfer to generate the caged radical pair **60**. When the temperature is raised, the K_{eq} of the first step decreases, lowering the overall rate constant.

$$\text{Ph}_2\text{Ge} \overset{\bigcirc}{\underset{\bigcirc}{\ominus}} : \; + \; \text{CCl}_4 \; \underset{k_{-1}}{\overset{\overset{fast}{k_1}}{\rightleftharpoons}} \; \overset{\overset{slow}{\underset{:\ddot{\text{Cl}}\diagdown\text{CCl}_3}{\downarrow}}}{\underset{\underset{63c}{\text{Ph}_2\text{Ge}\bigcirc:}}{}} \; \xrightarrow[\text{E.T.}]{} \; \left[\text{Ph}_2\overset{\cdot}{\text{Ge}}\text{Cl} \quad \overset{\cdot}{\text{CCl}_3} \right] \qquad (4.9)$$

$$\mathbf{60}$$
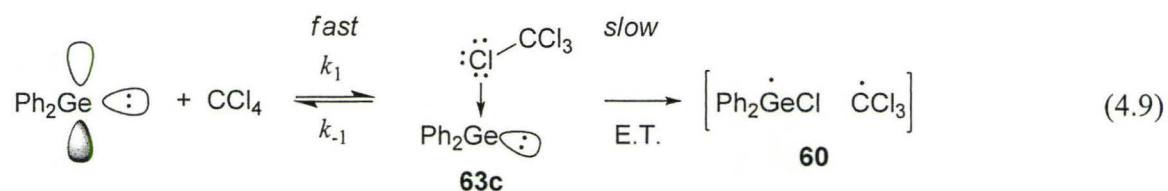
Unfortunately direct evidence for the existence of **63c** could not be obtained, even in a rigid matrix. This could be due simply to the small activation barrier to dissociative electron transfer. Similarly, we could not detect Ph_2GeCl radicals by LFP, most likely because germyl radicals are more reactive toward CCl_4 than GePh_2.[42] The Ph_2GeCl radical should absorb in the 290-350 nm region based on the UV spectra of similar germyl radicals.[43] In the reaction of SiPh_2 with CCl_4, the Ph_2SiCl radical has been detected by flash photolysis.[44] The rate constant for the reaction of SiPh_2 with CCl_4 is 1.4 $\times 10^9 \; \text{M}^{-1}\text{s}^{-1}$,[44] which is 400× faster than the rate constant for the analogous reaction with GePh_2. The rate constants for halogen atom abstraction by silyl and germyl radicals are roughly equal (ca. $10^8 \; \text{M}^{-1} \; \text{s}^{-1}$)[42] and because the Ph_2SiCl radicals are formed more rapidly their concentration can build up to detectable levels.

Our failure to detect the complex **63c** led us to study the reaction in THF. We reasoned that if **63c** is an intermediate in the reaction in hexanes, we should be able to impede the reaction by using a solvent that coordinates to the germylene. The results were quite different from expectation: we found that in THF there was no change in the products detected, only in the relative product yields with **58** becoming the major product (*vide supra*, eqs 4.3 and 4.8). The equilibrium constant for the complexation of GePh_2 with THF in hexane solution is $K_{eq} = 23,000 \pm 5,000 \; \text{M}^{-1}$,[45] and it is reasonable to expect

151

it will be of similar magnitude to this in neat THF. While **37** is the only species

detectable in neat THF, we wondered if its decay could be a manifestation of the reaction

of the free germylene. Assuming an initial germylene concentration of 10 μM and an

equilibrium constant for the complexation of GePh$_2$ with THF of K_{eq} = 23,000 M^{-1}, the

equilibrium concentration of germylene in THF will be 35 pM, ca. 3×10^6 times lower

than that of the complex. The measured rate constant (k_Q) will be the sum of k_{GePh2} and

$k_{complex}$ each corrected for the fraction F present at equilibrium (eq 4.10).[46] If we assume

that the *free* germylene reacts with CCl$_4$ at the diffusion limit (k_{diff} = 1.4×10^{10} M^{-1}s^{-1} in

THF at 25°C)[47] then the rate constant for the reaction of **37** with CCl$_4$ will be $k_{complex}$ =

4.2×10^6 M^{-1}s^{-1}.

$$k_Q = k_{GePh2}F_{GePh2} + k_{complex}F_{complex} \qquad [F_{GePh2} = 3.5 \times 10^{-6}] \qquad (4.10)$$

Nefedov and co-workers examined the effect of triphenylphosphine (PPh$_3$) on the

reaction of GeMe$_2$ with CCl$_4$. Upon generation of GeMe$_2$ in the presence of PPh$_3$ and

CCl$_4$ in benzene, they noted a much higher yield of the C-Cl insertion product

Me$_2$Ge(Cl)CCl$_3$ (**12**) (at the expense of Me$_2$GeCl$_2$) compared to the same reaction in the

absence of PPh$_3$.[48] The increased yield of **12** in the presence of PPh$_3$ is presumably due

to the fact that the germylene is complexed with a Lewis base. To examine this

possibility, the photolysis of **33a** (20 mM) was carried out in cyclohexane containing

small amounts of THF (60 mM) in addition to CCl$_4$ (50 mM). The reaction afforded a

similar product distribution to that observed in neat THF. Furthermore, photolysis of a

solution of **33a** (20 mM) in cyclohexane in the presence of CCl$_4$ (50 mM) and

triethylamine (NEt$_3$, 3 mM) gave the products **56:57:58** in a 1:1:60 ratio which can be

compared to the ratio of **56:57:58** = 12:10:16 observed in neat THF. Recall from Chapter

1 that the equilibrium constant for the Lewis acid-base complexation of

germylenes with amines (*e.g.* to give **68**) is considerably higher than the

corresponding K_{eq} for germylenes with ethers.
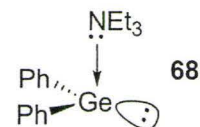
While there is no correlation of k_{CCl4} (**37a-f**) with standard Hammett σ constants,

there is a better correlation the inductive *F* parameters (ρ = -0.84 ± 0.16). The

implication of this result is that only the lone pair of the complex is involved in the rate-

determining step of the reaction; this seems reasonable because the *p*-orbital of

germylene is complexed with THF. The activation energy for the reaction of **37a** with

CCl$_4$ is positive (E_a = + 5.9 ± 0.4 kcal/mol), which is further evidence that a different

mechanism from that in hexanes operates in THF.

One mechanism considered for reaction of **37** with CCl$_4$ was an internal-S$_N$2

reaction (eq 4.11). If this mechanism is involved, the reaction of **37** with chloroform

should be quite similar to that measured for CCl$_4$ because the steric repulsion

encountered during the nucleophilic attack on carbon would be lower. The absolute rate

constants for the reaction of **37** with CHCl$_3$ is k_{CHCl3} = (2.4 ± 0.5) × 10^4 M^{-1}s^{-1}, which is

ca. 175 times slower than the rate constant for reaction with CCl$_4$. Thus based on the

slower rate constant with CHCl$_3$ than with CCl$_4$, this mechanism seems unlikely.

$$(4.11)$$

The second mechanism considered is an S_N2 reaction where the germanium lone

pair approaches the chlorine, adding electron density to the C-Cl σ^* orbital, resulting in

cleavage of the bond to give an ion pair **69**, as shown in eq 4.12. The ability of a solvent

to support the formation of an ion-pair is related to the magnitude of its dielectric

constant (ε), which is indeed higher in THF ($\varepsilon = 7.5$) than in cyclohexane ($\varepsilon = 2.0$).[49, 50]

Aside from the higher value of ε, THF has been shown to be an excellent solvent in terms

of its ability to solvate the resulting ions.[51] Once **69** has formed, ion pair combination

yields the observed major product **58**. If the halocarbon is changed to chloroform, the

rate constant should be lower because of the lower thermodynamic stability of the $CHCl_2$

anion vs. the CCl_3 anion, as estimated by the gas phase acidities of CH_2Cl_2 and $CHCl_3$.[52]

Indeed, a reduction in rate constant was observed with $CHCl_3$.

$$(4.12)$$
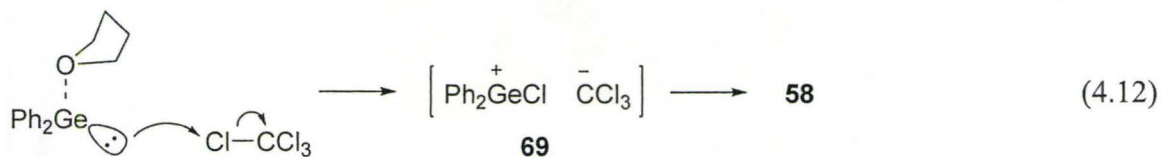
If we return to the reactivity of **37** in hexanes, recall that the product distribution

upon photolysis of **33a** in cyclohexane containing THF (60 mM) and CCl_4 (50 mM) is

similar to that observed in neat THF. In this case, the bulk dielectric of the solvent is

low, which should disfavour the formation of the ion pair; however, Szwarc has observed

154

that even addition of small concentrations of a good polarizing solvent to an otherwise inert medium can support the formation of ion pairs.[53] Furthermore, the yield of **58** is enhanced in the presence of NEt$_3$ presumably because the amine will more strongly stabilize the ion pair.[54]

Figure 4.16a shows the transient absorption spectra of a hexanes solution of **33a** (3 mM) containing THF (50 mM); the two transients are **DGa** (λ_{max} = 440 nm) and **37a** (λ_{max} = 350 nm). There is significant spectral overlap of **37a** with **DGa** and with the shorter wavelength transitions ($\leq$ 300 nm). The decay of **37a** was monitored as a function of CCl$_4$ concentration; however the decays recorded at 345 nm with concentrations of CCl$_4$ up to 232 mM did not fit well to first-order kinetics. In order to analyze theses decays, they were treated as the sum of two exponential decays (eq 4.13).

$$A = A_0 e^{-(k_{fast}' + k_{slow}')t} \qquad\qquad (4.13)$$

A plot of k_{fast}' vs. [CCl$_4$], shown in Figure 4.17, is scattered but was fit to a straight line for the purposes of estimating a rate constant (k_{fast} = (9.4 ± 7.0) × 10^6 M^{-1}s^{-1}). At the highest concentration of CCl$_4$ studied, the digermene can no longer be detected and the decay of **37a** fit well to a single first-order decay equation but at this point the intensity of the **37a** absorbance is relatively weak. Figure 4.16b shows the transient absorption spectra of the same solution in the presence of 232 mM CCl$_4$.

Despite the uncertainty of the rate constant estimated for the reaction of **37a** with CCl$_4$ in hexanes, its magnitude appears to be similar to the rate constant for the reaction

of **37a** with CCl_4 in THF, which is perhaps not surprising given the similar product

distribution in the two sets of solvents. Further experiments under these conditions will

be necessary in order to make more definitive conclusions.
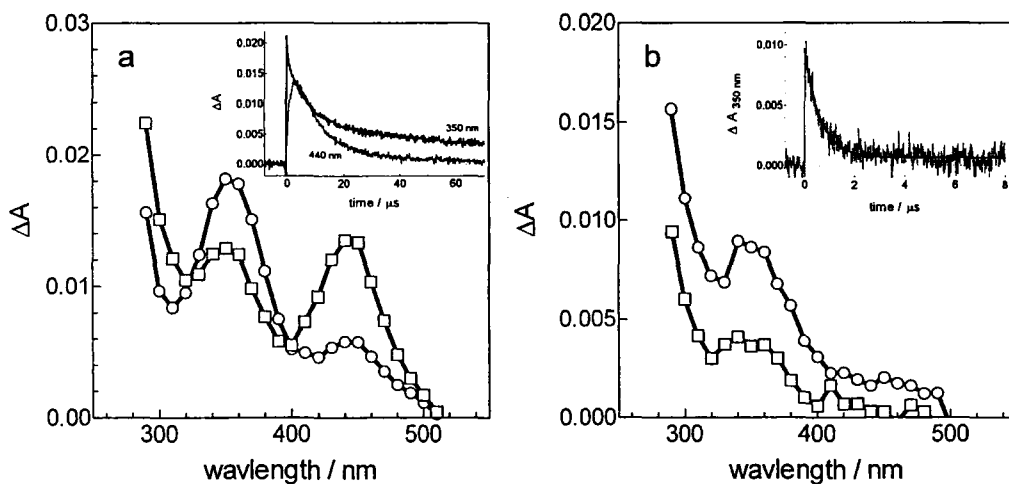
Figure 4.16. Transient absorption spectrum of **33a** in hexanes containing 50 mM THF and (a) 0 mM CCl_4, recorded 0-480 ns (o) and 3.20-3.68 μs (□) after the laser pulse, and (b) 232 mM CCl_4, recorded 80-128 ns (o) and 560-592 ns (□) after the laser pulse. The insets show the absorbance-time profiles at selected wavelengths. The black line is the fit of the decay to first-order kinetics (eq 2.19).
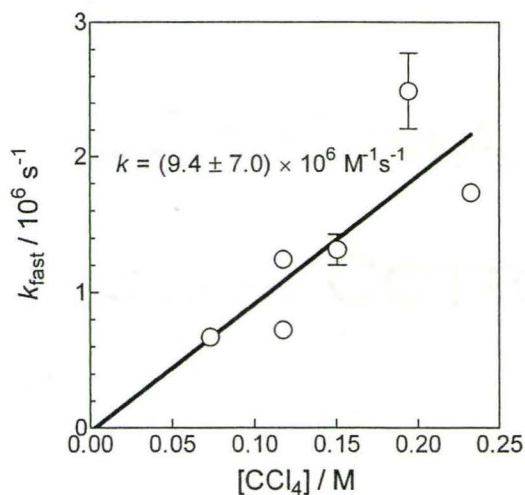
Figure 4.17. Plot of k_{fast} vs. [CCl$_4$] for the reaction of **37a** with CCl$_4$ in hexanes solution.

4.5. Summary

The reaction of GePh$_2$ with CCl$_4$ in hexanes leads to a complex mixture of products consistent with initial halogen atom abstraction by the germylene to yield a radical pair (GePh$_2$Cl/CCl$_3$). The dominate fate of this radical pair is dissociation. The major products are **56-58**, while the rest is higher MW oligogermanes. Kinetic studies in hexanes show that the reaction proceeds irreversibly with a rate-constant of $k_{GePh2-CCl4}$ = $(1.2 \pm 0.1) \times 10^7$ M^{-1}s^{-1}. The rate constants increase as the germylene becomes more electron-rich ($\rho = -0.38 \pm 0.10$), and the activation energy measured for GePh$_2$ is negative ($E_a = -0.7 \pm 0.7$ kcal/mol). These data, along with the product studies, are most consistent with a mechanism involving fast, reversible complexation between the germylene and the halocarbon (**63c**) which then undergoes a rate-determining dissociative inner sphere electron transfer within the complex to yield the Ph$_2$GeCl/CCl$_3$

157

radical pair **60**. Combination leads to the formal Cl-CCl₃ insertion product **58**, while cage escape results in **56** after a chlorine atom abstraction from CCl_4 by Ph_2GeCl. Product **57** likely results from the reaction of $GePh_2$ with HCl.

In THF, the product yields (**56** (33%), **57** (20%), **58** (49%)) are quite different from that in hexanes. Similar yields were also obtained when the germylene was generated in hexanes solution containing 50 mM THF. When the germylene was generated in the presence of 3 mM NEt_3, **58** was the only product detected. The rate constant for the reaction of **37a** with CCl_4 in THF is $k = (4.3 \pm 0.3) \times 10^6$ $M^{-1}s^{-1}$; these rate constants increased as the ability of the aromatic substituent to act as an inductive electron donor increased. The correlation of $\log k$ with F is $\rho = -0.84 \pm 0.16$. The activation energy is for the reaction of **37a** with CCl_4 is $E_a = +5.9 \pm 0.4$ kcal/mol. These results, along with kinetic experiments performed with $CHCl_3$, led to a proposed mechanism that involves an S_N2 reaction of **37** with CCl_4 to yield the ion pair **69** that combines to give **58**.

4.6. References

1. Ishikawa, M.; Nakagawa, K. I.; Katayama, S.; Kumada, M. *J. Organomet. Chem.* **1981**, *216*, C48.
2. Köcher, J.; Lehnig, M.; Neumann, W. P. *Organometallics* **1988**, *7*, 1201.
3. Tomoda, S.; Shimoda, M.; Takeuchi, Y.; Kajii, Y.; Obi, K.; Tanaka, I.; Honda, K. *J. Chem. Soc., Chem. Commun.* **1988**, 910.
4. Oka, K.; Nakao, R. *J. Organomet. Chem.* **1990**, *390*, 7.
5. Mochida, K.; Yoneda, I.; Wakasa, M. *J. Organomet. Chem.* **1990**, *399*, 53.
6. Mochida, K.; Adachi, M.; Wakasa, M.; Hayashi, H. *Phosph. Sulf. Sil. Rel. Elem.* **1999**, *150-151*, 237.

7.   Adachi, M.; Mochida, K.; Wakasa, M.; Hayashi, H. *Main Group Met. Chem.* **1999**, *22*, 227.

8.   Miller, K. A.; Bartolin, J. M.; O'Neill, R. M.; Sweeder, R. D.; Owens, T. M.; Kampf, J. W.; Banaszak Holl, M. M.; Wells, N. J. *J. Am. Chem. Soc.* **2003**, *125*, 8986.

9.   Tokitoh, N.; Ando, W. In *Reactive Intermediate Chemistry*, Moss, R. A.; Platz, M. S.; Jones, M., Jr., Eds. John Wiley & Sons: New York, 2004; pp 651-715.

10.   Kavara, A.; Cousineau, K. D.; Rohr, A. D.; Kampf, J. W.; Banaszak Holl, M. M. *Organometallics* **2008**, *27*, 1041.

11.   Neumann, W. P.; Schriewer, M. *Tetrahedron Lett.* **1980**, *21*, 3273.

12.   Bond Dissociation Energies. In *CRC Handbook of Chemistry and Physics, Internet Version*, 87 ed.; Lide, D. R., Ed. CRC Press/Taylor and Francis: Boca Raton, FL, 2007; pp 9-54.

13.   Clark, K. B.; Griller, D. *Organometallics* **1991**, *10*, 746.

14.   Satgé, J.; Massol, M.; Rivière, P. *J. Organomet. Chem.* **1973**, *56*, 1.

15.   Chateauneuf, J. E. *J. Am. Chem. Soc.* **1990**, *112*, 442.

16.   Sharutin, V. V.; Sharutina, O. K.; Pavlov, K. V.; Shcherbinin, V. V. *Zh. Org. Khim. (Eng. Trans.)* **1994**, *64*, 1051.

17.   Ohshita, J.; Toyoshima, Y.; Iwata, A.; Tang, H.; Kunai, A. *Chem. Lett.* **2001**, 886.

18.   Mochida, K.; Chiba, H. *J. Organomet. Chem.* **1994**, *473*, 45.

19.   Choi, N.; Tanaka, M. *J. Organomet. Chem.* **1998**, *564*, 81.

20.   Leigh, W. J.; Harrington, C. R. *J. Am. Chem. Soc.* **2005**, *127*, 5084.

21.   Davis, D. D.; Schmidt, J. F.; Neeley, C. M.; Hanrahan, R. J. *J. Phys. Chem.* **1975**, *79*, 11.

22.   Neumann, W. P. *Chem. Rev.* **1991**, *91*, 311.

23.   Su, M.-D. *Chem. Phys. Lett.* **2003**, *374*, 385.

24.   Chen, C.-H.; Su, M.-D. *Chem. Eur. J.* **2007**, *13*, 6932.

25.   Li, R.-E.; Sheu, J.-H.; Su, M.-D. *Inorg. Chem.* **2007**, *46*,

26.   Ando, W.; Itoh, H.; Tsumuraya, T. *Organometallics* **1989**, *8*, 2759.

27.   Enthalpy of Fusion. In *CRC Handbook of Chemistry and Physics, Internet Version*, 90 ed.; Lide, D. R., Ed. CRC Press/Taylor and Francis: Boca Raton, FL, 2009-2010; pp 6-130.

28.   Donth, E., *The Glass Transition. Relaxation Dynamics in Liquids and Disordered Materials*. Springer-Verlag: Heidelberg, 2001.

29.   Debenedetti, P. G.; Truskett, T. M.; Lewis, C. P.; Stillinger, F. H. *Adv. Chem. Eng.* **2001**, *28*, 21.

30.   Debenedetti, P. G.; Stillinger, F. H. *Nature* **2001**, *410*, 259.

31.   Ling, A. C.; Willard, J. E. *J. Phys. Chem.* **1968**, *72*, 1918.

32.   Ando, W.; Tsumuraya, T.; Sekiguchi, A. *Chem. Lett.* **1987**, 317.

33.   Leigh, W. J.; Huck, L. A.; Held, E.; Harrington, C. R. *Silicon Chem.* **2005**, *3*, 139.

34.   Toltl, N. P.; Leigh, W. J. *J. Am. Chem. Soc.* **1998**, *120*, 1172.

35.   Leigh, W. J.; Potter, G. D.; Huck, L. A.; Bhattacharya, A. *Organometallics* **2008**, *27*, 5948.

36. Nazran, A. S.; Gabe, E. J.; LePage, Y.; Northcott, D. J.; Park, J. M.; Griller, D. *J. Am. Chem. Soc.* **1983**, *105*, 2912.

37. Tukada, H.; Sugawara, T.; Murata, S.; Iwamura, H. *Tetrahedron Lett.* **1986**, *27*, 235.

38. Jensen, R. J.; Guettler, R. D.; Lyman, J. L. *Chem. Phys. Lett.* **1997**, *277*, 356.

39. Murakhtina, T.; Heuft, J.; Meijer, E. J.; Sebastiani, D. *Chem. Phys. Chem.* **2006**, *7*, 2578.

40. Atkins, P.; de Paula, J., *Physical Chemistry.* 7th ed.; W.H. Freeman & Co.: New York, 2002.

41. Houk, K. N.; Rondon, N. G. *J. Am. Chem. Soc.* **1984**, *106*, 4293.

42. Lalevée, J.; Blanchard, N.; Graff, B.; Allonas, X.; Fouassier, J. P. *J. Organomet. Chem.* **2008**, *693*, 3643.

43. Mochida, K.; Ichikawa, K.; Okui, S.; Sakaguchi, Y.; Hayashi, H. *Chem. Lett.* **1985**, 1433.

44. Moiseev, A. G.; Leigh, W. J. *Organometallics* **2007**, *26*, 6277.

45. Leigh, W. J.; Lollmahomed, F.; Harrington, C. R.; McDonald, J. M. *Organometallics* **2006**, *25*, 5424.

46. Leigh, W. J.; Li, X. *Organometallics* **2002**, *21*, 1197.

47. Murov, S. L.; Carmichael, I.; Hug, G. L., *Handbook of Photochemistry.* Dekker: New York, 1993.

48. Egorov, M. P.; Dvornikov, A. S.; Ezhova, M. B.; Kuz'min, V. A.; Kolesnikov, S. P.; Nefedov, O. M. *Organomet. Chem. USSR* **1991**, *4*, 582.

49. Permittivity (Dielectric Constant) of Liquids. In *CRC Handbook of Chemistry and Physics, Internet Version*, 90 ed.; Lide, D. R., Ed. CRC Press/Taylor and Francis: Boca Raton, FL, 2009-2010; pp 6-148.

50. Szwarc, M. *Acc. Chem. Res.* **1969**, *2*, 87.

51. Szwarc, M. In *Ions and Ion Pairs in Organic Reactions*, Szwarc, M., Ed. John Wiley & Sons: New York, 1972; Vol. 1, pp 1-26.

52. Bohme, D. K.; Lee-Ruff, E.; Young, L. B. *J. Am. Chem. Soc.* **1972**, *94*, 5153.

53. Shinohara, M.; Smid, J.; Szwarc, M. *J. Am. Chem. Soc.* **1968**, *90*, 2175.

54. Sandström, M.; Persson, I.; Persson, P. *Acta Chem. Scand.* **1990**, *44*, 653.

Chapter 5 – Reactions of Diarylgermylenes with 1,3-Dienes

5.1. Overview

There has been considerable interest in the reactions of silylenes and germylenes with alkenes and dienes, especially because of the potential for M-C bond formation (see Chapter 1). Silylenes and germylenes undergo (1+2)-cycloadditions with alkenes to yield the corresponding metalliranes (**13**) (eq 5.1).[1, 2] Metalliranes, particularly germiranes, are often thermally unstable and dissociate readily to the parent metallylene and alkene.[1, 3-8] Computational studies support the formation of a Lewis acid-base complex between the π-bond of the alkene and the metallylene (**70** – a "π-complex") prior to formation of **13**.[7, 9-13]

$$MR_2 \; + \; H_2C{=}CH_2 \; \rightleftharpoons \; \underset{\textbf{13}}{\overset{R_2}{\underset{\triangle}{M}}} \tag{5.1}$$
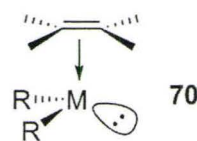
Silylenes react with 1,3-dienes to yield a vinylsilirane (**71**). If the silylene was generated thermally, **71** can undergo a rearrangement to a silacyclopentene (**19**). Compounds such as **19** derived from silylenes have a random stereochemistry and it has been proposed that the randomization is caused by a rearrangement such as that shown in eq 5.2, where the bonds can rotate within the intermediate.[8, 14-16] Tokitoh and co-workers have published one example of what they demonstrated was a direct (1+4) cycloaddition of a silylene with a diene to yield a silacyclopentene (eq 5.3).[17]

(5.2)

R = 2,4,6-(CH$_3$)$_3$C$_6$H$_2$
R' = 2,4,6-(CH(SiMe$_3$)$_2$)$_3$C$_6$H$_2$

(5.3)
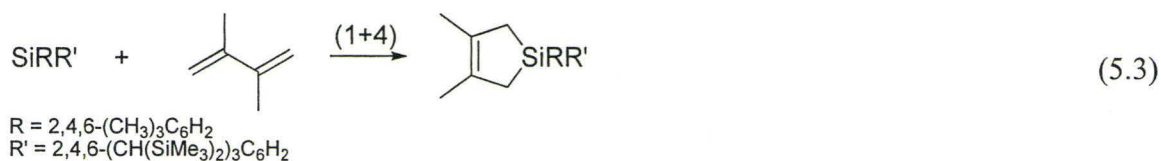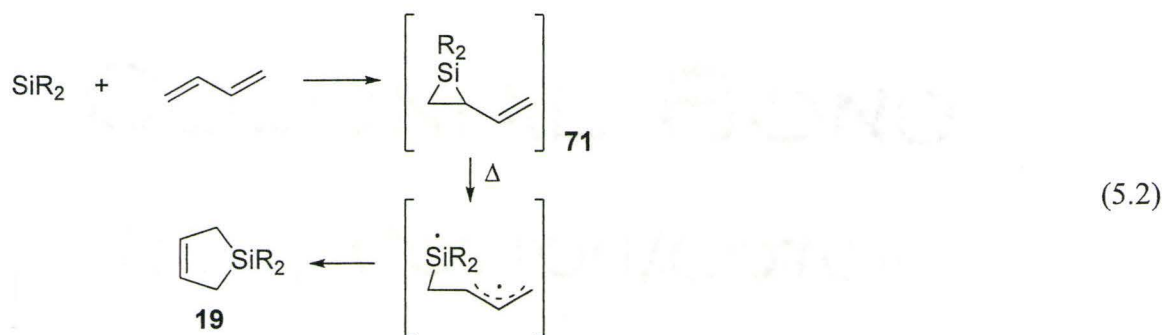
Germylenes react with 1,3-dienes stereospecifically to yield the chelotropic

formal (1+4) cycloaddition product **20** which lends support to the direct (1+4)

mechanism (eq 5.4).[18-20] Furthermore, it has been proposed that the germylene plays the

role of the nucleophile in this reaction.[20] In product studies, the formal

(1+2) cycloaddition product **72**, a vinylgermirane, is usually not observed.
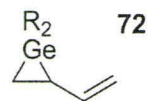
Early work from our group demonstrated that the reaction of **Ga** with isoprene forms the

vinylgermirane **24a** reversibly ($k = 5.5 \times 10^9$ M^{-1}s^{-1}; $K_{eq} \approx 6000$ M^{-1}) and the lifetime of

24a is ca. $\tau = 0.5$ ms.[8] The decay of **24a** was attributed to its rearrangement to the

corresponding germacyclopentene **23a**, as shown in eq 5.5.[8] A detailed computational

study on the reactions of MR$_2$ (M = Si, Ge, Sn) with 1,3-butadiene suggests that the

direct (1+4) cycloaddition to give the metallacyclopentene has a lower activation barrier

than rearrangement of the vinylmetallirane to yield the metallacyclopentene.[21]

$$GeR_2 \ + \ \diagup\!\!\diagup \longrightarrow \quad \overset{\underset{|}{Ge}}{\underset{R_2}{\bigcirc}} \ \mathbf{20} \tag{5.4}$$

$$GePh_2 \ + \ \diagup\!\!\diagup\!\!\diagdown \ \rightleftharpoons \ \overset{GePh_2}{\diagup} \longrightarrow \overset{GePh_2}{\bigcirc} \ \mathbf{23a} \tag{5.5}$$

24a $\tau = 0.5$ ms
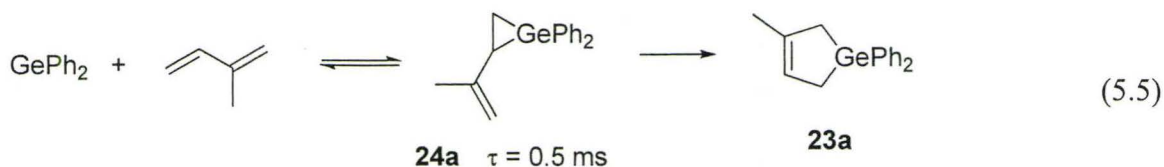
The objective of the present work was to study the reaction of germylenes with dienes in more detail. In particular, we were interested in determining whether **23** indeed forms via rearrangement of **24** or whether it forms from a direct (1,4)-cycloaddition reaction of GePh$_2$ with isoprene. In either case, kinetic studies employing our aryl-substituted germylenes would allow us make mechanistic conclusions with regards to the formation of both **23** and **24**.

5.2. Results

5.2.1. Product Studies

Photolysis of deoxygenated hexanes solutions of **33a-f** (0.02 M) containing isoprene (0.5 M) led to the formation of the corresponding germacyclopentenes (**24a-f**) as the only products detectable by GC/MS at up to ca. 40% conversion of the starting material. Compounds **24a,b,e** were identified by comparison of the mass spectra and retention times with independently prepared samples, while the identity of the others (**24c,d,f**) were inferred based on m/z of the M$^+$ ion and the similarity of the mass spectral fragmentation patterns to the other aryl analogues.

24

163
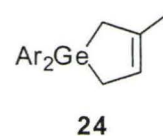
Photolysis of a solution of **33a** (0.03 M) in C_6D_{12} containing isoprene (0.2 M) resulted in the formation of **24a**, DMB, and a broadening of the aromatic and aliphatic regions of the ^{1}H NMR spectrum with increased photolysis time. Figure 5.1 shows the concentration vs. time plot. Because of the spectral overlap between the **33a** and **24a**, it was not possible to determine the concentration of the former in the experiment. Nevertheless, the yield of germylene produced can be assumed to be equal to the yield of DMB and we thus estimate that about 83% of the germylene is trapped by isoprene (eq 5.6). The "missing" $GePh_2$ in these experiments appears to oligomerize based on the broad aromatic resonances. In order to estimate the oligomer concentration, the aromatic regions of the NMR spectra that did not contain **24** or **33** (thus presumed to be the oligomer) were integrated and a concentration was assigned to this area assuming the oligomer was comprised of $(GePh_2)_n$ units. A MALDI mass spectrum of the product mixture shows at least 10 germanium containing compounds with MW 500-900 Da (see Figure 5.2). The most intense peak has an isotopic distribution consistent with two units of $GePh_2$ and four molecules of isoprene (plus 0-4 hydrogen atoms necessary to terminate the various radicals) (Figure 5.3). Increasing the temperature to 50°C resulted in a 10% increase in the relative yield of oligogermanes to **24a** compared to that obtained at 25°C.

$$\text{(5.6)}$$

33a   DMB 1.0 : **24a** 0.83 : 0.37
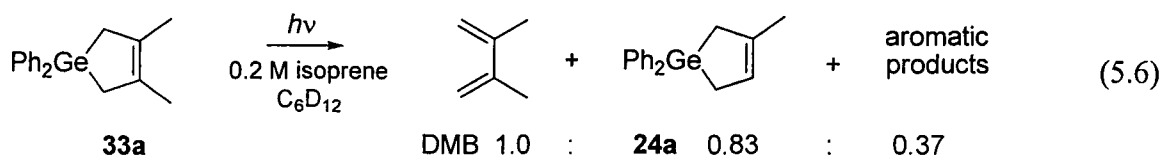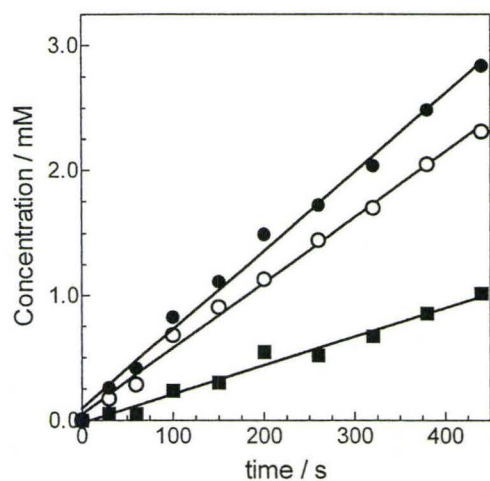
Figure 5.1. Product distribution upon 254 nm photolysis of **33a** (0.032 M) in C_6D_{12} in the presence of isoprene (0.2 M) as determined by ^1H NMR spectroscopy. DMB (●), **24a** (○), oligomers (■).
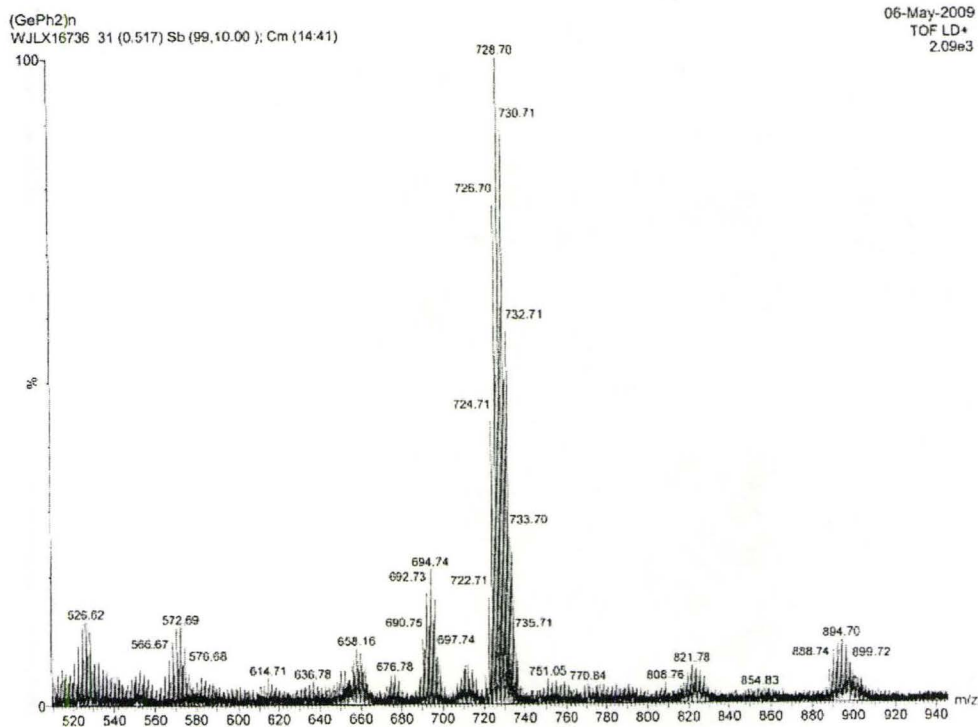
Figure 5.2. MALDI mass spectrum of the crude product mixture from photolysis of **33a** (0.02 M) in hexanes containing isoprene (0.3 M).
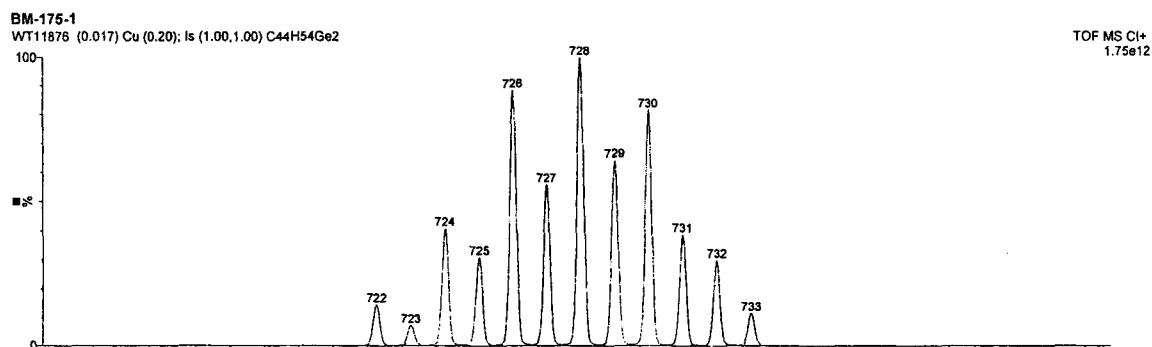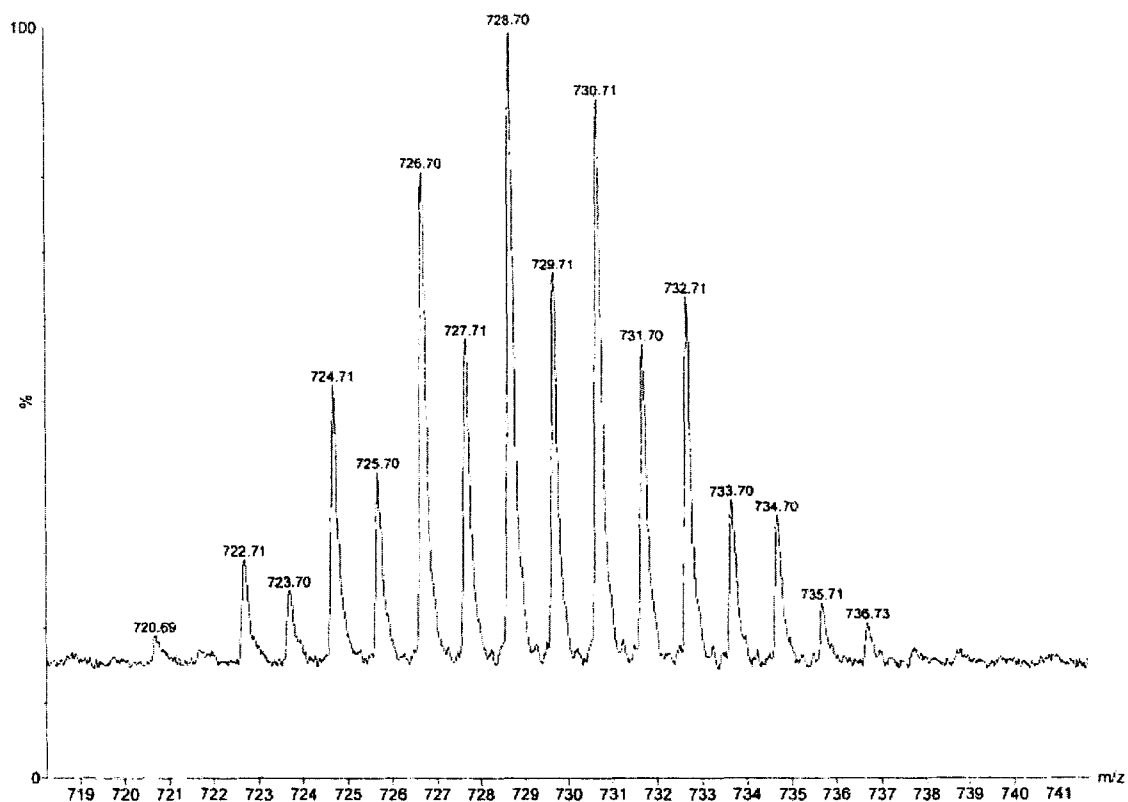
Figure 5.3. Expansion of the mass spectrum shown in Figure 5.2 (*top*); predicted mass spectrum of $(GePh_2)_2(isoprene)_4 + 2H$ (*bottom*). Note changing the number of hydrogen atoms will account for the lower intensity peaks observed but not predicted.

We wondered whether the formation of oligomers was the result of unexpected photochemistry of **33a**. Several years ago, Cam Harrington examined the thermal generation of GePh$_2$ from **65** in the presence of a 10× molar excess of DMB (eq 5.7).[22] A

re-examination of these data shows that the yield of **33a** from thermolysis of **65** is

roughly 83% (*i.e.* the trapping of $GePh_2$ by DMB is not 100% efficient). Figure 5.4

shows the concentration vs. time plot of this experiment – note that the decay of **65** does

not result in an equal yield of **33a**.

(5.7)
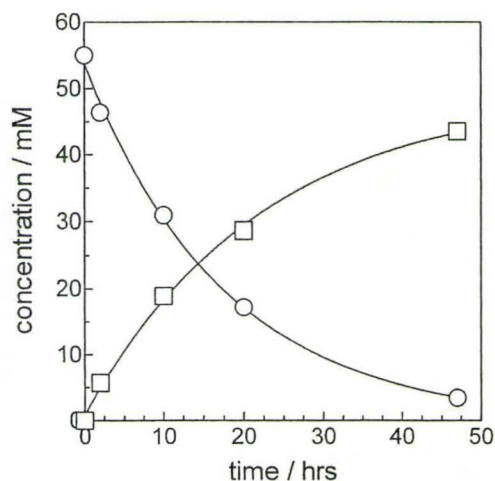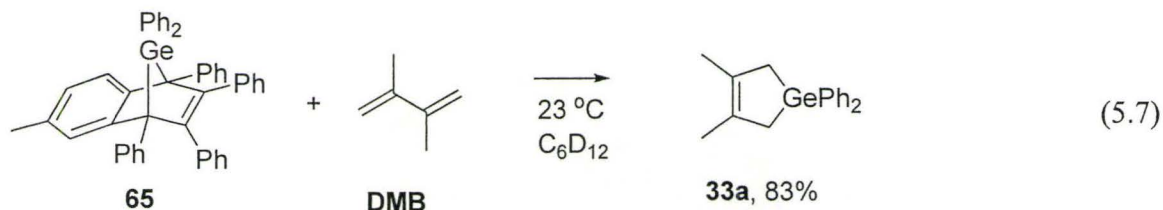
Figure 5.4. Thermal decomposition of 0.05 M **65** (○) in C_6D_{12} containing 0.5 M DMB (□) to yield **33a** (□) at 23 °C.

(Experiment performed by Cam Harrington; unpublished results.)

No other products, however, were visible in the ^1H NMR spectrum. Presumably

the missing germanium is due to germylene oligomerization which would cause gentle

broadening of the aromatic resonances. Unfortunately we were only able to analyze a

hard copy of these spectra and expansions of the regions of interest were missing. In any

case, we conclude that the product distribution described in equation 5.6 is a property of

the reaction of germylenes with dienes and not in the nature of germylene formation.

There are reports of products derived from one silylene (or germylene) and two molecules of diene, as shown in eq 5.8. This product is generally found only after prolonged reaction times in the presence of high substrate concentrations, so **73** is thought to be formed by reaction of the metallirane with free diene.[23, 24] We could not detect evidence for such a product from the reaction of $GePh_2$ with isoprene by NMR spectroscopy or GC/MS.

$$MR_2 \quad + \quad 2 \quad \text{[diene structure]} \quad \longrightarrow \quad \text{[cyclic product MR}_2\text{]} \underset{\textbf{73}}{} \tag{5.8}$$
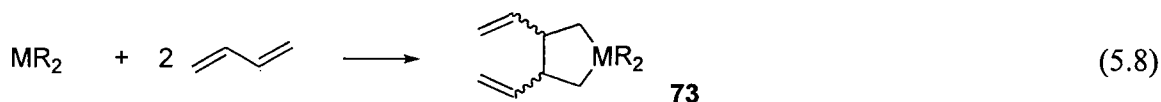
5.2.2. Kinetic measurements by laser flash photolysis

In the presence of isoprene, the transient decay profiles of the germylenes **Ga-g** are bimodal with a fast initial component superimposed on a long lived residual absorbance (plateau). The decay of the initial component increases with increasing concentrations of isoprene, along with a concomitant decrease in the intensity of the plateau, as shown in Figure 5.5. This behaviour is consistent with reversible scavenging of the germylene by the alkene ($1000 < K_{eq} < 25000$) and is in agreement with the kinetic behaviour previously described for the reaction of **Ga** with isoprene under similar conditions.[8]
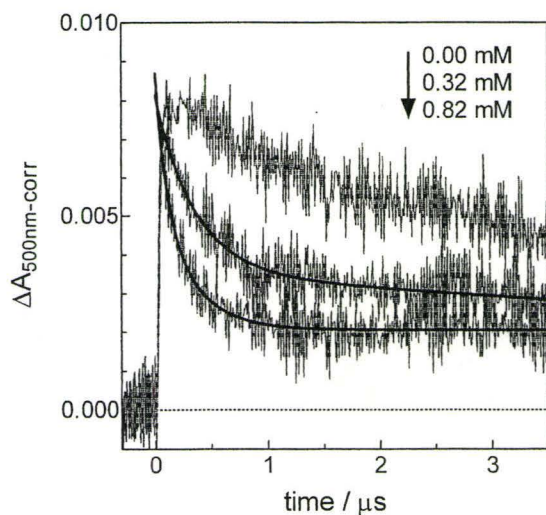
Figure 5.5. Effects of added isoprene on the (corrected) 500 nm absorbance of **Gb** in the presence of isoprene. The black lines in the 0.32 mM and 0.82 mM traces correspond to the non-linear least squares fit of the data to eq 5.9 and 2.19, respectively. *(Reprinted from reference 25 with permission. © 2009 American Chemical Society.)*

The presence of isoprene also resulted in the lengthening of the growth time and reduction in the maximum yield of the digermene, but did not affect the decay rate of the digermene, as shown in Figure 5.6. In order to obtain accurate kinetic data from the germylene decays, all data recorded at 500 nm were corrected to remove the underlying digermene contribution (see Chapter 3).
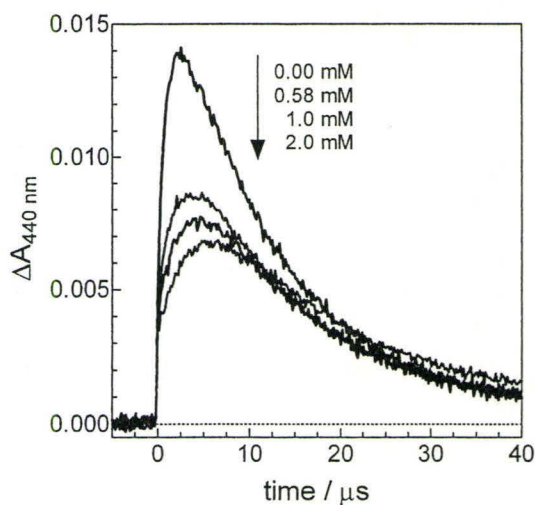
Figure 5.6. Effects of added isoprene on the 440 nm absorbance due to **DGf** in the presence of isoprene.

The bimodal germylene decay in the presence of isoprene is the sum of two components. The first component is the initial rapid decay (k_{fast}) which is the reaction of the germylene and isoprene approaching equilibrium. The second component is the slow residual decay of free germylene at equilibrium as it undergoes dimerization (k_{slow}). At low concentrations of isoprene, the decays are analyzed as the sum of two exponentials (eq 5.9) because k_{slow} cannot be neglected over the time scale monitored (*e.g.* see the 0.32 mM trace in Figure 5.5). At higher concentrations of isoprene, k_{fast} is the major component while k_{slow} is negligible over the time scale monitored – these traces are analyzed using a single exponential decay equation because the plateau is approximately constant (*e.g.* see the 0.82 mM trace in Figure 5.5). The resulting k_{fast} values are plotted against the concentration of isoprene to determine the forward rate constant for the reversible reaction.

$$A = A_0 e^{-(k_{fast}' + k_{slow}')t} \tag{5.9}$$

The equilibrium concentration of germylene is proportional to the ΔA value of the plateau (ΔA_{res}), but in cases where the analysis is the sum of two exponentials, the equilibrium concentration is not obvious. The procedure used to estimate the value of ΔA_{res} in such cases is shown in Figure 5.7.
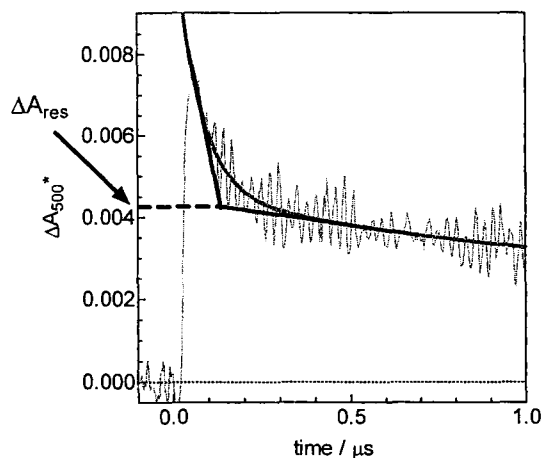
Figure 5.7. Corrected 500 nm transient decay trace for **33a** in hexanes containing 1.55 mM isoprene at 60°C, illustrating the procedure used for estimation of ΔA_{res} (the equilibrium absorbance of the germylene) in situations where the plateau is not constant over the time window monitored. The solid curved line is the fit of the data to two first-order exponential decays ($k_{decay} = k_{fast} + k_{slow}$) The value of ΔA_{res} is estimated as the break point in the bimodal decay. *(Reprinted from reference 25 with permission. © 2009 American Chemical Society.)*

An additional consideration is that isoprene absorbs a small portion of the laser light; as a result, with each successive addition of diene *less* germylene is produced. By determining the relative absorbances of the germylene precursor and isoprene at 248 nm at each concentration of diene, the correction to ΔA_{res} given in eq 5.10 was applied and K_{eq} was then calculated in the usual way (eq 5.11).

$$\Delta A_{0,corr} = \Delta A_0 \left(\frac{A_{33} + A_{isoprene}}{A_{33}} \right)_{248nm} \tag{5.10}$$

$$K_{eq} = \frac{(\Delta A_{0,corr} - \Delta A_{res})}{(\Delta A_{res})[isoprene]} \tag{5.11}$$

Upon the addition of isoprene a new transient is observed ($\lambda_{max} = 285$ nm) whose growth occurs concomitantly with the decay of the germylene on the same time scale (Figure 5.8a). This transient has previously been assigned to the vinylgermirane (**24a**)(eq 5.12)[8] and further support for this assignment will be discussed later. The spectrum of

24a overlaps with the S_0-S_2 absorbance bands of the germylene and digermene, so accurate kinetic measurements of the decay of the species are not possible until sufficient concentrations of isoprene have been added such that **24a** is the only product that can be detected. The spectrum shown in Figure 5.8b is an example of one recorded under such conditions. It is important to note that neither **33a** nor **23a** absorb significantly at wavelengths longer than 275 nm, as shown by their UV spectra in Figure 5.9.
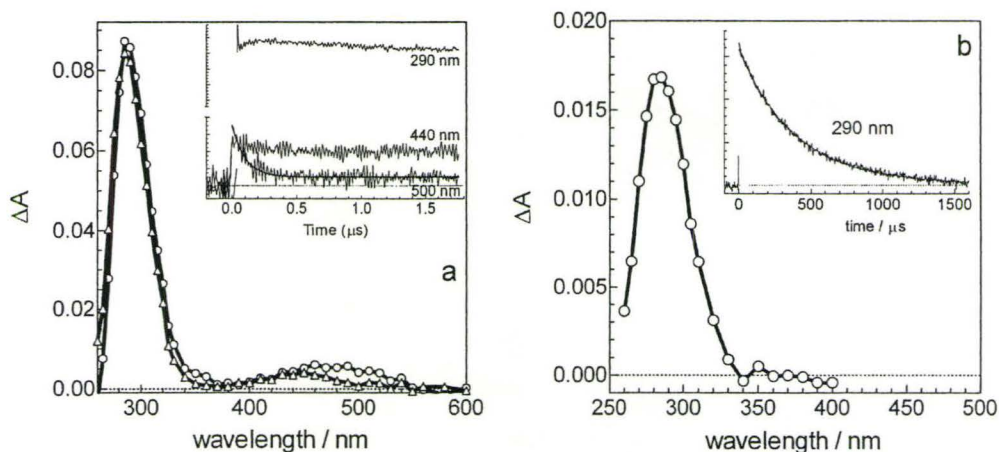
Figure 5.8. Transient absorbance spectra from laser flash photolysis of a solution of **33a** (3 mM in hexanes) containing (a) 1.5 mM isoprene at 25°C 48-54 ns (○) and 1.74-1.76 μs (●) after the laser pulse and (b) 50 mM isoprene at 27°C recorded 0-3.2 μs after the laser pulse. The insets show the absorbance-time profiles at selected wavelengths. *(Reprinted from reference 25 with permission. © 2009 American Chemical Society.)*
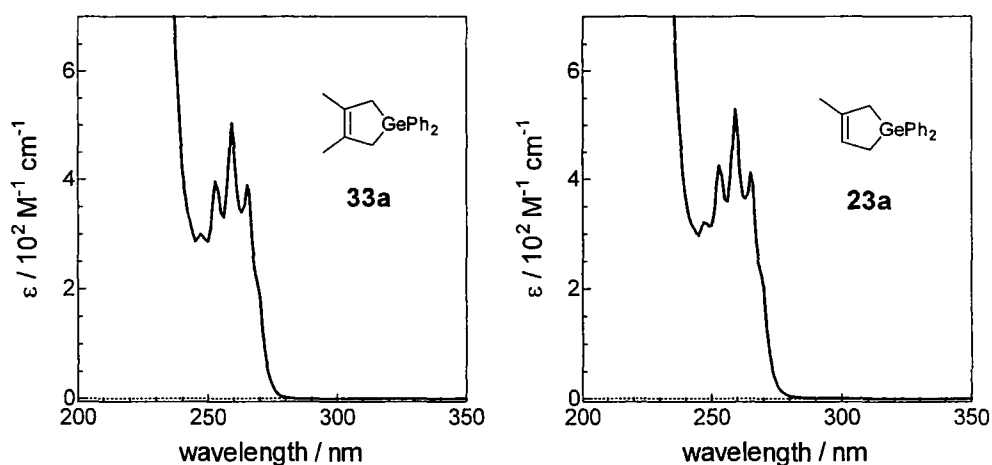
Figure 5.9. UV spectra of **33a** and **23a** in hexanes.

$$\text{GeAr}_2 \; + \quad \underset{k_{-1}}{\overset{k_1}{\rightleftharpoons}} \quad \text{Ar}_2\text{Ge} \qquad\qquad (5.12)$$

24a (λ_{max} = 285 nm)
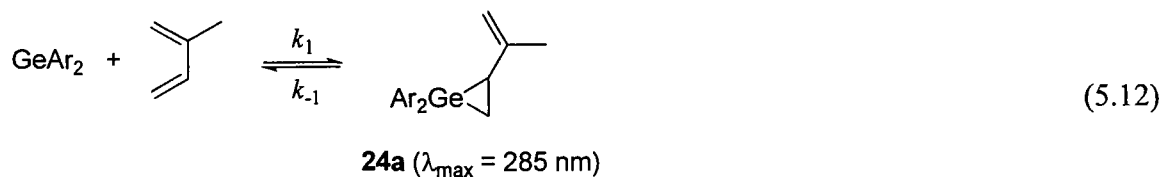
Plots of k_{decay} (k_{fast}) vs. [isoprene] were linear in each case, allowing the second

order rate constant (k_Q) for the approach to equilibrium to be calculated from the slope.

Plots of ($\Delta A_0/\Delta A_{res,Q}$) vs. [Q] were also linear and the equilibrium constant (K_{eq}) was

calculated from the slope as described above. Figure 5.10 shows examples of these plots

with the germylene **Gb**. Rate and equilibrium constants for the reactions of the

diarylgermylenes **Ga-g** with isoprene in hexanes were determined and these values are

listed in Table 5.1.
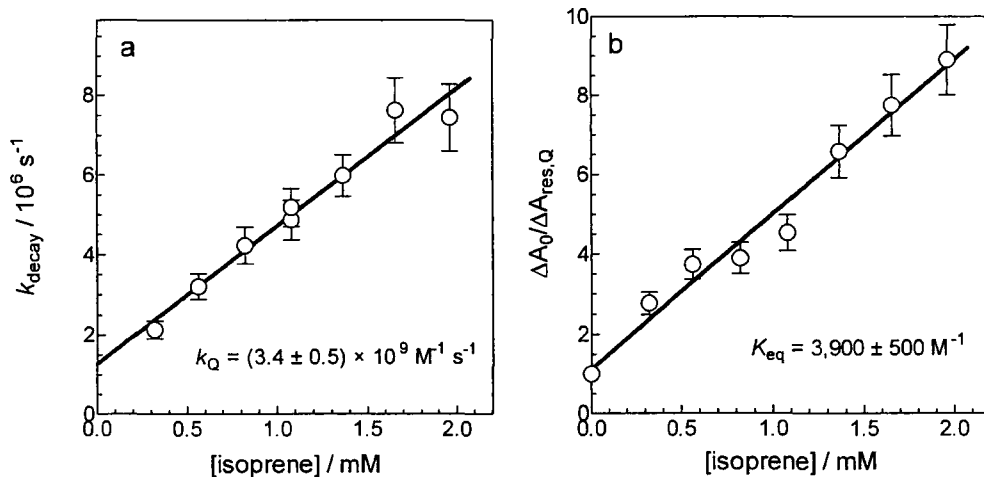
Figure 5.10. Plots of (a) k_{decay} vs. [Q] and (b) ($\Delta A_0/\Delta A_{res,Q}$) vs. [Q] for the reaction of **Gb** with isoprene in hexanes. *(Reprinted from reference 25 with permission. © 2009 American Chemical Society.)*

Table 5.1. Absolute forward rate (k_Q) and equilibrium constants (K_{eq}) for the reactions of **Ga-g** with isoprene and decay rate constants for the corresponding vinylgermiranes **24a-g** ($k_{24\text{-decay}}$) in hexanes.

		k_Q / 10^9 $M^{-1}s^{-1}$	K_{eq} / 10^3 M^{-1}	$k_{24\text{-decay}}$ / 10^3 s^{-1} [a]
a	(H)	5.2 ± 0.5	6.0 ± 1.5	2.52 ± 0.18
b	(3,4-Me$_2$)	3.4 ± 0.5	3.9 ± 0.5	1.34 ± 0.01
c	(4-Me)	4.3 ± 0.5	3.3 ± 0.6	1.82 ± 0.07
d	(4-F)	6.6 ± 1.4	1.7 ± 0.3	7.43 ± 0.07
e	(3-F)	4.8 ± 1.6	4.0 ± 1.0	9.54 ± 0.54
f	(4-CF$_3$)	2.5 ± 0.4	5.0 ± 0.5	14.5 ± 0.6
g	(3,5-(CF$_3$)$_2$)	1.6 ± 0.7 [b]	0.6 ± 0.3 [b]	487 ± 3

a. decays recorded at 290 nm in the presence of 50 mM isoprene. *b.* average $\pm$ σ from three independent determinations.

The decay of **Gg** cannot be treated in the same manner as **Ga-f** because of the unique complexity of the transient behaviour of this compound (see Chapter 2.9). To estimate a value of k_Q for the reaction of **Gg** with isoprene, we first calculated an

174

apparent rate constant by fitting the uncorrected 500 nm decays to first-order kinetics and

plotting the data in the usual way to obtain $k_{Q\text{-uncorr}}$. We then repeated this procedure for

Gb, **Gd**, and **Gf** and found that rate constants calculated from uncorrected decays were

1.25-1.65 times greater than those calculated from corrected decays. Therefore the value

of $k_{Q\text{-uncorr}}$ **Gg** was multiplied by a correction factor of (0.6 ± 0.1) to yield the value of k_Q

listed in Table 5.1. The calculation of K_{eq} was performed in the usual way because the

residual absorbance is not affected by the presence of the additional transient species

detected from **33g**.

The absorbance maxima of the vinylgermiranes **24a-g** ($\lambda_{max} = 285$ nm) do not

vary throughout the series, but the decay rate coefficients, which are listed in Table 5.1,

vary substantially as a function of substituent. We were unable to detect any changes in

the lifetimes of the vinylgermiranes over the range of 15-60 mM isoprene, indicating the

decay is not due to reaction of **24** with isoprene and must be a result of the formation of

23.

Hammett plots of k_Q, K_{eq}, and $k_{24\text{-decay}}$ are shown in Figure 5.11. The Hammett

plot of k_Q is distinctly concave, with the rates increasing as the electron withdrawing

capability is increased from mp-Me$_2$, reaching a maximum for the p-F analogue and then

decreasing as the electron withdrawing capability increases to mm-(CF$_3$)$_2$. K_{eq} shows no

regular variation with substituent, while $k_{24\text{-decay}}$ shows a reasonable positive correlation

with $\Sigma\sigma$.
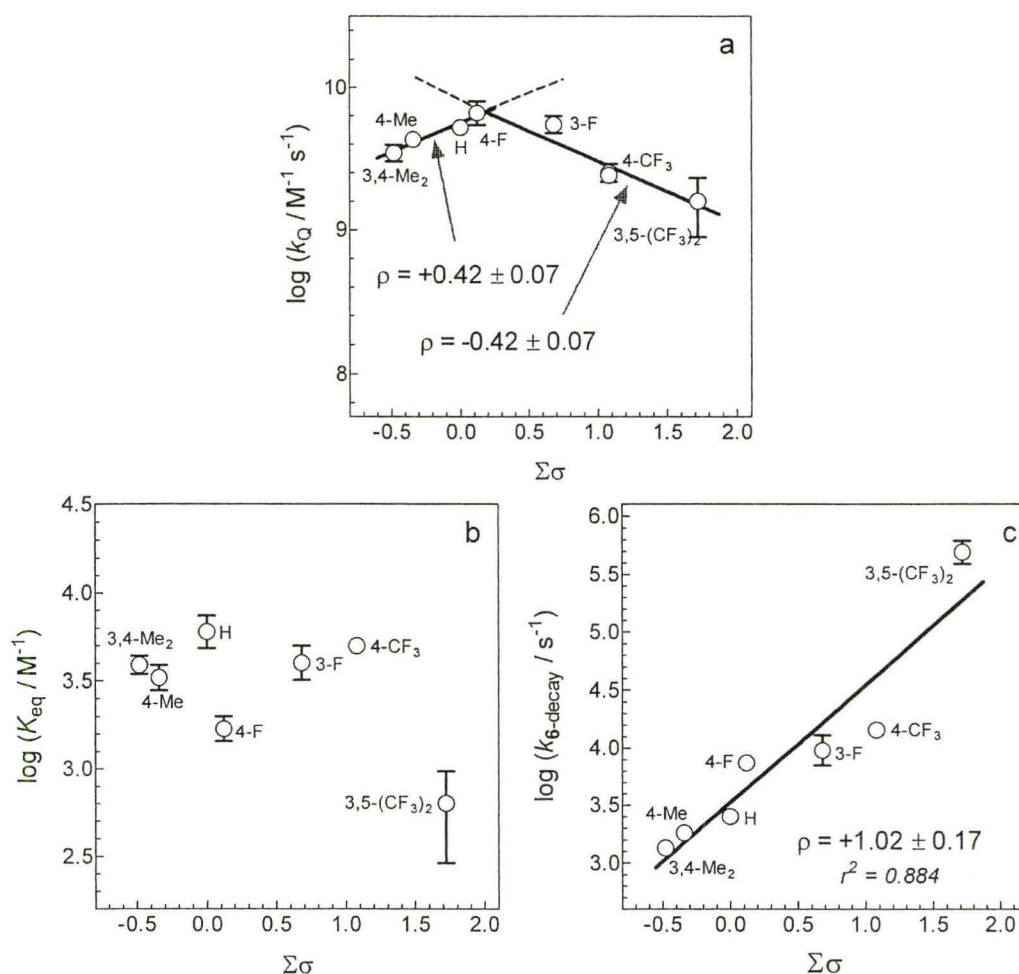
Figure 5.11. Hammett plots of the (a) forward rate and (b) equilibrium constants for the reaction of diarylgermylenes with isoprene and (c) of the first-order decay rate coefficient of the corresponding vinylgermiranes in hexanes. *(Reprinted from reference 25 with permission. © 2009 American Chemical Society.)*

The rate and equilibrium constants for the reactions of the germylenes **Ga** (H), **Gc** (CH$_3$) and **Gf** (CF$_3$) with isoprene were determined at several temperatures over the range of 14-61 °C. Table 5.2 lists the rate and equilibrium constants, while Figure 5.12 and Figure 5.13 show the resulting Arrhenius and van't Hoff plots; the Arrhenius and van't

Hoff parameters obtained from analysis of these data are shown in Table 5.3.

Table 5.2. Absolute rate and equilibrium constants for the reactions of germylenes **Ga,c,f** with isoprene in deoxygenated hexanes over the range of 13-62 °C. All values are corrected for the density change of the solvent with temperature.

	T / °C	k_Q / 10^9 $M^{-1}s^{-1}$	K_{eq} / 10^3 M^{-1}
Ga (H)	14.3	3.8 ± 0.5	13.2 ± 3.0
	25.0	5.2 ± 0.5	6.0 ± 1.5
	40.5	4.7 ± 0.4	2.8 ± 0.2
	61.0	3.3 ± 1.2	1.2 ± 0.1
Gc (Me)	13.0	4.1 ± 1.0	6.5 ± 1.9
	25.0	4.3 ± 0.5	3.3 ± 0.6
	41.8	5.2 ± 1.0	1.2 ± 0.4
Gf (4-CF$_3$)	13.5	2.8 ± 1.6	17.5 ± 6.0
	25.0	2.5 ± 0.4	5.0 ± 0.5
	45.7	9.3 ± 2.4	4.2 ± 0.8
	62.0	5.4 ± 3.0	0.6 ± 0.1
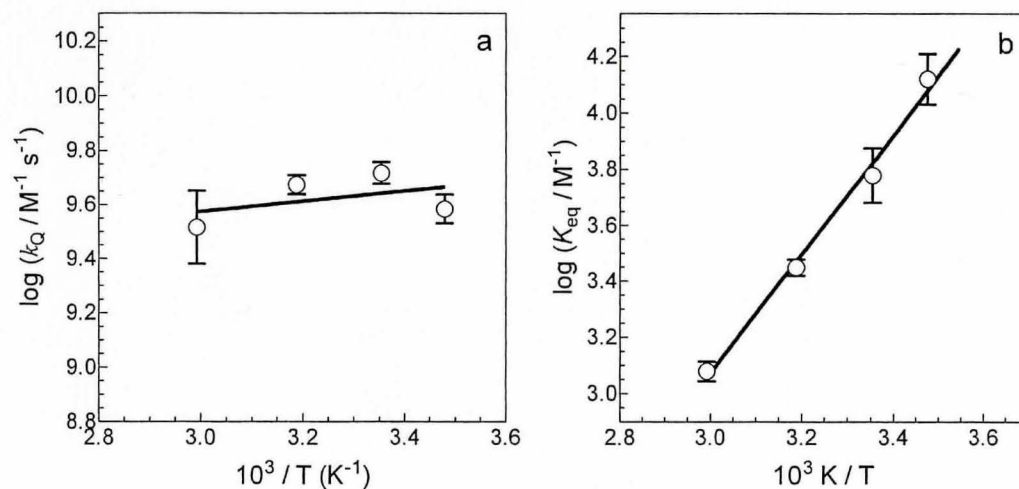
Figure 5.12. (a) Arrhenius and (b) van't Hoff plot for the reaction of **Ga** with isoprene in dry, deoxygenated hexanes solution over the range of 13-62 °C.
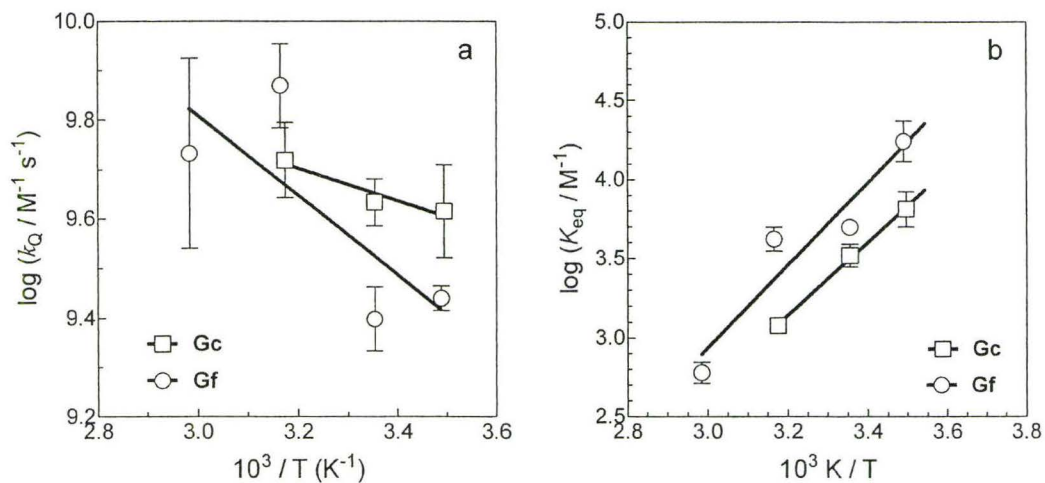
Figure 5.13. (a) Arrhenius and (b) van't Hoff plots for the reactions of **Gc** and **Gf** with isoprene in dry, deoxygenated hexanes solution over the range of 13-62 °C. *(Reprinted from reference 25 with permission. © 2009 American Chemical Society.)*

Table 5.3. Activation and thermodynamic parameters for the reactions of germylenes **Ga,c,f** with isoprene in hexanes.

	Ga (H)	**Gc** (Me)	**Gf** (CF₃)
E_a / kcal mol⁻¹	-0.9 ± 2.4	$+1.5 \pm 0.9$	$+3.7 \pm 4.2$
log A	9 ± 2	11 ± 1	12 ± 3
ΔH / kcal mol⁻¹	-9.7 ± 1.1	-10.5 ± 0.9	-12 ± 6
ΔS / cal K⁻¹ mol⁻¹	-15 ± 4	-19 ± 3	-21 ± 20
ΔG_{298} / kcal mol⁻¹	-5.2 ± 0.1	-4.8 ± 0.1	-5.0 ± 0.2

The effect of temperature on the formation and decay of the parent vinylgermirane **24a** was measured. Figure 5.14a shows the spectra of **33a** in hexanes recorded in the presence of 50 mM isoprene at 27°C and 51 °C. An increase in the decay rate coefficient with increasing temperature was observed. The Arrhenius plot of the decay rate coefficients, which is shown in Figure 5.14b, leads to an activation energy of $E_a \approx +11.8$ kcal/mol for the conversion of **24a** to **33a**. The maximum yield of the

178

vinylgermirane also decreased with increasing temperature. As shown in Figure 5.14a,

the maximum yield of **24a** decreases by a factor of ca. 1.65 upon increasing the

temperature from 27 °C to 51 °C. By estimating the K_{eq} values at these two temperatures

from the van't Hoff plot (Figure 5.12b), the estimated change in the maximum yield of

24a is 1.82, which is in good agreement with the observed value.

Table 5.4. Effect of temperature of the decay rate coefficient of the vinylgermirane **24a**.

T / °C	k_{decay} / 10^3 s^{-1}	T / °C	k_{decay} / 10^3 s^{-1}
10.6	0.81 ± 0.02	38.2	5.38 ± 0.27
14.3	1.11 ± 0.03	43.5	7.26 ± 0.43
19.3	1.75 ± 0.04	43.9	8.46 ± 0.52
25.5	2.20 ± 0.07	49.9	10.5 ± 0.6
34.1	3.86 ± 0.19	52.0	12.1 ± 1.0
34.5	4.17 ± 0.15		
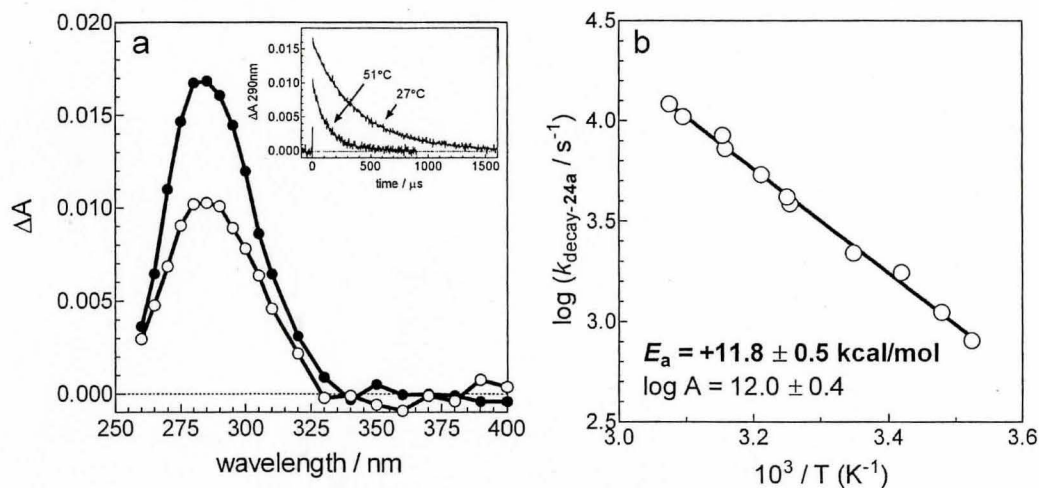
Figure 5.14. (a) Transient absorption spectra from photolysis of a solution of **33a** (3 mM) in the presence of 50 mM isoprene in hexanes at (●) 27 °C and (○) 51 °C. The inset shows the transient decay profiles recorded at 290 nm. (b) Arrhenius plot of k_{decay}**24a** in hexanes over the range of 11-52 °C. *(Reprinted from reference 25 with permission. © 2009 American Chemical Society.)*

The double bonds of isoprene are not equivalent so the possibility exists to form two different vinylgermiranes (**24** and **24′**). To determine whether this may lead to ambiguous results in the kinetic experiments, a flash photolysis experiment was carried out with DMB as the scavenger. There is only one possible vinylgermirane in this case (**64**), as shown in eq 5.13.

$$GeAr_2 \quad + \quad \text{isoprene} \quad \rightleftharpoons \quad \mathbf{64}$$

(5.13)

180
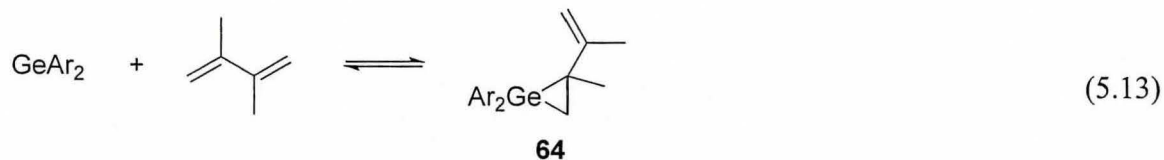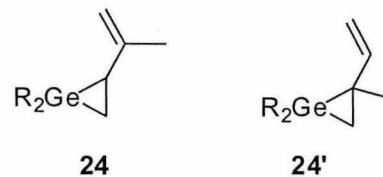
The form of the decays of $GePh_2$ in the presence of DMB is consistent with a

significantly smaller value of K_{eq} compared to that with isoprene. Figure 5.15a shows the

appearance of the decay of $GePh_2$ in the presence of various concentrations of isoprene;

even at higher concentrations of the diene, it is difficult to resolve the approach to

equilibrium. Given the limited number of data points in the initial fast decay, the forward

rate constant could only be estimated and was found to be roughly half of the value

determined for isoprene ($k_{DMB} = (2.3 \pm 1.0) \times 10^9$ $M^{-1}s^{-1}$). The equilibrium constant for

the reaction of $GePh_2$ with DMB was found to be $K_{eq} = 550 \pm 80$ M^{-1}, a value 12 times

lower than K_{eq} for the corresponding reaction of $GePh_2$ with isoprene. Given this lower

value of the equilibrium constant, we thus conclude that with isoprene there is a

preference for $GePh_2$ to form the vinylgermirane corresponding to reaction with the less

substituted of the two C=C bonds (*i.e.* **24** is formed preferentially to **24'**). The

vinylgermirane from the reaction of $GePh_2$ with DMB (**64**) can also be detected and

exhibits a $\lambda_{max} = 290$ nm. The decay coefficient of the species measured in the presence

of 30 mM DMB is fifty times more rapid than that of the corresponding isoprene-derived

vinylgermirane. The spectrum and decay profile of **64** are shown in Figure 5.15b.

Figure 5.15. (a) Effects of added DMB on the absorbance due to GePh$_2$ recorded at 500 nm (b) Transient absorption spectrum of **33a** in hexanes in the presence of 30 mM DMB. *Inset:* Decay of the **64** recorded at 290 nm. *(Reprinted from reference 25 with permission. © 2009 American Chemical Society.)*

The reaction of siliranes with methanol yields an isolable methoxysilane and this has been employed to infer the presence of siliranes in a reaction mechanism.[26, 27] For example, trapping of the vinylsilirane **74**, led to the methoxysilanes **75** and **76** as shown in eq 5.14.[27]

$$(5.14)$$

74   **75**   **76**

We wondered whether it would be possible to trap **24a** in a similar manner. The idea behind this experiment is shown in eq 5.15. The experiment would need to be designed with the appropriate concentrations of both methanol and isoprene such that a

sufficient amount of **24a** would be prepared and efficiently scavenged.
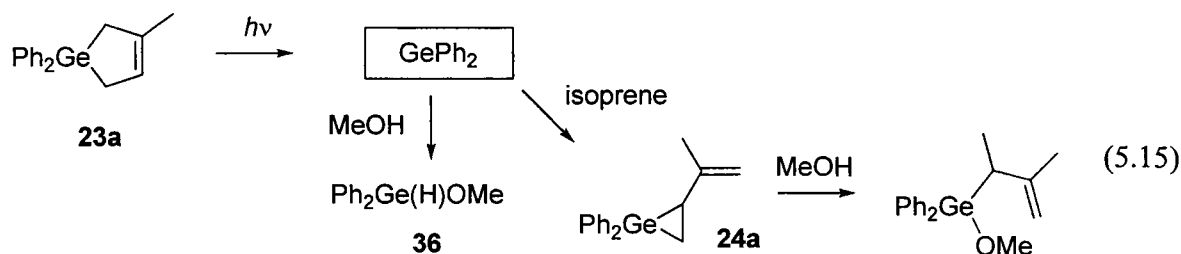
In order to estimate the appropriate concentrations of methanol and isoprene to use, a LFP experiment was performed to determine the rate constant for the reaction of **24a** with methanol. The germirane **24a** was formed from laser flash photolysis of a 3 mM solution of **33a** in hexanes containing 50 mM isoprene and its decay at 290 nm monitored in the presence of MeOH. The decay rate of **24a** increased in the presence of MeOH and the decays were fit to first-order kinetics. The plot of k_{decay} vs. [MeOH] exhibits distinct curvature (see Figure 5.16), indicating the reaction is not first-order in methanol. The data were therefore fit to an equation that includes an additional term to account for a reaction that is second-order in methanol (eq 5.16). The value of k_{MeOH} = $(3.7 \pm 1.5) \times 10^5$ M^{-1}s^{-1} is roughly seven orders of magnitude larger that the corresponding rate constant measured for the reaction of the vinylsilirane **74** with MeOH.[27] The value of k_{2MeOH} = $(2.3 \pm 0.5) \times 10^4$ M^{-2}s^{-1}.

$$k_{decay} = k_0 + k_{MeOH}[MeOH] + k_{2MeOH}[MeOH]^2 \tag{5.16}$$
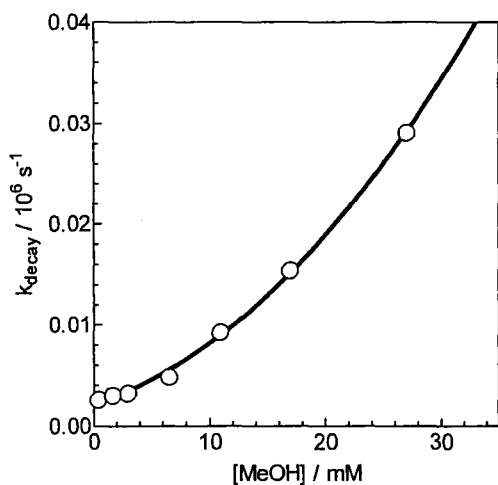
Figure 5.16. Plot of k_{decay} vs. [MeOH] for the reaction of **24a** with methanol in hexanes. The black line is the fit of the data to eq 5.16.

At ca. 30 mM methanol, the lifetime of the germirane has been reduced by a factor of 10, which should provide a sufficient yield of the methanol trapped germylene in the steady-state experiment. Therefore a solution of **23a** (35 mM) in C_6D_{12} containing isoprene (50 mM) and methanol (30 mM) was irradiated and the progress of the reaction monitored by ^1H NMR spectroscopy. Despite the similar magnitudes of the forward rate and equilibrium constants for the reactions of $GePh_2$ with methanol and isoprene (Methanol: $k_Q = 6.1 \times 10^9$ $M^{-1}s^{-1}$ and $K_{eq} = 3300$ M^{-1}.[28] Isoprene: $k_Q = 5.2 \times 10^9$ $M^{-1}s^{-1}$ and $K_{eq} = 6000$ M^{-1}.[8]), we were only able to detect the formation of **36a** throughout the experiment. This suggests that the changes to the absorbance-time profile of **24a** we observed in the presence of methanol were due to quenching of the free germylene rather than reaction with **24a**. In this case, the rate constants that were measured have no significance, and the experiment as designed (*i.e.* alcohol scavenging of the vinylgermirane) cannot be successful. In order to trap the vinylgermirane, presumably we would need to use a stronger nucleophile, such as methoxide.

5.3. Discussion

The kinetic product of the reaction of the germylene and isoprene is the (1+2)

cycloaddition product **24a**, which has been assigned as the transient at $\lambda_{max} = 290$ nm.[8]

Support for this assignment comes from the following observations: (1) The reaction of

GePh$_2$ with alkenes (*i.e.* not only dienes) leads to products with very similar transient

absorption spectra and lifetimes (*e.g.* GePh$_2$ in the presence of 4,4-

dimethyl-1-pentene gives a transient with $\lambda_{max} = 275$ nm and $\tau = 1.2$ ms,

which was assigned to germirane **18**.[8]) Although there have been no

reported UV-Vis spectra of stable germiranes, our results suggest that the S_0-S_1 transition

of 1,1-diphenylgermiranes is observed at ca. 285 nm regardless of the substituents on the

carbon framework. (2) Irradiation of **33a** in a hydrocarbon matrix (see Chapter 4) leads

to a single transient centered at 285 nm. Under these conditions, GePh$_2$ and DMB are

produced and the rigid medium prevents diffusion, so the only possible reactions are the

(1+4) cycloaddition to regenerate **33a** and the (1+2) reaction to generate the

vinylgermirane **64**.[27] (3) Generation of SiPh$_2$ in the presence of DMB led to the formation

of **21** ($\lambda_{max} = 290$ nm), which isomerizes over several hours to **22** (eq 5.17). Because of

the longer lifetime of the silirane, it could be characterized by ^{1}H NMR spectroscopy.[29]

(4) The lack of a Hammett correlation with K_{eq} rules out the possibility that the 290 nm

transient can be assigned to a π-complex (**70**) because such Lewis acid-base reactions

(*e.g.* with THF) have consistently shown strong correlations with Hammett σ values.

$$\text{(5.17)}$$

$$\lambda_{max} = 280 \text{ nm}$$
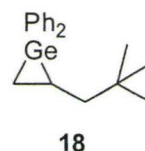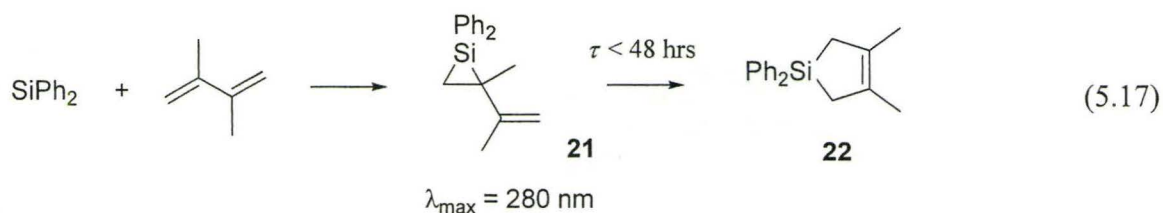
The Hammett plot of the forward rate constant is concave down. Such behaviour is typically associated with a multi-step mechanism wherein the rate-determining step changes with substituent.[30] The most likely candidate for a reaction intermediate is a π-complex (**77**), as shown in eq 5.18. The existence of these intermediates as minima on the reaction pathway has received support from computational studies (*vide supra*).[21]

$$\text{(5.18)}$$
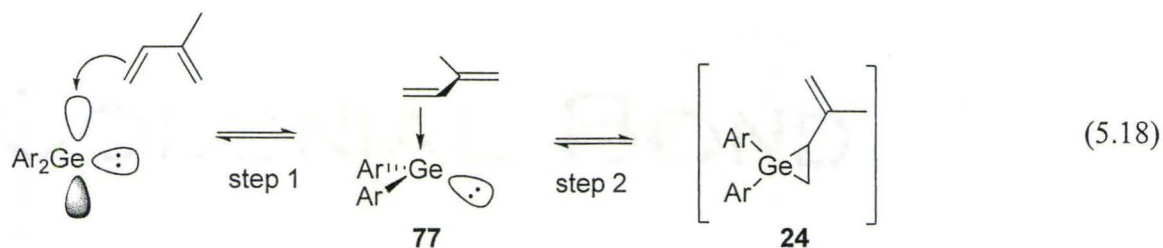
The first step of the reaction shown in eq 5.18 is a Lewis acid-base complexation and should accelerate with increasing electron withdrawing power of the substituents on the aryl rings. The second step involves formation of the two Ge-C bonds and should accelerate with electron donating substituents on the aryl rings because there will be a net movement of electron density away from the germanium to the more electronegative carbon atoms.

Consider the section of the Hammett plot which encompasses the relatively electron rich germylenes. With these germylenes, *step 2* should be favoured and *step 1* should be rate determining. When *step 1* is rate determining a positive ρ should be

observed. Now consider the region of the Hammett plot which encompasses the

relatively electron poor germylenes. With these germylenes *step 1* should be fast and

step 2 should be rate determining and a negative ρ value observed. Therefore, these

results are consistent with the two step mechanism shown in eq 5.18 for the formation of

vinylgermirane.

Additional support for the formation of a complex prior to reaction with the diene

comes from the observation that the rate constant for the reaction of $GeMe_2$-THF with

isoprene in THF solution is reduced by a factor of approximately four thousand compared

to that in hexanes.[31] Under these conditions, the $GeMe_2$-THF complex is the transient

with the highest concentration (ca. 10 μM) with the concentration of the free germylene

at roughly 35 pM (see Chapter 4). The ether blocks the initial nucleophilic attack of the

π-bond required for reaction between the germylene and diene.

Note that for a system which contains two consecutive equilibria, the rate

coefficient k_Q describes the *approach* to equilibrium and not the individual rate constants.

Laidler and co-workers have shown that the rate equation for such a system is given by

eq 5.19.[32] Because we cannot detect the intermediate, these microscopic rate constants

cannot be obtained.

$$-\frac{d[\mathbf{G}]}{dt} = \frac{k_1 k_2}{k_{-1} + k_2}[\mathbf{G}] - \frac{k_{-1} k_{-2}}{k_{-1} + k_2}[\mathbf{24}] \tag{5.19}$$

The decay of **24**, recorded under conditions where the system is flooded with

isoprene (50 mM) is sensitive to substitution and shows a modest correlation with

Hammett σ constants ($\rho = +1.0 \pm 0.2$, $r^2 = 0.88$; Figure 5.11c). Recall that we are

interested in determining how the major product (**23**) forms from the reaction of the

germylene with isoprene. Does the primary product, the vinylgermirane **24**, undergo a

[1,3]-sigmatropic rearrangement to yield **23**, or does **23** form from a direct (1,4)

cycloaddition reaction between the germylene and the diene (eq 5.20)?

(5.20)
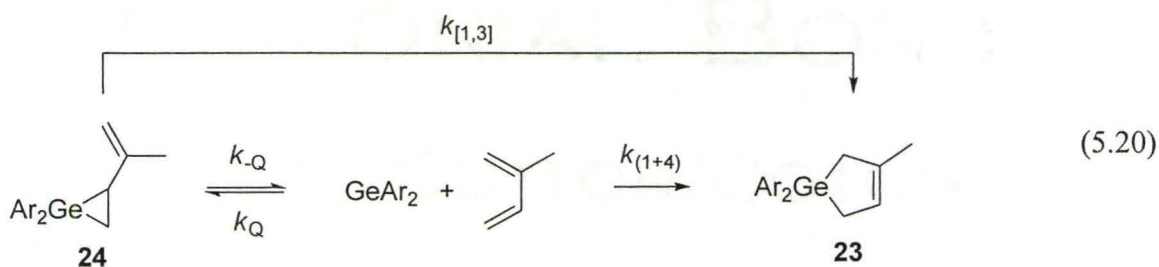
If **24** undergoes a [1,3]-sigmatropic rearrangement to **23**, the ρ value of the

Hammett plot suggests there is negative charge development at germanium in the

transition state. If **23** is formed from a direct (1+4) cycloaddition of the germylene and

diene, the rate equation describing the decay of the **24** is given in eq 5.21. These two

mechanisms are kinetically indistinguishable; however, we can estimate $k_{(1+4)}$ from the

decay of the **24**, as outlined in eqs 5.21-5.23. Thus the rate constant for the (1+4)

reaction can be obtained by multiplication of the K_{eq} and $k_{24\text{-decay}}$ (eq 5.24). Note that

these equations also indicate the decay of **24** should be insensitive to the concentration of

isoprene, and this was indeed observed in our experiments.

$$\frac{-d[24]}{dt} = \frac{d[23]}{dt} = k_{(1+4)}[\text{iso}][\mathbf{G}] \tag{5.21}$$

$$= k_{(1+4)}[\text{iso}]\left(\frac{[24]}{K_{eq}[\text{iso}]}\right) \tag{5.22}$$

$$= k_{(1+4)}\left(\frac{[24]}{K_{eq}}\right) \quad \therefore \quad k_{24-decay} = \frac{k_{(1+4)}}{K_{eq}} \tag{5.23}$$

$$\boxed{k_{(1+4)} = (k_{24-decay})(K_{eq})} \tag{5.24}$$

Table 5.5 lists the calculated $k_{(1+4)}$ values for all of the substituted analogues, while the corresponding Hammett plot is shown in Figure 5.17a. The plot reveals an excellent correlation of $k_{(1+4)}$ with Hammett σ constants, which leads to $\rho = +0.77 \pm 0.04$ ($r^2 = 0.987$). The positive ρ value is consistent with the germylene playing the role of the *electrophile* in the concerted (1+4)-cycloaddition. Furthermore, the strong Hammett correlation (which is better than that found with $k_{24-decay}$ alone) lends support for the direct (1+4) cycloaddition mechanism shown in eq 5.20.

We can also calculate the activation parameters of $k_{(1+4)}$ because the effect of temperature on K_{eq} and on $k_{24-decay}$ have already been determined (*vide supra*). The Arrhenius plot is shown Figure 5.17b; the activation energy is found to be $E_a = +2.2 \pm 0.5$ kcal/mol with log A = 8.8 ± 0.4. The activation energy for the (1+4) reaction is much higher than the activation energy for the (1+2) reaction, the latter of which is essentially zero.

Table 5.5. Absolute rates constants for the (1+4) cycloaddition reaction between **Ga-g** and isoprene in hexanes [$k_{(1+4)}$], calculated according to eq 5.24.

		$k_{(1+4)}$ / 10^6 M^{-1}s^{-1}
a	(H)	15.1 ± 4.6
b	(3,4-Me$_2$)	5.2 ± 0.7
c	(4-Me)	7.8 ± 1.7
d	(4-F)	12.6 ± 2.3
e	(3-F)	38 ± 12
f	(4-CF$_3$)	72 ± 9
g	(3,5-(CF$_3$)$_2$)	290 ± 145
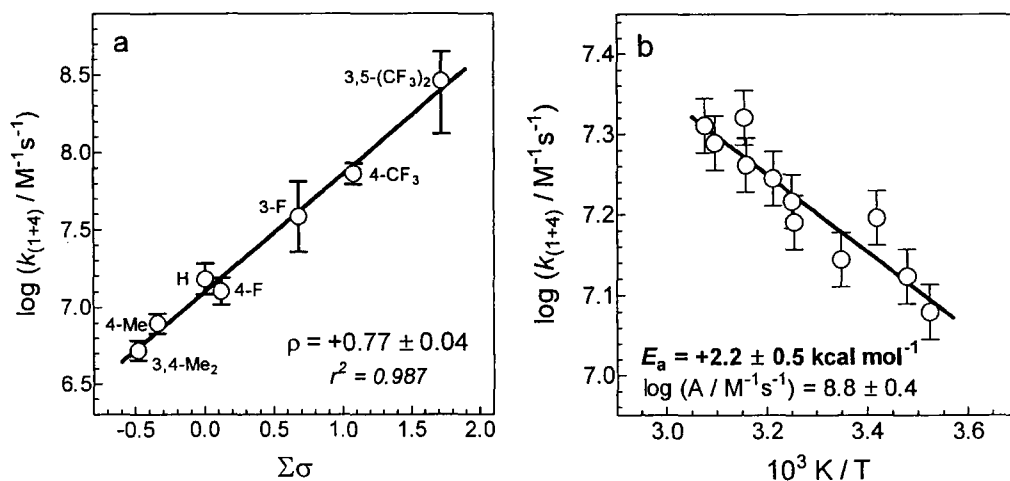
Figure 5.17. (a) Hammett plot of (1+4) cycloaddition rate constant ($k_{(1+4)} = K_{eq} \times K_{24\text{-}decay}$) between **Ga-g** and isoprene in hexanes. (b) Arrhenius plot for $k_{(1+4)}$ in hexanes over the temperature range of 11-52 °C, calculated using the measured ($k_{24\text{-}decay}$)$_T$ values and the (K_{eq})$_T$ values interpolated from the van't Hoff plot. *(Reprinted from reference 25 with permission. © 2009 American Chemical Society.)*

Recall that Köcher and Neumann proposed that GeMe$_2$ plays the role of the

nucleophile in its formal (1+4)-cycloaddition with dienes (see Chapter 1.4.6).[20] This

conclusion was based on the relative isolated yields of the germacyclopentene from the

reaction of $GeMe_2$ with various 1,4-disubstituted-1,3-dienes. The most efficient reaction occurred with electron poor dienes. We now know that this reaction is considerably more complex than just a (1+4) reaction, and their study was unable to address the (1+2) reaction. Furthermore, most of these diene substituents contain O and/or N; thus Lewis acid-base complexation between the germylene and diene substituents could have also affected the rate of oligomerization and therefore their interpretation of the results.

The decay rate coefficient of the vinylgermirane derived from the reaction of $GePh_2$ with DMB (64) is fifty times greater than the corresponding vinylgermirane derived from isoprene (24). It seems unlikely that the substitution of a single methyl group on the vinylgermirane would result is such a drastic change if the decay was due to a [1,3]-sigmatropic rearrangment. For example, in the all-carbon analogues shown in eq 5.25, the isomerization rate constants differ by only a factor of five and these reactions have a considerably higher activation energy than those associated with the process reflected in $k_{24\text{-decay}}$.[33] Calculation of the (1+4) cycloaddition rate constant for DMB is essentially the *same* as that with isoprene ($k_{(1+4)DMB} = (1.8 \pm 0.3) \times 10^7$ $M^{-1}s^{-1}$ at 25 °C)! Indeed, the additional methyl group should make little difference in the (1+4) cycloaddition.

$$\frac{k_{R=Me}}{k_{R=H}} = 5 \quad \text{(at 400 K)} \tag{5.25}$$
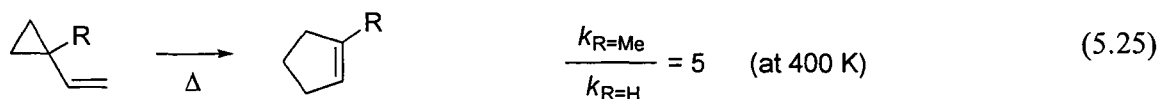
The thermodynamic and activation parameters associated with the (1+2)- and (1+4)-cycloaddition reactions of $GePh_2$ with isoprene are summarized in Table 5.6. The

enthalpy changes are also summarized in the reaction coordinate diagram in Figure 5.18.

A smaller activation energy for the (1+2) cycloaddition, along with $k_{(1+2)}$ about four-

hundred times greater than $k_{(1+4)}$, are consistent with the theoretical predictions of Nag

and Gaspar that the (1+4)-cycloaddition reaction of GeMe$_2$ with 1,3-butadiene has a

higher activation barrier than that for the (1+2) reaction.[21]

Table 5.6. Enthalpy and entropya changes for the (1+2) and (1+4) reactions of GePh$_2$ and
isoprene, and for the decay of **24** in hexanes.[a]

	ΔH / kcal mol^{-1}	$\Delta H^{\ddagger}$ / kcal mol^{-1}	ΔS / cal K^{-1} mol^{-1}	$\Delta S^{\ddagger}$ / cal K^{-1} mol^{-1}
(1+2)	-9.7 ± 1.1	≈ 0	-15 ± 4	-19 ± 4
(1+4)	b	$+1.5 \pm 0.3$	b	-20 ± 2
24 decay	b	$+11.2 \pm 0.4$	b	-5 ± 2

a. entropy reported at 25 °C; standard state is 1 M in hexanes at 298 K. *b.* cannot be determined.
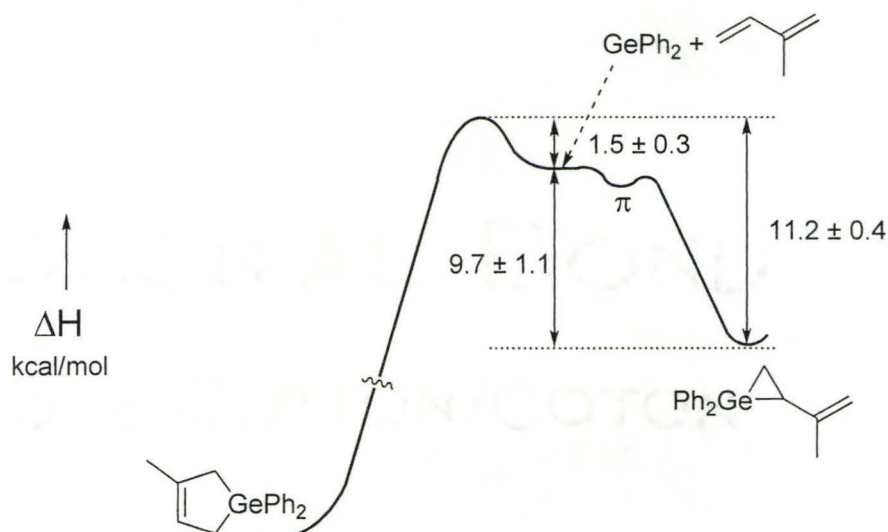
Figure 5.18. Reaction coordinate diagram showing the various enthalpy changes in
reaction GePh$_2$ and isoprene in hexanes. $\pi = \pi$-complex **77a**.

5.4. Summary

In hexanes solution, the diarylgermylenes **Ga-g** are scavenged by isoprene with roughly 80% efficiency to form the corresponding germacyclopentenes **23**. The primary product of the reaction is the corresponding vinylgermirane **24** formed by a (1+2) cycloaddition between the germylene and the diene. The equilibrium constants for the (1+2) reaction are *ca.* $K_{eq} = 1000\text{-}6000 \text{ M}^{-1}$ depending on the aromatic substituent but there is no regular variation with Hammett σ constants. The rate constants for the approach to equilibrium are $k_Q = 1\text{-}5 \times 10^9 \text{ M}^{-1}\text{s}^{-1}$ and the Hammett plot is concave (down). These data are consistent with the formation of an intermediate π-complex **77** prior to the formation of the vinylgermirane. The activation energy for the forward rate constant is essentially zero.

The vinylgermirane decay rate constant varies with aromatic substituent $k_{24\text{-decay}} = (1\text{-}500) \times 10^3 \text{ s}^{-1}$ and displays a reasonable Hammett correlation ($\rho = +1.02 \pm 0.17$; $r^2 = 0.88$). The decay rate increases markedly with temperature ($E_a = +11.8 \pm 0.5$ kcal/mol). From the decay of the vinylgermirane, the rate constant for the (1+4) cycloaddition reaction between the free germylene and isoprene is $k_{(1+4)} = (K_{eq\text{-}(1+2)})(k_{24\text{-decay}})$. These rate constants vary regularly with aromatic substituent ($\rho = +0.77 \pm 0.04$; $r^2 = 0.987$) and display a much better correlation with $\Sigma\sigma$ than do $K_{eq\text{-}(1+2)}$ or $k_{24\text{-decay}}$. The temperature dependence of the calculated $k_{(1+4)}$ values affords $E_{a\text{-}(1+4)} = +2.2 \pm 0.5$ kcal/mol and $\Delta S^{\ddagger} = -20 \pm 2 \text{ / cal K}^{-1} \text{ mol}^{-1}$. The higher activation energy of the (1+4) reaction compared to the (1+2) reaction agrees with recent theoretical predictions on the reaction of $GeMe_2$

with 1,3-butadiene.[21]

Our data support a reaction mechanism for the formation of the germacyclopentene involving direct (1+4) cycloaddition between $GePh_2$ and 1,3-dienes. The vinylgermirane is a kinetic product that mediates the rate of formation of the thermodynamically more stable germacyclopentene. We have been able to elucidate the electronic demands in both the (1+2) and (1+4) reactions (Figure 5.19) and quantitatively map most of the potential energy surface for the reaction of $GePh_2$ with isoprene.
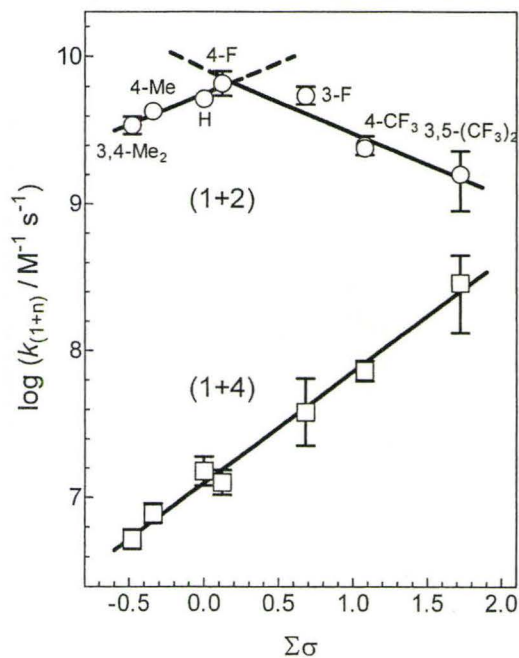
Figure 5.19. Hammett plot of the (1+2) and (1+4) cycloaddition reactions in hexanes. *(Reprinted from reference 25 with permission. © 2009 American Chemical Society.)*

5.5. References

1. Neumann, W. P. *Chem. Rev.* **1991**, *91*, 311.
2. Gaspar, P. P.; West, R. In *The chemistry of organic silicon compounds*, Rappoport, Z.; Apeloig, Y., Eds. John Wiley & Sons: New York, 1998; pp 2463-2568.
3. Tortorelli, V. J.; Jones, M., Jr.; Wu, S.-h.; Li, Z.-h. *Organometallics* **1983**, *2*, 759.
4. Boatz, J. A.; Gordon, M. S. *J. Phys. Chem.* **1989**, *93*, 3025.
5. Nagase, S. *Polyhedron* **1991**, *10*, 1299.
6. Horner, D. A.; Grev, R. S.; Schaefer, H. F., III *J. Am. Chem. Soc.* **1992**, *114*, 2093.
7. Birukov, A. A.; Faustov, V. I.; Egorov, M. P.; Nefedov, O. M. *Russ. Chem. Bull., Int. Ed.* **2005**, *54*, 2003.
8. Leigh, W. J.; Harrington, C. R. *J. Am. Chem. Soc.* **2005**, *127*, 5084.
9. Anwari, F.; Gordon, M. S. *Isr. J. Chem.* **1983**, *23*, 129.
10. Maier, E.; Olbrich, G. *Ber. Bunsen-Ges. Phys. Chem.* **1986**, *90*, 86.
11. Sakai, S. *Int. J. Quantum Chem.* **1998**, *70*, 291.
12. Su, M.-D.; Chu, S. Y. *J. Am. Chem. Soc.* **1999**, *121*, 11478.
13. Becerra, R.; Boganov, S. E.; Egorov, M. P.; Faustov, V. I.; Promyslov, V. M.; Nefedov, O. M.; Walsh, R. *Phys. Chem. Chem. Phys.* **2002**, *4*, 5079.
14. Lei, D.; Hwang, R.-J.; Gaspar, P. P. *J. Organomet. Chem.* **1984**, *271*, 1.
15. Clarke, M. P.; Davidson, I. M. T. *J. Chem. Soc., Chem. Commun.* **1988**, 241.
16. Lei, D.; Gaspar, P. P. *Res. Chem. Intermed.* **1989**, *12*, 103.
17. Takeda, N.; Tokitoh, N.; Okazaki, R. *Chem. Lett.* **2000**, 622.
18. Schriewer, M.; Neumann, W. P. *Angew. Chem. Int. Ed. Engl.* **1981**, *20*, 1019.
19. Ma, E. C.-L.; Kobayashi, K.; Barzilai, M. W.; Gaspar, P. P. *J. Organomet. Chem.* **1982**, *224*, C13.
20. Köcher, J.; Neumann, W. P. *J. Am. Chem. Soc.* **1984**, *106*, 3861.
21. Nag, M.; Gaspar, P. P. *Organometallics* **2009**, *28*, 5612.
22. Harrington, C. R.; Leigh, W. J.; Chan, B. K.; Gaspar, P. P.; Zhou, D. *Can. J. Chem.* **2005**, *83*, 1324.
23. Neumann, W. P.; Michels, E.; Köcher, J. *Tetrahedron Lett.* **1987**, *28*, 3783.
24. Bobbitt, K. L.; Gaspar, P. P. *J. Organomet. Chem.* **1995**, *499*, 17.
25. Huck, L. A.; Leigh, W. J. *Organometallics* **2009**, *28*, 6777.
26. Steinmetz, M. G.; Yu, C. *Organometallics* **1992**, *11*, 2686.
27. Leigh, W. J.; Huck, L. A.; Held, E.; Harrington, C. R. *Silicon Chem.* **2005**, *3*, 139.
28. Leigh, W. J.; Lollmahomed, F.; Harrington, C. R.; McDonald, J. M. *Organometallics* **2006**, *25*, 5424.
29. Moiseev, A. G.; Leigh, W. J. *Organometallics* **2007**, *26*, 6277.
30. Schreck, J. O. *J. Chem. Ed.* **1971**, *48*, 103.
31. Lollmahomed, F.; Huck, L. A.; Chitnis, S. S.; Harrington, C. R.; Leigh, W. J. *Organometallics* **2009**, *28*, 1484.
32. Krupka, R. M.; Kaplan, H.; Laidler, K. J. *Trans. Faraday Soc.* **1966**, *62*, 2754.
33. Elliott, C. S.; Frey, H. M. *J. Chem. Soc.* **1965**, 4289.

Chapter 6 – A Computational Study of the (1+2) Cycloaddition Reactions of Germylenes with Alkenes and Dienes

6.1. Introduction

Our group has studied the reactions of germylenes with alkenes and dienes (eq 6.1) over the past several years and a number of equilibrium constants for the (1+2) cycloaddition reactions of $GeMe_2$ and $GePh_2$ have been measured (Table 6.1 and 6.2). There are some trends in these K_{eq} values which prompted further investigation. Equilibrium constants for the reactions of $GePh_2$ with a number of C_6H_{12} alkene isomers in hexanes solution are listed in Table 6.1 and reveal a correlation between the K_{eq} values and the heats of formation (ΔH_f) of the alkenes (Figure 6.1). The reaction of $GePh_2$ with the alkenes becomes less favourable the greater the ΔH_f of the alkene.

$$GeR_2 \quad + \quad alkene/diene \quad \rightleftharpoons \quad R_2Ge\text{<}\!\!\!\!+\!R' \tag{6.1}$$

Table 6.1. Equilibrium constants for the reaction of $GePh_2$ with various six-carbon alkenes in hexanes, the corresponding free energy change of this reaction, and the heats of formation of the alkenes.

C_6H_{12}	K_{eq} / bar^{-1} [a,b]	$\Delta G_{298\,K}$/ kcal mol^{-1}	ΔH_f/ kcal mol^{-1} [b,c]
1-hexene	226 ± 37	-3.14 ± 0.37	-10.4
2-ethyl-1-butene	7.9 ± 0.4	-1.20 ± 0.12	-13.4
E-2-hexene	4.6 ± 0.3	-0.89 ± 0.17	-12.9
Z-2-hexene	2.4 ± 0.2	-0.51 ± 0.16	-12.5
2-methyl-2-pentene	0.16 ± 0.02	1.06 ± 0.30	-16.0

a. Measured by Saurabh Chitnis. Values measured in hexanes solution at 25 °C, and thus originally reported in units of M^{-1}. *b*. Standard state:1 bar and 298.15 K. *c*. Reference 1.
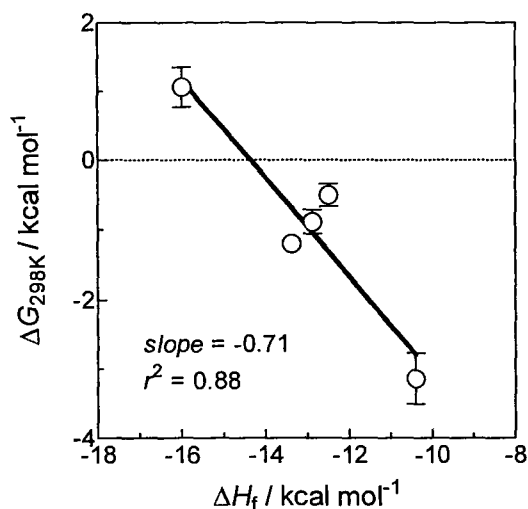
Figure 6.1. Plot showing the correlation between the $\Delta G_{298\,K}$ of reaction of $GePh_2$ with various C_6H_{12} alkenes and the ΔH_f of the corresponding alkene.

Equilibrium constants have been measured for the reactions of $GeMe_2$ and $GePh_2$ with isoprene, 4,4-dimethyl-1-pentene (DMP) and DMB (Table 6.2). These data also show that K_{eq} decreases with increasing substitution of the alkene; however, in this case we are interested in the effect of the germanium substituent on the stability of the germirane. The equilibrium constant for the reaction of each alkene with $GeMe_2$ is much greater than the corresponding value for the reaction with $GePh_2$.

Table 6.2. Equilibrium constants (in units of bar^{-1}) for the reactions of $GeMe_2$ and $GePh_2$ with isoprene, DMB, and 4,4-dimethyl-1-pentene (DMP).[a]

	$GeMe_2$ [b]	$GePh_2$
isoprene	≈ 800	240 ± 10 [c]
4,4-dimethylpentene (DMP)	≈ 800	100 ± 25 [c]
DMB	-	6.0 ± 0.8 [d]

a. Standard state: 1 bar and 298 K; values measured in hexanes solution at 25 °C, and thus originally reported in units of M^{-1}. *b.* Reference 2. *c.* Reference 3. *d.* Reference 4.

Recall from Chapter 5 that the (1+2) cycloaddition of germylenes with alkenes and dienes, the formation of an intermediate π-complex (**70**) has been proposed (eq 6.2).

Our group has employed the germacyclopentene **78** as a photochemical precursor to

GeH$_2$.[5] While a transient exhibiting germylene-like behaviour was indeed observed in

LFP experiments with **78** in hexanes, several aspects of its behaviour are not consistent

with what we would expect for free GeH$_2$ based on the extensive studies of the molecule

in the gas phase by Walsh *et al.*[6] One possible explanation for the unexpected behaviour

is that the observed species is a π-complex of GeH$_2$ with the diene co-product (**79**; see eq

6.3).

$$MR_2 + H_2C=CH_2 \rightleftharpoons \overset{H_{\prime\prime\prime}\equiv\prime\prime\prime H}{\underset{R^{\prime}}{\overset{H}{\underset{R\prime\prime\prime M}{\rightarrow}}}} \rightleftharpoons \overset{R_2}{\underset{13}{M}} \qquad (6.2)$$

70

$$\overset{Ph}{\underset{78}{H_2Ge\diagup}} \overset{h\nu}{\underset{hexanes}{\longrightarrow}} \left[GeH_2 + \overset{Ph}{\diagup} \right] \longrightarrow \overset{H_2Ge \ Ph}{\underset{\substack{\pi\text{-complex} \\ \lambda_{max} = 460 \text{ nm} \\ \mathbf{79}}}{\diagup}} \overset{x\,2}{\longrightarrow} \overset{H_2Ge=GeH_2}{\underset{\substack{\lambda_{max} = 385 \text{ nm} \\ \mathbf{80}}}{}} \qquad (6.3)$$

A better understanding of the effect of alkene substitution and germylene

substitution on the thermodynamics of (1+2)-cycloaddition reaction will be helpful in

explaining the trends in the K_{eq} values and the experimental observations described

above. We turned to computational chemistry to help address these questions. The first

part of this chapter outlines a computational DFT (ADF) study of the relative stabilities

of germiranes of GeMe$_2$ and GePh$_2$, with an emphasis on understanding the effect of

substitution on the germirane framework. The second part of this chapter places

emphasis on the reactions of GeH_2 and $GeMe_2$ with dienes to yield both the germirane

and the π-complex; Gaussian was used as the computational software for comparative

purposes to our earlier results and to other theoretical data in the literature.

6.2. Summary of previous computational studies on the (1+2) cycloaddition reactions of germylene with alkenes and dienes.

Previous computational studies in the reactions of germylenes with alkenes have

focused mainly on that of GeH_2 with ethylene (eq 6.4).[7-13] Table 6.3 summarizes the

enthalpy changes predicted by these calculations. In most cases, the existence of a π-

complex (81) as a minimum on the potential energy surface prior to the formation of the

germirane 82 is supported.

GeH₂ + H₂C=CH₂ ⇌ 81 ⇌ 82   (6.4)
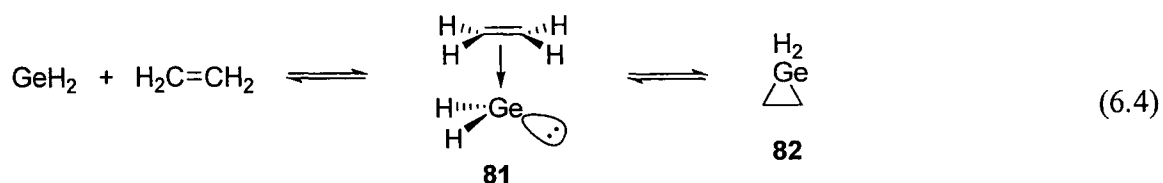
Table 6.3. Summary of computational data in literature on the (1+2) cycloaddition reaction of GeH$_2$ with ethylene.

		ΔH^{a}	Parameters	Reference
1	π–complex	-9.3	DZ+d SCF	7
2	germirane	-18.3	DZ+d CCSD//DZ+d SCF	7
3	π–complex	-10.5	MP4//MP2	8
4	germirane	-12.4	MP4//MP2	8
5	germirane	-27.4 ^{c}	B3LYP/6-31G*	9
6	germirane	-35.2	QCISD(T)/6-31G(3df,2p)	10
7	π–complex	-21.3	B3LYP/6-31G*	11
8	germirane	-24.8	B3LYP/6-31G*	11
9	π–complex	-11.6	PBE/TZ2P	12
10	germirane	-12.7	PBE/TZ2P	12
11	π–complex	-22	B3LYP/6-31G(d,p)	13
12	germirane	-26.4	B3LYP/6-31G(d,p)	13
13	π–complex	-13.6	B3LYP/6-311G(3df,3pd)	13
14	germirane	-16	B3LYP/6-311G(3df,3pd)	13
15	π–complex	- ^{d}	MP2/6-311G(3df,3pd)	13
16	germirane	-34.5	MP2/6-311G(3df,3pd)	13
17	π–complex	-15.6	CCSD(T)/6-311G(3df,3pd)	13
18	germirane	-22.4	CCSD(T)/6-311G(3df,3pd)	13

a. in kcal/mol, relative to the reactants at 298 K unless otherwise noted. *b*. 293 K. *c*. enthalpy conditions not reported. *d*. minimum not found.

Birukov *et al.* examined the effect of substitution on germanium as well as on the alkene by calculating the enthalpies of reaction of GeH$_2$ and GeMe$_2$ with ethylene and tetramethylethylene (TME) (Table 6.4, entry 1-8). The conclusions from these data are that alkyl substitution on both the germylene and alkene should make the reaction enthalpy to form both the π-complex and the germiranes more positive.

As part of a detailed computational study of the (1+2) and (1+4) reaction of metallylenes with 1,3-dienes, Nag and Gaspar calculated the free energies of reaction for

GeMe$_2$ with butadiene and GePh$_2$ with isoprene (see Table 6.4, entries 12-15 and Table

6.5, respectively).[14] The free energy of the reaction of GeMe$_2$ and GePh$_2$ with isoprene

has been measured in hexanes solution, as shown in Table 6.5.[2, 3] Also shown in Table

6.5 is that the B3LYP method underestimates the favourability of both reactions which

the authors note is due to the fact that B3LYP overestimates the stability of the free

germylene.[14]

Table 6.4. Summary of computational data in literature pertaining to the (1+2) cycloaddition reactions of GeR$_2$ (R = H, Me) with ethylene, tetramethylethylene (TME), and isoprene.

	System		ΔH^a	Parameters	Reference
1	GeH$_2$ + ethylene	π–complex	-11.6	PBE/TZ2P	12
2		germirane	-12.7	PBE/TZ2P	12
3	GeMe$_2$ + ethylene	π–complex	-^{b}	PBE/TZ2P	12
4		germirane	-8.4	PBE/TZ2P	12
5	GeH$_2$ + TME	π–complex	-3.3	PBE/TZ2P	12
6		germirane	-0.4	PBE/TZ2P	12
7	GeMe$_2$ + TME	π–complex	7.6	PBE/TZ2P	12
8		germirane	5.7	PBE/TZ2P	12
9	GeMe$_2$ + ethylene	germirane	-27.3 ^{c}	B3LYP/6-31G*	9
10		germirane	-17.73	B3LYP/LANL2DZ	15
11		germirane	-19.49	CCSD(T)/LANL2DZdp^e	15
12	GeMe$_2$ + butadiene ^{d}	π–complex	-12.1	CCSD(T)/cc-pVTZ^f	14
13		germirane	-23.2	CCSD(T)/cc-pVTZ^f	14
14		π–complex	-5.2	B3LYP ^{g}	14
15		germirane	-8.7	B3LYP ^{g}	14

a. in kcal/mol, relative to the reactants at 298 K unless otherwise noted. *b.* minimum not found. *c.* enthalpy conditions not reported. *d.* in the *s*-trans configuration. *e.* // B3LYP/LANL2DZ. *f.* // B3LYP/6-31G(d,p) for C, H and 6-311G(d,p) for Ge. *g.* /6-31G(d,p) for C, H and 6-311G(d,p) for Ge.

Table 6.5. Summary of data in literature on the (1+2) cycloaddition reactions of $GeMe_2$ and $GePh_2$ with 1,3-dienes to yield the germirane.

	System[b]	ΔG[a]	Parameters	Reference
1	$GeMe_2$ + isoprene	≈ -3.9	**experimental** (hexanes, 293 K)	2
2	$GeMe_2$ + butadiene	+3.2	B3LYP[c]	14
3	$GeMe_2$ + butadiene	-11.1	CCSD(T)/cc-pVTZ[d]	14
4	$GePh_2$ + isoprene	-3.2 ± 0.6	**experimental** (hexanes, 293 K)	3
5	$GePh_2$ + isoprene	+8.6	B3LYP[c]	14

a. in kcal/mol, standard state 298 K and 1 bar. *b*. for the calculations, the diene is in the *s*-trans configuration. *c*. 6-31G(d,p) for C, H and 6-311G(d,p) for Ge. *d*. B3LYP/6-31G(d,p) for C, H and 6-311G(d,p) for Ge.

6.3. The reactions of GeH_2, $GeMe_2$, and $GePh_2$ with alkenes and dienes. Computational results using ADF.

6.3.1. General Method

Preliminary structures of the alkenes, dienes and germiranes were obtained via molecular mechanics with the software Chem3D (11.0.1 CambridgeSoft), employing the MM2 force field.[16] The resulting structures were exported into the ADF DFT software (2008.01d; SCM)[17] for geometry optimization.[18, 19] These optimizations were gradient corrected (GGA) with the exchange and correlation functionals of Perdew and Wang (PW91)[20] and uncontracted Slater-type orbitals (STOs) of triple-ζ double-polarization (TZ2P) quality as basis functions, including all core electrons. Calculations were performed with the inclusion of relativistic effects (ZORA formalism).[21] Spectroscopic calculations used the time-dependent extension of density functional theory (TD-DFT) within ADF.[22-26] The adiabatic local density approximation (ALDA) was used for the exchange-correlation kernel[27, 28] and the differentiated static LDA expression was used with the Vosko-Wilk-Nusair parametrization.[29] All values were corrected for the zero-

point energy.

The iterative geometric energy convergence criterion was set at 4×10^{-4} Hartrees; smaller values either made the computational time unreasonably long or the computations failed to converge. In the calculation of the larger molecules **14** and **15**, the convergence criterion was raised to 1×10^{-3} Hartrees, and the basis set was reduced to TZP.

6.3.2. Results - geometry optimizations and thermodynamics

The computational parameters were initially chosen because we have previously found that the results produced agreed well with experimental data in the calculation of the structures of germylenes and stannylenes and the corresponding digermenes and distannenes.[30, 31] To determine whether the same parameters would be able to estimate the geometry of germiranes correctly, germiranes **14** and **15** were optimized and the results compared with values obtained by x-ray crystallography.[32] The agreement of the predicted geometries with experimental data is excellent, as shown in Table 6.6. The predicted free-energy change for the (1+2) cycloaddition to yield **14** is $\Delta G_{298\ K} = -2.88$ kcal/mol, which is more positive than expected based on the experimental observation.
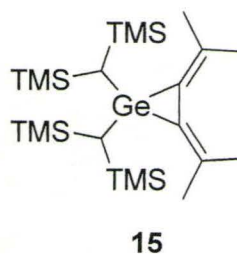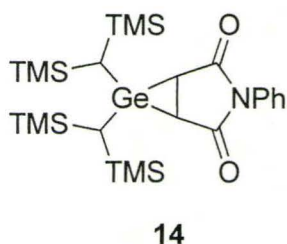
14   **15**

Table 6.6. Computational (PW91/TZP/ZORA) and x-ray crystal structure data for **14** and **15**. C_1 and C_2 are the carbon atoms of the three-membered ring.

	14		**15**	
	Calc.	Expt.[a,b]	Calc.	Expt.[a]
Ge-C_1 (Å)	2.00	1.92(2)/1.97(2)	1.97	1.95(1)
Ge-C_2 (Å)	2.01	1.98(2)/2.07(2)	1.97	1.96(1)
C_1-C_2 (Å)	1.52	1.51(3)/1.62(3)	1.45	1.46(2)
C_1GeC_2 (°)	44.6	45.0(8)/47.7(8)	43.4	44.0(5)

a. See reference 32. *b.* two independent molecules within the asymmetric unit.

Using these same methods the geometries of GeH_2, $GeMe_2$, $GePh_2$, the alkenes shown in Figure 6.2 and the germiranes shown in Figure 6.3 were calculated. Selected bond lengths and angles from the optimized structures are presented in two ways: Table 6.7 presents these data so that the trends in the structures of the germiranes derived from each germylene are evident, while Table 6.8 presents these same data so that the trends in the structures of the germiranes derived from each alkene are evident.
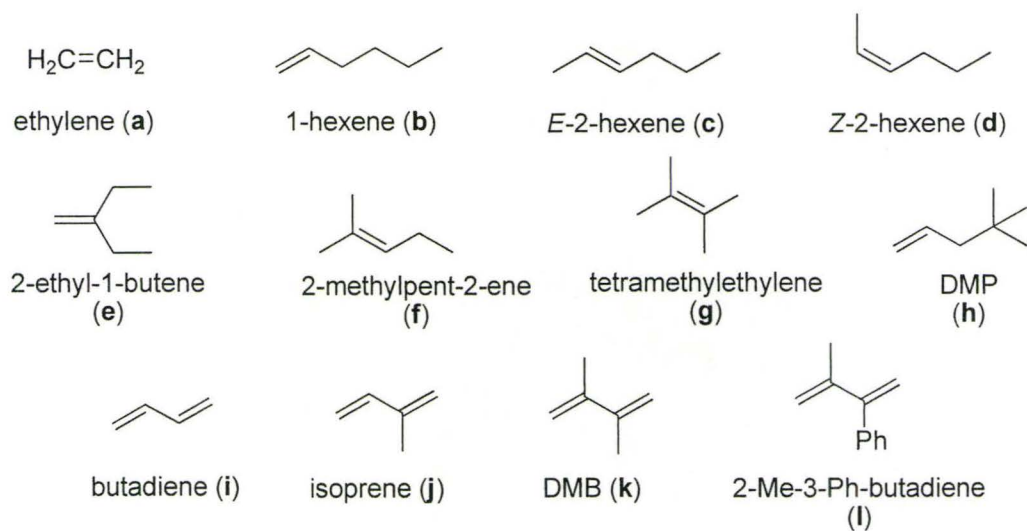
Figure 6.2. Alkenes and dienes investigated in this computational study.
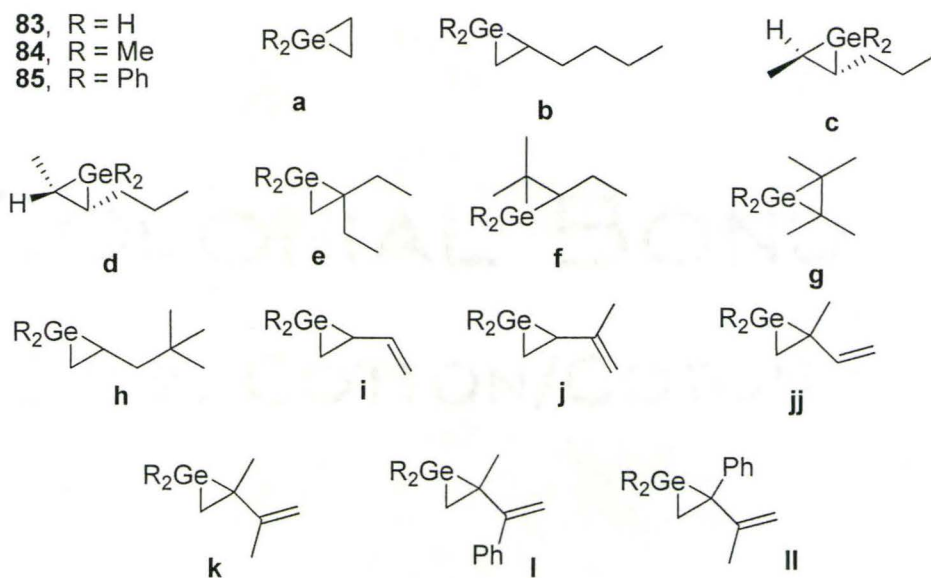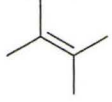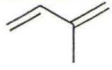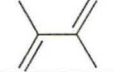
Figure 6.3. Germiranes investigated in this computational study.

Table 6.7. Summary of selected bond distances (Å) and angles (°) from the geometry optimized structures of the alkenes **a-l** and germiranes **83-85** (PW91/TZ2P/ZORA).

83		#[a]	C=C [b]	C-C [c]	Ge-C [d]	Ge-C [e]	C-Ge-C
a	ethene	0	1.331	1.533	1.962	1.962	45.98
b	1-hexene	1	1.334	1.532	1.957	1.957	46.08
g	TME	4	1.350	1.560	1.980	1.980	46.40
i	butadiene	1	1.342	1.533	1.945	1.993	45.82
l	2M3P	2	1.348	1.544	1.952	2.002	45.94
ll	2M3P	2	1.355	1.533	1.955	1.992	45.68
84							
a	ethene	0	1.331	1.547	1.958	1.958	46.53
b	1-hexene	1	1.334	1.546	1.963	1.965	46.34
c	E-2-hexene	2	1.336	1.548	1.968	1.968	46.31
d	Z-2-hexene	2	1.339	1.556	1.969	1.969	46.54
e	2-Et-butene	2	1.339	1.550	1.966	1.976	46.29
f	2-Me-2-p	3	1.342	1.557	1.975	1.978	46.41
g	TME	4	1.350	1.557	1.981	1.981	46.88
h	DMP	1	1.334	1.549	1.958	1.967	46.49
i	butadiene	1	1.342	1.548	1.947	2.001	46.15
j	isoprene	1	1.342	1.550	1.950	1.995	46.24
k	DMB	2	1.347	1.555	1.966	1.974	46.48
85							
a	ethene	0	1.331	1.539	1.962	1.956	46.26
b	1-hexene	1	1.334	1.546	1.956	1.965	46.44
c	E-2-hexene	2	1.336	1.544	1.966	1.970	46.19
d	Z-2-hexene	2	1.339	1.555	1.965	1.970	46.53
e	2-Et-butene	2	1.339	1.546	1.961	1.979	46.21
f	2-Me-2-p	3	1.342	1.557	1.969	1.979	46.46
g	TME	4	1.350	1.573	1.980	1.981	46.79
h	DMP	1	1.334	1.543	1.954	1.974	46.24
i	butadiene	1	1.342	1.545	1.944	2.005	46.02
j	isoprene	1	1.342	1.542	1.951	2.004	45.89
jj	isoprene-alt	2	1.347	1.547	1.946	2.025	45.81
k	DMB	2	1.347	1.537	1.960	2.004	45.62

a. number of alkyl substituents on the alkene. *b*. C=C of free alkene that will become the two carbons of the germirane framework. *c*. formerly the corresponding alkene carbons. *d*. bond to the less substituted carbon of the germirane moiety. *e*. bond to the more highly substituted carbon of the germirane moiety.

Table 6.8. Effect of germanium substituent on the geometry of the germirane for a given alkene or diene. Select bond distances (Å) and angles (°) from the geometry optimized structures of the alkenes **a-l** and germiranes **83-85** (PW91/TZ2P/ZORA).

		C-C ^{a}	Ge-C ^{b}	Ge-C ^{c}	C-Ge-C
83a		1.533	1.962	1.962	45.98
84a	$H_2C=CH_2$	1.547	1.958	1.958	46.53
85a		1.539	1.962	1.956	46.26
83b		1.532	1.957	1.957	46.08
84b		1.546	1.963	1.965	46.34
85b		1.546	1.956	1.965	46.44
83g		1.560	1.980	1.980	46.40
84g		1.557	1.981	1.981	46.88
85g		1.573	1.980	1.981	46.79
83i		1.533	1.945	1.993	45.82
84i		1.548	1.947	2.001	46.15
85i		1.545	1.944	2.005	46.02
83j		1.550	1.950	1.995	46.24
84j		1.542	1.951	2.004	45.89
83k		1.555	1.966	1.974	46.48
84k		1.537	1.960	2.004	45.62
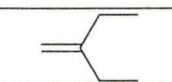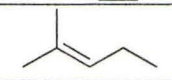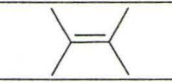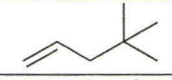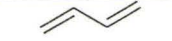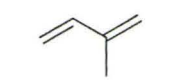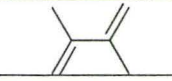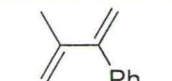
a. formerly the alkene carbons. *b.* bond to the less substituted carbon of the germirane moiety. *c.* bond to the more highly substituted carbon of the germirane moiety.

The energy changes associated with the cycloaddition reaction shown in eq 6.5 were calculated using eq 6.6 and are listed in Table 6.9.

$$GeR_2 \quad + \quad alkene/diene \quad \rightleftharpoons \quad R_2Ge\!\!\triangleleft\!\!-R' \qquad\qquad (6.5)$$
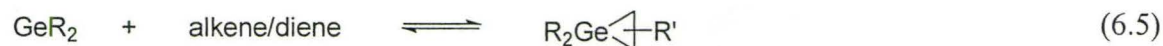
$$\Delta E = \Delta E_{germirane} - \Delta E_{GeR_2} - \Delta E_{alkene/diene} \qquad \text{where } E = G \text{ or } H \qquad (6.6)$$

Table 6.9. Calculated enthalpy and free energy changes (in kcal mol^{-1} at 298.15 K) for the (1+2) cycloaddition reactions of GeH$_2$, GeMe$_2$, and GePh$_2$. (PW91/TZ2P/ZORA)

		ΔH			ΔG		
		GeH$_2$	GeMe$_2$	GePh$_2$	GeH$_2$	GeMe$_2$	GePh$_2$
a	H$_2$C=CH$_2$	-18.32	-13.83	-13.1	-7.52	-2.11	0.11
b		-17.1	-12.54	-9.86	-6.4	-3.63	2.89
c		*a*	-10.57	-8.86	*a*	-2.32	5.4
d		*a*	-7.76	-5.19	*a*	0.03	6.96
e		*a*	-12.15	-11.08	*a*	-3.28	1.87
f		*a*	-6.26	-4.02	*a*	1.93	8.34
g		-10.25	-3.86	-2.12	3.89	5.59	14.71
h		*a*	-12.79	-12.65	*a*	-2.11	4.07
i		-14.56	-10.71	-8.77	-3.52	0.81	4.47
j		*a*	-9.19	-8.92	*a*	-0.08	5.08
jj		*a*	*a*	-7.26	*a*	*a*	5.19
k		*a*	-6.98	-8.71	*a*	1.82	6.07
l		-24.39	*a*	*a*	-14.38	*a*	*a*
ll	Ph	-26.85	*a*	*a*	-19.1	*a*	*a*

a. value not determined.

6.3.3. Discussion

There are some trends in the geometries of the germiranes that are apparent from these calculations. Consider the simplest cases of GeH$_2$, GeMe$_2$, and GePh$_2$ with

ethylene to yield **83a**, **84a**, and **85a**, respectively. The Ge-C bond lengths are in the order

of **84a** < **85a** ≈ **83a**. Furthermore, the C-C bond lengths of the germirane framework are

83a < **85a** < **84a**. These trends can be explained by considering the HOMO of **83a**

shown in Figure 6.4. This orbital is bonding with respect to both Ge-C bonds and anti-

bonding with respect to the C-C bond. Methyl groups are electron donors (relative to H

and Ph) and donation of electron density into the HOMO strengthens both interactions

leading to a decrease in the Ge-C bond length and an increase in the C-C bond length. It

is noted that the methyl and phenyl substituents on germanium do not alter the general

characteristics of the HOMO, as shown in Figure 6.4. The predicted changes in bond

lengths are consistent with expectation based on those observed with substituted

cyclopropanes.[33]

83a   **84a**   **85a**
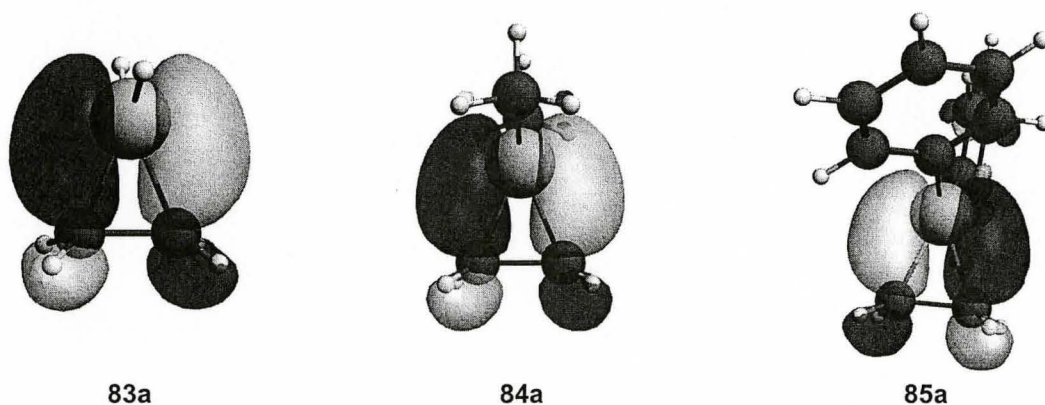
Figure 6.4. Highest-occupied molecular orbitals of **83a**, **84a** and **85a**.
(PW91/TZ2P/ZORA)

For the germiranes derived from the same alkene, the length of

bond 1 is usually longer than *bond 2*. The effect is most apparent with **84**

and **85** so steric repulsion between the substituents on the germanium (R)
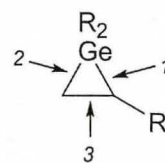
and the substituents on the carbon (R′) appears to be the largest contributing factor. The

lengths of the Ge-C bonds increase with the number of substituents on the carbon atoms

of the germirane framework. Steric repulsion between the R′ substituents also plays a

role because germiranes derived from TME display the longest Ge-C *and* C-C bond

lengths. If electronic effects were dominant, the Ge-C lengths in the germiranes derived

from TME should become shorter while the C-C bond should become longer, for the

reasons discussed in the preceding paragraph. Substituents on the carbon atoms of the

germirane framework do not alter the electron distribution in the HOMO (for example,

compare Figure 6.5 to Figure 6.4)
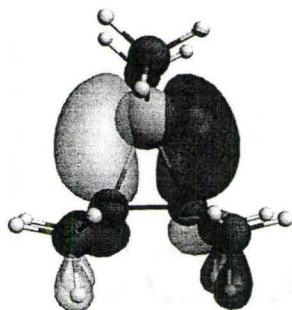
Figure 6.5. Highest-occupied molecular orbital of the germirane **84g** derived from $GeMe_2$ and TME. (PW91/TZ2P/ZORA)

Vinylgermiranes are predicted to have different geometries than germiranes

derived from non-conjugated alkenes. In these cases, *bond 1* is longer

than expected based solely on the number of R′ substituents while *bond 4*

is shorter than expected. Figure 6.6 illustrates this effect by comparing

the geometries of the germiranes derived from GeH_2 and butadiene (**83i**) and 1-hexene

(**83b**); the electron distribution in the corresponding frontier molecular orbitals are
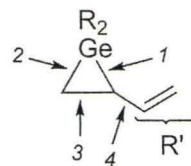
shown in Figure 6.7. The interaction between the π-bond of the vinyl

group and the adjacent Ge-C bond results in a net loss in electron density

in *bond 1* while there is additional bonding interaction in *bond 4*.
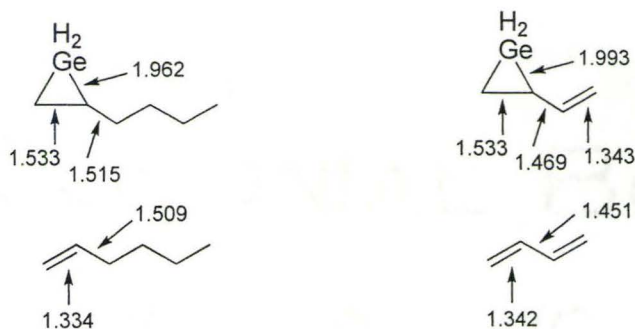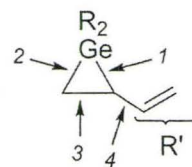
Figure 6.6. Select bond lengths (Å) in **83b**, **83i**, butadiene, and 1-hexene. (PW91/TZ2P/ZORA)
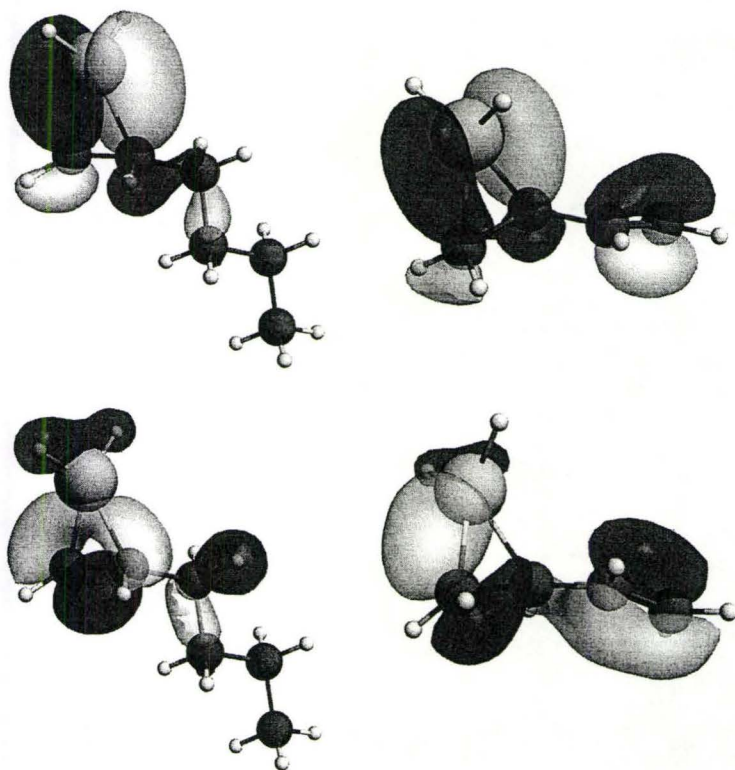
Figure 6.7. HOMO (top) and HOMO-1 (bottom) of **83b** and **83i**.

83b (1-hexene)   **83i** (butadiene)

The inverse relationship between the stabilities of the alkene and corresponding

germirane has already been established by experiment with $GePh_2$ as described in the

introduction. Such an effect is reasonable because with a more stable alkene there will be

a lower thermodynamic driving force to break the C=C bond and form the Ge-C bonds.

Table 6.10 lists the experimentally determined free energy changes for the reactions of

$GePh_2$ with a number of alkenes and dienes along with the corresponding values

predicted by theory; Figure 6.8 graphs the correlation. While the calculations

underestimate the free energy change for the reaction to form the germirane by 8

kcal/mol on average, the trend in ΔG as function of alkene substitution is predicted

correctly. Recall it has been suggested that DFT overestimates the stability of the free

germylene, which consequently leads to an underestimation of the driving force for the

reaction.[14]

Table 6.10. Experimental and calculated (PW91/TZ2P/ZORA) free-energy changes for
the reactions of various alkenes and dienes with $GePh_2$.[a]

	ΔG calc.	ΔG expt. [b]
1-hexene (**b**)	+2.89	-3.14 ± 0.37 [c]
E-2-hexene (**c**)	+5.40	-0.89 ± 0.17 [c]
Z-2-hexene (**d**)	+6.96	-0.51 ± 0.16 [c]
2-ethyl-1-butene (**e**)	+1.87	-1.20 ± 0.12 [c]
2-methyl-2-pentene (**f**)	+8.34	+1.06 ± 0.29 [d]
DMP (**h**)	+4.07	-2.67 ± 0.53 [d]
isoprene (**j**)	+5.08	-3.18 ± 0.55 [e]
DMB (**k**)	+6.07	-1.04 ± 0.31 [e]

a. Standard state:1 bar and 298.15 K. *b.* Values measured in hexanes solution at 25 °C, and thus originally
reported in units of M^{-1}. *c.* Measured by S. Chitnis. *d.* Reference 3. *e.* Reference 4.
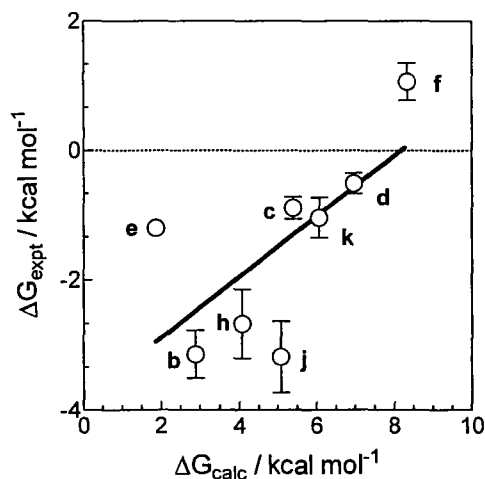
Figure 6.8. Comparison of the experimental and calculated (PW91/TZ2P/ZORA) free-energy changes at 298 K for the reactions of various alkenes and dienes with $GePh_2$. The line is the linear least-squares fit of the data.

The difference between the thermodynamic stabilities of the germiranes derived from the reaction of $GeMe_2$ and $GePh_2$ with alkenes/dienes has also been established by experiment; the reactions of $GeMe_2$ have a more negative ΔG than the corresponding reactions of $GePh_2$.[2,3] The calculations agree with these findings, showing that introduction of an alkyl or aryl group in place of a hydrogen atom at any of the three atoms of the germirane ring favours dissociation to the parent metallylene and alkene. It is likely that the origin of this effect is in the higher DSSE of GeR_2 vs. GeH_2. Walsh has shown that there is a positive correlation between the DSSE of silylenes and the electronegativity of the substituent on the silicon, presumably because the non-bonding electrons are held more closely to the silicon by substituents with a higher electronegativity ($DSSE_{SiH_2} \approx 19$ kcal/mol; $DSSE_{SiMe_2} \approx 32$ kcal/mol).[34] Reactions of $GePh_2$ with alkenes are less favourable than those with $GeMe_2$, perhaps because phenyl is more electronegative than methyl.[35] Conjugation of the phenyl π orbitals with the vacant

p orbital on the germanium may also lead to a higher DSSE. A more favourable

dissociation of $GePh_2$-derived germiranes could also result from steric repulsion of the

phenyl rings.

6.4. The reactions of GeH_2, $GeMe_2$, and $GePh_2$ with ethylene and dienes. Computations results using Gaussian.

6.4.1. General Method

Preliminary structures of the alkenes, dienes and germiranes were obtained via

molecular mechanics within the software Chem3D (11.0.1 CambridgeSoft), employing

the MM2 force field.[16] Alternatively, the structures from the ADF output were used.

Geometry and vibrational frequencies calculation were performed with Gaussian09[36]

employing Becke's hybrid functional (B3)[37] and the Lee, Yang, and Parr (LYP)[38]

correlation functional (B3LYP). Calculations for the structures derived from GeH_2 and

$GeMe_2$ were repeated using Grimme's modification of B3LYP, termed B2PLYP.[39, 40] In

all cases, the basis set was 6-311G employing (*d,p*) double polarization. Note that *d,p* is

often abbreviated **. The iterative geometric energy convergence criterion was set at

opt=tight.

The germiranes optimized in this study are shown in Figure 6.9 while the π-

complexes are shown in Figure 6.10. The results of these calculations are summarized in

the tables in Section 6.4.2.

83, R = H
84, R = Me
85, R = Ph

$R_2Ge\triangleleft$

a

R_2Ge

i

R_2Ge

j

R_2Ge

jj

R_2Ge

k

R_2Ge

l Ph

R_2Ge Ph

ll
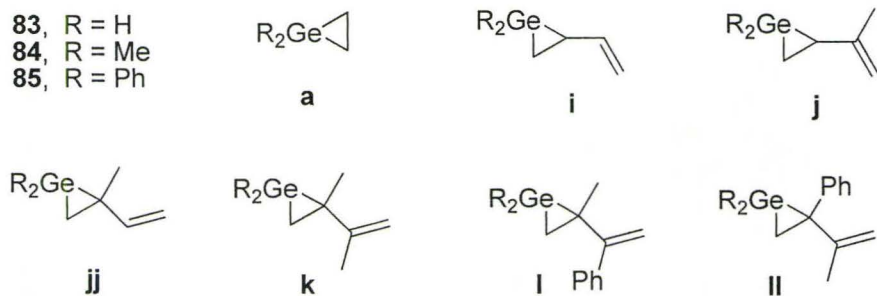
Figure 6.9. Germiranes investigated in the Gaussian computational study.

83C, R = H
84C, R = Me
85C, R = Ph

$R_2Ge\leftarrow\|$

a

R_2Ge

i

R_2Ge

j

R_2Ge

jj

R_2Ge

k

R_2Ge

l Ph

R_2Ge Ph

ll
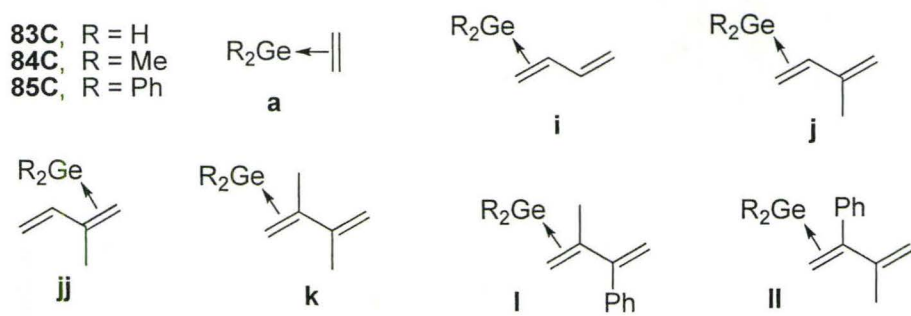
Figure 6.10. π-Complexes investigated in the Gaussian computational study.

6.4.2. Results – geometry optimizations and thermodynamics

Table 6.11. Summary of selected bond distances (Å) and angles (°) from the geometry optimized structures of the alkenes **a-l** and germiranes **83-85** (B3LYP/6-311G**).

83		#[a]	C=C[b]	C-C[c]	Ge-C[d]	Ge-C[e]	C-Ge-C
a	ethene	0	1.327	1.530	1.961	1.961	45.92
i	butadiene	1	1.337	1.536	1.951	1.995	45.76
j	isoprene	1	1.337	1.536	1.954	1.995	45.77
jj	isoprene-a	2	1.341	1.540	1.953	2.006	45.43
k	DMB	2	1.341	1.529	1.963	1.966	45.77
l	2M3P	2	1.341	1.542	1.951	2.012	45.77
ll	2M3P-a	2	1.343	1.542	1.954	2.002	45.87
84							
a	ethene	0	1.327	1.546	1.957	1.957	46.53
i	butadiene	1	1.337	1.551	1.948	1.999	46.35
j	isoprene	1	1.337	1.551	1.951	1.991	46.33
jj	isoprene-a	2	1.341	1.540	1.953	2.006	45.77
k	DMB	2	1.341	1.543	1.959	2.000	45.87
l	2M3P	2	1.341	1.551	1.956	1.985	46.34
ll	2M3P-a	2	1.343	1.555	1.952	2.006	46.24
85							
i	butadiene	1	1.337	1.545	1.948	1.999	46.07
j	isoprene	1	1.337	1.544	1.951	2.000	46.00
jj	isoprene-a	2	1.341	1.551	1.947	2.017	46.03
k	DMB	2	1.341	1.540	1.960	2.002	45.72
l	2M3P	2	1.341	1.545	1.954	1.998	46.01
ll	2M3P-a	2	1.343	1.550	1.952	2.012	46.02

a. number of alkyl substituents on the alkene. *b.* C=C of free alkene that will become the two carbons of the germirane framework. *c.* formerly the corresponding alkene carbons. *d.* bond to the less substituted carbon of the germirane moiety. *e.* bond to the more highly substituted carbon of the germirane moiety.

Table 6.12. Select bond distances (Å) and angles (°) from the geometry optimized structures of germiranes **83** and **84** (B2PLYP/6-311G**).

83		#[a]	C=C[b]	C-C[c]	Ge-C[d]	Ge-C[e]	C-Ge-C
a	ethene	0	1.331	1.532	1.958	1.958	46.05
i	butadiene	1	1.340	1.537	1.950	1.988	45.93
j	isoprene	1	1.340	1.537	1.953	1.988	45.90
jj	isoprene-a	2	1.343	1.540	1.953	1.997	45.89
k	DMB	2	1.344	1.530	1.962	1.989	45.54
l	2M3P	2	1.344	1.542	1.952	2.004	45.87
ll	2M3P-a	2	1.347	1.542	1.954	1.995	45.95
84							
a	ethene	0	1.331	1.548	1.954	1.954	46.68
i	butadiene	1	1.340	1.553	1.947	1.984	46.53
j	isoprene	1	1.340	1.554	1.949	1.984	46.52
jj	isoprene-a	2	1.343	1.557	1.949	1.995	46.48
k	DMB	2	1.344	1.530	1.962	1.989	45.54
l	2M3P	2	1.344	1.551	1.955	1.979	46.42
ll	2M3P-a	2	1.347	1.555	1.951	1.998	46.35

a. number of alkyl substituents on the alkene. *b.* C=C of free alkene that will become the two carbons of the germirane framework. *c.* formerly the corresponding alkene carbons. *d.* bond to the less substituted carbon of the germirane moiety. *e.* bond to the more highly substituted carbon of the germirane moiety.

Table 6.13. Select bond distances (Å) and angles (°) from the geometry optimized structures of the π-complexes **83C**, **84C**, and **85C** (B3LYP/6-311G**).

83C		#^{a}	C=C^b	C=C^c	Ge-C^d	Ge-C^e	Ge-C-C^f
a	ethene	0	1.327	1.381	2.218	2.474	83.39
i	butadiene	1	1.337	1.394	2.192	2.562	88.28
j	isoprene	1	1.337	1.391	2.211	2.584	88.62
jj	isoprene-a	2	1.341	1.376	2.520	2.446	76.91
k	DMB	2	1.341	1.373	2.539	2.501	75.70
l	2M3P	2	1.341	1.372	2.547	2.524	75.26
ll	2M3P-a	2	1.343	1.397	2.235	2.700	93.18
84C							
a	ethene	0	1.327	1.370	2.304	2.557	84.08
i	butadiene	1	1.337	1.394	2.217	2.609	89.52
j	isoprene	1	1.337	1.386	2.270	2.661	90.04
jj	isoprene-a	2	1.341	1.352	2.858	3.186	90.28
k	DMB	2	1.341	1.352	2.856	3.176	90.76
l	2M3P	2	1.341	1.352	2.879	3.109	86.70
ll	2M3P-a	2	1.343	1.355	2.871	3.239	93.07
85C							
i	butadiene	1	1.337	1.343	3.185	3.381	86.56
j	isoprene	1	1.337	1.345	3.028	3.273	88.16
ll	2M3P	2	1.343	1.351	3.082	3.523	97.47
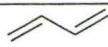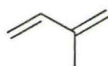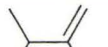
a. number of alkyl substituents on the alkene. *b.* C=C of free alkene that will coordinate to the germanium in the π-complex. *c.* complexed alkene C=C. *d.* the distance to the less substituted alkene carbon. *e.* the more substituted alkene carbon. *f.* the angle between the C-C bond of the alkene and the <u>shortest</u> Ge-C distance.

Table 6.14. Select bond distances (Å) and angles (°) from the geometry optimized structures of the π-complexes **83C** and **84C** (B2PLYP/6-311G**).

83C		#[a]	C=C[b]	C=C[c]	Ge-C[d]	Ge-C[e]	Ge-C-C[f]
a	ethene	0	1.327	1.391	2.169	2.429	82.94
i	butadiene	1	1.337	1.402	2.151	2.509	87.15
j	isoprene	1	1.337	1.400	2.166	2.526	87.42
jj	isoprene-a	2	1.341	1.386	2.458	2.327	78.43
k	DMB	2	1.341	1.383	2.474	2.369	77.64
l	2M3P	2	1.341	1.384	2.467	2.363	77.53
ll	2M3P-a	2	1.343	1.406	2.181	2.616	91.04
84C							
a	ethene	0					
i	butadiene	1	1.337	1.412	2.127	2.502	87.52
j	isoprene	1	1.337	1.407	2.156	2.532	87.96
jj	isoprene-a	2	1.341	1.355	2.781	2.947	83.23
k	DMB	2	1.341	1.412	2.127	2.502	87.52
l	2M3P	2	1.341	1.357	2.772	2.902	81.59
ll	2M3P-a	2	1.343	1.360	2.755	2.960	84.78
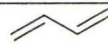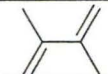
a. number of alkyl substituents on the alkene. *b*. C=C of free alkene that will coordinate to the germanium in the π-complex. *c*. complexed alkene C=C. *d*. the distance to the less substituted alkene carbon. *e*. the more substituted alkene carbon. *f*. the angle between the C-C bond of the alkene and the shortest Ge-C distance.

Table 6.15. Calculated enthalpy and free energy changes (in kcal mol^{-1} at 298.15 K) for the (1+2) cycloaddition reactions of GeH$_2$, GeMe$_2$, and GePh$_2$ to yield the germiranes **83-85**, respectively. (B3LYP/6-31G**)

		ΔH			ΔG		
		GeH$_2$	GeMe$_2$	GePh$_2$	GeH$_2$	GeMe$_2$	GePh$_2$
a	H$_2$C=CH$_2$	-15.86	-12.12	*a*	-4.11	-0.13	*a*
i		-10.99	-7.48	-3.8	+0.75	+4.28	+8.11
j		-10.21	-6.07	-2.7	+1.45	+5.53	+9.33
jj		-9.2	-5.25	-1.11	+2.86	+6.80	+11.3
k		-9.56	-5.91	-1.84	+2.28	+6.26	+10.56
l		-8.19	-4.12	-0.33	+3.84	+7.97	+12.68
ll	Ph	-8.96	-5.66	-0.94	+3.06	+6.64	+12.17

a. value not determined.

Table 6.16. Calculated enthalpy and free energy changes (in kcal mol^{-1} at 298.15 K) for the formation of the π-complexes **83C**, **84C** and **85C**. (B3LYP/6-311G**)

		ΔH			ΔG		
		GeH$_2$	GeMe$_2$	GePh$_2$	GeH$_2$	GeMe$_2$	GePh$_2$
a	H$_2$C=CH$_2$	+1.47	-3.52	*a*	-3.46	+7.13	*a*
i		-13.92	-5.3	-0.41	-2.96	+6.15	+8.30
j		-13.71	-4.66	-0.77	-2.8	+6.85	+8.25
jj		-8.96	-1.44	*a*	+1.6	+7.56	*a*
k		-8.92	-1.83	*a*	+1.59	+9.5	*a*
l		-8.08	-1.09	*a*	+2.37	+8.41	*a*
ll	Ph	-11.13	-0.94	-0.7	+0.35	+8.55	+9.01

a. value not determined due to extensive computational time.

Table 6.17. Calculated enthalpy and free energy changes (in kcal mol^{-1} at 298.15 K) for the (1+2) cycloaddition reactions of GeH$_2$, GeMe$_2$, and GePh$_2$ to yield the germiranes **83-85**, respectively. (B2PLYP/6-311G**)
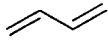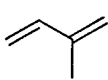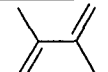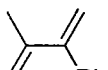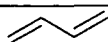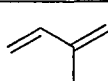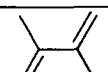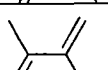
		ΔH		ΔG	
		GeH$_2$	GeMe$_2$	GeH$_2$	GeMe$_2$
a	H$_2$C=CH$_2$	-19.57	-16.55	-8.18	-5.36
i		-15.35	-12.68	-3.17	-0.85
j		-14.79	-11.58	-2.63	+0.23
jj		-14.2	-11.26	-1.66	+0.91
k		-14.87	-12.35	-2.57	-0.12
l		-13.96	-10.92	-1.37	+1.19
ll	Ph	-14.8	-12.89	-2.43	-0.54

Table 6.18. Calculated enthalpy and free energy changes (in kcal mol^{-1} at 298.15 K) for the formation of the π-complexes **83C** and **84C**. (B2PLYP/6-311G**)

		ΔH		ΔG	
		GeH$_2$	GeMe$_2$	GeH$_2$	GeMe$_2$
a	H$_2$C=CH$_2$	0.59	*nf*	-5.03	*nf*
i		-15.66	-8.45	-4.14	+3.38
j		-15.67	-8.08	-4.13	+3.73
jj		-11.3	-3.71	+0.04	+5.72
k		-11.4	-3.77	+0.08	+6.31
l		-10.99	-4.00	+0.40	+6.02
ll	Ph	-14.01	-3.96	-1.95	+6.68

nf. π-complex not found; computation minimized to germirane.

6.4.3. Discussion

The reactions of GeH_2, $GeMe_2$ and $GePh_2$ with alkenes and dienes were examined at the B3LYP and B2PLYP levels both using the 6-311G(d,p) basis set, including the germiranes and π-complexes. The latter method produces more negative values of ΔG and ΔH than the former and thus values that are closer to those determined experimentally. Grimme developed B2PLYP in response to the failure of many density functionals, particularly B3LYP,[41] to account for medium-range electron correlations (medium-range meaning electrons in adjacent bonds).[40] While the accuracy of the energy determination is increased with B2PLYP, at least with the calculations that pertain to the germiranes, approximately 10 times the computational resources are required. The geometries of the germiranes determined by the B3LYP/6-311G**, B2PLYP/6-311G**, and PW91/TZ2P are not significantly different.

It is noteworthy that of the methods PW91, B3LYP, and B2PLYP, PW91 produces energies changes for the cycloaddition reaction that are closest to experiment. We cannot reach such a conclusion yet with regards to the energy of the π-complexes because the corresponding calculations with ADF have yet to be completed. The ADF and Gaussian projects described in this chapter originally had different objectives; these projects were also completed at different times. The first step in making a complete comparison between the methods will be the calculations of the π-complexes with ADF. In addition, some of the holes in the data tables will be filled in.

Nag and Gaspar studied, among other things, the reaction of $GeMe_2$ with

butadiene (eq 6.7).[14] The geometry of **84i** using B3LYP/6-311G** was found to be

identical to that of Nag and Gaspar using B3LYP/(6-31G** C,H; 6-311G** Ge), which is

not surprising but nevertheless important to note. Figure 6.11 shows the π-complex **84Ci**

calculated by us and by Nag and Gaspar. The structural features are similar yet the

alkene is flipped (i.e. the plane containing all four alkene carbons has been rotated *ca.*

180°). Despite this difference the ΔH_{298} calculated by us for the reaction of GeMe$_2$ with

butadiene (eq 6.7) is -5.3 kcal/mol while for the same reaction Nag & Gaspar report -5.2

kcal/mol, suggesting that the potential energy surface is quite flat near the minimum

energy geometry of the π complex. A flat energy surface can lead to slight variations in

the final geometry of the calculations depending on the convergence criteria.

(6.7)
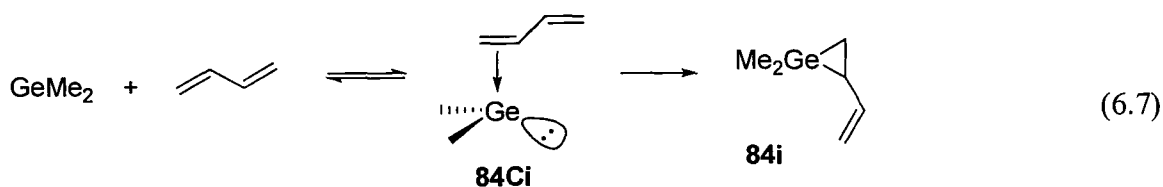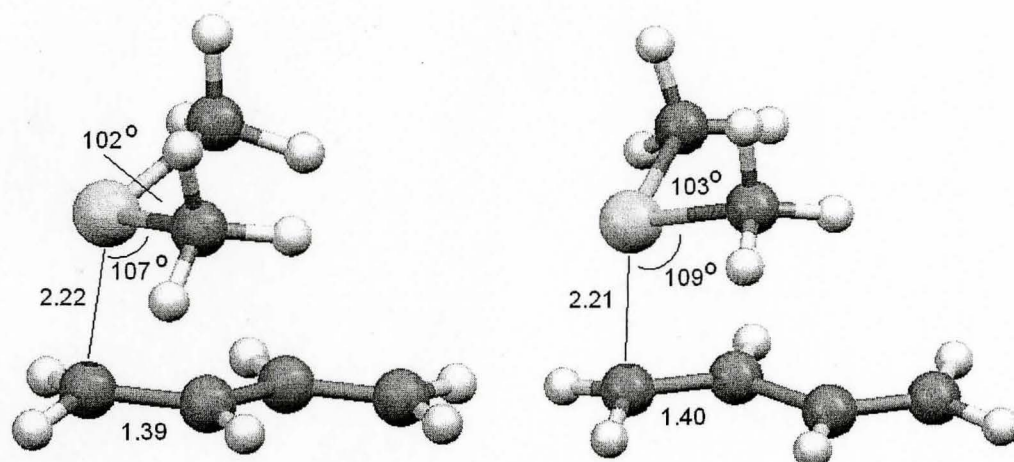
Figure 6.11. Optimized geometry of the π-complex **84Ci** calculated using B3LYP/6-311G** (*left*) and the geometry reported by Nag and Gaspar[14] using B3LYP/(6-31G** CH, 6-311G** Ge) (*right*).

In the π-complexes the germanium is generally situated in closer proximity to the terminal carbon of the diene with the substituents on the germanium oriented above the C=C bond (e.g. see Figure 6.12a). The length of the C=C bond within the π-complex is longer than that in the free alkene, consistent with delocalization of the electron density in the π-bond toward germanium. Examination of the HOMO (*e.g.* see Figure 6.12). shows the interaction between the germanium and the π-bond; the molecular orbital correlation diagram for this interaction is shown in Figure 6.13.
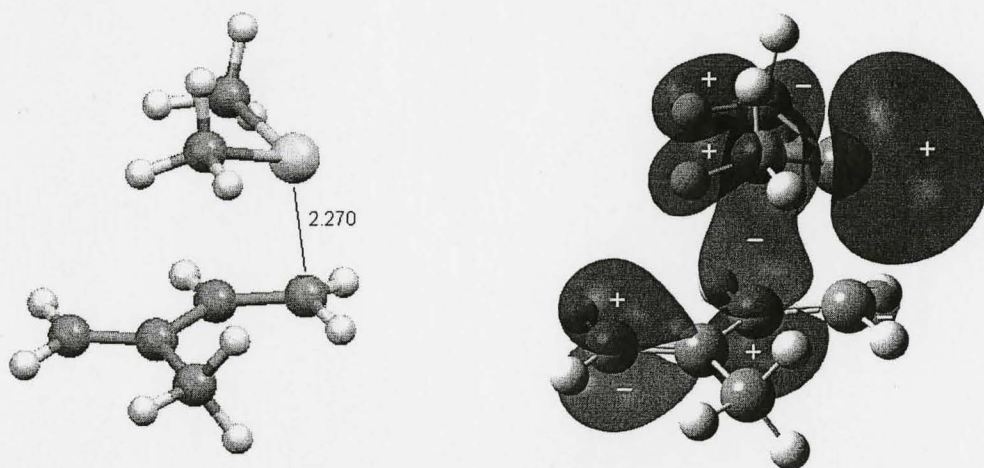
Figure 6.12. Geometry and HOMO of the π-complex of GeMe$_2$ and isoprene (**84Cj**). (B3LYP/6-311G**) Both diagrams are shown in the same orientation.
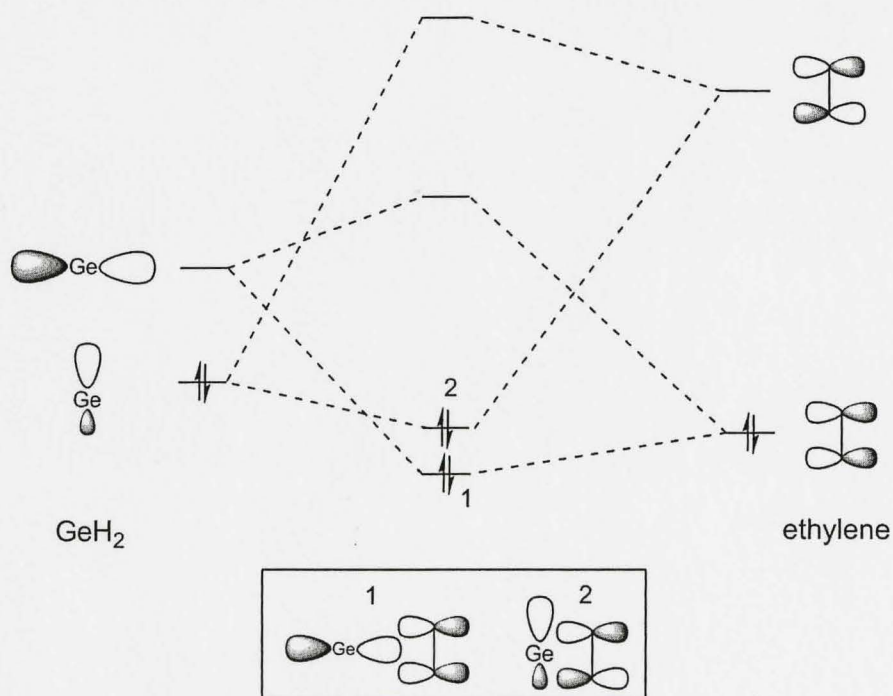
Figure 6.13. Molecular orbital correlation diagram showing the interaction between the germylene and the π-bond of an alkene.

When the alkene has large substituents (such as the phenyl rings of diene **I**) the substituents of the germanium are no longer above the C=C bond within the π-complex, which increases the distance between the germanium and the alkene (see Figure 6.14).
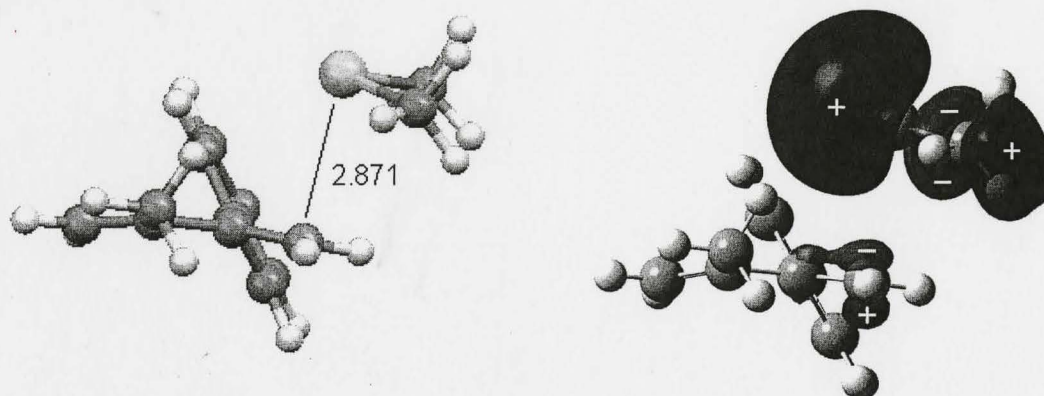
Figure 6.14. Geometry and HOMO of the π-complex of GeMe$_2$ and 2-methyl-3-phenylbutadiene (**84CII**) (B3LYP/6-311G**). Both diagrams are shown in the same orientation.

The free energy changes for the reaction of GeMe$_2$ and GePh$_2$ with an alkene/diene to form the germirane is more negative than the formation of the corresponding π-complex. This trend was observed at both the B3LYP and B2PLYP levels. The notable exceptions are the reactions of GeH$_2$ where the reaction to form the π-complexes with dienes have a more negative ΔG than the formation of the corresponding germiranes. (B2PLYP predicts that reaction of GeH$_2$ with the more highly substituted dienes will lead to the preferential formation of the germirane.) Analysis of the HOMO (using one of the π-complexes between GeH$_2$ and 2-methyl-3-phenylbutadiene as the example because this was the motivation for our study) shows a very strong bonding interaction between the germanium and the π-bond of the alkene

(Figure 6.15).
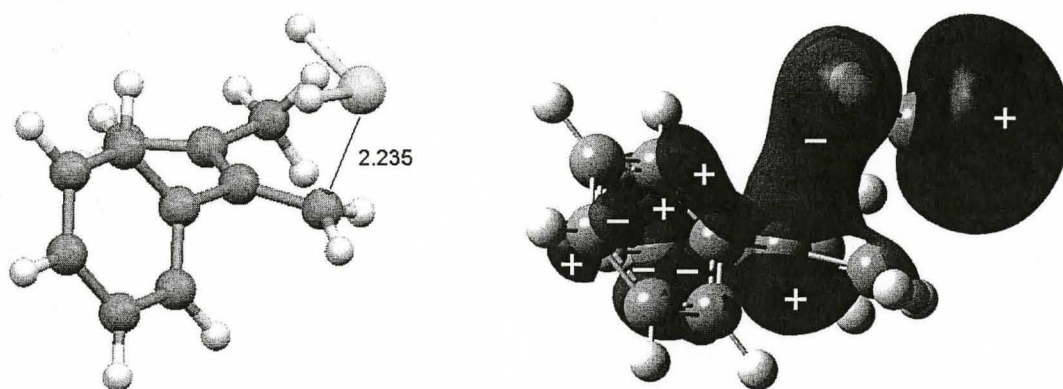
Figure 6.15. Minimum energy geometry (*left*) and HOMO (*right*) of **83Cll** (B3LYP/6-311G**). Both diagrams are shown in the same orientation.

6.5. Summary

The reaction of GeH_2, $GeMe_2$, and $GePh_2$ with alkenes and dienes were examined

using computational methods (ADF – PW91/TZ2P, Gaussian – B3LYP/6-311G** and

Gaussian – B2PLYP/6-311G**). This study was motivated by trends in experimental

data, particularly with regard to changes in the equilibrium constant for the (1+2)

cycloaddition reaction with changes in the substitution on both the germylene and the

alkene. The focus of this study was to determine the geometry of the (1+2) cycloaddition

product (germiranes) and the π-complexes along with the free energy change in the

reaction for a series of alkenes and dienes. Previous computational studies have shown

that DFT methods typically underestimate the stability of the products resulting from the

reaction of germylenes and alkenes. Nevertheless, we found that the trend predicted in

the free energy changes matched that determined by experiment and that PW91 produced

values that were closer to those determined experimentally. The reaction between a

germylene and an alkene to form the germirane becomes less favourable as the degree of

substitution on the alkene increases. The free energy change for the reaction of the

germylene with an alkene/diene to form the germirane is generally more negative than

the formation of the corresponding π-complex, except with GeH_2 where the π-complexes

with dienes are predicted to form preferentially at the B3LYP level and with less

hindered dienes at the B2PLYP level. Analysis of the HOMO within the π-complexes of

GeH_2 and 2-phenyl-3-methylbutadiene (**83CI** and **83CII**) shows a substantial bonding

interaction between the germanium and the alkene C=C bond. The higher stability of the

π-complex compared to the germirane may help explain the transient absorption spectra

of **78** in hexanes solution.

6.6. References

1. *CRC Handbook of Chemistry and Physics, Internet Version.* 90 ed.; CRC Press/Taylor and Francis: Boca Raton, FL, 2010.
2. Leigh, W. J.; Lollmahomed, F.; Harrington, C. R. *Organometallics* **2006**, *25*, 2055.
3. Leigh, W. J.; Harrington, C. R. *J. Am. Chem. Soc.* **2005**, *127*, 5084.
4. Huck, L. A.; Leigh, W. J. *Organometallics* **2009**, *28*, 6777.
5. Billone, P. S.; Beleznay, K. M.; Harrington, C. R.; Huck, L. A.; Ladowski, S.; Leigh, W. J. *manuscript in preparation*,
6. Becerra, R.; Walsh, R. *Phys. Chem. Chem. Phys.* **2007**, *9*, 2817.
7. Horner, D. A.; Grev, R. S.; Schaefer, H. F., III *J. Am. Chem. Soc.* **1992**, *114*, 2093.
8. Sakai, S. *Int. J. Quantum Chem.* **1998**, *70*, 291.
9. Su, M.-D.; Chu, S. Y. *J. Am. Chem. Soc.* **1999**, *121*, 11478.
10. Antoniotti, P.; Benzi, P.; Castiglioni, M.; Volpe, P. *Eur. J. Inorg. Chem.* **1999**, 323.
11. Becerra, R.; Boganov, S. E.; Egorov, M. P.; Faustov, V. I.; Promyslov, V. M.; Nefedov, O. M.; Walsh, R. *Phys. Chem. Chem. Phys.* **2002**, *4*, 5079.
12. Birukov, A. A.; Faustov, V. I.; Egorov, M. P.; Nefedov, O. M. *Russ. Chem. Bull., Int. Ed.* **2005**, *54*, 2003.
13. Joo, H.; Kraka, E.; Quapp, W.; Cremer, D. *Mol. Phys.* **2007**, *105*, 2697.
14. Nag, M.; Gaspar, P. P. *Organometallics* **2009**, *28*, 5612.

15. Su, M.-D. *Chem. Eur. J.* **2004**, *10*, 6073.

16. Allinger, N. L. *J. Am. Chem. Soc.* **1977**, *99*, 8127.

17. Baerends, E. J.; Autschbach, J.; Bérces, A.; Bickelhaupt, F. M.; Bo, C.; Boerrigter, P. M.; Cavallo, L.; Chong, D. P.; Deng, L.; Dickson, R. M.; Ellis, D. E.; Faassen, M. v.; Fan, L.; Fischer, T. H.; Guerra, C. F.; Gisbergen, S. J. A. v.; Götz, A. W.; Groeneveld, J. A.; Gritsenko, O. V.; Grüning, M.; Harris, F. E.; Hoek, P. v. d.; Jacob, C. R.; Jacobsen, H.; Jensen, L.; Kessel, G. v.; Kootstra, F.; Krykunov, M. V.; Lenthe, E. v.; McCormack, D. A.; Michalak, A.; Neugebauer, J.; Nicu, V. P.; Osinga, V. P.; Patchkovskii, S.; Philipsen, P. H. T.; Post, D.; Pye, C. C.; Ravenek, W.; Rodriguez, J. I.; Ros, P.; Schipper, P. R. T.; Schreckenbach, G.; Snijders, J. G.; Solà, M.; Swart, M.; Swerhone, D.; Velde, G. t.; Vernooijs, P.; Versluis, L.; Visscher, L.; Visser, O.; Wang, F.; Wesolowski, T. A.; Wezenbeek, E. M. v.; Wiesenekker, G.; Wolff, S. K.; Woo, T. K.; Yakovlev, A. L.; Ziegler, T. *ADF2009.01*, SCM, Theoretical Chemistry, Vrije Universiteit, Amsterdam, The Netherlands, http://www.scm.com.

18. Fonseca Guerra, C.; Snijders, J. G.; te Velde, G.; Baerends, E. J. *Theor. Chem. Acc.* **1998**, *99*, 391.

19. te Velde, G.; Bickelhaupt, F. M.; van Gisbergen, S. J. A.; Fonseca Guerra, C.; Baerends, E. J.; Snijders, J. G.; Ziegler, T. *J. Comput. Chem.* **2001**, *22*, 931.

20. Perdew, J. P.; Chevary, J. A.; Vosko, S. H.; Jackson, K. A.; Pederson, M. R.; Singh, D. J.; Fiolhais, C. *Phys. Rev. B* **1992**, *46*, 6671.

21. van Lenthe, E.; Ehlers, A.; Baerends, E.-J. *J. Chem. Phys.* **1999**, *110*, 8943.

22. Gross, E. K. U.; Kohn, W. *Adv. Quantum Chem.* **1990**, *21*, 255.

23. Gross, E. K. U.; Ullrich, C. A.; Gossmann, U. J., *Density functional theory of time-dependent systems*. Plenum: New York, 1995; p 149.

24. van Gisbergen, S. J. A.; Snijders, J. G.; Baerends, E. J. *J. Chem. Phys.* **1995**, *103*, 9347.

25. Gross, E. K. U.; Dobson, J. F.; Petersilka, M.; Nalewajski, R. F., *Density Functional Theory*. Springer: Heidelberg, 1996.

26. van Gisbergen, S. J. A.; Snijders, J. G.; Baerends, E. J. *Comput. Phys. Commun.* **1999**, *118*, 119.

27. van Gisbergen, S. J. A.; Snijders, J. G.; Baerends, E. J. *Phys. Rev. Lett.* **1997**, *78*, 3097.

28. van Gisbergen, S. J. A.; Snijders, J. G.; Baerends, E. J. *J. Chem. Phys.* **1998**, *109*, 10644.

29. Vosko, S. H.; Wilk, L.; Nusair, M. *Can. J. Phys.* **1980**, *58*, 1200.

30. Leigh, W. J.; Harrington, C. R.; Vargas-Baca, I. *J. Am. Chem. Soc.* **2004**, *126*, 16105. (Errata: *J. Am. Chem. Soc.* **2006**, *128*, 1394.).

31. Becerra, R.; Gaspar, P. P.; Harrington, C. R.; Leigh, W. J.; Vargas-Baca, I.; Walsh, R.; Zhou, D. *J. Am. Chem. Soc.* **2005**, *127*, 17469.

32. Ando, W.; Ohgaki, H.; Kabe, Y. *Angew. Chem. Int. Ed. Eng.* **1994**, *33*, 659.

33. Albright, T. A.; Burdett, J. K.; Whangbo, M. H., *Orbital Interactions in Chemistry*. John Wiley & Sons: New York, 1985; p 184.

34. Walsh, R. *Pure Appl. Chem.* **1987**, *59*, 69.
35. Wells, P. R. *Prog. Phys. Org. Chem.* **1968**, *6*, 111.
36. Frisch, M. J.; Trucks, G. W.; Schlegel, H. B.; Scuseria, G. E.; Robb, M. A.; Cheeseman, J. R.; Scalmani, G.; Barone, V.; Mennucci, B.; Petersson, G. A.; Nakatsuji, H.; Caricato, M.; Li, X.; Hratchian, H. P.; Izmaylov, A. F.; Bloino, J.; Zheng, G.; Sonnenberg, J. L.; Hada, M.; Ehara, M.; Toyota, K.; Fukuda, R.; Hasegawa, J.; Ishida, M.; Nakajima, T.; Honda, Y.; Kitao, O.; Nakai, H.; Vreven, T.; Montgomery, J., J. A.; Peralta, J. E.; Ogliaro, F.; Bearpark, M.; Heyd, J. J.; Brothers, E.; Kudin, K. N.; Staroverov, V. N.; Kobayashi, R.; Normand, J.; Raghavachari, K.; Rendell, A.; Burant, J. C.; Iyengar, S. S.; Tomasi, J.; Cossi, M.; Rega, N.; Millam, J. M.; Klene, M.; Knox, J. E.; Cross, J. B.; Bakken, V.; Adamo, C.; Jaramillo, J.; Gomperts, R. E.; Stratmann, O.; Yazyev, A. J.; Austin, R.; Cammi, C.; Pomelli, J. W.; Ochterski, R.; Martin, R. L.; Morokuma, K.; Zakrzewski, V. G.; Voth, G. A.; Salvador, P.; Dannenberg, J. J.; Dapprich, S.; Daniels, A. D.; Farkas, O.; Foresman, J. B.; Ortiz, J. V.; Cioslowski, J.; Fox, D. J. *Gaussian 09, revision A.02*, Gaussian, Inc.: Wallingford CT, 2009.
37. Becke, A. D. *J. Chem. Phys.* **1993**, *98*, 5648.
38. Lee, C.; Yang, W.; Parr, R. G. *Phys. Rev. B* **1988**, *37*, 785.
39. Grimme, S. *J. Chem. Phys.* **2006**, *124*, 034108.
40. Grimme, S. *Angew. Chem. Int. Ed.* **2006**, *45*, 4460.
41. Zhao, Y.; Truhlar, D. G. *Acc. Chem. Res.* **2008**, *41*, 157.

Chapter 7 – Reactions of Tetraaryldigermenes with Diethylamine, Acetic Acid, and Carbon Tetrachloride

7.1. Overview

The chapter describes the results of our product and kinetics studies of the reactions of digermenes with the scavengers $HNEt_2$, HOAc, and CCl_4. As mentioned in Chapter 1, relatively little is known about the reaction of amines with digermenes. Product studies have not been undertaken but the relative rate constants measured for the reactions of Ge_2Me_4 and Ge_2Ph_4 with H_2N^nBu in hexanes are suggestive of nucleophilic attack by the amine at germanium.[1] Prior to this work, the addition of a carboxylic acid across the Ge=Ge bond of a digermene had not been reported. The rate constants of Ge_2Me_4 and Ge_2Ph_4 with HOAc have been reported, and the data led to the suggestion that the reaction may involve rate determining protonation of the digermene.[1] Finally, digermenes have been reported to undergo formal double halogen atom abstraction from CCl_4 to yield the corresponding 1,2-dichlorodigermane.[2]

7.2. Product Studies of Digermene Reactions – Introduction

While digermenes **DGa-f** are used in the kinetic studies, they cannot be used for product studies because they are formed from dimerization of the corresponding germylenes (**Ga-f**), and anything that one may add to scavenge the digermene will also react with the germylene and quench the formation of the digermene. Instead, we have employed tetramesityldigermene (**DGm**) as the representative digermene for product studies because it can be prepared directly from photolysis of hexamesitylcyclotrigermane **86**.[3]

231

The steric bulk of the mesityl groups hinders significant dimerization of **DGm** so continued photolysis of a solution of **86** allows the concentration of **DGm** to build up.

As reported by Baines and co-workers, there are two general procedures that can be followed.[3] (1) Photolysis of **86** in toluene in the presence of $HSiEt_3$ yields **DGm** and **87**, the latter of which is formed from the reaction of $GeMes_2$ with $HSiEt_3$ (see eq 7.1).[4] (2) Photolysis of **86** in THF removes the necessity for $HSiEt_3$ because the extruded germylene forms a Lewis acid-base complex with THF, which itself then dimerizes to **DGm** (see eq 7.2).[5] The advantage of using THF is that the reaction mixture has fewer products because the coordinating solvent hinders dimerization of the digermene; furthermore a higher yield of the digermene results because the theoretical maximum yield is 1.5 equivalents relative to **86**.[3]

$$\underset{\textbf{86}}{\overset{\overset{\displaystyle Mes_2}{\underset{\displaystyle Mes_2Ge-GeMes_2}{Ge}}}{}} \quad \xrightarrow[\substack{\text{toluene}\\ HSiEt_3 \\ -(30\text{-}50)\ ^\circ C}]{hv} \quad \underset{\textbf{DGm}}{Mes_2Ge=GeMes_2} \; + \; GeMes_2 \;\Big\downarrow {}_{HSiEt_3} \tag{7.1}$$

$$Mes_2Ge(H)SiEt_3 \quad \textbf{87}$$

$$\textbf{86} \quad \xrightarrow[\substack{\text{THF}\\ -(30\text{-}50)\ ^\circ C}]{hv} \quad \underset{(1\ eq)}{\textbf{DGm}} \; + \; \underset{(1\ eq)}{GeMes_2} \quad {}_{THF}\Big\downarrow \tag{7.2}$$

$$\underset{(0.5\ eq)}{\textbf{DGm}} \quad \xleftarrow{\; \times 2\;} \quad Mes_2Ge \leftarrow O\!\!\!\bigcirc$$
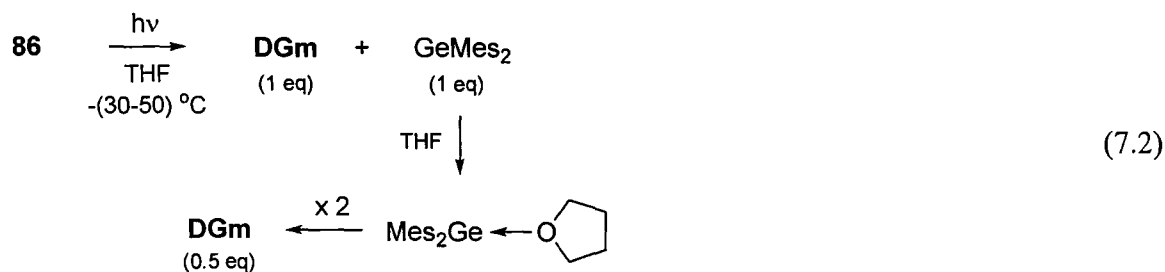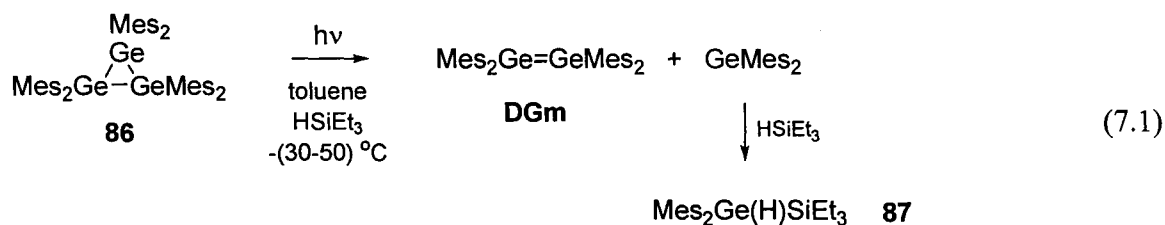
We have employed both of the above procedures in our work. In general, a dried and deoxygenated solution of **86** in either toluene or THF was cooled to between -30 and -50 °C (hereafter called -40 °C) and irradiated with 350 nm lamps for 4-8 hrs. Irradiation

was stopped and a solution of the appropriate scavenger (in the same solvent employed in

the photolysis) was cooled to -40 °C and added via syringe. In all cases the starting

concentration of **86** was 1.3 mM, while the concentration of the added scavenger was at

least 20 times greater than the maximum possible yield of the digermene. In these

hydrocarbon solvents, **DGm** is a bright yellow colour and addition of a scavenger that

reacts with the digermene causes the solution to become colourless.

7.3. Reaction of Tetraaryldigermenes with Diethylamine

7.3.1. Product studies

A solution of diethylamine in toluene, cooled to -40 °C, was added to a solution

of **DGm**, resulting in 0.25 M of the amine. After approximately 15 minutes, the solution

became colourless. The solvent was removed under a fine stream of nitrogen. TLC

analysis (1:1 DCM:hexanes) indicated the presence of a single product in addition to

residual **86**. The product was isolated by silica gel chromatography. The ^{1}H NMR

spectrum of the compound revealed it to be **88**, the product consistent with the addition of

water across the Ge=Ge double bond in **DGm**, based on comparison

with the previously reported ^{1}H NMR spectrum of the compound.[6]

$$\underset{\textbf{88}}{\overset{\text{H} \quad \text{OH}}{Mes_2Ge-GeMes_2}}$$
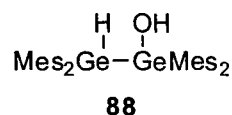
These results indicate that $HNEt_2$ is not sufficiently reactive

towards **DGm** to compete with adventitious water. We repeated the photolysis, this time

employing THF as the solvent. After thorough mixing of the amine with the solution of

DGm, the yellow colour of the digermene persisted. The reaction mixture was removed

from the cold bath and warmed to room temperature. The yellow colour remained even

after one hour at room temperature. The tube was transferred to the refrigerator (4 °C)

overnight; however, the yellow colour persisted for several days. After three days in the

refrigerator, the top portion of the solution was colourless, presumably due to the reaction

of **DGm** with O_2 introduced by diffusion through the septum; oxygen is known to react

with **DGm**.[5] It appears that **DGm** is not an appropriate digermene to study the products

of the reaction of digermenes with diethylamine. Future attempts to

study this reaction should therefore employ a less hindered digermene.

$$Ph_2Ge-GePh_2$$
$$Ph_2Ge-GePh_2$$
89
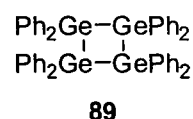
Tetraphenyldigermene is reportedly formed from photolysis of **89**,[7]

while tetramethyldigermene is reportedly formed from photolysis of **90** (eq 7.3).[2]

(7.3)
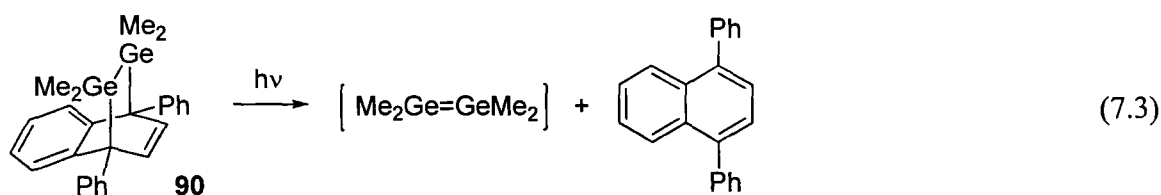
7.3.2. Kinetic Experiments

In the absence of added scavenger, the absorbance-time profiles of the digermenes

DGa,c,d,f, which form upon laser photolysis of **33a,c,d,f,** exhibit a growth followed by a

decay (for example, see the 0.00 mM trace in Figure 7.1a). Addition of sub-millimolar

concentrations of $HNEt_2$ to the solutions of **33a,c,d,f** leads to a decrease in the maximum

yield of the digermene, and faster rates of growth and decay of the species (see Figure

7.1a). These changes to the growth time and maximum yield of the digermene

absorbance-time profile are a result of the amine simultaneously quenching the

germylene (the digermene precursor). The decay portion of the traces were fit to first-

order kinetics, after the absorbance of the digermene began to decrease (see the black

lines in Figure 7.1a). The resulting k_{decay} values increased with the concentration of

added reagent (Figure 7.1b); due to the limited number of points, these data were fit to a

straight line although a slight curvature is exhibited in the plot of k_{decay} vs. [HNEt$_2$]. The

rate constants for the reactions of **DGa,c,d,f** with diethylamine vary by a factor of

approximately two throughout the series, as shown in Table 7.1.

Table 7.1. Absolute rate constants for the reaction of **DGa,c,d,f** with HNEt$_2$ in hexanes.

DG	k_Q / 10^9 M^{-1}s^{-1}
a (H)	2.4 ± 0.4
c (*p*-Me)	3.1 ± 0.3
d (*p*-F)	4.9 ± 0.5
f (*p*-CF$_3$)	5.8 ± 0.6
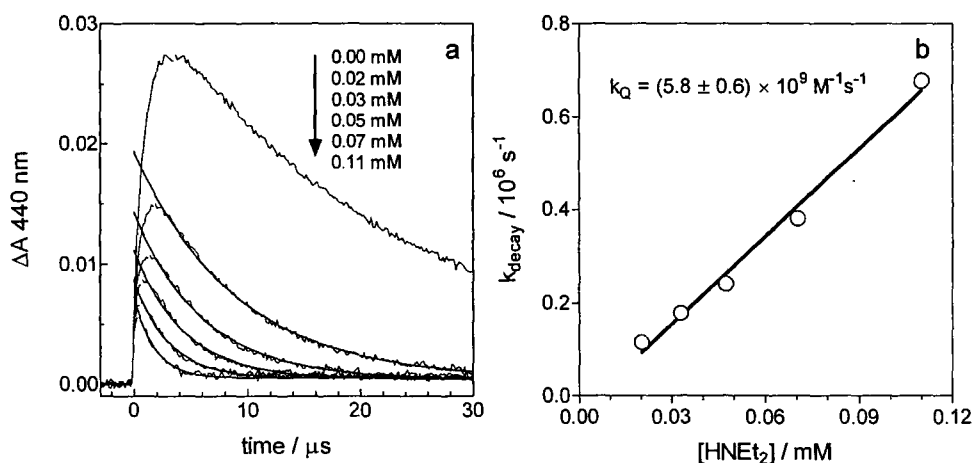
Figure 7.1. (a) Transient decay profiles of **DGf** in the presence of HNEt$_2$. The black lines are the non-linear least squares fit of the decays to first-order kinetics according to eq 2.19. (b) Plot k_{decay} vs. [Q] for the reaction of **DGf** with HNEt$_2$ in hexanes.

7.3.3. Discussion

The Hammett plot of the rate constants for the reaction of the digermenes

DGa,c,d,f with diethylamine is shown in Figure 7.2, and shows at best a weak correlation

with the Hammett σ values ($\rho = +0.12 \pm 0.07$). These data suggest a reaction mechanism

involving nucleophilic attack by the amine at a germanium of the digermene in the rate

determining step (see eq 7.4). Because of our inability to detect products from the

reaction of the **DGm** with diethylamine, we are unable to tell whether this initial step is

reversible or whether the reaction proceeds further to a product such as that consistent

with NH addition across the Ge=Ge bond (*e.g.* **91**). Because of the unfavourable

geometry in the intermediate complex for proton transfer, a second molecule of amine

may be required to catalyze the proton transfer, analogous to that proposed for the

reaction of germylenes with methanol.[1] If two molecules of amine are required in this

reaction, it may explain the curvature of the plot shown in Figure 7.1b.
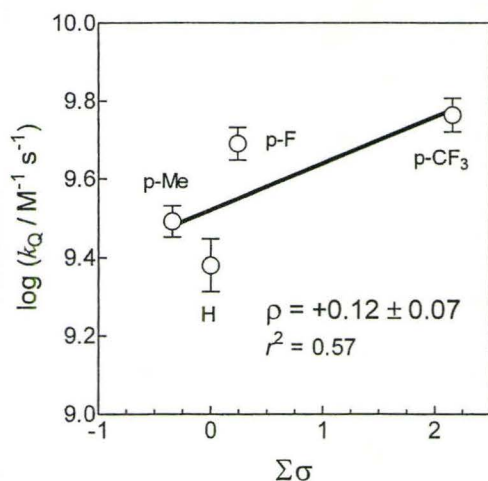
Figure 7.2. Hammett plot of the rate constants of the reaction of **DGa,c,d,f** with $HNEt_2$ in hexanes.

$$\text{(7.4)}$$
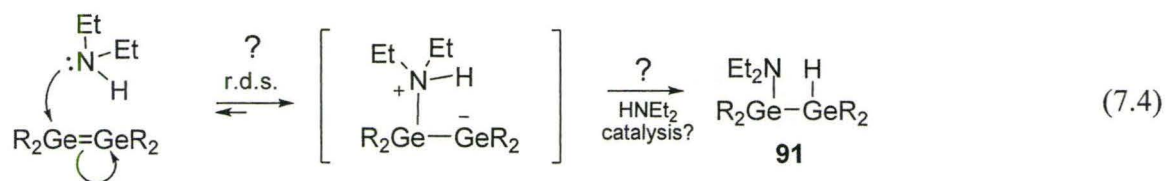
7.4. Reaction of Tetraaryldigermenes with Acetic Acid

7.4.1. Product studies

A solution of HOAc in toluene, cooled to -40 °C, was added to a solution of **DGm**, resulting in 20 mM HOAc. After mixing of the reagents and allowing the solution to stand for 60 minutes at this temperature, the characteristic yellow colour of the digermene persisted. The tube was removed from the cold bath, which caused the solution to become colourless within a few seconds. The solvent was removed and TLC analysis of the residue showed evidence for the formation of a single product. The product was isolated by silica gel chromatography as a colourless oil, which was analyzed by ^{1}H and ^{13}C NMR and infrared spectroscopy and mass spectrometry. The full list of spectral data are provided in Chapter 9, but the diagnostic clues to the identity of the compound were germyl hydride and acetyl methyl ^{1}H resonances at δ 6.32 and δ 1.88, respectively, coupled with the Ge-H and C=O infrared vibrations at ν 2077 and 1710 cm^{-1}, respectively, a carbonyl ^{13}C resonance at δ 172, and a molecular ion of $m/z = 682.2$ in the mass spectrum. The product was identified as **92**, the product of formal addition of the OH bond of the acid across the Ge=Ge bond of the digermene (eq 7.5).

$$\textbf{DGm} + \text{HOAc} \xrightarrow[\substack{\text{-40 °C} \\ \text{toluene}}]{} \underset{\textbf{92}}{\overset{\displaystyle \text{Mes}_2\text{Ge}-\text{GeMes}_2}{\overset{\displaystyle H \quad O}{\underset{}{|}}}} \tag{7.5}$$
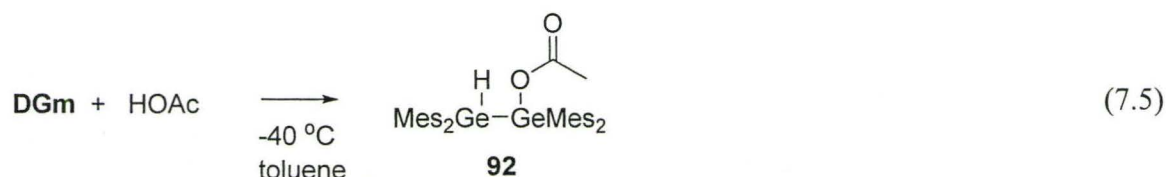
7.4.2. Kinetic studies

The presence of acetic acid affected similar changes to the absorbance-time profiles of the digermenes **DGa,c,d,f** as were observed with diethylamine. With increasing sub-millimolar concentrations of HOAc, the maximum yield of the digermene decreased, and the growth and decay rates of the species increased (see Figure 7.3a). The decay portion of the traces were fit to first-order kinetics, after the absorbance of the digermene began to decrease (see the black lines in Figure 7.3a). The resulting k_{decay} values increased in proportion to the concentration of added reagent as shown in Figure 7.3b. The rate constants for the reactions of **DGa,c,d,f** with HOAc are listed in Table 7.2, as are those for the reactions of **DGc,f** with DOAc. The rate constants obtained for the reactions of **DGc,f** with DOAc are not significantly different from those obtained with HOAc, indicating that a proton transfer does not occur in the rate determining step of the reaction.

Table 7.2. Absolute rate constants for the reaction of **DGa,c,d,f** with acetic acid and acetic acid-Od in hexanes.

| DG	k_{HOAc} / 10^7 M^{-1}s^{-1}	k_{DOAc} / 10^7 M^{-1}s^{-1}
a (p-H)	7.0 ± 0.4	-
c (p-Me)	4.0 ± 0.5	4.5 ± 0.8
d (p-F)	9.0 ± 1.0	-
f (p-CF$_3$)	36 ± 6	28 ± 3
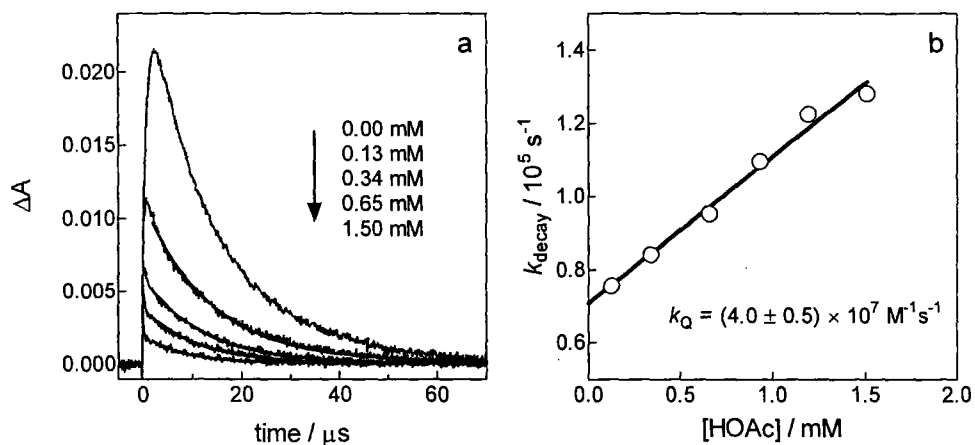
Figure 7.3. (a) Transient decay profiles of **DGc** in the presence of HOAc. The black lines are the non-linear least squares fit of the decays to first-order kinetics according to eq 2.19. (b) Plot of k_{decay} vs. [Q] for the reaction of **DGc** with HOAc.

7.4.3. Discussion

An excellent Hammett correlation with the rate constants for the reactions of

DGa,c,d,f with HOAc was found (ρ = +0.33 ± 0.01; see Figure 7.4) with the most

electron deficient digermene (**DGf**) reacting most rapidly. The absence of a significant

KIE on the rate constants rules out both a concerted addition of the acid to the digermene

as well as a two-step mechanism beginning with protonation. The latter is also mitigated

by the positive slope of the Hammett plot. A two-step mechanism beginning with rate-

determining nucleophilic addition of the acid, followed by a rapid intramolecular proton

transfer is consistent with these results, as shown in eq 7.6.
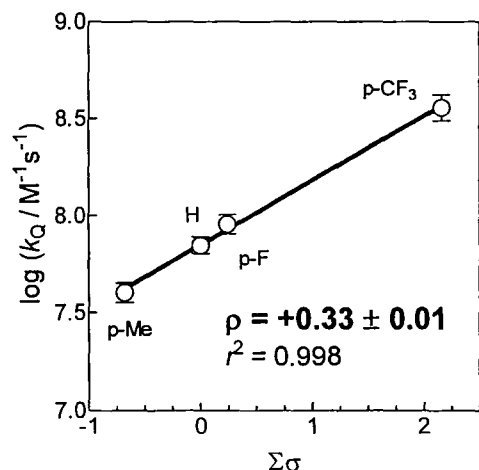
Figure 7.4. Hammett plot of the rate constants of the reactions of **DGa,c,d,f** with HOAc in hexanes.

$$(7.6)$$
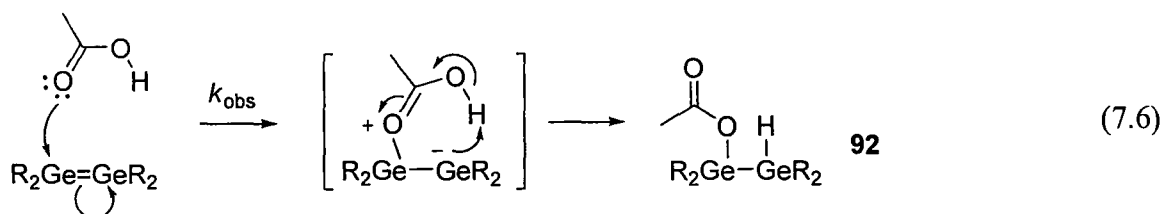
Samuel and Baines examined the reaction of **DGm** with the aldehyde **93**.[8] The final product was consistent with formal (2+2)-cycloaddition, as shown in eq 7.7. From this product distribution they proposed a mechanism involving nucleophilic attack of the carbonyl oxygen at germanium, leading to a zwitterionic intermediate.[8] Had the reaction followed a biradical mechanism, the cyclopropyl ring would open leading to different products.[9] A biradical mechanism was proposed for the reaction of tetramesityldisilene with **93**, based on the identification of the products shown in eq 7.8.[10, 11]

$$\tag{7.7}$$

$$\tag{7.8}$$
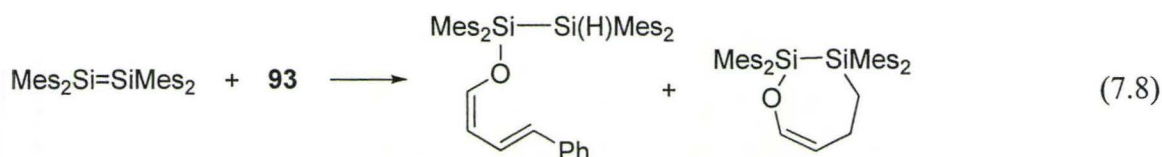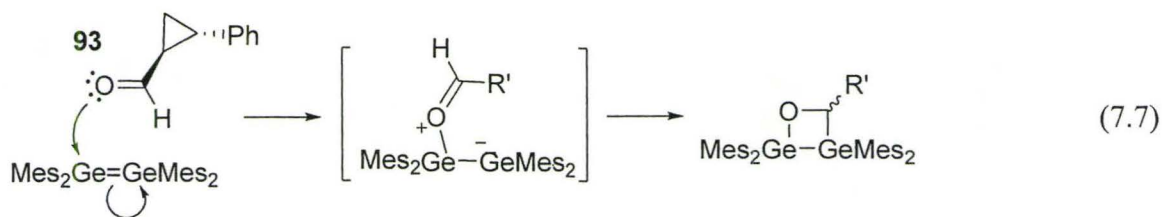
The rate constants for the reaction of the tetramethyldigermene (Ge_2Me_4) and tetraphenyldigermene (Ge_2Ph_4) with *n*-butylamine, methanol, and acetic acid in hexanes are listed in Table 7.3. Note that with H_2NBu and MeOH, Ge_2Ph_4 exhibits a faster rate constant than does Ge_2Me_4, whereas the reverse is true in the case of HOAc. Both the alcohol and the amine were proposed to react with the digermene by a mechanism involving initial nucleophilic attack at germanium by the substrate. The difference in rate constants was rationalized by the fact that Ge_2Ph_4 has a lower energy LUMO than Ge_2Me_4.[1, 12] It had been proposed that the reverse trend with HOAc is a result of a different mechanism, perhaps involving protonation of the digermene in the rate determining step.[12] Our results suggest that protonation does not occur in the rate determining step, at least not with the tetraaryldigermenes (**DGa,c,d,f**). The apparent anomaly in the rate constants with Ge_2Me_4 and Ge_2Ph_4 with HOAc, as well as the lack of a kinetic isotope effect, may be related to the oligomerization of the carboxylic acid that is known to occur in hexane solution.[13] Both rate constants were determined over roughly the same concentration range (< 0.5 mM HOAc) implying equal amounts of

oligomer would be present in each case – perhaps the approach of the acetic acid

oligomers to Ge_2Ph_4 is hindered by the larger phenyl groups.

Table 7.3. Absolute rate constants (k / 10^6 $M^{-1}s^{-1}$) for the reactions of Ge_2Me_4 and Ge_2Ph_4 with *n*-butylamine, methanol, and acetic acid in hexanes solution at 25 °C.

	Ge_2Me_4	Ge_2Ph_4
H_2NBu	50 [a]	3600 [c]
MeOH	3 [b]	20 [b]
HOAc	280 [a]	70 [d]

a. Reference 12. *b*. Reference 1. *c*. Reference 14. *d*. This work.

7.5. Reaction of Tetraaryldigermenes with CCl_4 in hexanes

7.5.1. Product studies

A solution of CCl_4 in toluene, cooled to -40 °C, was added to a solution of **DGm**, resulting in 0.35 M CCl_4. Upon mixing, the solution became colourless within a few seconds. The solvent was evaporated and the ^{1}H NMR spectrum of the residue showed evidence for the formation of several products; Figure 7.5 shows selected regions of the ^{1}H NMR spectrum of the product mixture. One of the products, 1,2-dichlorotetramesityldigermane (**94**), was identified by spiking the mixture with an independently prepared sample.[15] The yield of **94** was estimated to be approximately 20% from the contribution of the area of this peak to the total area (excluding **86** and **87**) in the aromatic region δ 6.50-8.85. Compound **87** was identified based on the similarity of the spectral data to that reported previously.[4]

We attempted to identify the other products by GC/MS analysis, but only

242

hexachloroethane (C_2Cl_6) could be identified by this method. While at least five germanium containing peaks were observed, the isotopic distributions were consistent with the presence of only one germanium atom per ion. The largest m/z of two of these peaks are consistent with the Ge(Cl)Mes$_2$ radical. Fragmentation of the Ge-Ge bond during mass spectral analysis has been previously observed.[16]
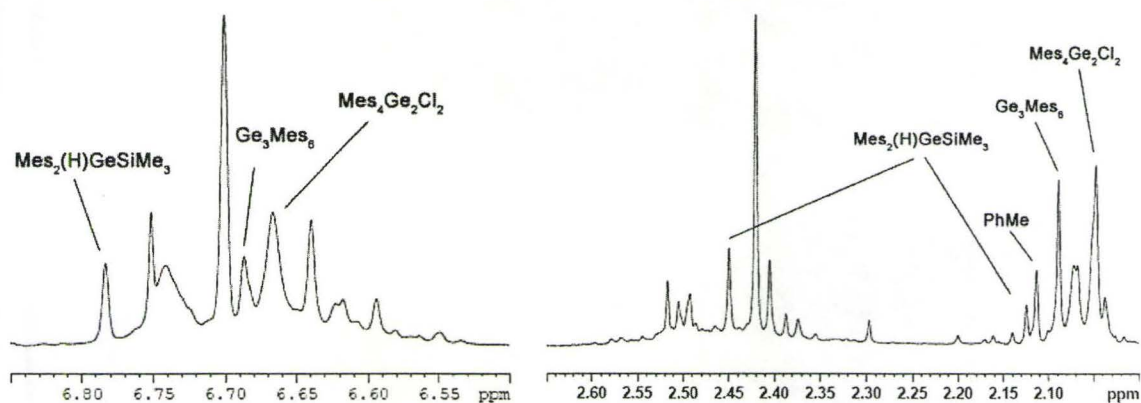
Figure 7.5. Select regions of the ^{1}H NMR spectrum (C_6D_6) of the products of CCl_4 quenching of **DGm**.

$$\textbf{DGm} \xrightarrow{\text{CCl}_4} \underset{\textbf{28 (ca. 20\%)}}{\overset{\overset{\displaystyle Cl\;\;\;Cl}{|\quad|}}{Mes_2Ge-GeMes_2}} \; + \; \underset{trace}{C_2Cl_6} \; + \; \text{other products} \qquad (7.9)$$
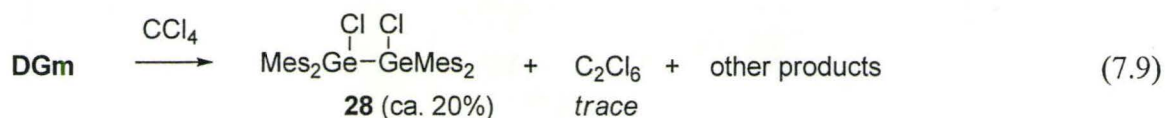
We wondered whether there may be a problem with our experimental procedure, so we repeated the experiment using $CHCl_3$ as the digermene scavenger. The reaction of **DGm** with $CHCl_3$ has been studied by Baines *et al.* (see eq 7.10).[17] In contrast to the results with CCl_4, addition of a -40 °C solution of $CHCl_3$ in toluene to a solution of **DGm** (resulting in 0.8 M $CHCl_3$) did not result in any immediate change in the appearance of the solution of **DGm**. After 30 minutes at -40 °C, the solution retained its original yellow

243

colour; the temperature was raised to -20 °C and after approximately five minutes at this temperature, the solution was colourless. The relatively slow reaction of $CHCl_3$ compared with CCl_4 is consistent with the relative rate constants that have been measured for the reactions of these halocarbons with **DGa** ($k_{CCl4} = 2 \times 10^6\ M^{-1}s^{-1}$ and $k_{CHCl3} < 10^5$ $M^{-1}s^{-1}$).[18] The solvent was evaporated and the ^1H NMR spectrum of the residue was obtained in C_6D_6. The spectrum was similar to that described by Baines *et al.*,[17] and consistent with the major products **95** and **87**, which were detected based on comparison to the reported chemical shifts in that solvent.[4, 17] We therefore conclude that the large number of products detected in the reaction of **DGm** with CCl_4 is likely not a result of problem with our experimental technique.

$$
\textbf{86} \quad \overset{\text{1) h}\nu,\ \text{PhMe, HSiEt}_3}{\underset{\text{2) CHCl}_3}{\longrightarrow}} \quad \underset{\textbf{(95, 25\%)}}{\overset{\overset{\text{Cl}}{|}\ \overset{\text{CHCl}_2}{|}}{\text{Mes}_2\text{Ge}-\text{GeMes}_2}} \quad + \quad \textbf{87} \qquad\qquad (7.10)
$$
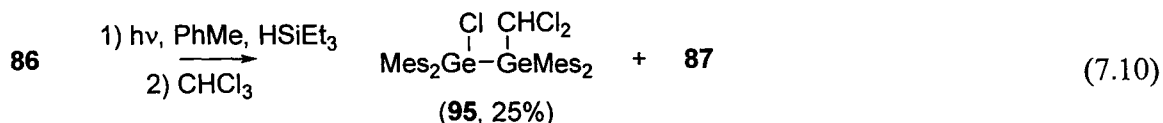
7.5.2. Kinetic studies

In the presence of millimolar concentrations of CCl_4, the maximum yields of the digermenes **DGa-f** were reduced, and their growth times and decay rates increased (see Figure 7.6a). The decay portion of the traces were fit to first-order kinetics, after the absorbance of the digermene began to decrease (see the black lines in Figure 7.6a). The resulting k_{decay} values increased in proportion to the concentration of added reagent as shown in Figure 7.6b. The absolute rate constants for the reactions of **DGa-f** with CCl_4 in hexanes are listed in Table 7.4.
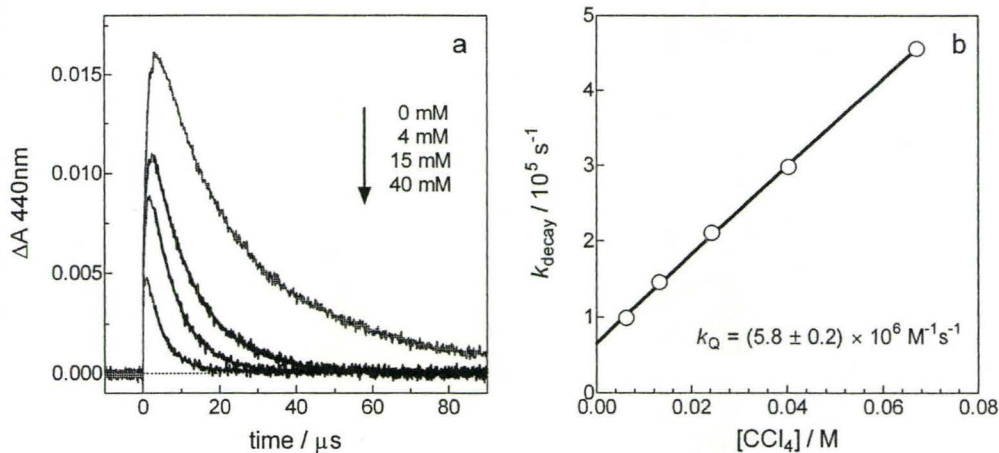
Figure 7.6. (a) Transient decay profiles of tetraaryldigermene **DGc** (CH$_3$) in hexanes containing CCl$_4$. The black lines are the fit of the decays to first-order kinetics according to eq 2.19. (b) Plot of k_{decay} vs. [CCl$_4$].

Table 7.4. Absolute rate constants for the reactions of the tetraaryldigermenes (**DGa-f**) with CCl$_4$ in hexanes.

DG	k_Q / 10^6 M^{-1}s^{-1}
a (H)	3.9 ± 0.5
b (mp-Me$_2$)	8.9 ± 1.0
c (p-Me)	5.8 ± 0.2
d (p-F)	2.5 ± 0.1
e (m-F)	1.3 ± 0.1
f (p-CF$_3$)	0.91 ± 0.08

A plot of the rate constants for the reaction of **DGa-f** with CCl$_4$ in hexane solution versus Hammett substituent constants is shown in Figure 7.7a. A reasonable correlation is observed, affording a Hammett ρ-value of -0.31 ± 0.03. Rate constants for the reaction of **DGa** with CCl$_4$ in hexane were also measured at several temperatures over the range of 10-60 °C. The Arrhenius plot is shown in Figure 7.7b, which led to the Arrhenius

parameters of $E_a = +4.3 \pm 0.8$ kcal/mol and log A = $+9.6 \pm 0.6$.
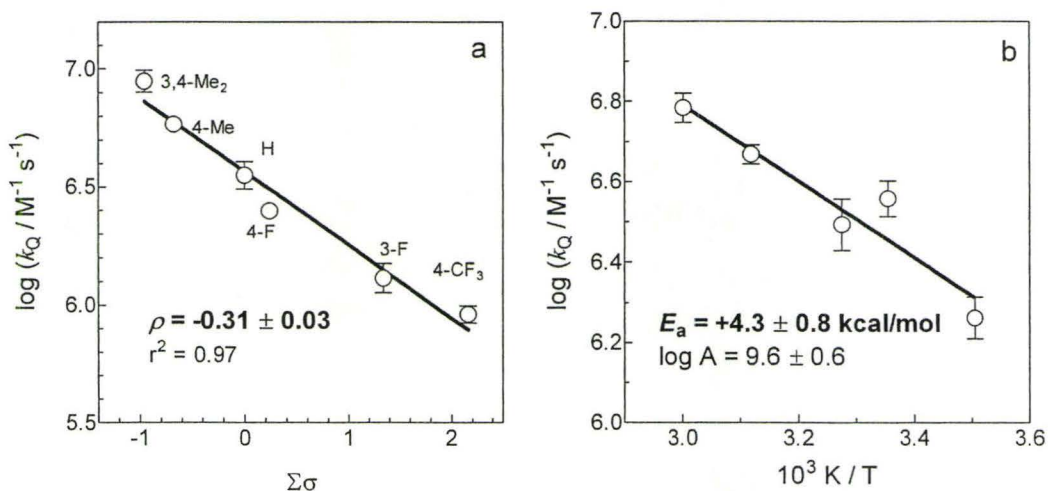
Figure 7.7. (a) Hammett Plot for the reaction of **DGa-f** with CCl_4 in hexanes at 25 °C. (b) Arrhenius plot for the reaction of **DGa** with CCl_4 in hexanes over 10-60 °C.

7.5.3. Discussion

Unlike the reactions of the digermenes with $HNEt_2$ and HOAc, the slope of the Hammett plot of the rate constants for the reaction of **DGa-f** with CCl_4 is negative, which implies that the digermene plays the role of the electron donor. The positive activation energy measured for the reaction of **DGa** with CCl_4 is consistent with the digermene being removed irreversibly in a single step. A mechanism consistent with our results is shown in eq 7.11, and involves a halogen atom abstraction from the halocarbon by the digermene as the first step. In this mechanism, the germanium should be polarized $\delta+$ in the transition state because of electron transfer to the halocarbon; the rate constants therefore increase with electron donating groups on the germanium.

(7.11)
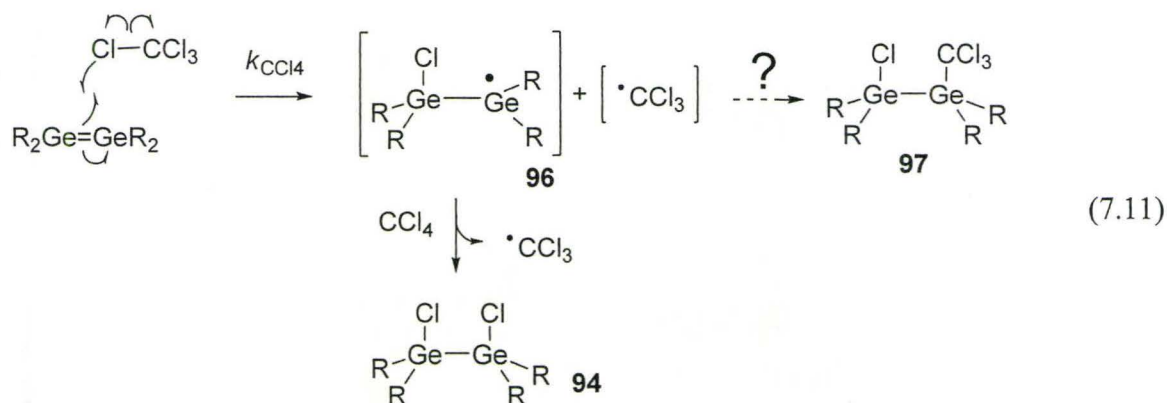
Initial chlorine atom abstraction from CCl_4 has been observed experimentally

with both disilenes[19] and digermenes[2] and has also been predicted to occur by

computational methods.[19-21] The resulting germyl radical intermediate (96) abstracts

another halogen atom from CCl_4 to yield the observed 1,2-dichlorodigermane product 94.

Clearly several other reactions also take place, as is evident from the ^1H NMR spectrum

of the product mixture. The most obvious question is whether the two radicals formed in

the first step combine, yielding the product resulting from formal $Cl-CCl_3$ *addition* to the

digermene (97). While we have not been able to identify 97, we can not rule it out as a

possible product as we did not attempt synthesis of the authentic sample.

7.6. Summary

Product formation in the reactions of the tetraaryldigermenes with $HNEt_2$ and HOAc was studied using the digermene **DGm**. Only with HOAc could a product be isolated and is consistent with a formal OH *addition* across the Ge-Ge double bond. Kinetic studies of this reaction ($k_{Ge2Ph4-HOAc} = (7.0 \pm 0.4) \times 10^7$ $M^{-1}s^{-1}$) suggest a two-step mechanism beginning with rate-determining nucleophilic attack of the carbonyl oxygen of the acid with the digermene ($\rho = +0.33 \pm 0.01$) followed by intramolecular proton transfer to the adjacent germanium atom. While products could not be detected in the reaction of **DGm** with the amines, the kinetic data ($k_{DGa-HNEt2} = (2.4 \pm 0.4) \times 10^9$ $M^{-1}s^{-1}$; $\rho = +0.12 \pm 0.07$) are consistent with nucleophilic attack by the amine.

Digermenes react with CCl_4 to yield the double halogen abstraction product **94** (20%) along with several other products that could not be identified. Kinetic studies show that the digermene plays the role of the electron donor in the rate determining step ($k_{DGa-CCl4} = (3.9 \pm 0.5) \times 10^6$ $M^{-1}s^{-1}$; $\rho = -0.31 \pm 0.03$). The positive activation energy ($E_a = +4.3 \pm 0.8$ kcal/mol) is consistent with a single-step halogen atom abstraction as the initial step.

7.7. References

1. Leigh, W. J.; Lollmahomed, F.; Harrington, C. R.; McDonald, J. M. *Organometallics* **2006**, *25*, 5424.
2. Mochida, K.; Kayamori, T.; Wakasa, M.; Hayashi, H.; Egorov, M. P. *Organometallics* **2000**, *19*, 3379.
3. Hurni, K. L.; Rupar, P. A.; Payne, N. C.; Baines, K. M. *Organometallics* **2007**, *26*, 5569.
4. Baines, K. M.; Cooke, J. A.; Vittal, J. J. *J. Chem. Soc., Chem. Commun.* **1992**, 1484.
5. Samuel, M. S.; Jennings, M. C.; Baines, K. M. *J. Organomet. Chem.* **2001**, *636*, 130.
6. Baines, K. M.; Cooke, J. A.; Dixon, C. E.; Liu, H.; Netherton, M. R. *Organometallics* **1994**, *13*, 631.
7. Mochida, K.; Adachi, M.; Wakasa, M.; Hayashi, H. *Phosph. Sulf. Sil. Rel. Elem.* **1999**, *150-151*, 237.
8. Samuel, M. S.; Baines, K. M. *J. Am. Chem. Soc.* **2003**, *125*, 12702.
9. Newcomb, M.; Toy, P. H. *Acc. Chem. Res.* **2000**, *33*, 449.
10. Samuel, M. S.; Jenkins, H. A.; Hughes, D. W.; Baines, K. M. *Organometallics* **2003**, *22*, 1603.
11. Hardwick, J. A.; Baines, K. M. *Organometallics* **2010**, *29*, 1305.
12. Leigh, W. J.; Lollmahomed, F.; Harrington, C. R. *Organometallics* **2006**, *25*, 2055.
13. Fujii, Y.; Yamada, H.; Mizuta, M. *J. Phys. Chem.* **1988**, *92*, 6768.
14. Leigh, W. J.; Harrington, C. R.; Vargas-Baca, I. *J. Am. Chem. Soc.* **2004**, *126*, 16105. (Errata: *J. Am. Chem. Soc.* **2006**, *128*, 1394.).
15. Cooke, J. A.; Dixon, C. E.; Netherton, M. R.; Kollegger, G. M.; Baines, K. M. *Synth. React. Inorg. Met. -Org. Chem.* **1996**, *26*, 1205.
16. Mallela, S. P.; Geanangel, R. A. *Inorg. Chem.* **1993**, *32*, 5623.
17. Samuel, M. S.; Jennings, M. C.; Baines, K. M. *Organometallics* **2001**, *20*, 590.
18. Leigh, W. J.; Harrington, C. R. *J. Am. Chem. Soc.* **2005**, *127*, 5084.
19. Kira, M.; Ishima, T.; Iwamoto, T.; Ichinohe, M. *J. Am. Chem. Soc.* **2001**, *123*, 1676.
20. Su, M.-D. *Inorg. Chem.* **2004**, *43* 4846.
21. Su, M. D. *J. Phys. Chem. A* **2004**, *108*, 823.

Chapter 8 – Future Directions

A simple extension of the work described in this thesis would be a more detailed examination of any germylene reactions not presented in this thesis using the same procedures (*e.g.* product studies and determination of substituent and temperature effects on the rate constants). Some interesting examples include the reactions of germylenes with alkenes and alkynes, metal hydrides, and Lewis acids, as described below.

Our group is beginning to look in detail at the reaction of germylenes with alkenes and alkynes. The initial results of some of these experiments were presented in Chapter 6. The results will eventually lead to a more detailed understanding of the (2+2) cycloaddition reactions of germylenes with unsaturated systems. As mentioned in Chapter 1, the utility of germylenes as catalysts for alkene polymerization has recently been demonstrated.

Germylene insertion into the MH bond (M = Si, Ge, Sn)[1, 2] is an interesting example of germylene insertion into a σ bond. The reaction is different from the other σ-bond insertion reactions (*e.g.* OH, NH) we have studied because the hydrogen has the opposite polarization (*i.e.* H δ-). The rate constants for the reactions of the germylenes GeMe$_2$, GeMePh, and GePh$_2$ with Group 14 hydrides increase as the strength of the MH bond decreases.[3-5] With GePh$_2$ the rate constants for reaction with Group 14 trialkylmetal hydrides decrease in the order $k_{SnH} \approx 120k_{GeH} \approx 6000k_{SiH}$ ($k_{HSnBu3} = 3.5 \times 10^9$ M^{-1}s^{-1} in hexanes at 25 °C).[3] Mochida and Hasegawa suggested that the germylene acts as a nucleophile in the reaction with silyl hydrides, based on the relative product

yields obtained from a competition experiment.[2] However, a computational study led to the prediction that the reaction of GeH_2 with hydrides begins with coordination of the hydrogen of the metal hydride with germanium, followed by an intramolecular reorganization as shown in eq 8.1.[6] In a gas-phase kinetic study by Walsh *et al*[7] on the reaction of GeH_2 with germane (GeH_4), a negative activation energy was observed, thus providing experimental evidence supporting the formation of an intermediate complex.

$$GeR_2 \ + \ HMR'_3 \ \rightleftharpoons \ \left(\begin{matrix} H-MR'_3 \\ \vdots \\ R_2Ge: \end{matrix} \right) \ \longrightarrow \ R_2Ge\begin{matrix} MR'_3 \\ \\ H \end{matrix} \qquad (8.1)$$

(M = Si, Ge, Sn)
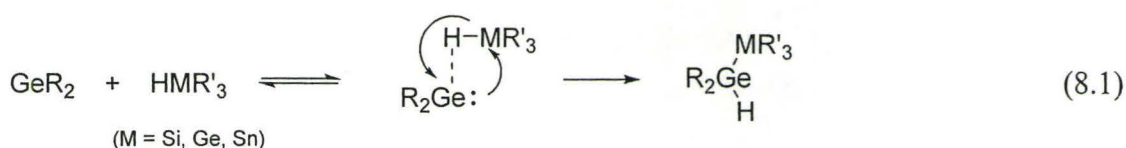
As described in this thesis, it is known that complexation of the germylene alters the reactivity. Neumann has studied the reactivity of the $GeMe_2$-water complex (**96**) with a focus on synthetic applications and has found that its chemistry is much different from free $GeMe_2$.[8] For example, **96** can act as a Michael donor in the reaction with α,β,γ,δ-unsaturated ketones, as shown in eq 8.2.[9]

$$(8.2)$$
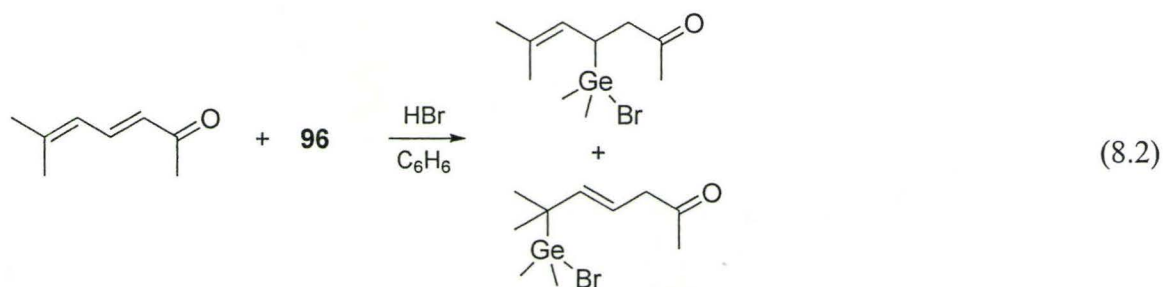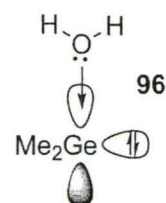
The increased electron density at the germanium is apparently sufficient to impart nucleophilic behaviour on the complex. The implications of this result for reactions with other scavengers have not been pursued in much detail. Our group has studied the

kinetics of the reaction of germylene-methanol and germylene-THF complexes with methane-sulfonic and acetic acids, CCl_4, and isoprene. Expanding the list of other scavengers and other complexes will be of interest. Mechanistic studies are presently underway in our group studying the reactions of germylene complexes (e.g. $GePh_2$-THF) with boranes (Lewis acids).

A long term goal of the group is to explore the excited state of germylenes, using two-photon laser[10] experiments. The first pulse (248 nm) will be used to generate the germylene, while a second pulse will promote the germylene to an excited state. This second laser pulse could be 308 nm for $GePh_2$ and should result in a S_0-S_2 excitation because this wavelength corresponds to the second lowest energy absorption. Internal conversion (IC) would lead to S_1, as shown Figure 8.1. These two photon experiments may allow us to measure the UV spectrum of a triplet germylene (G_{T1}). While there is no doubt that the singlet germylene is the ground state, some authors have reported the generation of triplet germylenes.[11] Generation of G_{S1} may lead to the formation of G_{T1} through intersystem crossing (ISC); although we have no information on which to estimate k_{ISC}, it will likely be quite fast because of the presence of the germanium atom (the heavy-atom effect).[12,13] Presumably the heavy atom effect will also facilitate ISC from G_{T1} to G_{S0}, so the triplet lifetime may be quite short. Once an efficient route to G_{T1} is determined, its reactivity could be studied in the same manner we have used to study the chemistry of G_{S0}.

Figure 8.1. State energy diagram of GePh$_2$. $\Delta E_{S0\text{-}S1}$ was estimated from the lowest energy absorption of GePh$_2$,[14] while $\Delta E_{S0\text{-}T1}$ was estimated from that calculated for GeMe$_2$.[15]

Determining reactivity trends in Group 14 divalent species is an important focus of the work in our group. Literature examining the chemistry of stannylenes is scarce relative to silylenes and germylenes.[16-20] The photochemistry of **97** was reported to extrude DMB and SnMe$_2$, as shown in eq 8.3:[21]

$$(8.3)$$

We have for some time been trying to determine an efficient synthesis of a photochemical precursor to diphenylstannylene, such as **98**. Our efforts have focused on the route shown in eq 8.4 (Mg* is activated magnesium[22]).

$$(8.4)$$

Approximately 100 mg of **98** was prepared, which was enough to record two transient absorption spectra by laser flash photolysis. The transient absorption spectra,

one recorded in hexanes and the other in hexanes containing 45 mM THF, are shown in

Figure 8.2a and b, respectively. In hexanes solution, a transient with long wavelength

absorption maxima at 500 nm and 380 nm is formed with the laser pulse and decays over

several microseconds. The tentative assignment of this transient is to stannylene $SnPh_2$.

In the presence of THF, the $SnPh_2$ can no longer be detected and a transient centered at

ca. 360 nm is observed; this behaviour is identical to that observed with

GePh$_2$ in the presence of THF and thus the transient at 360 nm is tentatively

assigned to the Lewis acid-base complex **99**. In order to continue this work,

the first task will be to identify a more efficient synthesis to **98**, ideally

following a method that does not involve the use of Mg*.

99

Ph_2Sn
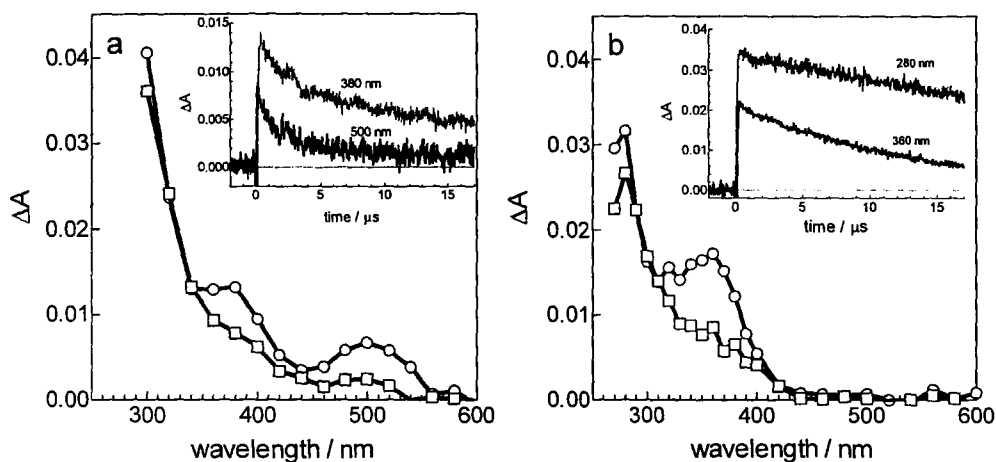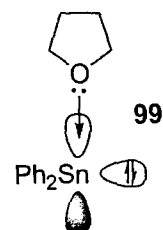
Figure 8.2. Transient absorption spectra from laser flash photolysis of **98** (*ca.* 0.003 M) in (a) hexanes, recorded 0.32-0.38 μs (○) and 3.84-3.97 μs (□) after the 248 nm laser pulse and (b) hexanes containing 45 mM THF, recorded 160-256 ns (○) and 12.32-12.48 μs (□) after the 248 nm laser pulse. The insets show the absorbance-time profile at selected wavelengths.

References

1.   Ma, E. C.-L.; Paquin, D. P.; Gaspar, P. P. *J. Chem. Soc., Chem. Commun.* **1980**, 381.
2.   Mochida, K.; Hasegawa, A. *Chem. Lett.* **1989**, 1087.
3.   Leigh, W. J.; Harrington, C. R. *J. Am. Chem. Soc.* **2005**, *127*, 5084.
4.   Leigh, W. J.; Lollmahomed, F.; Harrington, C. R. *Organometallics* **2006**, *25*, 2055.
5.   Leigh, W. J.; Dumbrava, I.; Lollmahomed, F. *Can. J. Chem.* **2006**, *84*, 934.
6.   Trinquier, G. *J. Chem. Soc., Faraday Trans.* **1993**, *89*, 775.
7.   Becerra, R.; Boganov, S. E.; Egorov, M. P.; Faustov, V. I.; Nefedov, O. M.; Walsh, R. *J. Am. Chem. Soc.* **1998**, *120*, 12657.
8.   Neumann, W. P.; Weisbeck, M. P.; Wienken, S. *Main Group Met. Chem.* **1994**, *17*, 151.
9.   Wienken, S.; Neumann, W. P. *Chem. Ber.* **1993**, *126*, 769.
10.   Scaiano, J. C.; Johnston, L. J. *Acc. Chem. Res.* **1988**, *21*, 22.
11.   Plyusnin, V. F.; Kaletina, M. V.; Leshina, T. V. *Russ. Chem. Rev.* **2007**, *76*, 931.
12.   Turro, N. J.; Ramamurthy, V.; Scaiano, J. C., *Principles of Molecular Photochemistry: An Introduction*. University Science Books: Sausalito, CA, 2009; p 231.
13.   Maeda, H.; Ishida, H.; Inoue, Y.; Merpuge, A.; Maeda, T.; Mizuno, K. *Res. Chem. Intermed.* **2009**, *35*, 939.
14.   Leigh, W. J.; Harrington, C. R.; Vargas-Baca, I. *J. Am. Chem. Soc.* **2004**, *126*, 16105. (Errata: *J. Am. Chem. Soc.* **2006**, *128*, 1394.).
15.   Su, M.-D.; Chu, S. Y. *J. Am. Chem. Soc.* **1999**, *121*, 4229.
16.   Neumann, W. P. *Chem. Rev.* **1991**, *91*, 311.
17.   Tokitoh, N.; Okazaki, R. *Coord. Chem. Rev.* **2000**, *210*, 251.
18.   Kira, M.; Ishida, S.; Iwamoto, T. *Chem. Rec.* **2004**, *4*, 243.
19.   Tokitoh, N.; Ando, W. In *Reactive Intermediate Chemistry*, Moss, R. A.; Platz, M. S.; Jones, M., Jr., Eds. John Wiley & Sons: New York, 2004; pp 651-715.
20.   Becerra, R.; Walsh, R. *Phys. Chem. Chem. Phys.* **2007**, *9*, 2817.
21.   Becerra, R.; Gaspar, P. P.; Harrington, C. R.; Leigh, W. J.; Vargas-Baca, I.; Walsh, R.; Zhou, D. *J. Am. Chem. Soc.* **2005**, *127*, 17469.
22.   Rieke, R. D.; Hanson, M. V. *Tetrahedron* **1996**, *53*, 1925.

Chapter 9 – Experimental

9.1. General

All synthetic preparations were carried out in flame-dried glassware under an

atmosphere of dry nitrogen or argon. Column chromatography was carried out using acid

washed 230-400 mesh silica gel (Silicycle). ^{1}H NMR and ^{13}C NMR spectra were

recorded on Bruker AV200, DRX500 or AV600 spectrometer in the specified perdeutero-

solvent (Cambridge Isotope Laboratories), $CDCl_3$ unless otherwise stated. Infrared

spectra were recorded as thin-films on sodium chloride plates using a Bio-Rad FTS-40

FTIR spectrometer and are uncorrected. Static UV/vis absorption spectra were recorded

on a Varian Cary 100 UV/vis spectrophotometer. Melting points were recorded using a

Mettler FP82 hot stage (controlled by a Mettler FP80 central processor) mounted on a

microscope and are uncorrected. Combustion analyses were performed by Guelph

Chemical Laboratories Ltd., Guelph ON <u>or</u> with a Thermo FlashEA 1112 elemental

analyzer using methionine as the calibrant (McMaster). High-resolution mass spectra

were recorded on a Micromass TofSpec 2E mass spectrometer using electron impact (70

eV) or chemical ionization (NH_3 reagent gas, positive ion mode). GC/MS analysis of

product mixtures was performed using a Varian Saturn 2200 GC/MS/MS system

equipped with a VF-5ms capillary column (30m×0.25mm; 0.25 μm; Varian, Inc.) using

electron impact or chemical ionization (MeOH reagent gas), where noted. MALDI mass

spectra were recorded on a Waters/Micromass MALDI MicroMX mass spectrometer

operating in reflectron mode (matrix: α-cyano-4-hydroxycinnamic acid). All *m/z* values

marked with an asterisk * indicate a cluster of peaks which contain one or more germanium atom; only the mass of the ^{74}Ge (or n^{74}Ge) peak is reported. X-ray crystallographic analysis was performed in the McMaster Analytical X-Ray (MAX) Diffraction Facility on a single crystal (in each case, grown from slow evaporation of hexanes), mounted and cooled to -100 °C on a SMART APEX II diffractometer with a 3 kW sealed tube Mo generator. The structures were solved by Drs. James Britten, Hilary Jenkins, and/or Laura Harrington. **When not in use, all compounds were stored at -20 °C in vials that had been purged with nitrogen or argon.**

9.2. Solvents

Hexanes (EMD-Omnisolv), diethyl ether (Caledon) and THF (Caledon) were dried by passage through activated alumina under nitrogen using a Solv-Tek solvent purification system. THF was also distilled from a Na/K amalgam. Methanol (Caledon Caledon, HPLC grade or J. T. Baker, absolute), methanol-*Od* (Aldrich), and 1,4-dioxane (Caledon) were used as received. For chromatographic purposes hexanes (Caledon) and dichloromethane (Caledon) were used as received. Cyclohexane-*d12*, benzene-*d6* and THF-*d8* were used as received.

9.3. Commercial Reagents

For synthetic applications, the following reagents were purchased from Aldrich and used as received: isoprene, 2,3-dimethylbutadiene, bromobenzene, 1-bromo-4-methylbenzene, 1-bromo-4-fluorobenzene, 1-bromo-3-fluorobenzene, 1-bromo-4-trifluorobenzene, 1-bromo-3,5-bis(triflouromethyl)benzene, 1-bromo-2,4,6-

trimethylbenzene, cupric chloride, carbon tetrachloride, lithium aluminum hydride, t-butyl lithium. Other synthetic reagents used as received: $GeCl_4$ (Gelest Inc. or Teck-Cominco Metals Ltd.), 1,1,3,3-tetramethlydisiloxane (Gelest), magnesium (EM Science, >99%), triphenylbismuth (Gelest).

For photolysis experiments (steady state, laser flash): Glacial acetic acid (Caledon), acetic acid-Od (Aldrich), and methanol (J.T. Baker) were used as received. N-Butylamine and N,N-diethylamine (Aldrich) were refluxed over KOH and distilled. Ethyl acetate (Caledon) was dried by passage through activated silica gel. THF was dried as described above. Methanesulfonic acid (Aldrich) was distilled under vacuum before use. Sodium methoxide solutions were prepared by dissolving sodium in methanol. Carbon tetrachloride (Aldrich) and toluene (Caldeon) were refluxed over P_2O_5 and distilled. Chloroform (Caledon) was washed with an equal volume of distilled water (×3), dried with $MgSO_4$, and then refluxed and distilled over P_2O_5 (×2). Isoprene and DMB were distilled or passed as neat liquids through a short column of silica gel.

For low temperature matrix experiments: 3-methylpentane (spectrophotometric grade) was used as received (Aldrich). Chloroform-d (Cambridge Isotope Laboratories) was obtained from 1 mL ampoules and used immediately after opening. Carbon tetrachloride (Aldrich) was refluxed over P_2O_5 and distilled.

9.4. Synthesis

9.4.1. Diarylgermacyclopentenes

$$\text{(9.1)}$$
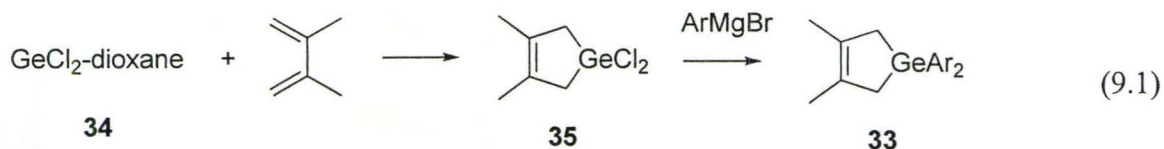
The syntheses of **33a-f** all followed the scheme outlined in eq 9.1. Compounds **34**, **35** and **33a** were prepared as previously described.[1] GeCl$_2$-dioxane (**34**) was obtained as white crystals, which were washed several times with pentane and used without further purification or identification. Care must be taken to minimize exposure of **34** to air for prolonged periods. **1,1-Dichloro-3,4-dimethyl -1-germacyclopent-3-ene** (**35**, bp 56 °C/0.2 mmHg): ^{1}H NMR: δ = 1.81 (s, 6H, CH$_3$), 2.23 (s, 4H, CH$_2$). The boiling point[2] and ^{1}H NMR spectrum[3] are in good agreement with literature values.
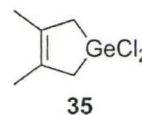
The synthesis of **33c**, prepared from the reaction of **35** with 4-methylphenyl-magnesium bromide, is used as a specific example to illustrate the synthesis of the germacyclopentenes. For **33a,c-g**, the corresponding aryl bromides used to make the Grignard reactions are commercially available. For the synthesis of **33b**, 1-bromo-3,4-dimethylbenzene was synthesized by S. Chitnis following a reported procedure.[4]

3,4-Dimethyl-1,1-di-(4-methylphenyl)-1-germacyclopent-3-ene (**33c**, mp 62.0-63.0 °C): A 2-neck round bottom flask equipped with a stir-bar, condenser, and dropping funnel was charged with freshly ground magnesium turnings (1.05 g, 43 mmol) and dry THF (75 mL). A solution of 1-bromo-4-methylbenzene (6.5 g, 38 mmol) in dry THF (30

mL) was added to the dropping funnel. A single crystal of iodine was added to the round bottom flask, followed by approximately 5 mL of the solution from the dropping funnel. The reaction was stirred until initiation (indicated by the disappearance of the yellow colour). Once the reaction initiated, the remaining solution was added dropwise over 30 minutes and the mixture stirred overnight.

The dropping funnel was then charged with a solution **35** (3.91 g, 17.3 mmol) in THF (45 mL) and the flask was cooled in an ice bath. The solution was then added dropwise over 1 hr and the mixture left to stir overnight at room temperature. The reaction was quenched with 1 M HCl (150 mL) and the mixture transferred to a separatory funnel with ether (150 mL). The organic layer was removed and the aqueous portion extracted with ether (2 × 50 mL). The combined organics were washed with sat. $NaHCO_3$ (1 × 50 mL), brine (1 × 50 mL), and water (1 × 50 mL), dried ($MgSO_4$), and evaporated to give a pale yellow oil (4.89 g, 14.5 mmol, 84%). The oil was passed through a silica column (hexanes, 15 cm height, 230-400 mesh, 25 mm diameter) to remove the polar contaminants to give a colourless oil, from which the product crystallized, usually upon cooling in the fridge (4 °C). Further purification was achieved by recrystallization from hot hexanes; recrystallization was repeated until GC/MS analysis showed that the ratio of the peak areas of **33**:Ar_2 was 99.9>0.1.

3,4-Dimethyl-1,1-di-(4-methylphenyl)-1-germacyclopent-3-ene (33c;

mp 81.4 – 83.7 °C). ^{1}H NMR, δ = 1.78 (s, 6H, C^8H_3), 1.98 (s, 4H, C^6H_2), 2.36 (s 6H, C^5H_3), 7.19 (d, 4H, J = 7.8 Hz, C^3H), 7.42 (d, 4H, J = 7.8 Hz, C^2H); ^{13}C NMR, δ =19.55 (C8), 21.56 (C5), 25.80 (C6), 129.11(C2), 130.91(C7), 134.32
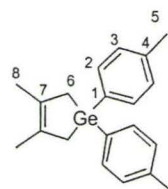
(C3), 134.91 (C1), 138.69 (C4). IR: 2914 cm^{-1} (m,br), 1911 (w), 1497 (m), 1440 (m,br), 1264 (m), 1171 (m), 1157 (m), 1087 (m), 799 (s), 742 (m), 667 (m). MS: m/z = 338.1* (38), 256.0* (100), 181.1 (94), 164.9* (46), 139.0* (15). HRMS: $C_{20}H_{24}Ge$ calc. 338.1090; found 338.1078. Anal. calc. for $C_{20}H_{24}Ge$: C 71.28, H 7.18; found: C 70.91, H 6.99.

1,1-bis(3,4-dimethylphenyl)-3,4-dimethyl-2,5-dihydro-1H-germole (33b; m.p. 62.0-63.0 °C). (*Synthesis by S. Chitnis*) ^{1}H NMR, δ = 1.77 (s, 6H, H^3), 1.96 (s, 4H, H^1), 2.25 (s, 6H, H^{11}), 2.26 (s, 6H, H^{10}), 7.13 (d, 2H, J = 7.2 Hz, H^8), 7.25 (d, 2H, J = 7.2 Hz, H^9), 7.28 (s, 2H, H^5). ^{13}C NMR, δ = 19.58 (C^3), 19.84 (C$^{10\ or\ 11}$), 19.85 (C$^{10\ or\ 11}$), 25.79 (C^1), 129.61 (C^8), 130.90 (C^2), 131.96 (C^9), 135.47 (C$^{4\ and\ 5}$ by 2D NMR), 136.50 (C^7), 137.58 (C^6). MS, m/z (intensity): 366.1* (40), 284.1* (90), 209.1* (100), 179.0 (75), 145.1 (30), 91.1 (40), 67.1 (70). HRMS: $C_{22}H_{28}{}^{74}Ge$: calc.: 366.1407, found: 366.1386. IR, cm^{-1} (intensity): 3092 (w), 3048 (m), 2998 (s), 2967 (s), 2915 (s), 2584 (s), 2780 (w), 2724 (w), 1890 (w), 1762 (w), 1447 (s), 1098 (s), 810 (s). Anal. calc. for $C_{22}H_{28}Ge$: C 72.37, H 7.73, found: C, 72.43; H, 7.90.

3,4-Dimethyl-1,1-diphenyl-1-germacyclopent-3-ene (33a). ^{1}H NMR, δ = 1.79 (s, 6H, CH$_3$), 2.01 (s, 4H, CH$_2$), 7.30-7.45 (m, 6H, ArH), 7.45-7.60 (m, 4H, ArH). The spectrum agrees with data reported elsewhere.[1, 3]
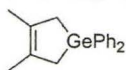
33a

1,1-Di-(4-fluorophenyl)-3,4-dimethyl-1-germacyclopent-3-ene (33d; mp 83.1 – 84.8

°C). ^{1}H NMR, δ = 1.80 (s, 6H, C$^8H_3$), 2.00 (s, 4H, C$^6H_2$), 7.07 (dd, 2H,

J = 9, 9 Hz, C^3H), 7.46 (dd, 2H, J = 9, 6 Hz, C^2H); ^{13}C NMR, δ =19.51

(C8), 25.82 (C6), 115.55 (d, $^2J_{C-F}$ = 20 Hz, C3), 130.87 (C7), 133.40

(C1), 136.00 (d, $^3J_{C-F}$ = 7 Hz, C2), 163.81 (d, $^1J_{C-F}$ = -248 Hz, C4). IR: 2911 cm^{-1} (m,br),

1893 (w), 1587 (s), 1496 (m), 1230 (m), 1162 (m), 1086 (m), 821 (m), 743 (m), 670 (w).

MS: m/z = 346.1* (50), 262.0* (58), 169.0* (100), 152.1 (88), 92.9* (70). HRMS:

$C_{18}H_{18}F_2$Ge calc.346.0588; found 346.0564. Anal. calc. for $C_{18}H_{18}F_2$Ge: C 62.68, H

5.26; found: C 63.07, H 5.56.
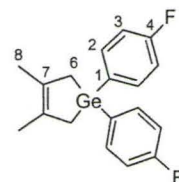
1,1-bis(3-fluorophenyl)-3,4-dimethyl-1-germacyclopentene (33e; mp 46.0-47.1°C) ^{1}H

NMR, δ = 1.86 (s, 6H, H$_9$), 2.09 (s, 4H, H$_7$), 7.05 (ddd, 2H, J = 8.6, 8.6,

2.7 Hz, H_4), 7.19 (dd, 2H, J = 8.4, 2.7 Hz, H_2), 7.26 (d, 2H, J = 7.2 Hz,

H_6), 7.34 (ddd, 2H, J = 7.7, 7.7, 5.4 Hz, H_5). ^{13}C NMR, δ =19.48 (C_9),

25.53 (C_7), 116.10 (d, $^2J_{C-F}$ = 21 Hz, C_4), 120.69 (d, $^2J_{C-F}$ = 19 Hz, C_2),

129.83 (C_6), 130.04 (d, $^3J_{C-F}$ = 7 Hz, C_5), 130.84 (C_8), 140.64 (C_1), 162.88 (d, $^1J_{C-F}$ = 250

Hz, C_3). IR, cm^{-1} (intensity): 3062 (m), 2907 (m), 1598 (m), 1577 (m), 1475 (m), 1440

(w), 1416 (m), 1260 (m), 1211 (m), 1173 (w), 1161 (w), 1097 (m), 897 (m), 862 (m), 782

(m), 741 (m). MS, m/z (intensity): 346.0* (40), 262.0* (25), 168.9* (25), 152.1 (100),

92.9 (30). HRMS: $C_{18}H_{18}F_2$^{74}Ge: calc.: 346.0588, found: 346.0574. Anal. calc. for

$C_{18}H_{18}F_2$Ge, C 62.68, H 5.26; found, C 63.00, H 5.28.
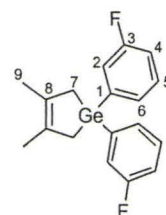
3,4-Dimethyl-1,1-bis-(4-trifluoromethylphenyl)-1-germacyclopent-3-ene (**33f**, mp

59.2 – 60.0 °C); ^{1}H NMR, δ = 1.80 (s, 6H, C^8H_3), 2.06 (s, 4H, C^6H_2), 7.62 (s, 8H, all

ArH); ^{13}C NMR, δ = 19.46 (C8), 25.44 (C6), 124.28 (q, $^1J_{C\text{-}F}$ = -272 Hz,

C5), 124.96 (C3), 130.86 (C7), 131.38 (q, $^2J_{C\text{-}F}$ = 32 Hz, C4), 134.60

(C2), 142.66 (C1). IR: 2915 cm^{-1} (m,br), 1925 (w), 1607 (m), 1394 (m),

1325 (s), 1167 (s), 1129 (s), 1058 (s), 1019 (m), 826 (m), 690 (m). MS: m/z = 446.1*

(19), 271.1 (69), 252.1 (77), 219.0 (46), 126.0 (26). HRMS: $C_{20}H_{18}F_6Ge$ calc.446.0524;

found 446.0501. Anal. calc. for $C_{20}H_{18}F_6Ge$: C 53.99, H 4.08; found: C 54.06, H 4.02. A

single crystal x-ray structure was determined for this compound (Figure 9.1).[5]
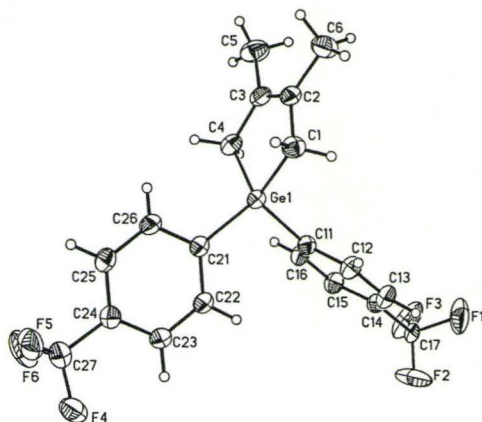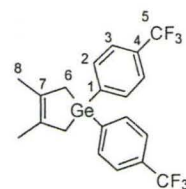
Figure 9.1. The molecular structure of **33f** drawn with 50% probability ellipsoids. Atoms C17, F1, F2 and F3 are disordered but the disorder is not shown for clarity.[5] *Reproduced with permission of the International Union of Crystallography (http://journals.iucr.org/)*

3,4-Dimethyl-1,1-bis[3,5-bis(trifluoromethyl)phenyl]germacyclopent-3-ene (**33g**, mp

76.6-77.4 °C) ^{1}H NMR: δ = 1.84 (s, 6H, H-1), 2.15 (s, 4H, H-3), 7.89

(s, 4H, H-5), 7.92 (s, 2H, H-7); ^{13}C NMR: δ = 19.39 (C-1), 25.30 (C-

3), 123.47 (q, J = 273 Hz, C-8), 123.60 (C-7), 130.77 (C-2), 131.70

(q, J = 33 Hz, C-6), 133.98 (C-5), 140.10 (C-4); IR (film, cm^{-1}): 2987 (m), 2927 (m),
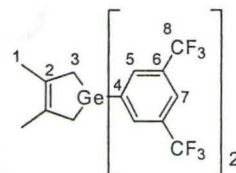
1832 (w), 1616 (w), 1445 (w), 1357 (s), 1280 (s), 1167 (s), 1127 (s), 984 (w), 894 (m);

MS: (EI, m/z (%)) = 582.0* (28), 563.0* (6), 388.0 (100), 369.0* (10), 286.9* (15), 194.0

(48); HRMS: calc. for $C_{22}H_{16}F_{12}Ge$ ([M]$^+$) = 582.0276; found, 582.0298. Anal. calc. for

$C_{22}H_{16}F_{12}Ge$, C 45.48%, H 2.78%; found, C 45.83%, H 2.39%.

9.4.2. Molecules associated with germylene product studies:

Compounds **66**[6] and **23a**[1] were prepared as previously described. The analogues

of **23a** (**23b** and **23e**) were prepared in an analogous fashion to **23a** using the appropriate

Grignard reagent.

1,1-diphenylgermetane (66). ^{1}H NMR, δ = 1.98 (t, 4H, 7.7 Hz), 2.42 (pentet, 2H, 7.5

Hz), 7.36-7.46 (m, 6H), 7.56-7.66 (m, 4H). The spectrum agrees with data

reported elsewhere.[6]

3-Methyl-1,1-diphenyl-1-germacyclopent-3-ene (23a). (*Synthesis by S.*

Ladowski) ^{1}H NMR, δ = 1.91 (s, 3H, CH$_3$), 1.94 (s, 2H, CH$_2$), 2.04 (s, 2H,
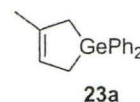
CH$_2$), 5.78 (s, 1H, alkene), 7.38-7.42 (m, 6H, ArH), 7.55-7.59 (m, 4H, ArH). The

spectrum agrees with data reported elsewhere.[1]

1,1-bis(3,4-dimethylphenyl)-3-methyl-1-germacylopent-3-ene (23b)

^{1}H NMR, δ = 1.84 (br s, 5H, H $^{4 \text{ and } 5}$), 1.94 (s, 2H, H^1), 2.25 (s, 6H, H^{12}

$^{\text{or } 13}$), 2.26 (s, 6H, H$^{12 \text{ or } 13}$), 5.70 (s, H, H^3), 7.13 (d, 2H, J = 7.2 Hz, H^{10}),

7.25 (d, 2H, J = 7.2 Hz, H^{11}), 7.28 (s, 2H, H^{11}).^{13}C NMR, δ = 19.33
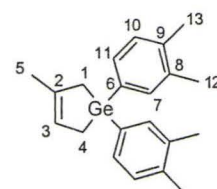
(C^1), 19.83 (C$^{12 \text{ or } 13}$), 19.88 (C$^{12 \text{ or } 13}$), 22.68 (C^5), 22.89 (C^4), 125.41 (C^3), 129.64 (C^{10}),

264

131.88 (C^{11}), 135.40 (C^7), 135.43 (C^8), 136.55 (C^9), 137.47 (C^6), 140.28 (C^2). MS, m/z

(intensity): 352.1* (8), 284.1* (12), 210.1 (100), 195.1 (53), 179.1 (19). HRMS: calc. for

$C_{21}H_{26}{}^{74}Ge$, 352.1246; found: 352.1234. IR, cm^{-1} (intensity): 2998 (br, s), 2917 (br, s),

1637 (w), 1494 (m), 1447 (s), 1377 (m), 1147 (w), 1098 (s), 810 (m), 720 (m).

1,1-bis(3-fluorophenyl)-3-methyl-1-germacyclopentene (23e) ^{1}H NMR, δ = 1.86 (s,

3H, H_3), 1.89 (s, 2H, H_{10}), 2.00 (s, 2H, H_7), 5.63 (s, H, H_9), 7.06 (m, 2H,

H_4), 7.19 (dd, 2H, H_2, J = 8.5, 2.6 Hz), 7.26 (m, 2H, H_6), 7.31 (m, 2H,

H_5). ^{13}C NMR, δ = 19.16 (C_7), 22.54 (C_{11}), 22.66 (C_{10}), 116.19 (d, J = 21

Hz, C_4), 120.63 (d, J = 18 Hz, C_2), 125.18 (C_9), 129.75 (C_6), 130.10 (d, J

= 7.5 Hz, C_5), 140.15 (C_8), 140.58 (C_1), 162.90 (d, J = 250 Hz, C_3). MS, m/z (intensity):

332.0* (52), 262.0* (40), 198.1* (20), 152.1 (100), 92.9* (38). HRMS: $C_{18}H_{18}F_2{}^{74}Ge$:

calc.: 332.0432, found: 332.0437. IR, cm^{-1} (intensity): 3036 (m), 3004 (m), 2911 (br, m),

2060 (br, w), 1576 (s), 1475 (s), 1416 (s), 1260 (s), 1214 (s), 1161 (m), 1096 (s), 865 (s).
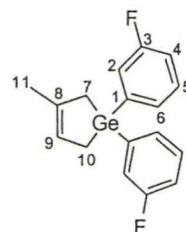
1,1,2,2-tetraphenyl-1,2-bis(trimethylsilyl)digermane $(GePh_2(SiMe_3))_2$ was obtained

from C. Harrington. Synthesis and characterization are reported elsewhere.[7]

Chlorodiphenylgermane (57) was prepared following the method of Kunai and co-

workers.[8] The product was isolated from the crude reaction mixture as a colorless oil by

Kugelrohr distillation (T = 100°C, P = 0.2 mmHg). ^{1}H NMR: δ = 6.56 (s, H), 7.46-7.54

(m, 6H, *ortho/para*), 7.63-7.73 (m, 4H, *meta*). ^{13}C NMR: δ = 128.9 (*meta*), 130.8 (*para*),

133.8 (*ortho*), 135.3 (*ipso*). MS [m/z (I)]: 263.0* (15), 227.0* (13), 185.9* (100), 151.0*

(48), 108.9* (49), 79.1* (60). HRMS: $C_{12}H_{10}{}^{74}GeCl$ (M-H) calc. 262.9683; found

262.9675. IR (cm^{-1}): 3071 (m), 3052 (m), 3008 (br, w), 2076 (br, s), 1484 (m), 1433 (s),

1334 (w), 1305 (w), 1095 (s), 1027 (w), 998 (w), 855 (br, w).

Trichloro(trichloromethyl)germane (61) was prepared following the method of

Nefedov and co-workers.[9] $GeCl_2$-dioxane (10.3 g, 44 mmol) was dissolved in CCl_4 (150

mL) and refluxed for 4 hrs under nitrogen. The reaction mixture was stirred under

vacuum (~0.1 mmHg) at ambient temperature until the solvent had been removed,

yielding the crude product as a pale yellow solid. While still under vacuum, the flask was

gently warmed with a water bath (ca. 40-50 °C) and the product, a white solid, sublimed

onto a cold-finger cooled to –(30-40)°C using dry-ice/iso-propanol. Yield: 8.68 g (29

mmol, 66%) The melting point was measured in a sealed tube (mp 104-106 °C; lit. 106-

107 °C)[9]. MS: $[m/z$ (I)]: 297.7* (3) $[M^+]$, 260.8* (80) $[M-Cl]^+$, 178.8* (28) $[M-CCl_3]^+$,

159.9* (18), 116.9 (100).

Chloro(trichloromethyl)diphenylgermane (58) A 2-neck 250 mL round bottom flask,

fitted with a dropping funnel and a condenser, was charged with Cl_3GeCCl_3 (0.80 g, 2.7

mmol) and anhydrous ether (20 mL). The dropping funnel was charged with freshly

prepared PhMgBr (10.8 mmol, 4 eq) in ether (50 mL). The Grignard reagent was added

dropwise over 40 minutes, causing the formation of white insoluble salts. After the

addition was complete, the mixture was allowed to stir for 2 hr at room temperature. The

solvent was removed under vacuum and the residue was washed with pentane (5 × 20

mL). The combined washes were filtered and the solvent removed under vacuum to yield

a yellow oil (0.66 g). The product was isolated from the crude reaction mixture by

Kugelrohr distillation, with a majority of the product, a colorless oil, distilling at 110-120

°C (P = 0.05 mmHg). Isolated yield 0.10 g (0.3 mmol, 11 %). ^1H NMR (C_6D_{12}) = 7.34-

7.42 (m, 6H); 7.79-7.87 (m, 4H). ^{1}H NMR (CD$_3$CN) = 7.55-7.59 (m, 4H, *ortho*); 7.61-

7.67 (m, 2H, *para*); 7.87-7.91 (m, 4H, *meta*). ^{13}C NMR (CD$_3$CN) = 92.05 (CCl$_3$); 130.19

(*ortho*); 130.69 (*ipso*); 133.09 (*para*); 135.38 (*meta*). [Note: the ^{13}C shift of CCl$_3$ is

consistent with literature data for this group on Ge.[10-12]] GC/MS, (Saturn, CI), m/z =

344.7* (20)(M-Cl)$^+$, 299.2* (44), 201.3 (100), 161.1 (30), 159.2 (50). GC/MS, (Saturn,

EI), m/z = 263.2* (100)(M-CCl$_3$)$^+$. MS (Micromass, CI) (*m/z*, intensity): 306.9* (7),

280.0* (4), 263.0* (18), 151.0* (8), 108.9* (9), 94.1 (24), 93.1 (28), 78.0 (100). HRMS:

calc. for C$_{12}$H$_{10}$^{74}GeCl (M-CCl$_3$)$^+$: 262.9683; found: 262.9621. IR (cm^{-1}, intensity):

3075 (m), 3055 (m), 1960 (w), 1885 (w), 1816 (w), 1585 (w), 1485 (s), 1434 (s), 1092

(s), 998 (s).

Attempts to crystallize the compound were unsuccessful; however, slow

evaporation of a hexane solution in contact with atmospheric moisture led to the

formation of colorless crystals of trichloromethyldiphenylgerminol (**62**) (mp 65.6-67.7

°C) ^{1}H NMR (CD$_3$CN) = 7.50-7.54 (m, 4H, *ortho*); 7.56-7.60 (m, 2H, *para*); 7.82-7.87

(m, 4H, *meta*). IR (cm^{-1}, intensity): 3375 (br, m), 1961 (w), 1882 (w), 1810 (w), 1481

(m), 1431 (s), 999 (s).
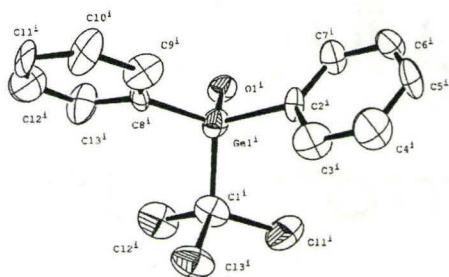
Figure 9.2. ORTEP diagram of **62** (50% probability ellipsoids). H atoms omitted for clarity.

Table 9.1. Crystal data and structure refinement for **62.**

Empirical formula	$C_{13}H_{11}Cl_3GeO$
Temperature	173(2) K
Wavelength	0.71073 Å
Formula weight	362.16
Crystal system	Triclinic
Space group	P-1
Unit cell dimensions	a = 13.651(5) Å, α = 88.545(8)°
	b = 14.244(5) Å, β = 85.854(8)°
	c = 15.712(5) Å, γ = 84.987(7)°
Volume	3035.0(19) Å^3
Z	8
Density (calculated)	1.585 Mg/m^3
Absorption coefficient	2.531 mm^{-1}
F(000)	1440
Crystal size	0.40 × 0.30 × 0.10 mm^3
Theta range for data collection	1.30 to 20.87°
Index ranges	-12 ≤h ≤13, -14 ≤k ≤14, -11 ≤l ≤5
Reflections collected	21095
Independent reflections	6337 [R(int) = 0.2301]
Completeness to theta = 20.87°	99.0 %
Absorption correction	Numerical
Max. and min. transmission	0.7859 and 0.4308
Refinement method	Full-matrix least- squares on F^2
Data / restraints / parameters	6337 / 15 / 601
Goodness-of-fit on F^2	0.956
Final R indices [I>2sigma(I)]	R1 = 0.0681, wR2= 0.1129
R indices (all data)	R1 = 0.2014, wR2 = 0.1536
Largest diff. peak and hole	0.589 and -0.697 e.Å^{-3}

9.4.3. Molecules associated with digermene product studies

Hexamesitylcyclotrigermane (**86**)[13] and 1,2-dichlorotetramesityldigermane (**94**)[14] were prepared as previously described. Spectra agreed well with reported data.

Hexamesitylcyclotrigermane (86): ^{1}H (C$_6$D$_6$), δ = 2.09 (s, 18H, p-Me), 1.90-2.70 (br s, 36H, o-Me), 6.674 (s, 12H, ArH). **1,2-dichlorotetramesityldigermane (94)**: ^{1}H (C$_6$D$_6$), δ = 2.05 (s, 12H, p-Me), 2.15-2.90 (br s, 24 H, o-Me), 6.667 (s, 8H, ArH).

9.5. Steady-State Photolysis Experiments

9.5.1. General

Solutions of **33x** were prepared in the appropriate solvent, spiked with the appropriate scavenger, and internal standard (Si_2Me_6 for NMR experiments or dodecane for GC/MS experiments). Aliquots of these solutions were then transferred to the appropriate quartz vessel (either an NMR tube or 15 mL [diameter 2 cm] tube). The solutions were purged for several minutes with argon and sealed. Samples were irradiated within a Rayonet® photochemical reactor (Southern New England Ultraviolet Co.) equipped with a merry-go-round apparatus and RPR2537 (254 nm) lamps. The progress of the reaction was periodically monitored by NMR or GC/MS. The relative yields of the products were then calculated from the relative slopes of the individual concentration vs. time plots.

9.5.2. Quantum yield of germylene extrusion (trapping with methanol)

The quantum yields for the extrustion of $GeAr_2$ from **33a-g** were all determined in the same manner (See Chapter 2.1.4). As an example, the first such experiment is described in more detail:

Compounds **33a-d** were each dissolved in C_6D_{12} (1.0 mL), such that the concentration was $(2.0 \pm 0.3) \times 10^{-2}$ M. To each solution was added methanol CH_3OH (0.2 M) and Si_2Me_6 (1 μL) as an internal standard. Approximately 700 μL of each solution was placed in a quartz NMR tube and degassed. The Rayonet photochemical

reactor equipped was equipped with 2 × 254 nm lamps. NMR spectra were obtained after 0, 1, 2, 3, and 4 minutes of photolysis, using the solvent peak (δ = 1.38 ppm) as a reference, and integrating the Si_2Me_6 peak to 1.000. Four minutes of photolysis time resulted in roughly 20% conversion. Visible in the spectrum after photolysis were 2,3-dimethyl-1,3-butadiene, as well as the germylene-methanol insertion product (**36**).

bis(4-methylphenyl)(methoxy)germane (36c): ^1H (C_6D_{12}), δ = 2.30 (s, 6H, C^5H_3), 3.50 (s, 3H, OCH_3), 6.05 (s, H, GeH), 7.10 (d, 4H, J = 7.8 Hz, C^3H), 7.39 (d, 4H, J = 7.8 Hz, C^2H);
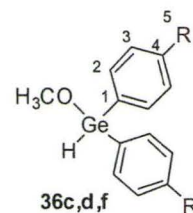
bis(4-fluorophenyl)(methoxy)germane (36d): ^1H (C_6D_{12}), δ = 3.53 (s, 3H, OCH_3), 6.10 (s, H, GeH), 7.00 (m, 4H, C^3H), 7.44 (m, 4H, C^2H).

bis(4-trifluoromethylphenyl)(methoxy)germane (36f): ^1H (C_6D_{12}), δ = 3.58 (s, 3H, OCH_3), 6.19 (s, H, GeH), 7.60 (d, 4H, J = 7.8 Hz, C^3H), 7.63 (d, 4H, J = 7.8 Hz, C^2H).

bis(3,4-dimethylphenyl)(methoxy)germane (36b) ^1H (C_6D_{12}): δ = 2.21 (s, 6H, ArMe), 2.22 (s, 6H, ArMe), 3.49 (s, 3H, OMe), 6.02 (s, H, GeH), 7.06 (d, 2H, J = 7.2 Hz, H-2), 7.23 (d, 2H, J = 7.2 Hz, H-3), 7.29 (s, 2H, H-1).
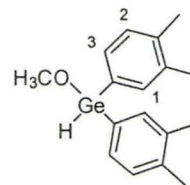
bis(3-fluorophenyl)(methoxy)germane (36e) ^1H (C_6D_{12}): δ = 3.56 (s, 3H, OCH_3), 6.11 (s, H, GeH), 6.98-7.03 (m, 2H, ArH). Remaining aromatic proton resonances are obscured by **33e.**

bis(3,5-bis(trifluoromethyl)phenyl)(methoxy)germane (36g): ^1H (C_6D_{12}), δ = 3.63 (s, 3H, OMe), 6.32 (s, 1H, GeH), 7.95 (s, 2H, p-H), 8.00 (s, 4H, o-H).

9.5.3. Germylene scavenging with acetic acid

Solutions of **33c,d,f** in hexanes containing HOAc (0.4 M) were irradiated for two hours in parallel with 2 × 254 nm lamps. The solvent and excess HOAc were removed under high vacuum to afford yellow oils, the ^{1}H NMR spectra of which showed high conversion (> 80%) of the starting material to a single product (>90 % yield). These products were unstable towards silica gel chromatography or GC/MS and thus could not be isolated. Compounds **40c,d,f** were thus identified on the basis of the following spectroscopic data, obtained on the crude reaction mixtures.

bis(4-methylphenyl)germyl acetate (40c): ^{1}H NMR, δ = 2.11 (s, 3H, OAc), 2.38 (s, 6H, C$^5H_3$), 6.63 (s, 1H, GeH), 7.25 (d, 4H, J = 7.9 Hz, C^3H), 7.57 (d, 4H, J = 7.5 Hz, C^2H); ^{13}C NMR, δ = 21.68 (C5), 22.15 (COCH$_3$), 129.47 (C2), 129.86 (C1), 134.60 (C3), 140.80 (C4), 174.64 (C=O); IR, ν (cm^{-1}) = 2087 (m), 2041 (w), 1700 (s); HRMS, calc. C$_{16}$H$_{17}$GeO$_2$ (M-H), 316.0519; found, 316.0512.

bis(4-fluorophenyl)germyl acetate (40d): ^{1}H NMR, δ = 2.12 (s, 3H, OAc), 6.65 (s, H, GeH), 7.13-7.18 (m, 4H, C^3H), 7.64-7.67 (m, 4H, C^2H); ^{13}C NMR, δ = 22.00 (COCH$_3$), 116.13 (d, $^2J_{C\text{-}F}$ = 20 Hz, C3), 128.49 (C1), 136.70 (d, $^3J_{C\text{-}F}$ = 7 Hz, C2), 164.70 (d, $^1J_{C\text{-}F}$ = 251 Hz, C4), 174.66 (C=O). IR, ν (cm^{-1}) = 2049 (m, br), 1699 (s); HRMS, calc. C$_{14}$H$_{11}$F$_2$GeO$_2$ (M-H), 322.9939; found, 322.9997.

40c,d,f
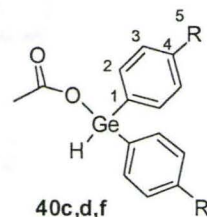
bis(4-trifluoromethylphenyl)germyl acetate (40f): ^{1}H NMR, δ = 2.16 (s, 3H, OAc), 6.75 (s, H, GeH), 7.70 (d, 4H, J = 8.4 Hz, C^3H), 7.79 (d, 4H, J = 8.4 Hz, C^2H); ^{13}C NMR,

δ = 21.81 (COCH_3), 123.95 (q, $^1J_{C\text{-}F}$ = 272 Hz, C5), 125.47 (C2), 133.03 (q, $^2J_{C\text{-}F}$ = 32

Hz, C4), 135.00 (C3), 137.85 (C1), 174.74 (C=O). IR, ν (cm^{-1}) = 2101 (m, br), 1702 (s);

HRMS, calc. for $C_{16}H_{11}F_6GeO_2$ (M-H), 422.9875; found, 422.9908.

9.5.4. Germylene scavenging with CCl$_4$

(a) For reactions monitored by NMR (C_6D_{12} or THF-d_8 solvent) the standard procedure
was followed using 2 × 254 nm lamps. Reaction products were identified by spiking the
mixture with authentic samples as well as by a GC/MS analysis at the end of the
experiment.

(b) For reactions monitored by GC/MS only, solutions of the compounds (0.22-0.50 M)
were prepared in dry cyclohexane or THF (5 mL). The standard procedure was followed
with 2 × 254 nm lamps. The solution was spiked with the dodecane (1 mM) to use as an
integration standard and CCl$_4$ (0.05 M). If applicable, THF or triethylamine was added
as well. Over the course of the photolysis, aliquots were removed and monitored by
GC/MS. After each aliquot was removed, the tube was re-purged with argon. Reaction
products were identified by spiking the mixture with authentic samples.

9.5.5. Germylene scavenging with isoprene

(a) For those monitored by NMR: The standard procedure was followed (2 × 254 nm
lamps). The yield of the GePh$_2$-containing oligomers (10H) were calculated by
subtracting the integrals of the aromatic proton signals due to **33a** + **23a** (10H) from the
total integral over δ 6.79-7.83.

(b) For those monitored by GC/MS only: The standard procedure was followed (6 × 254 nm lamps for 20 minutes) using hexanes solvent. In each case, the chromatogram showed evidence of only a single photolysis product, which eluted at a slightly shorter retention time compared to that of the starting compound. The products were identified as the corresponding 1,1-diaryl-3-methylgermacyclopent-3-enes **23b-g** based on their mass spectra (Table 9.2). The identity of **23b,e** in the photolysate from **33b,e** was further confirmed by spiking the mixture with an authentic sample.

Table 9.2. Low-resolution mass spectral data of 1,1-diaryl-3-methylgermacyclopent-3-enes **23c,d,f,g**. *m/z* values marked with * indicate ions containing ^{74}Ge

23c	*p*-Me	324.2*(24), 256.3*(100), 181.5 (20), 165.2 (12).
23d	*p*-F	332.3*(70), 264.4*(100), 233.5*(12), 152.3 (35), 93.2*(35).
23f	*p*-CF$_3$	432.1*(52), 413.3* (12), 271.3 (85), 252.4 (100).
23g	*mm*-CF$_3$	568.3*(50), 549.7*(22), 389.3 (20), 388.6 (100).

9.5.6. Digermene scavenging with acetic acid

A solution of hexamesitylcyclotrigermane (**86**; 18 mg, 1.9×10^{-5} mol) in dry toluene (15 mL) was placed in a 15 × 150 mm quartz tube and sealed with a rubber septum. Triethylsilane (0.05 mL, 3.1×10^{-4} mol) was then injected via syringe and the solution was deoxygenated with a fine stream of argon for 30 min. It was then placed in a Pyrex dewar containing 3:1 2-propanol/methanol, cooled to <-30 - 50°C with dry ice, and photolysed with 12 × RPR3500 lamps in a Rayonet® photochemical reactor for three hours. Addition of acetic acid (0.2 mL, 3.5×10^{-3} mol) to the cold solution caused no change in the characteristic yellow color due to **DGm**, so was removed from the dewar

and allowed to warm to room temperature. The solution turned colorless after ca. 10

minutes at ca. 20 °C. The solvent and excess HOAc were removed under vacuum to

yield a pale yellow oil. The ^{1}H NMR spectrum of the crude mixture showed two

products present, in addition to residual starting material and $Mes_2Ge(H)(SiEt_3)$, the

product resulting from the trapping of Mes_2Ge with triethylsilane. The mixture was

purified using column chromatography (silica; 1:1 dichloromethane:hexanes). Residual

86 (2 mg) was recovered, followed by 1-hydroxy-1,1,2,2-tetramesityldigermane (**88**, 2

mg), formed from traces of water present in the system.[15] The major product was a white

solid which was identified as

1-acetoxy-1,1,2,2-tetramesityldigermane (92, 8 mg, 1.2×10-5 mol, 63%):

^{1}H (C$_6$D$_6$), δ = 1.88 (s, 3H, OAc), 2.06 (s, 6H, *p*-C*H*$_3$ A), 2.08

(s, 6H, *p*-C*H*$_3$ B), 2.36 (s, 12H, *o*-CH$_3$ A), 2.40 (s, 12H, *o*-

C*H*$_3$ B), 6.32 (s, H, Ge*H*), 6.70 (s, 4H, Ar*H* A), 6.72 (s, 4H,
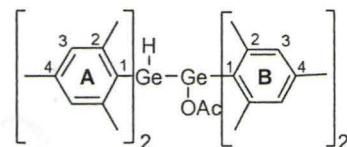
Ar*H* B); ^{13}C (CDCl$_3$): δ = 21.12 (*p*-CH$_3$, A&B - there are two overlapping signals here

that can be resolved in benzene-*d*6), 23.37 (COCH$_3$), 23.80 (*o*-CH$_3$ A), 24.52 (*o*-CH$_3$ B),

128.63 (C3 A), 129.42 (C3 B), 134.51 (C1 A), 136.76 (C1 B), 138.39 (C4 A), 138.92 (C4

B), 142.83 (C2 A), 143.77 (C2 B), 172.01 (C=O). ^{1}H (CDCl$_3$), δ = 1.98 (s, 3H, OAc),

2.11 (s, 12H), 2.18 (s, 12H), 2.23 (s, 12H), 5.90 (s, H, Ge*H*), 6.72 (s, 4H, Ar*H* A), 6.75 (s,

4H, Ar*H* B); ^{13}C (C$_6$D$_6$): δ = 20.98, 21.02, 23.01, 24.18, 24.80, 129.19, 129.90, 135.15,

137.58, 138.56, 139.05, 143.21. 144.03, 171.09. IR, υ (cm-1) = 2964 (s, br), 2922 (s, br),

2077 (w), 2034 (w), 1710 (s), 1698 (s), 1602 (m), 1448 (m, br), 1264 (s), 1017 (m), 847

(m); MS (CI), m/z (I) = 682.2* (9), 621.1* (90), 563.1* (17), 503.1* (11), 431.2* (17),

371.1* (95), 312.1* (48), 253.0* (32), 192.0* (100); HRMS, Calc. for $C_{38}H_{48}O_2Ge_2$, 682.2061; found, 682.2087.

9.5.7. Digermene scavenging with CCl_4

The procedure described in Section 9.5.6 was used to generate the digermene (including reagent amounts). Addition of a solution of CCl_4 in toluene (0.2 mL, 3.5×10^{-3} mol) (pre-cooled to -30 °C) to the cold solution caused immediate disappearance (within seconds) of the characteristic yellow color due to **DGm**. The solvent and excess CCl_4 were removed under vacuum to yield a pale yellow oil. The ^1H NMR was shown in Chapter 4. The product **94** was identified by co-spiking of the mixture with the authentic sample.

9.6. Low temperature matrix photolyses.

A solution of **66** ($A_{254\ nm} \approx 0.8$) in 3-methylpentane (Aldrich spectrophotometric grade) was sealed in a cuvette ($2 \times 1 \times 1$ cm; Suprasil quartz) with a rubber septum and degassed by bubbling with a fine stream of argon for 5 minutes. If applicable, $CDCl_3$ or CCl_4 were added through the septum via microliter syringe. The sample was placed in an Oxford^{TM} Optistat liquid nitrogen cryostat equipped with an Oxford^{TM} ITC601 temperature controller. Liquid nitrogen was used to cool the cyrostat to 78 K. The entire assembly was placed in a Rayonet photochemical reactor equipped with 12×254 nm. UV/vis spectra were recorded by moving the entire unit into the UV spectrometer.

9.7. Laser Flash Photolysis

Laser flash photolysis experiments employed the pulses from a Lambda Physik Compex 120 excimer laser, filled with $F_2/Kr/Ne$ (248 nm; ca. 25 ns; 100 ± 5 mJ or $F_2/Ar/Ne$ (193 nm; 20-25 ns; ca. 50 mJ) mixtures, and a Luzchem Research mLFP-111 laser flash photolysis system. The latter has been modified to incorporate an external 150 W high pressure xenon lamp as monitoring source, powered by a Kratos LPS-251HR power supply. A Pyrex filter between the sample cell and monochromator protects the latter from scattered laser light from the when the monitoring wavelength is < 330 nm. The laser is at 90° relative to the monitoring beam and hits the sample cell through a through a 5 mm diameter circular slit.[1]

Solutions of **33** were prepared in a calibrated 100 mL reservoir, fitted with a glass frit to allow bubbling of argon through the solution for at least 30 minutes prior to and then throughout the duration of each experiment. Concentrations were such that the absorbance at the excitation wavelength was between *ca.* 0.7 and 0.9. The solutions were pumped from the reservoir through Teflon tubing connected to a 7 × 7 mm Suprasil flow cell using a Masterflex[TM] 77390 peristaltic pump. The glassware, sample cell, and transfer lines were dried in a vacuum oven (65-85 °C) before use. The flow cell was placed in a thermostatted sample compartment:

(a) Experiments at 25 °C: the solution temperatures were measured with a Teflon-coated copper/constantan thermocouple inserted into the sample compartment in close proximity to the sample cell.

(b) Experiments other than 25 °C: a modified flow cell was employed that allowed

insertion of the Teflon-coated copper/constantan thermocouple directly into the

sample solution.

Reagents were added directly to the reservoir by microliter syringe as aliquots of standard

solutions. Transient absorbance-time profiles at each concentration of scavenger are the

signal-averaged result of 7-40 laser shots. Decay rate constants were calculated by non-

linear least squares analysis of the transient absorbance-time profiles using the Prism 5.0

software package (GraphPad Software, Inc.) and the appropriate user-defined fitting

equations, after importing the raw data from the Luzchem mLFP software and applying

the necessary corrections to remove the minor contributions from the corresponding

digermenes at low substrate concentrations (as described in the text). Rate constants

were calculated by linear least-squares analysis of decay rate-concentration data

(generally 4-7 points) that spanned as large a range in transient decay rate as possible.

Rate constants determined at temperatures other than 25°C were corrected for thermal

solvent expansion: hexanes[16] and THF[17].

9.8. References

1. Leigh, W. J.; Harrington, C. R.; Vargas-Baca, I. *J. Am. Chem. Soc.* **2004**, *126*, 16105. (Errata: *J. Am. Chem. Soc.* **2006**, *128*, 1394.).
2. Mazerolles, P.; Manuel, G. *Bull. Soc. Chim. Fr.* **1966**, 327.
3. Manuel, G.; Mazerolles, P.; Lesbre, M.; Pradel, J.-P. *J. Organomet. Chem.* **1973**, *61*, 147.
4. Lollmahomed, F.; Huck, L. A.; Chitnis, S. S.; Harrington, C. R.; Leigh, W. J. *Organometallics* **2009**, *28*, 1484.
5. Huck, L. A.; Harrington, L. E.; Britten, J. F.; Leigh, W. J. *Acta Cryst.* **2007**, *E63*, m1282.
6. Toltl, N. P.; Leigh, W. J. *J. Am. Chem. Soc.* **1998**, *120*, 1172.

7. Harrington, C. R.; Leigh, W. J.; Chan, B. K.; Gaspar, P. P.; Zhou, D. *Can. J. Chem.* **2005**, *83*, 1324.
8. Ohshita, J.; Toyoshima, Y.; Iwata, A.; Tang, H.; Kunai, A. *Chem. Lett.* **2001**, 886.
9. Kolesnikov, S. P.; Perl'Mutter, B. L.; Nefedov, O. M. *Dokl. Akad. Nauk SSSR (Eng. trans.)* **1971**, *196*, 594.
10. Egorov, M. P.; Dvornikov, A. S.; Ezhova, M. B.; Kuz'min, V. A.; Kolesnikov, S. P.; Nefedov, O. M. *Organomet. Chem. USSR* **1991**, *4*, 582.
11. Komoriya, H.; Kako, M.; Nakadaira, Y.; Mochida, K. *Organometallics* **1996**, *15*, 2014.
12. Nemes, G.; Escudié, J.; Silaghi-Dumitrescu, I.; Ranaivonjatovo, H.; Silaghi-Dumitrescu, L.; Gornitzka, H. *Organometallics* **2007**, *26*, 5136.
13. Ando, W.; Tsumuraya, T. *J. Chem. Soc., Chem. Commun.* **1987**, 1514.
14. Cooke, J. A.; Dixon, C. E.; Netherton, M. R.; Kollegger, G. M.; Baines, K. M. *Synth. React. Inorg. Met. -Org. Chem.* **1996**, *26*, 1205.
15. Baines, K. M.; Cooke, J. A.; Dixon, C. E.; Liu, H.; Netherton, M. R. *Organometallics* **1994**, *13*, 631.
16. Density of Solvents as a Function of Temperature. In *CRC Handbook of Chemistry and Physics, Internet Version*, 87 ed.; Lide, D. R., Ed. CRC Press/Taylor and Francis: Boca Raton, FL, 2007; pp 15-25.
17. Postigo, M.; Mariano, A.; Mussari, L.; Camacho, A.; Urieta, J. *Fluid Phase Equilib.* **2003**, *207*, 193.